Astroglial connexins in adult neurogenesis: Mechanistic insight from mutant mice

Dissertation

zur

Erlangung des Doktorgrades (Dr. rer. nat)

der

Mathematisch-Naturwissenschaftlichen Fakultät

der

Rheinische Friedrich-Wilhelms-Universität Bonn

Vorgelegt von

Jiong Zhang

aus

Shanghai

Bonn, Juni 2013

Angefertigt mit Genehmigung der Mathematisch-Naturwissenschaftlichen Fakultät der Rheinischen Friedrich-Wilhelms-Universität Bonn

Gutachter:

Erstgutachter: Prof. Dr. Martin Theis
Zweigutachter: Prof. Dr. Klaus Willecke

Tag der Promotion: 11. 10. 2013
Erscheinungsjahr: 2013

Erklärung:

Hiermit versichere ich, dass diese Dissertation von mir selbst und ohne unerlaubte Hilfe angefertigt worden ist. Es wurden keine anderen als die angegebenen Hilfsmittel benutzt. Ferner erkläre ich, dass die vorliegende Arbeit an keiner anderen Universität als Dissertation eingereicht wurde.

Bonn, Juni 2013

……

Jiong Zhang

Acknowledgements

First, I would like to express my sincere gratitude to my supervisor Prof. Dr. Martin Theis, who gave me the opportunity to perform PhD thesis in his research group and for his valuable advice, scientific guidance and constant encouragement throughout the course of this work. I also would like to express my deep gratitude to Prof. Dr. Christian Steinhäuser for his constructive discussions, critical suggestions and overall excellent organization during my PhD thesis.

I would like to thank Prof. Dr. Klaus Willecke, Prof. Dr. Walter Witke and Prof. Dr. Volkmar Gieselmann for accepting my request to be the members of the examination committee and for their time and efforts in reviewing this work.

In addition, my sincere and special thanks go to Prof. Dr. Lampe (Fred Hutchinson Cancer Research Center, Seattle, USA), Prof. Dr. Brehm (University of Veterinary Medicine Hannover, Hannover, Germany), Prof. Dr. Volkmar Gieselmann and Dr. Marc Sylvester (Institute of Biochemistry and Molecular Biology, University Hospital of Bonn) as well as Mrs. Alexandra Klein (Institute of Physiology I, University Hospital of Bonn) for their good collaboration.

I also would like to express the appreciation to my colleagues Dr. Peter Bedner and Mrs. Stephanie Griemsmann for helping me with the coupling study and sharing of their experience. I thank all other members of Institute of Cellular Neurosciences, especially Anja Matijevic, Joana Fischer and Ina Fiedler for excellent technical assistance.

A special gratitude and love goes to my family. I am deeply and forever indebted to my parents for their abiding love, continuous support and encouragement throughout my entire life. Finally, I want to express my deepest love and thanks to my wife Wei for her support, understanding and taking care of me during the most difficult time of our stay in Germany.

Learn from yesterday, live for today, hope for tomorrow.
The important thing is not to stop questioning.

Albert Einstein (1879-1955)

Table of Contents

Abbreviations

Abbreviations

αMHC	alpha myosin heavy chain
℃	centigrade
µg	microgram
µl	microlitre
µm	micrometer
µM	micromolar
ACN	acetonitrile
ACSF	artificial cerebrospinal fluid
APS	ammonium persulfate
ATP	adenosintriphosphate
BBB	blood brain barrier
BCA	bicinchonic acid assay
BDNF	brain derived neurotrophic factor
Biocytin	N-biotinyl-L-lysine
BLBP	brain lipid-binding protein
BMP	bone morphogenetic protein
bp	base pairs
BrdU	5-brom-2-desoxyuridin
CA	cornu ammonis
cAMP	cyclic adenosinmonophosphate
CDC2	cyclin-dependent kinase 2
CK1	casein kinase 1
CNS	central nervous system
CREB	cAMP response element-binding protein
Cx	connexin
DCX	coublecortin
DEPC	diethylpyrocarbonate
DG	dentate gyrus
dH_2O	double distilled water
DKO	double knockout
DNA	desoxyribonucleic acid
dNTP	2-desoxy-nucleoside-5-triphosphate
E. coli	*Escherichia coli*
e.g.	for example
ECFP	enhanced cyan fluorescent protein
ECL	enhanced chemiluminescence
EDTA	ethylene diaminetetraacetic acid
EEG	electroencephalogram
EGFP	enhanced green fluorescent protein
ERT	estrogen receptor
et al.	*et altera* and others
floxed	flanked by loxP sites
GABA	γ-aminobutyric acid
GCL	granule cell layer
GFAP	glial fibrillary acidic protein
GFP	green fluorescent protein
GJC	gap junction channel
GLAST	glutamate aspartate transporter
GLT-1	glutamate transporter-1
GS	glutamine synthetase
H	hour
HC	hippocampus
HCs	hemichannels
HEPES	4-2-hydroxyethyl-1-piperazineethanesulfonic acid
HPLC	high-performance liquid chromatography
HRP	horse radish peroxidase
i.e.	*it est*
i.p.	intraperitoneal injection
IAA	iodoacetamide

ICC	immunocytochemistry
IF	immunofluorescence
IHC	immunohistochemistry
IP	immunoprecipitation
IR-DIC	infrared differential interference contrast
IRES	internal ribosomal entry site
KA	kainic acid
KDa	kilo Dalton
KO	knockout
L	litre
loxP	locus of crossing over of P1
LSM	laser scanning microscop
LTD	long term depression
LTP	long term potentiation
M	molar
m/z	mass to charge ratio
MAPK	mitogen-activated protein kinase
mg	milligram
Min	minutes
mM	millimolar
MS	mass spectrometry
MTLE	mesial temporal lobe epilepsy
MΩ	megaohm
NDS	normal donkey serum
NeuN	neuronal nuclei antigen
NG2	neuroglycan 2
NGS	normal goat serum
nM	nanomolar
NMDA	N-Methyl-D-Aspartate
NP40	nonidet P-40
NSC	neural stem cell
nt	nucleotides
ODDD	oculodentodigitale dysplasia
ORF	open reading frame
PBS	phosphate buffered saline
PCR	polymerase chain reaction
PDGFR	platelet derived growth factor receptor
PDZ	PSD-95/Dlg-A/ZO-1
PFA	paraformaldehyde
pH	a negative decimal logarithm of the hydrogen ions concentration
PKA	protein kinase A
PKC	protein kinase C
pm	picomoles
PN	postnatal
ppm	parts per million
Prox1	prospero homeobox protein-1
PVDF	polyvinylidine fluoride
RG-like cell	radial glia-like cell
RIPA	RNA immunoprecipitation assay
RNA	ribonucleic acid
rpm	revolutions per minute
RT	room temperature
s.d.	standard deviation
s.e.m.	standard error of the mean
S100ß	S100 calcium binding protein ß
SDS-PAGE	sodium dodecyl sulfate-polyacrylamide gel electrophoresis
Sec	seconds
SGZ	subgranular zone
Shh	sonic hedgehog
SLM	stratum Lacunosum moleculare
SO	stratum Oriens
SP	stratum pyramidale

SR	stratum radiatum
SR101	sulfat rhodamine 101
ß-Gal	ß-galactosidase
SVZ	subventricular zone
TAP	transient amplifying cell
TBST	Tris-buffered saline and Tween20
TCEP	Tris-(2-carboxyethyl)-phosphine
TEMED	N,N,N',N'-tetramethyl-ethylene-diamine
TetO	tetracycline operator
TIF2	transcriptional intermediary factor 2
TLE	temporal lobe epilepsy
TRITC	tetramethyl rhodamine isothiocyanate
TTA	tetracycline transactivator
U	enzyme unit
UTR	untranslated region
UV	ultraviolet
V	volts
v/v	volume per volume
VEGF	vascular endothelial growth factor
w/v	weight per volume
WB	Western Blot
WT	wild type
X-gal	5-bromo-4-choro-indolyl-ß-D-galactopyranoside
ZO-1	zonula occludens-1
ZONAB	ZO-1 associated nucleic acid-binding protein

Amino acids

Amino acid	3-Letter	1-Letter	Molecular weight of amino acid (Da)
Alanine	Ala	A	71,0
Arginine	Arg	R	157,2
Asparagine	Asn	N	114,1
Asparatic acid	Asp	D	114,0
Cysteine	Cys	C	103,1
Glutamic acid	Glu	E	128,1
Glutamine	Gln	Q	128,1
Glycine	Gly	G	57,0
Histidine	His	H	137,1
Isoleucine	Ile	I	113,1
Leucine	Leu	L	113,1
Lysine	Lys	K	129,1
Methionine	Met	M	131,1
Phenylalanine	Phe	F	147,1
Proline	Pro	P	97,1
Serine	Ser	S	87,0
Threonine	Thr	T	101,1
Tryptophan	Trp	W	186,2
Tyrosine	Tyr	Y	163,1
Valine	Val	V	99,1

1. Introduction

Adult hippocampal neurogenesis is one of the most exciting topics at the frontier of neuroscience. Adult-born hippocampal neurons continuously integrate into the preexisting neural circuit under the regulation of intrinsic and extrinsic factors, demonstrating a unique form of neuroplasticity. Advances in our understanding of adult neurogenesis in hippocampus will not only clarify the basic principles of learning and memory, but also may lead to develop new strategies for cell replacement therapy after brain injury or age related neurodegenerative diseases. Despite exciting novel findings over the last five decades, the molecular mechanisms underlying such dynamic process are still not fully understood. This work focuses on the function and regulation of astrocytic gap junctions in adult hippocampal neurogenesis, which are suggested to be essential for maintaining the capacity of neural stem cell proliferation and neural development.

1.1 Hippocampus

1.1.1 Anatomy and function of the hippocampus

The hippocampal formation is a bilateral structure found within the temporal lobes of the hemispheres (Fig. 1.1). The Bolognese anatomist Giulio Cesare Aranzi (circa 1564) was the first to coin the name “hippocampus” to this part of brain, because of its stunning structure similarity to the seahorse. The hippocampal formation consists of three parts: the dentate gyrus (DG), the C*ornu Ammonis* (also ammon’s horn, CA) and the subiculum.

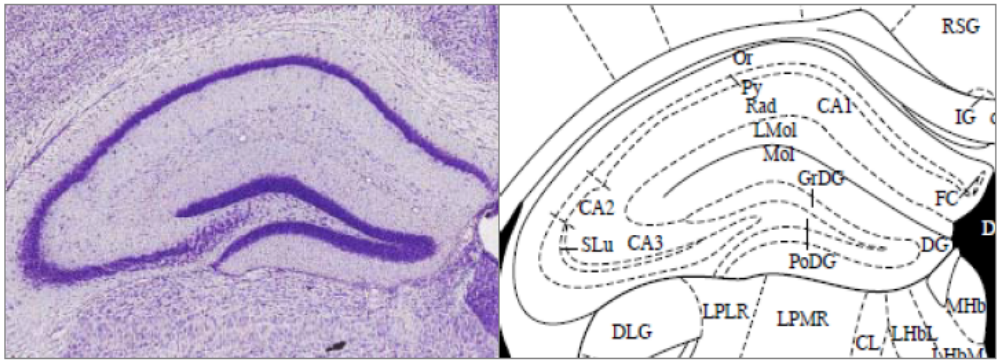

Fig. 1.1: Anatomy of the mouse hippocampus. Following structures are illustrated in coronal plates and diagrams: stratum oriens (Or), pyramidal cell layer (Py), stratum radiatum (Rad), stratum lacunosum moleculare (L.Mol), stratum moleculare (Mol), dentatus gyrus (DG), granular layer of dentate gyrus (GrDG, hilus), polymorph layer (PoDG) also referred to as the hilus, stratum ludicum (SLu) und cornu ammonis regions 1-3 (CA1, CA2, CA3) (Paxinos and Franklin, 2011).

The DG forms a "V" shaped structure, embedded in the most proximal part of the hippocampal formation. DG is also stratified into clearly separated layers. The most

superficial layer is referred to as the *stratum moleculare*. It lies closest to the hippocampal fissure. This layer mainly consists of dendritic trees of the granule cells and is receiving perforant path inputs from the entorhinal cortex. The granule cell layer or *stratum granulosum* forms the principle cell layer of the DG. The polymorphic layer is often referred to as hilus, which consists of axons of dentate granule cells and interneurons, termed mossy fibers. The subgranular zone (SGZ) lies in-between the granule cell layer (GCL) and the hilus. This narrow strip is one of the only two widely acknowledged regions to date that retain adult neurogenesis (for details see below).

The *Cornu Ammonis* (CA) subfield forms the area between the subiculum and the DG (Lorente de No R., 1934). It is subdivided into CA1, CA2 and CA3. The polymorphic layer of the dentate gyrus is also termed as CA4. The lamination of the CA is largely the same for all subfields. However, only CA3 has a layer called the *stratum lucidum*, whereas this layer is absent in CA1 and CA2. The most superficial layer is the *stratum lacunosum moleculare*, followed by *stratum radiatum*, *stratum lucidum*, *stratum pyramidale* or pyramidal cell layer and *stratum oriens.* The *stratum oriens* contains the basal dendrites of the glutamatergic pyramidal cells, and a variety of GABA-ergic interneurons. The *stratum pyramidale* is a narrow U-shaped principal cell layer. Direct below the pyramidal cell layer in the CA3 are the mossy fiber axons from the granule cells of the DG, termed *stratum lucidum*. The *stratum radiatum* contains CA3 to CA3 associational connections and *Schaffer collaterals*, which are the projection forward from CA3 to CA1. The *stratum lacunosum moleculare* contains perforant path fibers from the entorhinal cortex and apical dendrites of pyramidal cells.

The subiculum is positioned between the CA1 subfield and the entorhinal cortex, as well as a range of subcortical structures. There is general agreement that the subiculum has three principal layers: a polymorphic layer, a stratum moleculare and a narrow principal cell layer with large pyramidal cells, together with a mixture of smaller interneurons. The principal neurons of the subiculum are populated very large in size and shape (Amaral and Witter, 1995). All portions of CA1 send its primary projection to all regions of the subiculum, which in turn projects to the entorhinal cortex. Therefore, the subiculum is the main output structure of the hippocampus (Witter and Groenewegen, 1990; Amaral et al., 1991; O'Mara et al., 2001).

The current view is that the hippocampus has been causally implicated in three main functions: learning and memory, emotional responses and spatial navigation. The hippocampus is called the “gateway to memory”. All mammals require their hippocampus for certain types of learning. However, the hippocampus is not believed to be the primary storage area but processes and consolidates so-called declarative information relating items in space and time, which can be contrasted with nondeclarative memory including learned skills and habits (Martin and Morris, 2002). The hippocampus has also an important role in the formation of new memory about experienced events (episodic memory). Together with

neocortical regions the long-term memory of declarative and episodic contents is considered an essential prerequisite of human consciousness and self-awareness. The second major line of function relates the hippocampus to emotion, which was proposed by James W. Papez (1937). The hippocampus as one of several limbic structures has been extensively studied in emotional behavior. One of them is neurobiologically based depression. The functional differentiation of the hippocampus along the septo-temporal axis within the context of adult hippocampal neurogenesis suggests that neurogenesis in the ventral dentate gyrus may be preferentially involved in regulation of emotion. Current evidence indicates that adult hippocampal neurogenesis may be required for some of the behavioral effects of antidepressants (Sahay and Hen, 2007). In the 1970s the discovery of place cells in the hippocampus led to a universal agreement that spatial navigation plays an important role in hippocampal function (O' Keefe and Nadel, 1978). In the CA1 and CA3 regions place cells are considered to be pyramidal cells, whereas those in DG are believed to be granule cells. Corresponding to the cells “place field” whenever an animal is in a specific location, place cells exhibit a high rate of firing. Together with head direction cells in the presubiculum (Taube et al., 1990) and grid cells (Hafting et al., 2005) in the entorhinal cortex form the system of spatial orientation in rodents.

1.1.2 Adult hippocampal neurogenesis: history and current status

For more than 100 years, a central dogma of neuroscience declared that the generating functionally integrated neurons from progenitor cells occur exclusively during the prenatal phase of development in the mammalian central nervous system (CNS; Gross 2000). Indeed, there are few views of the brain development that had existed with contrary evidence at the turn of the 20th century (Hamilton, 1901; Allen, 1912). However, using the methods of the time, it was unclear whether the cells undergoing mitosis subsequently became glia or neurons (Ramon y Cajal, 1913). In the 1960s, Joseph Altman and his colleagues performed a series of pioneering studies using [^{3}H]-thymidine autoradiography to label dividing cell populations and trace their fates. This approach provided the first anatomical evidence for a constitutive presence of newly generated neurons in the DG of the hippocampus (Altman and Das, 1965), neocortex (Altman and Das, 1966) and olfactory bulb (Altman, 1969). Although these surprising observations were published in the most prestigious journals of the time, such as the Journal of Comparative Neurology, Science, and Nature, these findings were not readily accepted by the majority of biologists or dismissed as unimportant mainly because the identification of the new neurons was based solely on their morphology as a result of the unavailability of neuron specific markers (Gross, 2000). Another reason was that there was no concept of stem cells in the adult brain at that time. Without stem cells the idea of adult

neurogenesis conflicted with the central principle of neuroscience known in the 1960s (Kempermann et al., 2004). In some sense, Altman's discovery of adult neuogenesis was a discovery made before its time.

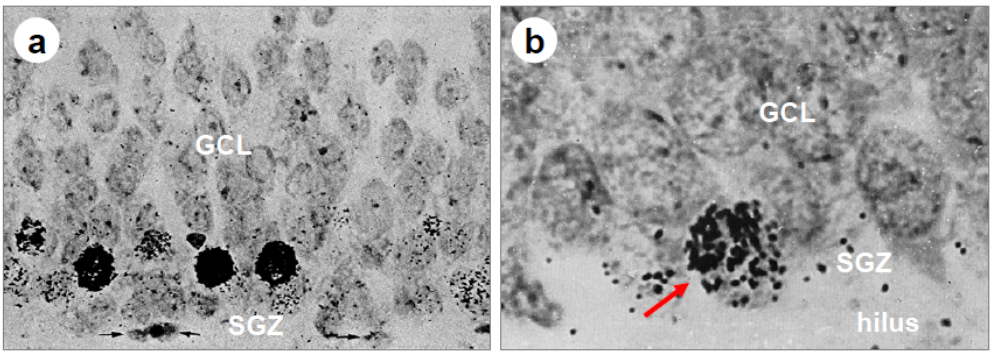

Fig. 1.2: ^{3}H-thymidine autoradiograms of labeled granule cell near the hilus of the DG of an adult rat. a: Pattern of granule cell labeling. Note the earlier generated outer granule cells are unlabeled, and heavily and lightly labeled granule cells are confined to the deep row close to the hilus. **b:** Enlarged picture shown one ^{3}H-thymidine labeled precursor cell in the SGZ of adult rat (red arrow) (Altman, 2011) (Memoir: The discovery of adult mammalian neurogenesis, Springer, modified).

In the late 1970s, direct support for Altman's claim of adult neurogenesis came from a series of electron microscopy studies. They showed that [^{3}H]-thymidine labelled cells in the dentate gyrus and olfactory bulb of adult rats have the ultrastructural characteristics of neurons, such as dendrites and synapses, but not of astrocytes or oligodendrocytes (Kaplan and Hinds, 1977). In the 1980s, these new neurons were demonstrated receive synaptic inputs (Kaplan and Bell, 1983) and extend axon projections to their target area (Stanfield and Trice, 1988). Meanwhile, a series of studies of adult neurogenesis in songbirds started to provide evidence for functional roles of postnatal neurogenesis in seasonal song learning (Nottebohm, 2004). In the 1990s, the field was revolutionized by the introduction of bromodeoxyuridine (BrdU), a synthetic thymidine analogue, as another S-phase marker of the cell cycle (Gratzner, 1982). Adult neurogenesis was identified in the hippocampus and the olfactory bulb of mammals, including humans (Lois and varez-Buylla, 1993; Gage et al., 1995; Kuhn et al., 1996; Eriksson et al., 1998). Adult neural stem cells were first isolated from the adult CNS of rodents (Reynolds and Weiss, 1992) and later from humans (Kukekov et al., 1999). Today, it is widely accepted that neurogenesis occurs in two regions of the adult mammalian brain: the subventricular zone (SVZ) of the lateral ventricle, giving rise to neurons which migrate into the olfactory bulb and the SGZ in the DG of the hippocampal formation (Doetsch, 2003). There is evidence for adult neurogenesis in several additional areas, including the neocortex, striatum, amygdala and substantia nigra, but this has been difficult to replicate consistently other than under pathological conditions, such as ischemia (Gould, 2007). Adult neurogenesis has become a prime topic in neuroscience research because of its implications

for the learning and memory, neuropsychiatric disorders and treatment of neurodegenerative disorders and essentially all diseases that involve a loss of neurons - in cases of Parkinson's disease, for example (Bjorklund and Lindvall, 2000). The discovery of adult neurogenesis caused a paradigm shift in the neurosciences.

1.1.3 Function and regulation of adult hippocampal neurogenesis

Adult hippocampal neurogenesis is a complex muti-step process that begins with the proliferation of precursors in the SGZ, followed by neuronal differentiation, migration and morphological and physiological maturation with neuronal characteristics, and ends with the functional integration of newborn neuron into the existing circuitry (Ming and Song, 2005).

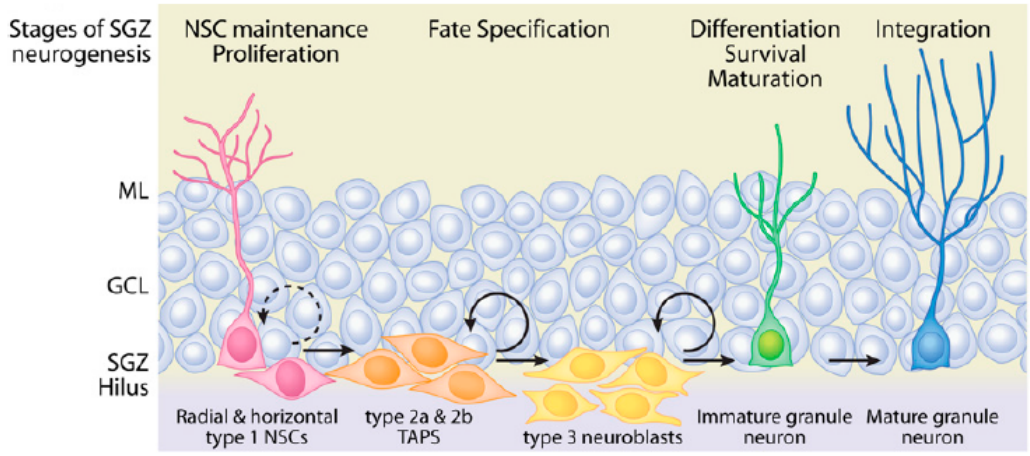

Fig. 1.3: Adult neurogenesis in the SGZ of the dentate gyrus. Developmental stages during adult hippocampal neurogenesis: 1, activation of radial glia-like cell (neural stem cells (NSCs); pink; type-1) in the SGZ; 2, proliferation of transient amplifying cells (TAP; orange; type-2a,b); 3, generation of neuroblasts (yellow, type-3); 4, integration of immature neurons (green); 5, maturation of newborn granule cells (blue). The progression from type-1 cells to mature granule neurons in adult SGZ is a multistep process with distinct stages (labeled on top) and is controlled by the sequential expression of transcription factors. ML: molecular layer; GCL: granule cell layer; SGZ: subgranular zone (Hsieh, 2012).

Adult neurogenesis is bi-directionally regulated by many factors, both intrinsic and extrinsic. Intrinsic factors expressed by stem cells and progenitors that control different neurogenic phases. By contrast, external factors are produced by surrounding cells to act on stem cells and progenitors. SGZ progenitor cells receive excitatory glutamatergic inputs from the entorhinal cortex and GABA-ergic inputs mostly from the interneurons within the dentate gyrus. Destruction of the perforant pathway, the main glutamatergic afference to DG, increases cell proliferation, thus indicating that glutamate exerts an inhibitory influence (Cameron et al., 1995). In contrast to glutamate, direct GABA-ergic input promotes the differentiation of type-2 hippocampal progenitors (Tozuka et al., 2005). Adult neural

progenitors are also regulated by a variety of key extrinsic morphogens like Wnt/beta-catenin, Notch, and Sonic hedgehog (Shh). Interestingly, several growth factors have been found to regulate SGZ neurogenesis, e.g. vascular endothelial growth factor (VEGF) and brain-derived neurotrophic factor (BDNF). In addition to the intracellular signaling pathways downstream of the growth factors, neurotrophins, and morphogens, a variety of intracellular mechanisms have been implicated in the regulation of adult neurogenesis. Among these, several transcription factors have been shown to play critical roles in postnatal neurogenesis (Table 1.1).

Signal	Effect on neurogenesis	Reference
Extrinsic *Morphogens*		
Wnt	Increases neurogenesis Required for neuronal differentiation Stimulates NSC proliferation/self-renewal	(Lie et al., 2005) (Kuwabara et al., 2009) (Qu et al., 2010)
Notch	Required for NSC proliferation, maintenance Required for dendritic arborization	(Ables et al., 2010) (Breunig et al., 2007)
Shh	Required for progenitor proliferation	(Lai et al., 2003)
BMP	Promotes neuroblast survival	(Lim et al., 2000)
Growth factors		
BDNF	Increases neurogenesis Required for dendritic arborization	(Scharfman et al., 2005) (Bergami et al., 2008)
VEGF	Increases neurogenesis	(Jin et al., 2002)
Neurotransmitters		
Glutamate	Required for progenitor proliferation Required for neuronal survival, migration	(Cameron et al., 1995) (Tashiro et al., 2006)
GABA	Increases progenitor differentiation Required for dendritic arborization Required for NSC quiescence	(Tozuka et al., 2005) (Ge et al., 2006) (Song et al., 2012)
Intrinsic *Transcription factors*		
CREB	Required for neuronal survival	(Jagasia et al., 2009)
Tbr2	Required for differentiation of neuronal precursors	(Hodge et al., 2012)
Sox2	Required for NSC/neuronal progenitor proliferation	(Ferri et al., 2004)
NeuroD	Required for survival, maturation of neuroblasts	(Gao et al., 2009)

Tab. 1.1: Overviews of intrinsic and extrinsic factors which regulate adult NCSs in the SGZ.

In the SGZ newborn neurons migrate only a short distance into the granule cell layer. A recent study suggested that Reelin pathway as guidance cue may be involved in migration of

newborn cells in the DG (Gong et al., 2007). Two-4 weeks after neuronal birth, the initial depolarization by GABA plays a critical role in the maturation of newborn granule cells (Ge et al., 2006). The Disrupted-in-schizophrenia (DISC1) protein controls dendritic growth and physiological maturation in newborn dentate granule cells (Duan et al., 2007). Within 4 weeks after birth many newborn neurons die, and their survival is influenced by the animals' experience, such as spatial learning and exposure to an enriched environment (Kee et al., 2007; Tashiro et al., 2007).

Once a newborn cell has reached its target and becomes a mature neuron, a central question remains to be answered: What is the functional significance of this biological phenomenon in mammals? 'Function' is the key criterion for determining whether adult neurogenesis is successful and has truly generated new neurons. 'Function' in adult hippocampal neurogenesis can be considered on cellular, circuitry, system and behavioral levels (Ming and Song, 2011). At the cellular level, newborn granule cells display special properties that are distinct from their mature counterparts. Synaptically connected newborn neurons exhibit hyperexcitability and enhanced synaptic plasticity of their glutamatergic inputs during a critical period of maturation in the hippocampus, which may allow newly integrated adult-born neurons to make a unique contribution to information processing (Wang et al., 2000; Schmidt-Hieber et al., 2004). At the circuitry level, decreased SGZ neurogenesis by radiation led to a reduction of long-term potentiation (LTP) in the DG (Snyder et al., 2001). One potential mechanism is a strongly deceased sensitivity of newly generated neurons to perisomatic GABA-ergic inhibition from interneurons during the critical period (Ge et al., 2008). It is at the systems level in which most of the work related to the functions of adult neurogenesis has taken place. Computational models of adult neurogenesis have suggested that the addition of new neurons may alter neural network properties and distinct roles for adult-born neurons at different stages of neuronal maturation (Aimone and Gage, 2011). At the behavioral level, elimination of dividing cells with the antimitotic agent methylazomethanol acetate (MAM) disrupts trace eye-blink conditioning and trace fear conditioning, but not contextual fear conditioning and spatial memory, all of which are considered hippocampus-dependent forms of memory (Shors et al., 2001). There is also correlative data suggesting a link between adult neurogenesis and hippocampus-dependent learning. The acquisition phase of the Morris water maze and genetically determined baseline levels of hippocampal neurogenesis was significant correlated (Kempermann and Gage, 2002). Adult hippocampal neurogenesis has also been suggested to be required for certain antidepressant-induced behavioral responses (Sahay and Hen, 2007).

1.2 Glial cells in the Central Nervous System

The CNS consists of two main cell populations: neurons and glial cells (Greek: glue). Glial cells make up most of the cells in the brain. The mouse brain has roughly 65% of these cells; this ratio grows to 90% in humans (Allen and Barres, 2009). On the basis of morphology, function and location, glial cells in the CNS are classified as astrocytes, microglia and oligodendrocytes. Recently, a fourth cell type was reported, the so-called polydendrocytes (Nishiyama et al., 2009), or NG2 glia (Peters, 2004). Traditionally, glial cells were considered as "supporting cells" of the nervous system. However, it is now becoming increasingly clear that these cells have more functions: Glial cells express a variety of ion channels including glutamatergic and non-glutamatergic receptors (Verkhratsky and Steinhauser, 2000; Verkhratsky and Kirchhoff, 2007; Domingues et al., 2010). Glia cells also play a role in adult neurogenesis (Doetsch, 2003) and in the regulation of extracellular potassium ion concentration (Ransom and Sontheimer, 1992; Newman and Reichenbach, 1996).

1.2.1 Astrocytes

In the CNS astrocytes are the most abundant cell type with very diverse morphologies (Reichenbach and Wolburg, 2005). In grey matter, astrocytes are described as protoplasmic which are spherical and bushy. Astrocytes in the white matter are more elongated, process-bearing and less bushy, giving them a fibrous appearance (Kimelberg and Nedergaard, 2010). A common feature, however, is that the astrocyte is a star shaped cell with multiple fine processes which bear so-called endfeet. Endfeet contact the basal lamina of blood vessels and the pial surface (Butt and Ransom, 1989). A second characteristic is extensive coupling by a variety of gap junctions (for details see below). Glial fibrillary acidic protein (GFAP) is an intermediate filament protein important for the cytoarchitectural stability of the cell (Liedtke et al., 1998). GFAP is considered as a specific marker for astrocytes (Bignami et al., 1972; Ludwin et al., 1976) and cells from the astrocytic lineage. GFAP expression in astrocytes varies dependent on brain regions, i.e., in the hippocampus all astrocytes express GFAP, whereas only 15% of astrocytes express GFAP in the cortex (Verkhratsky and Butt, 2007). After brain injury and disease, GFAP expression increases during reactive gliosis (Eng et al., 2000; Middeldorp and Hol, 2011). S100β, a calcium binding protein, is also mainly expressed in astrocytes in the hippocampus as well as in the cortex (Boyes et al., 1986; Ogata and Kosaka, 2002). Recent results show that S100ß is involved in the regulation of astrocytic proliferation and activation (Brozzi et al., 2009). In addition to S100β and GFAP, astrocytes are also labelled by glutamine synthetase (GS), an ATP-dependent

glutamate-to- glutamine converting enzyme predominantly expressed by astrocytes (Norenberg and Martinez-Hernandez, 1979). Except astrocytes S100ß and GS were also reported in other cell types: S100ß in NG2 cells (Nishiyama et al., 2009) and GS in a fraction of oligodendrocytes (Miyake and Kitamura, 1992).

Astrocytes have been reported to contribute in a number of active functions in the brain. In the hippocampus astrocytes are involved in spatial buffering of extracellular potassium homeostasis, allowing discrete and precise encoding of synaptic signals and neurotransmission (Wallraff et al., 2006). Astrocytes contain glycogen and are providing neurons with energy and neuritis which are essential for synaptic plasticity (Ullian et al., 2001; Slezak and Pfrieger, 2003). Astrocytes express transporters for uptake of many neurotransmitter including glutamate, GABA and glycine (Swanson, 2005). In the case of the glutamate - glutamine cycle, astrocytes remove up to 80 % of glutamate from the synaptic cleft mostly by the glutamate transporter GLT-1 (Verkhratsky and Butt, 2007). Glutamate removal from the synaptic cleft is considered crucial for normal synaptic function. Another important function is the neuron-glia communication via intracellular astrocytic Ca^{2+} signalling pathways, by which astrocytes process synaptic information and modulate synaptic transmission and plasticity through the release of gliotransmitters (Perea et al., 2009). Astrocytes are also required for the formation and maintenance of the blood brain barrier (BBB; Bauer et al., 2005). The BBB is constituted by endothelial cells equipped with continuous tight junctions. Astrocytic endfeet completely surround the capillary walls, indicating a role in regulating local blood flow via release of Prostaglandin E_2 (PGE_2) by astrocytes (Zonta et al., 2003; Takano et al., 2006). Astrocytic gap junctions mediate some other functions via intracellular coupling. These functions are described in chapter 1.3.1.

1.2.2 Radial glia-like cells in the neurogenic niche

As one of astrocytic type, radial glia cells are NSCs and generate neurons in early embryonic CNS development. Radial glia cells play a major role for patterning and migrating neurons during brain histogenesis. In mammalian species, these cells transdifferentiate into astrocytes when neuronal migration is completed (Schmechel and Rakic, 1979). Importantly, it has been clearly demonstrated that radial glia cells with stem cell properties (radial glia-like cell, RG-like cell) give rise to neurons and glial cells in restrict brain regions throughout adulthood (Gage, 2000; Doetsch, 2003; Kempermann et al., 2004). In the adult mammalian brain such restricted brain regions are termed neurogenic niches. Neurogenic niches are defined as microenvironments that anatomically house stem cells and functionally control their development *in vivo*. The SGZ of the DG is one of the only two such neurogenic niches under physiological conditions. SGZ was simply the border between the GCL of the DG and

the hilus. The term SGZ was coined by Altman in a study on neurogenesis in 1975 (Altman and Bayer, 1975). RG-like cells, astrocytes, endothelial cells, ependymal cells, microglia, immature/mature neurons, and progeny of adult neural precursors are among major cellular components of the adult neurogenic niche (Ming and Song, 2011).

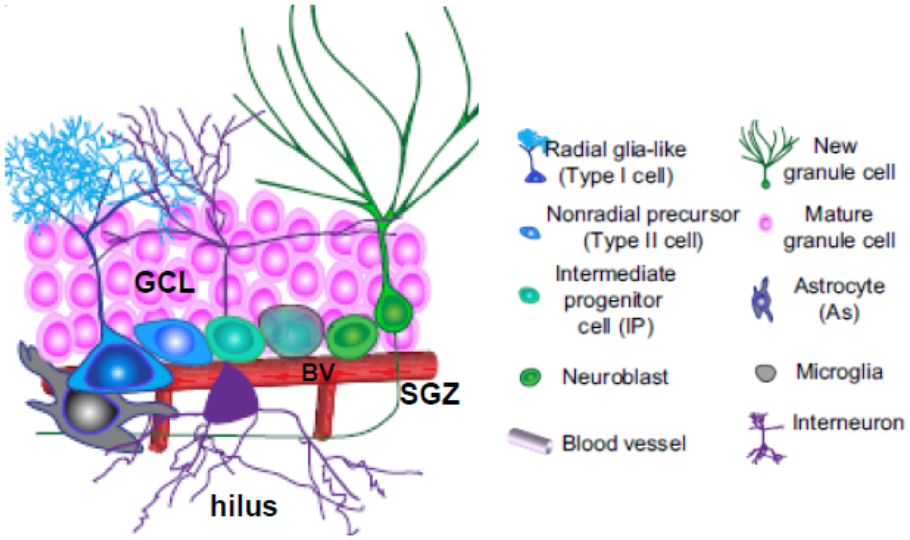

Fig. 1.4: Cell types and the architecture of the adult neurogenic niche in the SGZ. This illustration shows the relationships of RG-like cells to transit-amplifying progeny and their neuronally restricted progeny. Only those interactions identified as being specifically between the RG-like cells and progenitor cells are noted. Major interactions are cited in the text. SGZ: RG-like cells and astrocytes are in close proximity to blood vessels (BV, red). Neural precursors are found in foci of dividing cells, frequently at the junction of blood vessels, suggesting mutual co-regulation. GCL: granule cell layer; SGZ: subgranular zone (Ming & Song, 2011, modified).

RG-like cells exhibit a characteristic morphology with the soma located in the SGZ and a long process extending through the GCL. These processes play a role as a scaffold upon which newly formed neurons can migrate from the SGZ to the GCL. Typically, they express nestin as well as GFAP (Fukuda et al., 2003; Filippov et al., 2003; Seri et al., 2004). Evidence supporting RG-like cells as NSCs comes from anti-mitotic treatment recovery (Seri et al., 2001), genetic ablation (Garcia et al., 2004), and transgenic fate-mapping (Ahn and Joyner, 2005; Lagace et al., 2007; Dranovsky et al., 2011). RG-like cells often divide asymmetrically, inducing one new stem cell and one neuronal precursor cell per division (Doetsch, 2003). In the SGZ quiescent RG-like cells (Type-1 cells) generate proliferative precursors known as intermediate progenitors (Type-2a/b cells), which give rise to neuroblasts (Type 3 cells) and then immature neurons. In addition to their role as NSCs, astrocytes are also suggested to be sensors and regulators of the environment within hippocampal neurogenic niches (Doetsch et al., 1997; Seri et al., 2004). Astrocytic gap junction-mediated coupling can form a syncytium (Giaume et al., 2010), which may allow them to propagate signals locally or throughout the whole niche. Thus, astrocytes seem to be regulating proliferation and differentiation of NSCs. With endfeet surrounding the blood

vessels, astrocytes may serve as an interface to modulate influences of endothelial and growth factors as well as the availability of cytokines in the basal lamina. Astrocytes express a number of secreted and membrane-attached factors which contribute to the neurogenic niche through contact-mediated cues and by secreting diffusible signals (Song et al., 2002; Lie et al., 2005; Barkho et al., 2006). Ependymal cells and astrocytes are coupled by gap junctions (Zahs, 1998). Therefore, local signals, ions, metabolites and second messengers between neighboring cells can be coordinated within the neurogenic niche (Kumar and Gilula, 1996; Sohl et al., 2005). In the SGZ, microglia also actively regulates adult neurogenesis by phagocytosing apoptotic corpses of newly generated neurons from the niche (Sierra et al., 2010). Recent studies have revealed the dynamic and plastic relationship between newborn progeny and neural precursors via feedback. For example, local interneurons release GABA, which in turn regulates cell proliferation as well as maturation and synaptic integration of newborn neurons in the adult SGZ (Tozuka et al., 2005; Ge et al., 2006). Moreover, mature neurons release glutamate, regulating the survival of newborn neurons through an NMDAR-dependent mechanism (Tashiro et al., 2006). The functional and anatomical components within the SGZ neurogenic niche are still not clear. Any diffusible molecules secreted by local cells can impact the fate of neural precursors. Neighboring cells within the niche can also exert their influence via direct cell-cell communication.

1.3 Gap junctions

Gap junctions represent conduits that permit the direct trafficking of small molecules between two adjacent cells. In mammals gap junction-mediated communication is reported in almost all cell types except skeletal muscle, erythrocytes, thrombocytes and sperm cells (Gilula et al., 1978). Generally, gap junctions are characterized by adjacent cell membranes narrowed down to 2-4 nm instead of the usual 20-30 nm (Revel and Karnovsky, 1967). Gap junctions occur as a plaque of up to thousands of single gap junctional channels (GJC; Kumar and Gilula, 1996). Each adjacent cell contributes a hemichannel (also called connexon) composed of six protein subunits, termed connexins (Cx). Connexins are transmembrane proteins characterized by a cytoplasmic amino terminus, four transmembrane domains, two extracellular and one cytoplasmic loop and a regulatory carboxy terminal region. Depending on their molecular composition, three different types of gap junction channels have been described: 1) homomeric / homotypic, 2) heterotypic and 3) heteromeric. Homotypic gap junctions contain two identical types of hemichannels and heterotypic channels contain two different hemichannels, whereas homomeric hemichannels are composed of identical

connexins and heteromeric are composed of different connexins in a hemichannel (Sohl et al., 2005; Fig. 1.5). So far, 20 different connexin genes in mouse and 21 genes in the human genome have been described (Sohl and Willecke, 2003). According to their molecular weight, the connexins are classified into different isoforms, i.e. a connexin protein with the molecular weight of 43 kDa is called Cx43 (Beyer et al., 1989).

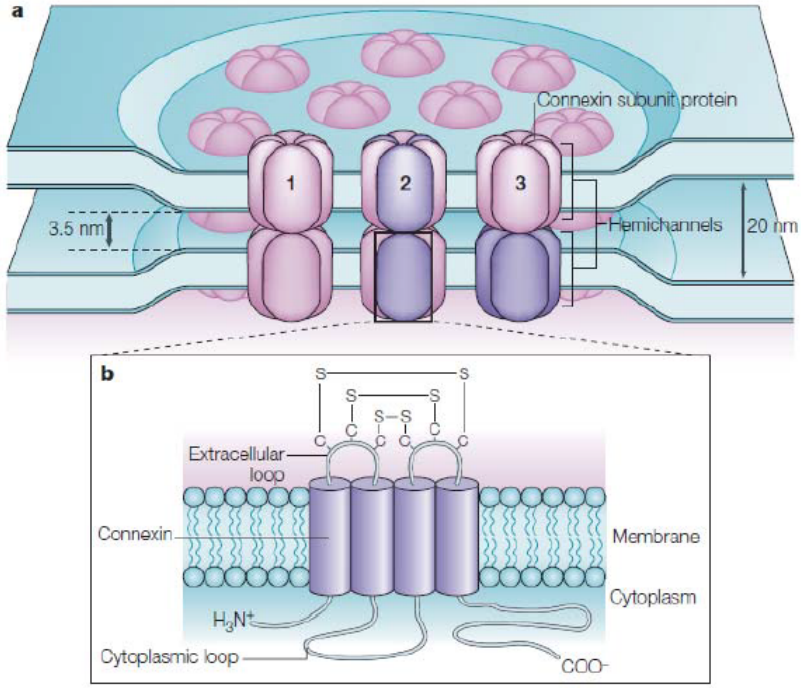

Fig. 1.5: Organization and topology of gap junction plaques. a: Hemichannel in plasma membranes of two adjacent cells can dock to each other forming a gap junctional channnel. Each connexon (hemichannel) consists of six connexin subunits of the same connexin isoform (1, homomeric) or different connexin isoforms (2, heteromeric). Gap junctions containing two identical connexons are termed homotypic (1,2), whereas composing different connexons are called heterotypic (3). **b:** Connexins are transmembrane proteins containing four transmembrane domains, an amino-terminal domain, cytoplasmic loop and carboxy-terminal domain and two extracellular loops. The extracellular loops are interacted by disulfide bonds (SS) between the highly conserved cystein residues (Söhl et al., 2005).

Gap junction channels (GJC) allow passive diffusion of small metabolites such as: glucose (Rouach et al., 2008), amino acids, nucleotides (Bennett and Verselis, 1992), potassium (Wallraff et al., 2006) and sodium (Langer et al., 2012), as well as second messengers like cAMP, Ca^{2+} and IP_2 (Bruzzone et al., 2001; Bedner et al., 2012), with a molecular weight up to 1-1.2 kDa (Harris, 2007). Furthermore, connexons can also function as hemichannels (HCs) that enable the exchange of molecules and ions between the cytoplasm and the external medium, thereby supporting autocrine and paracrine actions (Spray et al., 2006; Giaume and Theis, 2010).

In the CNS, depending on the brain region, neurons express mainly three different types of connexins namely Cx36, Cx45 and Cx57 (Sohl et al., 2005). Neuronal connexins were

shown to mediate electrical coupling and form functional electrical synapses which facilitate fast oscillatory networks and synchronisation (Bennett and Zukin, 2004). By contrast, Cx43, Cx30 and Cx26 are the three main connexin types in CNS astrocytes (Giaume and Theis, 2010).

1.3.1 Astrocytic gap junctions

Cx43 (*GJA*1) was the first type of gap junction which was identified in astrocytes (Dermietzel et al., 1989), followed by two additional astrocytic connexins, namely Cx30 (*GJB*6; Nagy et al., 1999) and Cx26 (*GJB*2; Nagy et al., 2001). An *in vitro* study of Cx43 KO mice observed the expression of Cx40, Cx45 and Cx46 in astrocyte cultures (Dermietzel et al., 2000). Moreover, single-cell RT-PCR demonstrated astrocytic mRNA expression of Cx32 and Cx40 in hippocampal slices (Blomstrand et al., 2004). However, their presence *in vivo* and potential role under physiological condition remained unclear.

Dual whole-cell patch clamp studies showed that astrocytes are functionally coupled to each other by GJCs (Kettenmann and Ransom, 1988; Ransom and Kettenmann, 1990). Specific deletion of Cx43 in astrocytes led to about 50 % reduction in the tracer coupling (Theis et al., 2003), whereas mice lacking Cx30 showed only 20 % reduced gap junctional coupling (Gosejacob et al., 2011). Interestingly, in Cx43 and Cx30 double knock out (dKO) mice interastrocytic coupling in the CA1 was completely inhibited (Wallraff et al., 2006). Thus, Cx43 and Cx30 are considered as the two major Cxs allowing intercellular gap junctional communication between hundreds of astrocytes in a certain brain area. Their relative expression levels vary in the different developmental stage and brain region (Nagy and Rash, 2000). The detection of Cx43 expression is very early in development, around the twelfth day of gestation in radial glia processes. As development proceeds, Cx43 expression increases and is detectable throughout the brain. Cx30 is expressed in astrocytes relative late during the third postnatal week (Nagy et al., 1999). Immunostaining results showed that Cx30 and Cx43 are clearly co-expressed at junctional plaques of mature grey matter astrocytes. The major regional expression difference of these two Cxs is that there is no Cx30 expression in astrocytes of white matter tracts (Nagy et al., 1999).

Interastroglial gap junctions are prominent and contribute to several brain functions. As a result of neuronal activity, extracellular potassium is elevated (Heinemann and Lux, 1977). However, a high extracellular potassium concentration impairs neuronal excitability. Therefore, potassium spatial buffering serves as a main mechanism of potassium removal from the extracellular space and is important for normal neuronal function (Kofuji and Newman, 2004). A recent study showed that astrocytic Cx43 and Cx30 are required for removal of elevated extracellular potassium near synapses of active neurons and also

control the accumulation of potassium during synchronized neuronal firing (Wallraff et al., 2006). Mice lacking Cx30 and Cx43 in astrocytes showed a lower threshold for the generation of spontaneous and induced epileptiform activity (Wallraff et al., 2006). Moreover, astroglial connexins were also involved in the clearance of the extracellular glutamate during synaptic activity via modulating the extracellular space volume (Pannasch et al., 2011). Due to the interface between blood vessels and neurons, as well as an astroglial syncytium coupled by gap junctions, astrocytes provide metabolites from the bloodstream for neurons to sustain their activity (Rouach et al., 2008). In addition, Cx43 might be involved in regulating the gene expression via their C-terminus interactions with ß-catenin through Wnt/ß-catening signalling pathway (Theis et al., 2005). According to two other reports, astroglial connexins mediated also cell adhesion for radial migration (Elias et al., 2007; Cina et al., 2009) and modulation of purinergic receptors by the C-terminal domain of Cx43 (Scemes, 2008).

1.3.2 Role of astrocytic gap junctions in neurogenesis

Astrocytic connexins have a strong impact on neurogenesis. Cx43 as a predominant component of gap junctions is expressed in both adult neurogenic niches SVZ and SGZ (Miragall et al., 1997; Menezes et al., 2000; Theis et al., 2003; Peretto et al., 2005). Except Cx43, Cx30 and Cx26 mRNA and protein are also detected in RG-like cells (Typ-1; Kunze et al., 2009; Imbeault et al., 2009). In Type-2a progeny, but not Type-2b or Type-3 neuronal committed progenitors additionally express Cx37, Cx40 and Cx45. Interestingly, increases in Cx26 protein expression inhibited Cx43, Cx45 and Cx40 protein levels, and altered the subcellular localization of Cx30. These changes are associated with decreased neurogenesis (Imbeault et al., 2009).

The mechanism, by which astrocytic connexins regulate neurogenesis may be through gap junction coupling, cell-cell adhesion and hemichannel activity. Besides forming gap junctional coupling, glial Cxs allow direct communication between the cells and the extracellular environment via hemichannels (Bennett et al., 2003). Thus, Cx43 in adult neurogenic regions may coordinate the communication between neighboring and distant cells within the niche either through gap junctions or hemichannels. There is evidence that hemichannels regulate the initiation and propagation of calcium waves between clusters of cells during cortical neurogenesis (Weissman et al., 2004). Cx43 hemichannels have been implicated in the division of neural progenitor cells in the developing retina (Pearson et al., 2005) and developing cortex (Liu et al., 2010a) via purinergic signaling. More recently, one study described that Cx45 hemichannels rather than gap junctions potentiate precursor cell

proliferation via ATP signaling in the mouse subventricular zone (Khodosevich et al., 2012). Cx43 may also act as a cell-cell adhesion unit to tether glioma cells and mediates the invasion via their C-terminus (Lin et al., 2002). Cx26, which is expressed in the SVZ may have similar regulatory roles in stem cell proliferation and morphological plasticity (Mercier and Hatton, 2001). Specific deletion of Cx43 using transgenic mice or by RNA interference led to deficits in neuronal migration that were mainly attributed to adhesive functions of Cxs, although the role of the C-terminal cytoplasmic tail of Cx43 in this process is under debate (Elias et al., 2007; Cina et al., 2009). In addition to adhesion and hemichannel activity, Cx43 and Cx30 mediate intercellular coupling between RG-like cells, which is required for proliferation and subsequently neurogenesis in the SGZ (Kunze et al., 2009). Mice lacking Cx30 and Cx43 in astrocytes show an almost 90% reduction of proliferation and about 20% decrease in the number of granule cells in the GCL of the DG. These results suggest that astrocytic gap junction coupling of RG-like cells is important for intact neurogenesis in the adult brain (Kunze et al., 2009).

1.3.3 Phosphorylation of gap junctions

Connexins as integral membrane proteins are highly regulated. One of the regulatory possibilities is post-translational phosphorylation (Lampe and Lau, 2004; Solan and Lampe, 2005). The effect of connexin phosphorylation depends on cell types, stages of the cell cycle, three-dimensional environment and extracellular matrix interactions (Laird, 2005). Many connexins i.e. Cx31, Cx32, Cx36, Cx37, Cx40, Cx43, Cx45, Cx46, Cx50 and Cx56 are phosphoproteins (Solan and Lampe, 2009), while Cx26 is not phosphorylated at all (Traub et al., 1989). Without question, as a most widely expressed connexin and predominant connexin in most cell lines the majority of phosphorylation studies focuses on the Cx43 protein. The C-terminal domain of Cxs varies widely in length and is thought to play key roles for regulatory phosphorylation (Lampe and Lau, 2004). In Cx43, the 17 kDa C-terminal domain extends freely into the cytoplasm and appears to be the primary region that becomes phosphorylated. So far, there are no reports of phosphorylation of the N-terminal domain or in its cytoplasmic loop (Solan and Lampe, 2009). Today, at least 14 of the 21 serines and 2 of the tyrosines between amino acids 245-382 in the cytoplasmic tail region of Cx43 can be phosphorylated (Marquez-Rosado et al., 2012).

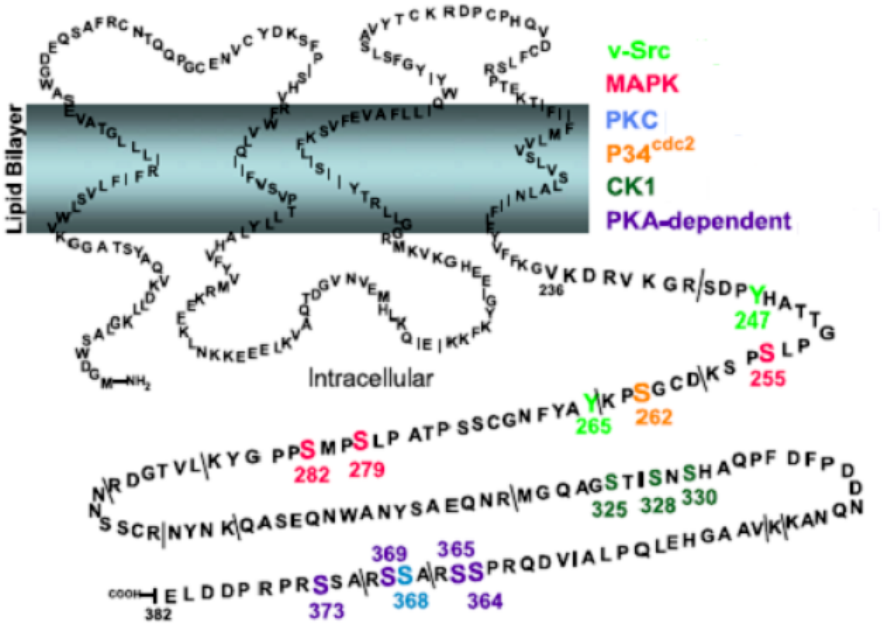

Fig. 1.6: Phosphorylation sites in the carboxy-terminal region of Cx43. Residues phosphorylated by known kinases are indicated in different colors. Scr-lime green; MAPK-red; PKC-blue; P34cdc2-orange; CK1-dark green; PKA-dependent-purple. The lines dividing the sequence represent tryptic cleavage sites (Solan and Lampe, 2005).

The pioneering work of Musil and Goodenough has shown that Cx43 is differentially phosphorylated throughout its life cycle (Musil et al., 1990; Musil and Goodenough, 1991). By polyacrylamide gel electrophoresis (SDS-PAGE) analysis, Cx43 shows multiple electrophoretic isoforms, including at least two slower migrating forms (termed P1 and P2), and a faster migrating form that includes non-phosphorylated Cx43 (P0 or NP). Following alkaline phosphatase treatment two slower migrating forms co-migrate with the faster migrating form, indicating phosphorylation is the primary covalent modification detected in their differences in electrophoretic mobility. According to the cell types, the profile of band migration can vary due to differences in gap junction assembly (Musil et al., 1990). The P0 form was suggested for newly synthesized Cx43, whereas the P1 and P2 form was suggested for mature Cx43 (Musil et al., 1990). Notably, there is no evidence that the P2 form is more phosphorylated than the P1 form, which is only due to specific migration changes corresponding to specific phosphorylation sites. Moreover, 2-4 kDa shifts between three Cx43 phosphorylated forms in SDS-PAGE are not simply due to the addition of the phosphate molecular weight (80 Da), but to the conformational changes. Phosphospecific antibodies have shown that the P2 isoform is linked to phosphorylation of Ser325/Ser328/Ser330 (Lampe et al., 2006), whereas phosphorylation of Ser365 is involved in the shift to P1 (Solan et al., 2007).

Connexin phosphorylation can regulate gap junctional communication by a variety of mechanisms including modulating channel open probability, unitary conductance,

degradation, and trafficking. However, most of these alterations are due to activation of several protein kinases, which in turn target phosphorylation sites. These kinases including protein kinase A (Atkinson et al., 1995; Yogo et al., 2006), protein kinase C (Reynhout et al., 1992; Lampe, 1994), mitogen-activated protein kinase (Lau et al., 1992; Cameron et al., 2003), Src kinase (Loo et al., 1995; Pahujaa et al., 2007; Gangoso et al., 2012), Cyclin-dependent kinase 2 (Lampe et al., 1998; Kanemitsu et al., 1998), Casein kinase 1 (Cooper and Lampe, 2002), can lead to increased Cx43 phosphorylation. The activation of Src, PKC, MAPK and CDC2 led to a reduction of gap junctional communication, whereas CK1 and PKA increase the communication (Lampe and Lau, 2004; Axelsen et al., 2006; Pahujaa et al., 2007). The regulation of Cx43 protein by the tyrosine kinase Src is one of the best understood mechanisms that play a central role in gap junction communication. Src may directly phosphorylate at two tyrosine residues of Cx43. Src can also indirectly activate MAPK to phosphorylate Cx43 via expression of platelet-derived growth factor receptor (PDGFR). In addition, Scr may induce pleiotropic effects to activate PKC. Moreover, Src may work together with other kinases, such as CDC2 to regulate intercellular coupling. All these reactions reduce the gap junctional communication. In contrast, when the activity of Src is inhibited by PKA, then this increases the gap junctional communication (Pahujaa et al., 2007). Not only Cx43 phosphorylation is correlated with alterations in junctional coupling (Warn-Cramer et al., 1998), but also its dephosphorylation is linked to reduced gap junctional coupling (Godwin et al., 1993; Oelze et al., 1995).

1.4 The Cre/loxP system: benefits and pitfalls

In the CNS, transgenic mice are suitable models for the investigation of gene and protein function *in vivo.* There are two major approaches in gene manipulation, namely the targeted deletion of gene, resulting in so called knock-out mice, or in replacements, so called knock-in mice. During the last decades several gene manipulation strategies have been developed (Evans and Kaufman, 1981; Thomas and Capecchi, 1987). One common method for the functional analysis of targeted gene can be achieved by homologous recombination of vector constructs into the genome of mouse embryonic stem cells (Nagy et al., 2003). However, the probability of recombination is very low between 1: 10^6 and 1: 10^7 (Thomas and Capecchi, 1987). Moreover, it might affect early developmental stages in which the targeted gene plays a role. Thus, it is impossible to limit the gene functional analysis, for example, only in the postnatal or adulthood due to pleiotropic effects.

To overcome these critical limitations the Cre/loxP systeme can be used for conditional deletion or activation of genes in a specific cell type or region of the brain (Sauer and Henderson, 1988; Tsien et al., 1996). The Cre recombinase derived from the *E. Coli* bacteriophage P1 with a molecular mass of 38 kDa (Sternberg et al., 1986). Under the control of a cell-type specific promoter binds the Cre recombinase to a 34 bp long recognition sites which are called loxP sites. The target gene flanked by loxP sites is called “floxed” DNA. The core sequences in recognition sites determine their orientation. If both sites are orientated in the same direction, the floxed allele will be excised and one loxP site remains, in contrast, when the sites point in different directions, the floxed gene will be inverted (Fig. 1.7).

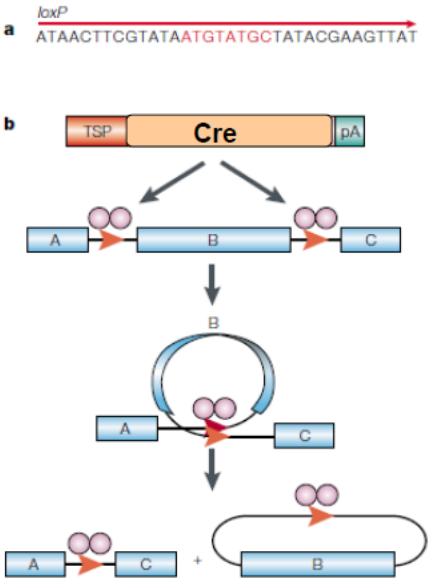

Fig. 1.7: Schematic illustration of the Cre/LoxP recombination system. a: The 34 bp loxP sites consist of two inverted 13 bp repeats (black) and flank an 8 bp core sequence (red). The core sequence determines its orientation (red arrows). **b:** Cre recombinase dimers (pink) bind to their recognition sites and mediate the excision of the target DNA sequence between the loxP sites, when both sites have the same orientation. TSP: tissue specific promotor; pA: polyadenylation site (Lewandoski, 2001).

The Cre/loxP system benefits from a direct linkage between gene deletion and reporter activation, which allow a quick and easy monitoring of the recombination status and cell type specific deletion of the target gene. For Cx43 gene deletion in the CNS, using reporter genes like ß-galactosidase (ß-Gal) driven by promoter elements of the human glial fibrillary acidic protein (hGFAP-Cre) has been used extensively (Theis et al., 2003). In astrocytes, such approach was used for direct linkage between the hGFAP-Cre mediated loss of *GJA*1 (Cx43) gene expression and *lacZ* reporter activation (Theis et al., 2003). More recently, a floxed Cx43 point mutation mouse line was generated. An astrocyte-directed Cx43 point mutation was obtained by interbreeding with nestin-Cre transgenic mice, and Cre activity leading to

expression of this mutated Cx43 protein was monitored by gain of enhanced green fluorescent protein (EGFP) expression (Dobrowolski et al., 2008).

Even though the Cre/loxP system has obvious advantages, it still has certain limitations (Schmidt-Supprian and Rajewsky, 2007). For example, our group described repeated spontaneous inactivation of the hGFAP-Cre transgene (Requardt et al., 2009). Although the mechanism responsible for hGFAP-Cre silencing remains unclear, a rigid quality control of mice with astrocyte directed gene inactivation is suited to maintain the activity status of hGFAP-Cre within the transgenic colony. In contrast to spontaneous loss of Cre activity, several other Cre transgenic lines displayed also spontaneous germ-line activity (Schmidt-Supprian and Rajewsky, 2007; Martens et al., 2010; Wicksteed et al., 2010). Using the myosin heavy chain promoter Cre (MyHC-Cre) for cardiomyocyte-specific deletion of Cx43 a spontaneous ubiquitous deletion of the floxed Cx43 in addition to cardimyocyte-specific deletion was reported (Eckardt et al., 2004). More recently, we observed that the widely used hGFAP-Cre and nestin-Cre transgenes exhibit similar germ-line recombination activity in the CNS (described in this work). Several pitfalls can be circumvented by using inducible Cre transgenes, i.e. CreERT (Metzger et al., 1995; Hirrlinger et al., 2006) and dual reporter approaches for identification of Cre efficacy (Degen et al., 2012). For instance, to assess Cre mediated recombination at the level of individual alleles we can simultaneously combine one floxed Cx43 allele with recombination-activated *LacZ* reporter and other floxed Cx43 allele with recombination-activated enhanced cyan fluorescent protein (ECFP) reporter to assess deletion of individual alleles (Degen et al., 2012).

2. Aim of the thesis

The impact of the Cx43 mutations in adult hippocampal neurogenesis had to be investigated after activation of the mutant gene using hGFAP-Cre or nestin-Cre expressing mice. However, the widely used Cre transgene exhibits several critical limitations, including e.g. spontaneous ectopic Cre activity (Eckardt et al., 2004; Korets-Smith et al., 2004) and spontaneous loss of Cre activity (Schulz et al., 2007; Requardt et al., 2009). To overcome these limitations of the Cre/loxP system, the first goal of my work was to establish a quality control method for Cre mediated gene specific activation or deletion and to investigate the possible mechanism underlying such phenomenon.

Previous studies provided evidence that in the developing embryonic neocortex the expression of connexin or formation of gap junctions modulate proliferation and differentiation of astrocytes (Weissman et al., 2004). A recent study underlined the importance of gap junctions in so called RG cells during embryonic neurodevelopment, which mediate neuronal migration through adhesive interactions with the cytoskeleton (Elias et al., 2007). More recently evidence from our group showed that the ablation of Cx30 and Cx43 in RG-like cells led to a strong decrease in proliferation and the number of granule neurons in the adult dentate gyrus (Kunze et al., 2009). The second and main purpose of this work was to investigate in detail by which mechanism would connexions affect adult neurogenesis: coupling, adhesion, hemichannel or control of gene expression. Therefore, three transgenic mice with conditional mutation of Cx43 in astrocytes, as well as with additional, unrestricted deletion of Cx30 (Teubner et al., 2003) were raised and compared with WT mice. Mice expressing the point mutation Cx43G138R showed selective loss of intercellular coupling, but preserved adhesion and hemichannel function (Dobrowolski et al., 2008; Dobrowolski et al., 2009). Cx43K258stop mice carry a C-terminal (CT) truncation of Cx43, which still showed intercellular coupling in transfected HeLa cells (Maass et al., 2004). Cx43D378stop mice lacking the last five amino acid residues of the CT still revealed functional gap junction channels and normal coupling properties (Lubkemeier et al., 2013), but adhesive interactions should be affected. I investigated these transgenic mice with combined patch-clamp recording, biocytin injection, immunohistochemistry and immunoblotting to study the interastrocytic and RG-like cell coupling *in situ*, as well as the proliferation and neurogenesis in the adult hippocampus.

Phosphorylation of one or multiple residues in the CT domain of Cx43 may regulate gap junctional communication (Solan and Lampe, 2009). It is absolutely critical to understand the sites, patterns of connexin phosphorylation and its function for the intercellular communication under normal and pathologic conditions. For this purpose, the third aim of my work was to study the phosphorylation of Cx43 in the hippocampus by using immunoblotting,

immunoprecipitation and mass spectrometry in a mouse model of temporal lobe epilepsy (TLE).

3. Animals, Materials & Methods

3.1 Animals

Maintenance and handling of animals used in this study was according to local government regulations. All mice were bred and maintained under specific pathogen-free (SPF) conditions. Mice were kept under standard housing conditions (12 h/12 h dark-light cycle, food and water ad libitum). All transgenic lines were backcrossed at least 10 times to C57BL/6. All measures were taken to minimize the number of animals used.

3.1.1 Cx43fl/fl: hGFAP-Cre mice

In Cx43fl (*lacZ*) animals, the Cx43 coding regions are floxed. The floxed sequence is followed by a *lacZ* gene which encodes β-galactosidase reporter equipped with a nuclear localization signal (Theis et al., 2001). Mice lacking Cx43 in astrocytes were obtained by interbreeding of Cx43fl/fl mice with hGFAP-Cre mice (Theis et al., 2003). After the excision of Cx43, the expression of β-galactosidase is activated under the control of the Cx43 gene regulatory elements. Expression of the hGFAP-Cre transgene was not restricted to astrocytes, but also in neurons and ependyma due to Cre expression in radial glia during development (Malatesta et al., 2003; Garcia et al., 2004).

3.1.2 Cx43flG138R/flG138R: nestin-Cre mice

Oculodentodigital dysplasia (ODDD) is a dominant negatively inherited disorder with several characteristic abnormalities of the fingers and toes, eyes, face and teeth (Judisch et al., 1979). ODDD is caused by mutations in the human *GJA*1 gene, coding for Cx43 protein (Paznekas et al., 2003). A mouse model for ODDD, the Cx43flG138R mouse, has been described (Dobrowolski et al., 2008). The human Cx43G138R point mutation was inserted into the WT mouse Cx43 gene and generated Cx43G138R/+ mice showed all phenotypes known for ODDD in human patients with a corresponding variability. To generate a conditional mouse model for astrocyte-specific activation of the Cx43G138R mutation the homozygous Cx43flG138R mice were mated with nestin-Cre expressing mice (Tronche et al., 1999). The Cre-recombinase activity led to deletion of the loxP-flanked Cx43WT region and at the same time expresses the Cx43G138R-internal ribosomal entry site (IRES)-eGFP cassette under the control of the Cx43 regulatory elements.

3.1.3 Cx43fl/K258stop: hGFAP-Cre mice

The Cx43K258stop mice expressing a C-terminally truncated Cx43 protein (Cx43K258stop) in place of WT protein, in which Cx43 is lacking the last 125 amino acid residues of the cytoplasmic C-terminal domain. Due to a defect of the epidermal barrier more than 97%

homozygous Cx43K258stop mice die shortly after birth (Maass et al., 2004). Former studies showed that decreasing the Cx43K258stop gene dosage by crossing with mice heterozygous for a Cx43 knockout allele rescued the lethal epidermal phenotype (Maass et al., 2007). Therefore, we raised Cx43fl (*lacZ*)/K258stop; hGFAP-Cre heterozygous mice carrying one Cx43K258stop allele and a Cx43fl (*lacZ*) allele which is deleted in the CNS by virtue of the hGFAP-Cre transgene to investigate the effect of truncated Cx43 in adult neurogenesis.

3.1.4 Cx43flD378stop/flD378stop: hGFAP-Cre mice

Cx43D378stop mice express a mini-truncated form of the Cx43 gene lacking the last five amino acid residues (DDLEI) of the C-terminal binding motif for scaffolding protein zonula occludens-1 (ZO-1). Recent data show that ablation of this region leads to the occurrence of severe ventricular arrhythmias and sudden arrhythmic death in all homozygous Cx43D378stop mice (Lubkemeier et al., 2013). To overcome the early postnatal lethality and for our adult neurogenesis study, we generate a conditional mouse model for astrocyte-specific activation of the Cx43D378stop mutation by interbreeding the homozygous Cx43flD378stop mice with hGFAP-Cre expressing mice (Zhuo et al., 2001). Unlike other Cx43 mutation mice, Cx43D378stop mice reveal functional gap junction channels and normal coupling properties in cardiomyocytes.

3.1.5 Cx43ki-ECFP mice

Cx43fl (ECFP)/fl (*lacZ*) is a novel conditional KO mouse line combining a floxed Cx43 allele with recombination activated *lacZ* reporter and a floxed Cx43 allele with recombination activated enhanced cyan fluorescent protein (ECFP) reporter, Cre-mediated recombination at the level of individual alleles could be assessed. It was shown that the widely used hGFAP-Cre transgene deletes both Cx43 alleles in the majority of hippocampal astrocytes. (Degen et al., 2012). The Cx43ki-ECFP mouse line was generated by breeding Cx43fl (ECFP) mice, with PGK-Cre mice (Lallemand et al., 1998). In Cx43ki-ECFP mouse one allele of Cx43 is deleted in all cells of the body, and ECFP is expressed instead.

3.1.6 Cx30-/- mice

Cx30-deficient mice were generated by Teubner et al. (2003). In these mice the Cx30 coding region has been replaced with a *lacZ* reporter sequences under control of Cx30 gene regulatory elements. The *lacZ*-encoded β-galactosidase contains a nuclear localization signal. In order to study the role of astrocytic coupling in neurogenesis, we raise mice with Cx43 mutation and deficient for Cx30 by interbreeding Cx30 deficient mice with animal expressing several Cx43 mutations as mentioned before.

3.2 Materials

3.2.1 Chemicals

Chemicals were purchased from Applied Biosystems (California, USA), Applichem (Darmstadt, Germany), Biostatus (Shepshed, UK), B.Braun (Melsungen, Germany), Carl Roth (Karlsruhe, Germany), Dianova (Hamburg, Germnay), Invitrogen (Darmstadt, Germany), Merck (Darmstadt, Germany), Millipore (Darm stadt, Germany), Promega (Madison, USA), Qiagen (Hilden, Germany), Riedel-de-Haën (Seelze, Germany), Roche (Manheim, Germany), Sakura (Netherlands), Sarstedt (Nümbrecht, Germany), Sigma Aldrich (Munich, Germany), Thermo Scientific (Waltham, MA, USA). Vector Laboratories (Burlingame, USA), PCR Primers were ordered from MWG Eurofins (Ebersberg, Germany).

3.2.2 Solutions and reagents (commercial)

2-Mercaptoethanol
Aqua polymount
Acetic acid
Acrylamide solution (Rotiphorese Gel 30 (37, 5:1)
Biocytin
CepetorKH (1mg/ml)
Chloroform
Draq5
Dimethyl Sulfoxide (DMSO)
Ethanol
Ethidium Bromide (10mg/ml)
Entellan
Gel Code blue safe protein stain
Glutaraldehyde
Hoechst 33258
Hydrogen peroxide solution (H_2O_2)
Isopropanol
Ketamin 10%
Methanol
Mountant Permafluor
Normal Goat Serum (NGS)
Normal Donkey Serum (NDS)
Paraformaldehyde
Protease and phosphatase single using inhibitor

PermaFluor mounting medium

Restore Western Blot stripping buffer

Roti-liquid barrier marker

Roti-Load buffer (4x)

Sterile Water

Streptavidine-Cy3

Sucrose

Tissue-Tek (O.C.T compound)

TritonX-100

Tween-20

Tetramethylethylenediamine (TEMED)

VectaShield mounting medium

3.2.3 Kits used

Product	*Company*
DAB substrate Kit for peroxidase	Vector Laboratories
Go taq flexi DNA polymerase	Promega
Super Signal West dura extended duration substrate	Pierce
In-gel tryptic digestion Kit	Thermo Scientific
Immunoprecipitation Kit-Dynabeads Protein A	Invitrogen
Pierce BCA protein assay Kit	Pierce
Vectastain Elite ABC Kit	Vector Laboratories

3.2.4 Buffers and solutions

3.2.4.1 Solutions for genotyping

Solution	*Concentration*	*Contents*
Laird-Lysis-Buffer (pH 8,5)	100 mM 200 mM 5 mM 0,2 % (w/v)	Tris-HCl NaCl EDTA SDS ad. 4 µl Proteinase K pro 500 µl, before using
Proteinase	K 20 mg/ml stock	Proteinase K ad. 50 ml aliquots à 1 ml at -20℃

TBE-Puffer (10 x)	1 M 0,83 M 10 mM	Tris-Base Boricacid EDTA
Ethidium Bromide	10 % (10 mg/ml)	diluted in 1 x TBE

3.2.4.2 Solutions for immunostaining

Solution	*Concentration*	*Contents*
Blocking solution	5-10 % (v/v) 0,3-0,5 % (v/v)	NGS TritonX-100 diluted in 1 x PBS (pH 7,4)
Primary antibody solution	5 % (v/v) 0,1-0,3% (v/v)	NGS TritonX-100 diluted in 1 x PBS (pH 7,4)
Secondary antibody solution	1-5 % (v/v)	NGS diluted in 1 x PBS (pH 7,4)
Blocking solution for biocytin	10 % (v/v) 2 % (v/v)	NGS TritonX-100 diluted in 1 x PBS (pH 7,4)
Antibody solution for biocytin visualization	2 % (v/v) 0,1 % (v/v)	NGS TritonX-100 diluted in 1 x PBS (pH 7,4)
Hoechst nuclei staining solution	1 % (v/v)	diluted in 1 x PBS (pH 7,4) stored at -20°C
Draq5 nuclei staining solution	0,1 % (v/v)	diluted in 1 x PBS (pH 7,4) stored at 4°C

3.2.4.3 Solutions for immunohistochemistry

Solution	*Concentration*	*Contents*
$MgCl_2$ stock solution	50 mM	Magnesium chloride
EGTA stock solution (pH 8,0)	100 mM	EGTA diluted with dH_2O
Deoxycholat stock solution	10 % (w/v)	Sodium deoxycholate
Na_2HPO_4 stock solution (pH 9,0)	500 mM	Na_2HPO_4
NaH_2PO_4 stock solution (pH 4,7)	500 mM	NaH_2PO_4
K_3 $[Fe(CN)_6]$ stock solution	0,5 M	Potassium ferricyanide at 4°C, light protected

K_4 [$Fe(CN)_6$] stock solution	0,5 M	Potassium ferrocyanide at 4°C, light protected
X-Gal stock solution	4 % (w/v)	X-Gal in N,N'-Dimethylformamide at 4°C, light protected
lacZ-basic solution (pH 7,4)	100 mM 1,25 mM 2 mM	Trisodium phosphate (Na_2HPO_4/NaH_2PO_4 5:1) $MgCl_2$ EGTA
lacZ-fixation solution	0,2 % (v/v)	Glutaraldehyde in *lacZ*-basic solution fresh prepare
lacZ-washing solution	0,01 % (v/v) 0,2 % (v/v)	Deoxycholate Nonidet P40 diluted in *lacZ*-basic solution
lacZ-substrate solution	5 mM 5 mM 4 % (v/v)	K_3 [$Fe(CN)_6$] stock K_4 [$Fe(CN)_6$] stock X-Gal stock solution diluted in *lacZ*-washing solution, sterile-filtered at 4°C, light protected
Eosin-staining solution	0,1 % (w/v)	Eosin Y sterile-filtered
BrdU working solution	0,75 % (w/v)	Bromdesoxyuridine dissolved in 0,9 % NaCl
BrdU blocking solution	0,6 % (v/v)	H_2O_2 in TBS (pH 7,5)
TBS solution (pH 7,5)	100 mM 150 mM	Tris-base NaCl
HCl	2 N (mol/L)	Hydrogen chloride diluted in dH_2O
H_3BO_3	0,1 M	Boric acid diluted in dH_2O

3.2.4.4 Buffers for immunostaining

Buffer	*Concentration*	*Contents*
Phosphate buffered saline (PBS, pH 7,4, 10 x)	1,5 mM 2,7 mM 8,3 mM 1,7 mM	NaCl KCl Na_2HPO_4 NaH_2PO_4 dissolved in dH_2O

PBS with sodium azide	0,01 % (w/v)	NaN_3 dissolved in PBS
Paraformaldehyde (PFA, pH 7,4)	4 % (w/v)	dissolved 40 g PFA first in 800ml dH_2O, heat to 60℃ adding 1 M NaOH until solution clear then ad 100 ml PBS (1 x) to 1L
Cryoprotection solution	30 % (w/v)	Sucrose in PBS (1 x)

3.2.4.5 Buffers for SDS-PAGE gel

Contents 2 x gels à 1,5 mm	**Stacking gel** (4%)	**Resolving gel** (10%)	(12%)
Rotiphorese gel 30	1,3 ml	10,5 ml	12 ml
Stacking gel (pH 6,8)	2,5 ml	-	-
Resolving gel (pH 8,8)	7,5 ml	7,5 ml	7,5 ml
dH_2O	6,2 ml	12 ml	10,5 ml
TEMED	6 µl	18 µl	18 µl
APS (10 %)	60 µl	180 µl	180 µl

Tab. 3.1: Composition of SDS-PAGE used to prepare two gels.

3.2.4.6 Buffers for Western blotting

Buffer	*Concentration*	*Contents*
Protein lysis buffer (RIPA buffer, modified) (pH 7,5)	50 mM 150 mM 0,5 % (v/v) 0,5 % (w/v) 1 % (v/v)	Tris-base NaCl Nonidet P-40 (NP40) Sodium Deoxycholate TritonX-100 sterile-filtered, at -20℃
Complete Mini tablet	1 x tablet	dissolved in 10 ml lysis buffer, fresh prepare
APS stock buffer	10 % (w/v)	Ammonium persulfate dissolved in dH_2O stored at 4℃
SDS stock buffer	10 % (w/v)	Sodium dodecyl sulfate dissolved in dH_2O
Stacking gel buffer (pH 6,8)	0,5 M 0,4 % (v/v)	Tris-base SDS stock buffer sterile-filtered, at 4℃
Resolving gel buffer (pH 8,8)	1,5 M 0,4 % (v/v)	Tris-base SDS stock buffer sterile-filtered, at 4℃

"Laemmli" sample buffer (4x) (pH 6,8)	62,5 mM 3 % (v/v) 10 % (v/v) 0,01 % (w/v) 5 % (v/v)	Tris-HCl SDS stock buffer Glycerin Bromphenol blue 2- Mercaptoethanol dissolved in dH_2O, stored at 4℃
SDS-running buffer (1x) (pH 8,3)	0,25 M 1,92 M 1 % (v/v)	Tris-base Glycine SDS stock buffer dissolved in 5L dH_2O
Transfer buffer (5x) (pH 8,3)	50 mM 0,1 M 0,8 M	Tris-HCl Tris-Base Glycine dissolved in 2L dH_2O
Transfer buffer (1x)	20 % (v/v) 20 % (v/v)	Transfer buffer (5 x) Methanol diluted in dH_2O
Washing blot buffer (pH 6,3)	8,5 mM 1,7 mM 50 mM 0,1 % (v/v)	Tris-HCl Tris-Base NaCl Tween 20 dissolved in 2 L dH_2O
Blocking buffer (for Cx43CT antibodies)	5 % (w/v)	Milk powder dissolved in washing blot buffer
Blocking buffer (for Cx43NT antibodies)	1 % (w/v)	Milk powder dissolved in PBS

3.2.4.7 Buffers for immunoprecipitation and in-gel digestion

Buffer	*Concentration*	*Contents*
HEPES stock buffer (pH 7,4)	100 mM	HEPES dissolved in 100 ml dH_2O
Cytospin lysis buffer (pH 4,8-5,0)	120 mM 0,15 mM 10 mM 25 % (v/v) 2 mM 5 mM 5 mM	KCl $CaCl_2$ KH_2PO_4 HEPES stock buffer EGTA $MgCL_2$ L-glutathione (4℃) dissolved in 100 ml dH_2O, sterile-filtered, stored at -20℃

Protease and phosphatase Inhibitor	1 % (v/v)	diluted in lysis buffer fresh prepare
Tris-HEPES-running buffer (pH 8,0)	100 mM 100 mM 0,1 % (w/v)	Tris-base HEPES SDS dissolved in dH_2O
Trypsin stock solution (10x)	20 µg	lyophilized trypsin dissolved in 20 µl trypsin storage solution, aliquot 5 µl, stored at -20℃
Trypsin working solution (1x)	10 % (v/v)	Trypsin stock (10 x) diluted in dH_2O stored at -20℃
Destaining solution	80 mg 50 % (v/v)	Ammonium bicarbonate Acetonitrile (ACN) diluted in 20 ml dH_2O stored at 4℃
Digestion buffer	25 mM	Ammonium bicarbonate diluted in 5 ml dH_2O stored at 4℃
Reducing buffer	50 mM	TCEP dissolved in digestion buffer, prepare just before use
Alkylation buffer (5x)	500 mM	IAA dissolved in dH_2O light protected, at 4℃
Activated trypsin	10 % (v/v)	Trypsin working solution diluted in digestion buffer prepare just before use

3.2.5 Antibodies

3.2.5.1 Primary antibodies

Antigen	*Species*	*Dilution ratio*	*Company/Reference*
α-Tubulin	mouse	IB: 1: 10,000	Sigma Aldrich
BLBP	rabbit	IF: 1: 200	Abcam
BrdU	rat	IF: 1: 500	AbD Serotec
β-galactosidase	rabbit	IF: 1: 500 Paraffin: 1: 5000	Invitrogen

β-galactosidase	Chicken	IF: 1: 500 Paraffin: 1: 500	Abcam
Cre recombinase	mouse	IF: 1: 500	Chemicon
Cre recombinase	rabbit	IB: 1: 1000	Millipore
Cx43CT	rabbit	IF: 1: 500 IB: 1: 5000 IP: 1: 10	Sigma Aldrich
Cx43CT	rabbit	IF: 1: 500 IB: 1: 1000 IP: 1: 10	C. Schlieker, 2000
Cx43NT1	mouse	IF: 1: 250 IB: 1: 200	FHCRC
Cx30	rabbit	IF: 1: 500 IB: 1: 250	Invitrogen
DCX	goat	IF: 1: 100	Santa Cruz Biotech
GFP	mouse	IF: 1: 500	Invitrogen
GFP	rabbit	IB: 1:1000	Invitrogen
GFP	chicken	IF: 1: 500	Abcam
GFAP	mouse	IF: 1: 500	Chemicon
GFAP	rabbit	IF: 1: 500 Paraffin: 1: 1000	Dako
Ki67	rabbit	IF: 1: 500	Novocasta
NeuN	mouse	IF: 1: 500	Millipore
Prox1	rabbit	IF: 1: 2500	Chemicon
TIF-2	mouse	Paraffin: 1: 100	BD Transduction Lab.
VASA (DDX4)	rabbit	Paraffin: 1: 100	Abcam

Tab. 3.2: Used primary antibodies in studies. IF: Immunofluorescence; IB: Immunoblot; IP: Immunoprecipitation

3.2.5.2 Secondary antibodies

Antigen	*Species*	*Dilution ratio*	*Company*
Anti mouse HRP	sheep	IB: 1:10,000	GE Healthcare
Anti rabbit HRP	donkey	IB: 1: 10,000	GE Healthcare
Anti rat biotinylated	donkey	IF: 1: 500	Jackson Immunores.
Alexa fluor 488	donkey anti goat	IF: 1: 200	Molecular probes
Alexa fluor 488	goat anti mouse	IF: 1: 500 Paraffin: 1: 2000	Molecular probes
Alexa fluor 488	goat anti rabbit	IF: 1: 500 Paraffin: 1: 2000	Molecular probes
Alexa fluor 488	goat anti chicken	IF: 1: 500	Molecular probes

Alexa fluor 546	goat anti rabbit	Paraffin: 1: 2000	Molecular probes
Alexa fluor 594	goat anti mouse	IF: 1: 500	Molecular probes
Alexa fluor 594	goat anti rabbit	IF: 1: 500	Molecular probes
Alexa fluor 674	donkey anti rabbit	IF: 1: 300	Molecular probes
Alexa fluor 674	goat anti mouse	IF: 1: 500	Molecular probes
Alexa fluor 674	goat anti rabbit	IF: 1: 500	Molecular probes
Streptavidin Cy3	anti biocytin	IF: 1: 400	Sigma Aldrich
Streptavidin Cy2	anti biocytin	IF: 1: 400	Sigma Aldrich

Tab. 3.3: Used secondary antibodies in studies. IF: Immunofluorescence; IB: Immunoblot.

3.2.6 Primers for mice genotyping

Primers	*Sequence (in 5'-3' direction)*	*Transgene*
Cx30 wt-5	GGT ACC TTC TAC TAA TTA GCT TGG	Cx30KO
Cx30 wt-3	AGG TGG TAC CCA TTG TAG AGG AAG	
Cx30 LacZ-3	AGC GAG TAA CAA CCC GTC GGA TTC	
fw poly A	GGG GGT GAA GGA GTT TTC AGC AGT GC	Cx43flG138R
fw loxP	GCA CTT GGT AGG TAG AGC CTG TCA GGT C	
in kod reg Cx43	GCT TCC CCA AGG CGC TCC AGT CAC CC	
Cx43 delCT-HO3	GCA TCC TCT TCA AGT CTG TCT TCG	Cx43K258stop
RO-delCT	CAA AAC ACC CCC CAA GGA ACC TAG	
vor poly A	GGG GGT GAA GGA GTT TTC AGC AGT GC	Cx43D378stop
vor loxP	GCA CTT GGT AGG TAG AGC CTG TCA GGT C	
in kod reg Cx43	GCT TCC CCA AGG CGC TCC AGT CAC CC	
Cx43 del forw	GGC ATA CAG ACC CTT GGA CTC C	Cx43floxed
UMPR	TCA CCC CAA GCT GAC TCA ACC G	
fw loxP	GCA CTT GGT AGG TAG AGC CTG TCA GGT C	Cx43CFP
DSP-CFP	AAG AAG TCG TGC TGC TTC ATG TGG	
in kod reg Cx43	GCT TCC CCA AGG CGC TCC AGT CAC CC	
Cx43 del forw	GGC ATA CAG ACC CTT GGA CTC C	Cx43del
Cx43 del rev	TGC GGG CCT CTT CGC TAT TAC G	
GFAP LZ1	ACT CCT TCA TAA AGC CCT CG	GFAP-Cre
Cre LZ4	ATC ACT CGT TGC ATC GAC CG	
up nestin Cre	TCC CTT CTC TAG TGC TCC ACG TCC	Nestin-Cre
intere rev	TCC ATG AGT GAA CGA ACC TGG TCG	
intcre up	TTT GCC TGC ATT ACC GGT CGA TGC	Inter-Cre
intcre rev	TCC ATG AGT GAA CGA ACC TGG TCG	

Tab. 3.4: Primers used for each transgenic mice.

3.2.7 Laboratory instruments

Equipment	*Company*
Axiophot	Carl Zeiss, Carlzeiss microimaging GmbH, Göttingen, Germany
Binocular	Moticam, Xiamen, China
Centrifuges	Eppendorf GmbH, Wesseling, Germany
Cryostat	Microm HM560, Thermoscientific
DynaMag Magnet	Invitogen, Darmstadt, Germany
Gel electrophoresis chamber	Biorad, Munich, Germany
Genegnome Syngene bioimaging	Synaptics ltd. Cambridge, England
GeneFlash Syngene bioimaging	Synaptics ltd. Cambridge, England
Heat block	VWR, Darmstadt, Germany
Incubator	BINDER, USA
Leica TCS confocal	Leica Microsystems, Wetzlar, Germany
Microwave	Severin, Germany
Mini-Protean 3 cell	Biorad, Munich, Germany
Novex Minicell WB module	Invitrogen, Darmstadt, Germany
PCR machines (MyCycler Thermal cycler)	Biorad, München, Germany
pH meter	Mettler Toledo, Giessen, Germany
Refrigerators (4℃ & -20℃)	Liebherr GmbH, Biber ach, Germany
Refrigerators (-80℃)	Thermo Fischer Scientific, Bonn, Germany
Rotator mixer	Grant-Bio, UK
Shaker	Heidolph Rotomax120
Shaking Incubator (GFL)	Progen Scientific, London, England
Shaking water bath	Memmert GmbH, Schwabach, Germany
Table top small centrifuge	VWR, Darmstadt, Germany
Table top centrifuge (Centrifuge5424)	Eppendorf GmbH, Wesseling, Germany
Cooling centrifuge	HERAEUS Fresco17 centrifuge, Thermo Fischer Scientific, Bonn, Germany
Vibratome (VT1000S)	Leica, Nussloch, Germany

Vortexer	VWR, Darmstadt, Germany
WB power supply	Biorad, Munich, Germany
Weigh balance	ACCULAB, Sartorius group
Water bath	P-D Industriegesellscaft GmbH, Germany

3.2.8 General lab materials

Material	*Company*
Agarose	Invitrogen
Cell culture materials	Sarstedt, Grenier Bio-one, Millipore, Germany
Cell scrapers, Tubes	Sarstedt, Germany
Gloves	Ansell ltd, Staffordshire, UK
Hybond ECL Nitrocellulose membrane	Amsterdam, UK
Mice surgery equipment	Fine Science Tools (F.S.T), Germany
Microscopic slides	Thermoscientific, Braunsweig, Germany
Pasteur pippetts	Carl-Roth
Pipette tips	Greiner GmbH, Frickenhausen, Germany
Pippetts, PCR tubes	BRAND
Protein gels (4-20 %)	Pierce, Rochford, USA
PVDF membrane	Millipore, Schwalbach, Germany
Sterile filters	Millipore, Schwalbach, Germany
Syringes, Venofix safety	Braun, Melsungen, Germany
Whatman paper	Whatman International, Maidstone, UK

3.3 Methods

3.3.1 Isolation of genomic DNA from mouse tail tips

Genomic tail tip DNA was prepared as described previously. Briefly, 4 weeks old mice tails were cut and incubated in Laird buffer (Laird et al., 1991) supplemented with Proteinase K (20U/ml) at 55℃ overnight (O/N) in a water bath. The tail lysates were precipitated in isopropanol by centrifuging at 13,000 rpm for 15 min at room temperature (RT). The supernatant was discarded; the DNA pellet was washed in 70 % ethanol and centrifuged again at 13,000 rpm for 5 min. The DNA pellet was air dried for one hour and dissolved in an appropriate volume of double distilled water. For routine genotypic analysis, genomic DNAs from tail biopsies were used for PCR with different primers.

3.3.2 PCR analysis of transgenic mice

The polymerase chain reaction (PCR) is now a common technique used for amplification of DNA fragments *in vitro* (Mullis and Faloona, 1987). The method relies on several thermal cycling reactions for melting and replication of target DNA region, where attached by two primers through complementary base pairing. Almost all PCR applications need a heat-stable DNA polymerase, such as *Taq*-polymerase, an enzyme originally isolated from bacterium *Thermus aquaticus*. For further analysis of PCR products agarose gel electrophoresis is performed for separation of DNA fragments by their size and charge. Due to the phosphate groups negative charged DNA move to the anode and the migration velocity is proportional to their molecular mass. For visualization of DNA under ultraviolet light commonly added ethidium bromide to bind with nucleic acid. To determine the presence of transgene the PCR products were run on 1,2 % agarose gels at 110 V for 1-1,5 h. At same time, a DNA ladder was run along with the samples to estimate the molecular size. PCR reaction mixes and programs for genotyping are shown in the following:

3.3.2.1 Detection of the Cx30-/- transgene

Reaction mixture	Volume (µl)
DNA	1,0
Cx30 wt-5 (20 pmol/µl)	1,0
Cx30 wt-3 (20 pmol/µl)	1,0
Cx30 LacZ-3 (20 pmol/µl)	1,0
$MgCl_2$ (25 mM)	2,0
5 x PCR-buffer	5,8
dNTP's (2,5 mM)	1,0
Tag-Polymerase (500 U)	0,1
dH_2O	12,1
Total	25

Program	Temperatur (℃)	Time
1	94	5 min
2	92	45 sec
3	60	45 sec
4	72	45 sec
5	Go to step 2	35 x
6	72	10 min
7	10	forever

Tab. 3.5: Reaction mixture and program for detection of the Cx30-/- transgene. Cx30+/+: 544 bp; Cx30-/-: 460 bp.

3.3.2.2 Detection of the Cx43flG138R transgene

Reaction mixture	Volume (µl)
DNA	1,0
fw poly A (20 pmol/µl)	1,0
fw loxP (20 pmol/µl)	1,0
in kod reg Cx43 (20 pmol/µl)	1,0
$MgCl_2$ (25 mM)	1,7
5 x PCR-Puffer	5,0
dNTP's (10,0 mM)	0,5
Tag-Polymerase (500 U)	0,1
dH_2O	13,7
Total	25

Program	Temperatur (°C)	Time
1	95	5 min
2	94	1 min
3	65	1 min
4	72	1 min
5	Go to step 2	34 x
6	72	10 min
7	10	forever

Tab. 3.6: Reaction mixture and program for detection of the Cx43flG138R transgene. Cx43+/+: 350 bp; Cx43flG138R: 400 bp.

3.3.2.3 Detection of the Cx43K258stop transgene

Reaction mixture	Volume (µl)
DNA	2,0
Cx43delCT-HO3 (50 µM)	0,2
RO-delCT (50 µM)	0,2
$MgCl_2$ (25 mM)	2,0
5 x PCR-Puffer	5,0
dNTP's (10,0 mM)	0,5
Tag-Polymerase (500 U)	0,2
dH_2O	14,9
Total	25

Program	Temperatur (°C)	Time
1	95	5 min
2	94	30 sec
3	62	45 sec
4	72	1 min
5	Go to step 2	39 x
6	72	10 min
7	8	forever

Tab. 3.7: Reaction mixture and program for detection of the Cx43K258stop transgene. Cx43+/+: 851 bp; Cx43K258stop: 452 bp.

3.3.2.4 Detection of the Cx43flD378stop transgene

Reaction mixture	Volume (µl)
DNA	1,0
vor poly A (20 pmol/µl)	1,0
vor loxP (20 pmol/µl)	1,0
in kod reg Cx43 (20 pmol/µl)	1,0
$MgCl_2$ (25 mM)	1,7
5 x PCR-Puffer	4,0
dNTP's (10 mM)	0,5
Tag-Polymerase (500 U)	0,1
dH_2O	9,7
Total	20

Program	Temperatur (°C)	Time
1	95	5 min
2	95	1 min
3	61	1 min
4	72	1 min
5	Go to step 2	34 x
6	72	10 min
7	10	forever

Tab. 3.8: Reaction mixture and program for detection of the Cx43flD378stop transgene. Cx43+/+: 350 bp; Cx43flD378stop: 400 bp.

3.3.2.5 Detection of the Cx43flox transgene

Reaction mixture	Volume (µl)
DNA	1,0
Cx43delforw (25 µM)	1,0
UMPR (25 µM)	1,0
$MgCl_2$ (25 mM)	1,0
5 x PCR-Puffer	5,0
dNTP's (2,5 mM)	1,0
Tag-Polymerase (500 U)	0,2
dH_2O	14,8
Total	25

Program	Temperatur (°C)	Time
1	94	4 min
2	94	2 min
3	65	1 min
4	72	1 min 30 sec
5	Go to step 2	25 x
6	72	10 min
7	8	for ever

Tab. 3.9: Reaction mixture and program for detection of the Cx43flox transgene. Cx43+/+: 500 bp; Cx43flox: 650 bp.

3.3.2.6 Detection of the Cx43del transgene

Reaction mixture	Volume (µl)
DNA	1,0
Cx43delforw (25 µM)	1,0
Cx43delrev (25 µM)	1,0
$MgCl_2$ (25 mM)	2,5
5 x PCR-Puffer	5,0
dNTP's (2,5 mM)	1,0
Tag-Polymerase (500 U)	0,2
dH_2O	13,3
Total	25

Program	Temperatur (°C)	Time
1	95	5 min
2	94	30 sec
3	62	45 sec
4	72	1 min 30 sec
5	Go to step 2	40 x
6	72	10 min
7	8	for ever

Tab. 3.10: Reaction mixture and program for detection of the Cx43del transgene. Cx43del: 670 bp.

3.3.2.7 Detection of the Cx43ki-ECFP transgene

Reaction mixture	Volume (µl)
DNA	1,0
fw loxP (20 pmol/µl)	1,0
DSP-CFP (20 pmol/µl)	1,0
in kod reg Cx43 (20 pmol/µl)	1,0
$MgCl_2$ (25 mM)	2,0
5 x PCR-Puffer	5,0
dNTP's (10 mM)	0,5
Tag-Polymerase (500 U)	0,1
dH_2O	13,4
Total	25

Program	Temperatur (°C)	Time
1	95	5 min
2	95	30 sec
3	65	30 sec
4	72	1 min
5	Go to step 2	30 x
6	72	10 min
7	10	forever

Tab. 3.11: Reaction mixture and program for detection of the Cx43ki-ECFP transgene. Cx43+/+: 340 bp; Cx43flCFP: 395 bp; Cx43ki-ECFP: 700 bp.

3.3.2.8 Detection of the GFAP-Cre transgene

Reaction mixture	Volume (µl)
DNA	1,0
GFAP LZ1 (25 pmol/µl)	1,0
Cre LZ4 (25 pmol/µl)	1,0
$MgCl_2$ (25 mM)	2,0
5 x PCR-Puffer	5,0
dNTP's (2,5 mM)	1,0
Tag-Polymerase (500 U)	0,2
dH_2O	13,8
Total	25

Program	Temperatur (°C)	Time
1	94	1 min
2	94	1 min
3	60	1 min
4	72	1 min
5	Go to step 2	30 x
6	72	10 min
7	10	forever

Tab. 3.12: Reaction mixture and program for detection of the GFAP-Cre transgene. GFAP-Cre: 190 bp.

3.3.2.9 Detection of the nestin-Cre transgene

Reaction mixture	Volume (µl)
DNA	1,0
up-nestin-Cre (25 pmol/µl)	0,2
intcre_rev (25 pmol/µl)	0,2
$MgCl_2$ (25 mM)	2,0
5 x PCR-Puffer	2,5
dNTP's (10,0 mM)	0,2
Tag-Polymerase (500 U)	0,5
dH_2O	18,4
Total	25

Program	Temperatur (°C)	Time
1	95	5 min
2	94	30 sec
3	60	50 sec
4	72	1 min 30 sec
5	Go to step 2	36 x
6	72	10 min
7	8	forever

Tab. 3.13: Reaction mixture and program for detection of the nestin-Cre transgene. nestin-Cre: 650 bp.

3.3.2.10 Detection of the inter-Cre transgene

Reaction mixture	Volume (µl)
DNA	1,0
intcre up (25 pmol/µl)	1,0
intcre rev (25 pmol/µl)	1,0
$MgCl_2$ (25 mM)	2,0
5 x PCR-Puffer	5,0
dNTP's (10,0 mM)	1,0
Tag-Polymerase (500 U)	0,2
dH_2O	13,8
Total	25

Program	Temperatur (°C)	Time
1	94	1 min
2	94	1 min
3	60	1 min
4	72	1 min
5	Go to step 2	30 x
6	72	10 min
7	10	forever

Tab. 3.14: Reaction mixture and program for detection of the inter-Cre transgene. inter-Cre: 400 bp.

3.3.3 Immunohistochemistry

Immunohistochemistry was carried out on mice at age p60 or at age p90-120 for intercellular coupling analysis.

3.3.3.1 Cardiac perfusion and fixation

To get well preserved brain sections for immunohistochemistry transcardiac perfusion was carried out. First, mice were anesthetized with intraperitoneal injection of Cepetor-KH (1 mg/ml) and Ketamin (10 %) in a ratio of 3:2. Using small scissors to open the ribcage and to expose the pericardium, which was followed by the insertion of a 25-G needle into the left ventricle. The right atrium was cut for the blood to flow out. During the whole perfusion process, 30 ml PBS (pH 7,4) was slowly injected to remove blood, followed by further pumping of 30 ml 4 % PFA for fixation. A successful perfusion was indicated by the animal becoming rigid. Later, the skull was opened and the brain isolated, then fixed again in 4 % PFA overnight at 4℃. The next day the brain was transferred to sucrose solution in PBS (30 %) for at least 3 days.

3.3.3.2 Cryoprotection and sectioning

Three days after immersion in sucrose solution, brains were cryoprotected in Tissue-tek (Sakura), frozen and stored first at -80℃. Generally, free floating coronal sections (40 µm) were cut on a cryostat (Microm HM560) and collected in 24-well plates filled with PBS (pH 7,4) and 0,01 % sodium azide for longer preservation at 4℃. Depending on the purpose, like X-Gal staining, 10-20 µm thin sections were produced. Such sections were mounted directly onto histological slides. The sections were air-dried for one hour at RT to prevent them from falling off the slides during incubations. Slides containing cryostat sections can be stored at -80℃ for up to 12 months.

3.3.3.3 Immunostaining procedure

The coronal sections were washed three times in PBS (pH 7,4) for 10 min each and then incubated in blocking solution (5-10 % NGS, 0,3-05 % TritonX-100 in PBS) for 2 h at RT. Subsequently, sections were incubated in appropriate primary antibodies diluted in blocking solution (5 % NGS, 0,1-0,3 % TritonX-100 in PBS) overnight at 4℃ with gentle shaking. Applied primary antibodies were listed in Tab. 3.2. For Ki-67, BLBP and DCX stainings, sections were incubated with the mentioned primary antibodies for 48 h at 4℃, respectively. After incubation with the appropriate secondary antibodies for 2 h at RT sections were washed three times in PBS, followed by nuclei staining with Hoechst 33258 (1:100) or alternatively with Draq5 (1:1000) for 10 min at RT. Applied secondary antibodies are listed in Tab. 3.3. Brain sections were mounted onto specimen slides using Permafluor or Vectashield

and covered by cover slips. For double and triple immunofluorescence, the same procedure was performed with suitable primary and corresponding secondary antibodies.

3.3.3.4 X-Gal and eosin immunohistochemistry

The *lacZ* gene encodes the enzyme β-galactosidase (ß-Gal), which metabolized the colourless substrate X-Gal (5-bromo-4-chloro-3-indolyl-b-D-galactopyranoside) into an insoluble blue precipitate. The X-Gal staining demonstrates cell nuclei, whereas cytoplasm and extracellular matrix are obtained by counterstaining with the eosin Y solution. X-Gal and eosin staining of thin sections was performed according to Theis et al., 2001. Perfusion and fixation of mice brains or hearts are described previously in section 3.3.3.1. Solutions and materials are listed before (3.2.4.3). Frozen sections (10-20 µm) were first fixed in *lacZ*-fixation solution for 5 min, rinsed three times in *lacZ*-washing solution for 5 min each. Subsequently, sections were incubated in *lacZ*-substrate solution overnight at 37℃ in dark. On the following day, sections were washed three times in *lacZ*-washing solution for 5 min each and counterstained with eosin-staining solution for 3-5 min. To obtain a desired colour intensity, sections were washed several times in distilled water, followed by application of coverslips with entellan and air-dried at RT.

3.3.3.5 BrdU immunohistochemistry

BrdU (5-bromo-2-deoxyuridine), an analogue of thymidine, can be incorporated specifically into the DNA structure of dividing cells both *in vitro* and *in vivo* (Gage, 2000). BrdU labeling is currently the most used technique for monitoring neural progenitor cell proliferation in a variety of neurogenesis studies, including human (Miller and Nowakowski, 1988; Seki and Arai, 1995; Kuhn et al., 1996; Eriksson et al., 1998; Gage, 2000). The experimental design and BrdU administration protocol are illustrated in Fig. 3.1.

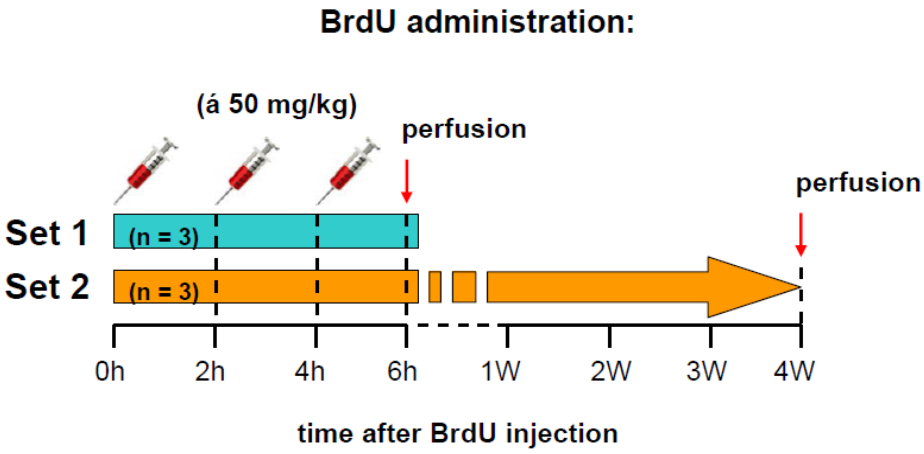

Fig. 3.1: The experimental design and BrdU administration protocol. Schematic illustration of the experimental design. Prior to perfusion all animals received intraperitoneal (i.p.) injections of the proliferation

marker BrdU three times with the interval of two hours on one day and separated into two groups. Set 1 animals were sacrificed 2 h after last injection, whereas set 2 groups were perfused 4 weeks later.

As an exogenous marker BrdU (50 µg/g body weight; Sigma Aldrich) was dissolved in 0,9 % saline and stored at -20℃. All animals at age p60 were received three times intraperitoneal (i.p.) injections with the interval of two hours on one day. Mice were sacrificed either 2 h or 4 weeks following the last BrdU administration to map the fate of proliferating cells. Animals were deeply anesthetized and perfused transcardially, followed by cryoprotection and sectioning as described above. Free floating sections (40 µm) were treated for 30 min with H_2O_2 (0,6 %) in TBS (pH 7,5) to block endogenous peroxidase. After washing sections were denaturized in 2 N HCl for 30 min at 37℃ to expose the antigen of DNA, followed by rinsing in borate buffer (pH 8,5) for 10 min. Then, sections were blocked in TBS with 3 % donkey serum and 0,1 % TritonX-100 (TBS-plus) for 1 h at RT. Subsequently, sections were incubated in primary antibody (rat monoclonal anti-BrdU 1: 500; AbD Serotec) in TBS-plus overnight at 4℃. Next day, after rinses in TBS, sections were incubated in the secondary antibody (biotinylated donkey anti-rat 1: 500; Jackson Immunoresearch) for 4 h at RT. For immunohistochemical detection of BrdU incorporation, sections were treated in an avidin-biotin peroxidase reagent (Vectastain Elite ABC kit; Vector Laboratories) for 1 h. After another set of rinses in TBS, a nickel-intensified DAB (3, 3'-diaminobenzidine) substrate kit (Vector Laboratories) was used for peroxidase reaction. After peroxidase staining sections were thoroughly washed and mounted with entellan. For immunofluorescence triple-labeling of BrdU, Prox1 and DCX, sections were treated in the same way described previously for the immunoperoxidase staining. Briefly, sections were first incubated with primary antibody rat anti-BrdU (1: 500, AbD Serotec) overnight at 4℃, followed by biotinylated donkey anti-rat antibody (1:500, Jackson Immunoresearch) staining for 4 h at RT. Then, sections were incubated with streptavidin Cy3 (1: 500, Sigma Aldrich) overnight at 4℃. On the following day, sections were incubated in a mixture of two antibodies (goat anti-doublecortin, 1:200, Santa Cruz Biotechnologies; rabbit anti-Prox1, 1:2500, Chemicon) for 48 h at 4℃. After a set of rinses in TBS, a mixture of secondary antibodies (Alexa Fluor 488 donkey anti-goat for DCX, Alexa Fluor 674 donkey anti-rabbit for Prox1) was applied for 4 h at RT. Subsequent the sections were rinsed again in TBS and coverslipped in the permafluor mounting medium (Thermo Fischer Scientific).

3.3.3.6 Paraffin immunohistochemistry and immunofluorescence

For light microscopy and immunostaining, three sectioning techniques are routinely carried out: free floating sections, thin sections on the slides and paraffin embedded sections. In cooperation with Prof. Dr. Brehm (Anatomisches Institut, Tierärzliche Hochschule Hannover), immunofluorescence of fixed paraffin-embedded testis and ovary sections were performed.

Testis and ovary were dehydrated by graded ethanol solutions, followed by graded xylene solutions and liquid paraffin: 70 % Ethanol 20 min (1 x), 95 % Ethanol 20 min (2 x), 100 % Ethanol 20 min (2 x), Xylene 20 min (2 x), Paraffin (65°C) 30 min (2 x). The tissue was removed from liquid paraffin and placed into a mold. The wax was allowed to solidify until it formed a block that could be held in the microtome (Microm, Germany). 5 µm serial sections were mounted on Superfrost slides (Metzel-Gläser, Germany) and dried at 37°C for 16 hours to bond the tissue to the glass. Slides and blocks were stored at room temperature until they were used. Before each staining, sections were de-waxed in xylene for 5 min (3 x), and rehydrated through serial ethanol solutions: 100 % 5 min (1x), 90 % 5 min (1 x), 80 % 5 min (1 x), 70 % 5 min (1 x), 50 % 5 min (1 x) to PBS (pH 7,4). After deparaffinization and rehydration, sections were treated with 3 % H_2O_2 and blocked with bovine serum albumin (BSA, 5 %) for 30 min each, and then incubated with the polyclonal anti-β-Gal antibody (1:5000) or a polyclonal anti-GFAP antibody (1:1000, DAKO, Hamburg) overnight at 4°C, respectively. For visualization, the DAKO EnVision+ System/rabbit, horseradish peroxidase (DAKO, Hamburg, Germany) was used in accordance with the manufacturer's protocol. Intermediate washing steps were performed using TBS (10 mM Tris pH 8.0, 150 mM NaCl) containing 0.05 % Tween20 (TBST). After staining with diaminobenzidine, the sections were thoroughly washed in running tap water for 10 min and counterstained with hematoxylin (ß-Gal) or without counterstaining (GFAP). Finally, they were dehydrated in a series of graded ethanol solutions, cleared in xylene, mounted with Eukitt (Sigma Aldrich, Munich, Germany) and images were aquired using an Axioskop connected to an Axiocam (Zeiss, Jena, Germany).

For double β-Gal immunofluorescence stainings (ß-Gal and TIF-2), deparaffinised and rehydrated sections were boiled at 96-99°C for 20 m in in sodium citrate buffer (pH 6.0), let cool down, permeabilized with 0,2 % Triton X-100 in TBS for 45 min and blocked with 20 % NGS for 20 min at room temperature. Then, sections were incubated overnight at 4°C with the primary anti β-Gal antibody (1:5000) and monoclonal mouse anti-TIF-2 antibody (1:100, BD Transduction Laboratories, Heidelberg, Germany). This step was followed by the incubation with a mix of the secondary antibodies (goat anti-rabbit antibody conjugated to Alexa fluor 546 (red, 1:2000, A11040, Invitrogen) and goat anti-mouse antibody conjugated to Alexa fluor 488 (green, 1:2000, A11029, Invitrogen) for 45 min and washed again. Washing steps were performed using TBST. After 5 min in aqua dest, sections were mounted with ProLong Antifade (Invitrogen, Karlsruhe, Germany), viewed under a Zeiss Axiovert 200 M fluorescence microscope and images were acquired with the Zeiss software AxioVision (Zeiss, Jena, Germany).

For β-Gal and VASA double immunofluorescence stainings, deparaffinised and rehydrated sections were microwave treated at 600 W in sodium citrate buffer (pH 6.0) for 2 x 5 min, let

cool down, permeabilized with 0,2 % Triton X-100 in TBS for 45 min and blocked with 20 % NGS for 20 min at room temperature. Then, sections were incubated overnight at 4℃ with a mix of the primary antibodies (chicken anti β-Gal antibody (1:500, Abcam, ab9361, Cambridge, UK) and polyclonal rabbit anti-DDX4 (VASA) antibody (1:100, Abcam, ab13840). Then, sections were incubated with a mix of the secondary antibodies (goat anti-chicken antibody conjugated to Alexa fluor 546 (red, 1:2000, A11040, Invitrogen) and goat anti-rabbit antibody conjugated to Alexa fluor 488 (green, 1:2000, A11029, Invitrogen) for 45 min and washed again. All intermediate washing steps were performed using TBST. Images were acquired with a Zeiss Axiovert 200 M fluorescence microscope and the Zeiss software AxioVision (Zeiss, Jena, Germany).

3.3.3.7 Image acquisition and processing

Images were taken with a digital SPOT camera (Diagnostic Instruments, Sterling Heights, MI) and MetaView software (Universal Imaging, West Chester, PA), using an Axiophot microscope (Carl Zeiss, Göttingen, Germany) equipped with fluorescence optics. Using appropriate filter sets fluorescent illumination was acquired by excitation/emission wavelengths of 340/425 nm (blue), 500/550 nm (green) and 580/ 630 nm (red). Alternatively, light images for BrdU immunohistochemistry were taken with a Binocular (Moticam, Xiamen, China) supplied with a digital camera. For higher resolution and cell colocalization, images were acquired with confocal laser scanning microscopy (Leica TCS, Pulheim, Germany). Image processing and quantification were performed using ImageJ software (NIH, Bethesda, USA). Several optical sections, at 1 µm intervals through the depth of the slice, were digitally combined to yield the final images. Only general adjustments of color, contrast and brightness were made.

3.3.3.8 Quantification and statistical analysis

Quantification of proliferating cells was achieved by counting the number of positively stained nuclei within the SGZ of the DG using z-stack micrographs. Ki67-positive cells were quantified in a 1-in-5 series of sections totaling to 5 sections (i.e., 10 DG sections) throughout the whole rostrocaudal extension of the DG. BrdU-positive cells in the SGZ and colocalization studies were counted using a confocal laser scanning microscope (Leica TCS). Images were acquired in sequential scanning mode, where only one laser and the respective detection line are active at a time to exclude cross-bleeding between the three different channels. Colocalization was confirmed by z-series through the cell soma allowing the definite assessment of overlap between the antigens. The percentage of BrdU-positive cells expressing Prox1 only, or Prox1 and DCX were assessed by the colocalization studies. Prox1-positive cells were counted in a 1-in-5 series of sections with intervals of 240 µm

throughout the rostrocaudal span of the GCL. To define the counting box, confocal laser micrographs of the GCL were obtained using 40 x objectives at 1 µm intervals to a final depth of 4 µm. The counting box has dimensions of 150 x 50 x 4 μm^3 and was embedded entirely within the section. The left side of the counting box is positioned 250 µm away from the outermost margin of the GCL flexure and was perpendicularly oriented to the longitudinal axis of the GCL. Cell nuclei that were located completely inside the counting frame and those that crossed through its right side were counted, whereas nuclei that crossed the left plane were not considered. BLBP-positive cells were also counted in a 1-in-5 series of sections, with a counting box of 220 x 170 x 30 μm^3 that was located 50 µm beyond the tips of the hilus perpendicularly to the longitudinal axis of the GCL. Only BLBP-positive cells in the SGZ with a process extending into the GCL were counted. Data analysis was performed using SPSS (PASW statistics version 18) for windows. Mean values of cells per DG (Ki67, Prox1, BLBP and BrdU) were calculated and assessed with the Mann-Whitney U- or Kruskal-Wallis H-test for significant differences between groups. Data are given as mean ± SD unless otherwise noted. A difference in probability value $P < 0.05$ was considered statistically significant.

3.3.3.9 Electrophysiology and biocytin visualization

Patch-Clamp recordings were carried out by Dr. Peter Bedner and Mrs. Stephanie Griemsmann in our institute. The measurements of biocytin tracer coupled astrocytes or RG-like cells were performed as described previously (Theis et al., 2003; Wallraff et al., 2006; Kunze et al., 2009). Mice aged 90 to 120 postnatal days were anesthesized by Isofluran, decapitated and the brains were quickly removed. Twohundred µm thick coronal sections were cut on a vibratome (VT1000S, Leica, Nussloch, Germany). Then, slices were stored in artificial cerebrospinal fluid (ACSF) containing (in mM): 126 NaCl, 3 KCl, 2 $MgSO_4$, 2 $CaCl_2$, 10 glucose 1.25 NaH_2PO_4, 26 $NaHCO_3$, equilibrated with 95 % O_2 and 5 % CO_2 to a pH of 7.4 at RT. For some experiments slices were incubated in ACSF added with 1 µM SR101 (Invitrogen) at 35°C. Whole-cell voltage-clamp recording model was performed for the intercellular coupling in the stratum radiatum of CA1 or in the SGZ of DG. Slices were transferred to a recording chamber and continuously perfused with carbogenized ACSF. Cells were visualized using an upright microscope equipped with an infrared DIC system (Eclipse E600FN, Nikon) at 600-fold magnification. Experiments were performed on cells identified by endogenous fluorescence or staining with the astrocyte marker SR101 (SR101, Invitrogen) (Nimmerjahn et al., 2004; Kafitz et al., 2008). Pipettes were fabricated from borosilicate glass (Science Products) and had a resistance of 2 to 6 MΩ when filled with internal solution containing (in mM): 130 K-gluconate, 1 $MgCl_2$, 3 Na_2-ATP, 20 HEPES, 10

EGTA, 0.5 % N-biotinyl-L-lysine (Biocytin, Sigma); pH 7.2. Currents were recorded employing either an EPC-7 or EPC-8 patch clamp amplifier (Heka, Lambrecht, Germany) and monitored by TIDA software (Heka). Data were sampled at 6 to 30 kHz and filtered at 3 to 10 kHz. Input and series resistance were regularly checked by applying a 10 mV depolarisation step. The holding potential in acute slices was -80 mV. Biocytin injections were performed only one cell per slice for 20 min, afterwards slices were immediately fixed overnight in 4 % paraformaldehyde (PFA) in 0.1 M phosphate buffered saline (PBS), pH 7.4 at 4℃. After wash and rinsing in PBS (pH 7,4), slices were blocked with solution consisting of 10 % NGS and 2 % TritonX-100 in PBS for 2 h at RT. Subsequently, sections were incubated with streptavidin Cy3 or Cy2 (for Cx43K258stop RG-like cell slices) (Sigma Aldrich, 1: 300) overnight at 4℃. Next day, slices were washed with PBS three times and co-stained with anti-GFP (Cx43G138R mice) or anti-ß-Gal (Cx43K258stop mice) antibodies to confirm the mice genotype. Finally, slices were mounted in the permafluor mounting medium (Thermo Fischer Scientific) and images were taken by Axiophot microscope (Carl Zeiss) with a 20 x objective as described above.

3.3.4 Western Blot

3.3.4.1 Sample preparation

Mice were sacrificed by cervical dislocation, and the brain was immediately isolated. The cerebellum was first removed into an eppendorf tube and quick-frozen in liquid nitrogen. Then, the olfactory bulbs were cut off with part of frontal cortex and the rest of brain was put on a coronal plane. The hippocampus was separated carefully and collected into a tube and frozen in liquid nitrogen. For the phosphorylation studies only the dorsal part of the hippocampus was used to compare the phosphorylated Cx43 in the ipsilateral versus the contralateral side. The tissues were stored at -80°C or subsequent prepared in a modified RNA Immuno- Precipitation Assay (RIPA) lysis buffer (50 mM Tris, 150 mM NaCl, 0.5 % Nonidet P40, 0.5 % Na-DOC, 1 % Triton X-100, 0.5 % SDS) supplemented with Roche Complete Mini protease inhibitor cocktail, 1 tablet/10 ml (Roche, Mannheim, Germany). For phosphorylation study the same lysis buffer was added with protease and phosphatase single using inhibitor 100 µl/10 ml (Thermo Scientific, Bonn, Germany). Then, the tissue was homogenized with a plastic pestle in a 1.5 ml tube in about 300 µl lysis buffer, then disrupted with a prechilled 27 gauge needle (Braun, Melsungen; Germany) and supersonic slat (until homogeneous). After incubation on ice for ~30 min, supernatants were collected by centrifugation for 30 min at 13,000 x g at 4℃. Total protein content was assayed with BCA (Pierce, Bonn, Germany) method using 5 µl supernatant of each sample.

3.3.4.2 SDS-PAGE, Blotting and detection

Depending on the purpose of the experiment, 30-50 µg total protein per sample was used for immunoblot studies. Lysates were mixed with “Laemmli” sample buffer (62.5 mM Tris-Cl, pH 6.8, 3 % SDS, 0.01% bromophenol blue, 5 % β-mercaptoethanol, 10 % glycerol) and denatured by heating for 10 min at 65°C. After that samples were spin briefly and separated with 10 % or 12 % SDS resolving gel for 1-1,5 h at 0,06 mA in denaturing conditions. To estimate the protein size, Novex (Invitrogen) standard was loaded along with the samples. Nitrocellulose membrane (Aamsterdam) or PVDF (polyvinylidene fluoride) membranes (Millipore) were used for electroblotting of separated proteins for 2 h at 500 mA running condition. Membranes were blocked with 5 % milk powder in TBS (pH 7.4) containing 0.05 % Tween-20 and incubated overnight at 4°C on a rotator with primary antibodies: rabbit polyclonal anti-Cx43CT (1:5000, Sigma, Steinheim, Germany), rabbit polyclonal anti-Cx43CT (1: 1000, C. Schlieker, 2000), mouse monoclonal anti-Cx43NT (1:200, Fred Hutchinson Cancer Research Center (FHCRC), Seattle, USA), rabbit polyclonal anti-Cx30 (1: 250, Invitrogen, Darmstadt, Germany), rabbit polyclonal anti-Cre (1:1000, Merck, Darmstadt, Germany), mouse monoclonal anti-α-tubulin (1:10,000, Sigma, Steinheim, Germany). Secondary antibodies used: goat-anti-mouse HRP conjugate (1:10,000, GE Healthcare, Little Chalfont Buckinghamshire, UK) goat-anti-rabbit HRP conjugate (1:10,000, GE Healthcare). All antibodies, including secondary antibodies, were diluted in 5 % milk powder in TBS (pH 7.4) containing 0.05 % Tween-20, except for the mouse monoclonal anti-Cx43NT antibody, which was diluted in 1 % milk powder in TBS (pH 7.4). Equal loading of the lanes was confirmed by α-tubulin staining of the same membrane. For stripping, Pierce “Restore” stripping buffer was used for all blots for 20 min at RT. Membranes were usually re-blocked after stripping for 2 h at room temperature. For visualisation of HRP, the Super signal West Dura substrate (Pierce) was used and chemiluminescence was detected with the Gene Gnome digital documentation system (Synoptics, Cambridge, UK).

3.3.4.3 Quantification and statistical analysis

Raw data analysis and densitometry were performed with Gene Tools quantification software (Synoptics, Cambridge, UK). After subtracting the background ratio for each band, the intensity of the target proteins was normalized to the values from their α-tubulin loading controls, respectively. The normalized values of control samples were set to 100% for statistical analysis. A difference in probability value $P < 0.05$ was considered statistically significant using student’s t-test. Data are presented as mean ± SEM.

3.3.5 *In vivo* phosphorylation

To study the effect of Cx43 phosphorylation on intracellular coupling, a mass spectrometry (MS)-based proteomic analysis was performed.

3.3.5.1 Immunoprecipitation

The first step in the analysis of a protein complex is the purification of the Cx43 protein from hippocampus in sufficient quantity for mass spectrometric identification. This is the most critical and often the most time-consuming step. Various approaches to purify protein complexes were developed; one of them is the immunoprecipitation (IP) method. Hippocampi from five mice (i.e., 10 hippocampi) were homogenized with a glass pestle in 1000 µl cytospin lysis buffer (120 mM KCl, 0,15 mM $CaCl_2$, 10 mM KH_2PO_4, 25 % HEPES, 2 mM EGTA, 5 mM $MgCL_2$, 5 mM L-glutathione) supplemented with protease and phosphatase inhibitor 100 µl/10 ml (Thermo Scientific, Bonn, Germany) to prevent enzymatic protein degradation during extraction and purification procedures. Then, crude lysates were disrupted with a prechilled 27 gauge needle (Braun, Melsungen, Germany) and supersonic slat was used three times for 10 sec each until the tissue was completely homogeneous. After incubation on ice for 30 min, supernatants were collected by centrifugation for 30 min at 13,000 x g at 4℃. Total protein content was assaye d with a BCA method (Pierce, Bonn, Germany) according to the manufacturer instructions. To capture immunoprecipitated Cx43 complexes a protein A-Dyna bead kit (Invitrogen) was used. All the IP steps were performed at 4℃ on the ice. Hundred µl (3 mg) beads were tra nsferred into a test tube followed by separation and removal of supernatant on the magnet. Cx43 antibodies (Sigma, 0,5 mg/ml, 20 µl) were diluted in 200 µl antibody binding & washing buffer and added to beads. For binding of antibody on the beads the complex was incubated with rotation for 1 h at RT. Later, the supernatant on the magnet was removed and the beads were resuspended by gently pipetting in 200 µl binding & washing buffer. For IP of target Cx43, hippocampal lysates (1000 µg) were incubated with beads-antibody complex overnight at 4℃ with rotation. In each case, the same amount of sample proteins were incubated with only beads overnight as negative control. On the next day, the tube was placed on the magnet and the supernatant was transferred to a clean tube for further quality control. The beads- antibody-antigen complex was washed in 200 µl washing buffer for three times and transferred to a new clean tube to avoid co-elution of proteins bound to the tube wall. Non-denaturing elution of target antigen was carried out by adding 30 µl elution buffer to the complex and incubation with rotation for 10 min at RT. After dissociation of the complex the supernatant containing eluted antigen was transferred to a clean tube for detection of proteins in 1-D gel electrophoresis. The target protein was separated in a 4-20 % polyacrylamide gel (Pierce, Rockford, USA) for 1 h at 180 V with Tris-HEPES running buffer (100 mM Tris-base, 100 mM

HEPES, 0,1 % SDS). To visualize Cx43 band a Coommassie G-250 dye-based reagent (GelCode Blue Safe Protein Stain, Thermo Scientifc) was used for staining protein on gel.

3.3.5.2 In-gel digestion

The gel was first incubated with GelCode Blue Safe Protein Stain for 3 h at RT on a shaking, followed by destaining in ultrapure water overnight at 4℃. In-gel digestion was performed on the following day by using a trypsin based digestion kit (Thermo Scientific, Bonn, Germany). Protein band of interest was excised from the gel using a clean scalpel and cut into 2 x 2 mm pieces. Gel pieces were incubated in 200 µl destaining solution (80 mg ammonioum bicarbonate, 50% acetonitrile in 20 ml dH_2O) at 37℃ for 30 min with shaking. Remove and discard destaining solution from the tube and repeat the step once more. For high-sequence coverage samples were reduced and alkylated by using first 30 µl reducing buffer (50 mM TCEP in digestion buffer) at 60 ℃ for 10 min, foll owed by incubation in alkylation buffer (500 mM IAA in dH_2O) in the dark for 1 h at RT. After discarding alkylation buffer from tube samples were washed by 200 µl destaining buffer again for 15 min at 37℃ with shaking. Subsequently, gel pieces were incubated in 50 µl acetonitrile for 15 min at RT and dried in the air for 10 min. Gel pieces were swollen by adding 10-20 µl of activated trypsin solution (10 % trypsin working solution in digestion buffer) to the tube and further incubated for 15 min at RT. Finally, samples were digested in 25 µl digestion buffer (25 mM ammonium bicarbonate in dH_2O) overnight at 30 ℃ with shaking, followed by rem oving digestion mixture in a clean tube on the next day. Samples were stored at 4℃ until MS analysis.

3.3.5.3 Mass spectrometry

Mass spectrometry (MS) is a powerful tool for the identification and characterization of protein post-translational modification, including phosphorylation. In cooperation with Dr. Marc Sylvester (Institute for Biochemistry and Molecular Biology, University Hospital Bonn), MS-based Cx43 phosphorylation studies were performed. For peptide preparation, proteins from Cx43-immunoprecipitation samples were eluted with “Laemmli” buffer and separated on SDS-PAGE. Slices in the molecular weight range of Cx43 were excised and subjected to tryptic in gel digestion (Rosenfeld et al., 1992; Jeno et al., 1995). In brief, proteins were reduced with 20 mM DTT, slices washed with 100 mM ammonium bicarbonate, and proteins alkylated with 40 mM iodoacetamide (IAA). The slices were washed again and dehydrated with acetonitrile. Slices were dried in a vacuum concentrator and incubated with 400 ng sequencing grade trypsin at 37℃ overnight. The pep tide extract was dried in a vacuum concentrator and stored at -20℃. For liquid chroma tography-mass spectrometry (LC-MS) analysis, dried peptides were dissolved in 7 µl 0.1 % formic acid (solvent A). 1,7 µl were injected onto a C18 trap column (20 mm length, 100 µm inner diameter). Bound peptides

were eluted onto a C18 analytical column (200 mm length, 75 µm inner diameter, both columns from NanoSeparations, Nieuwkoop, Netherlands). Peptides were separated during a linear gradient from 0 % to 35 % solvent B (80 % acetonitrile, 0.1 % formic acid) within 40 min at a flow rate of 400 nl/min. The nano-HPLC (high-performance liquid chromatography) was coupled online to an LTQ Orbitrap Velos mass spectrometer (Thermo Fisher Scientific, Bremen, Germany). Peptide ions between 395 and 1800 m/z were scanned in the orbitrap detector with a resolution of 30,000 (maximum fill time 400 ms, AGC target 10^6). The 25 most intense precursor ions (threshold intensity 5000) were subjected to collision induced dissociation with multiple stage activation and fragments analyzed in the linear ion trap. Fragmented peptide ions were excluded from repeat analysis for 15 s. Raw data processing and analysis of database searches were performed with Proteome Discoverer software 1.3 (Thermo Fisher Scientific). Peptide identification was done with an in house Mascot server version 2.3 (Matrix Science Ltd, London, UK) and the Sequest search node in Proteome Discoverer. MS2 data was searched against mouse sequences from SwissProt (release 2012-07) and a minimized Cx43 database for increased sensitivity. Precursor ion m/z tolerance was 6.5 ppm, fragment ion tolerance 0.6 Da. b- and y-ion series were included. Semittryptic peptides with up to two missed cleavages were searched. Carbamidomethylation was set as a static modification of cysteines. The following dynamic modifications were allowed: phosphorylation of serine, threonine, and tyrosine, oxidation of methionine, and the acetylation of the protein N-terminus. The PhosphoRS2.0 node was used for scoring of the phospho-site assignment (Taus et al., 2011). Spectra with low scoring identifications and phospho-localizations were inspected manually. Mascot results from searches against SwissProt were sent to the percolator algorithm version 1.17 (Kall et al., 2008) as implemented in Proteome Discoverer 1.3.0.339.

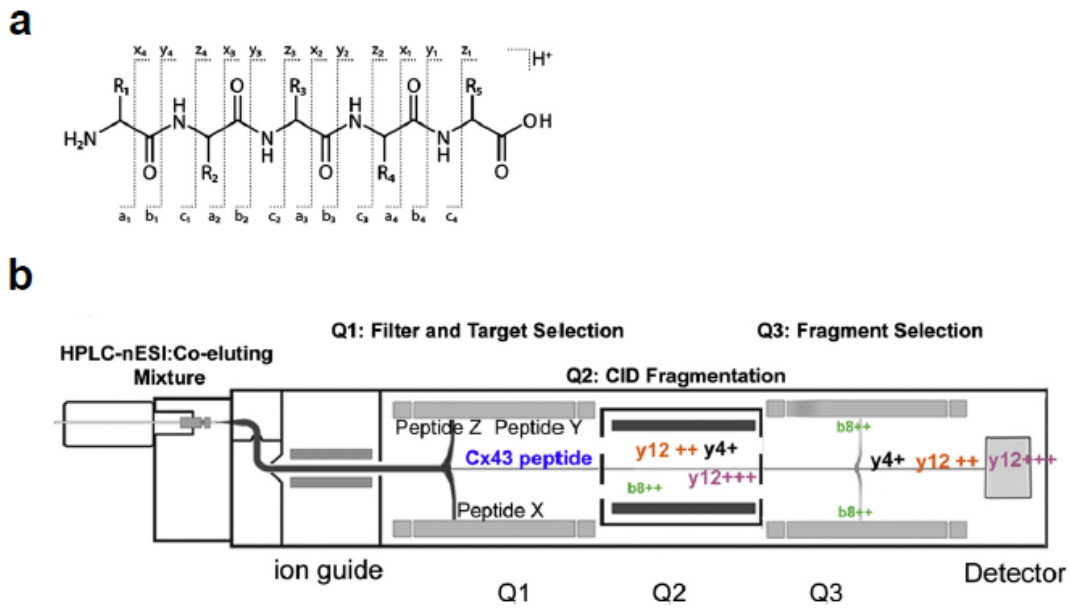

Fig. 3.2: Overview of a multiple reaction monitoring triple quadrupole (MRM-QQQ) MS experiment. a: Positional cleavage along the peptide backbone results in C-(a-, b-, and c-) or N-terminal (x-, y- and z-) ions. collision-induced dissociation (CID) experiment typically produce b- and y-ions. **b:** During an MRM run, Q1 selects peptides based on m/z for transfer to the Q2 CID collision cell. Product ions, called transitions, are then specifically selected as they pass through a Q3 isolation window. Each set of transitions at a given liquid-chromatography (LC)-elution time uniquely identifies a target protein (Chen et al., 2012, modified).

4. Results

The Cre/loxP system of site-specific recombination is a powerful tool to manipulate cell-type restricted deletions in the mouse (Nagy, 2000; Gaveriaux-Ruff and Kieffer, 2007), even though it has certain drawbacks (Schmidt-Supprian and Rajewsky, 2007) and the application of various conditional gene expressions systems are discussed with regard to their efficacy and accuracy. These include detrimental effects of Cre overexpression (Schmidt et al., 2000; Forni et al., 2006; Lee et al., 2006), spontaneous ectopic Cre activity (Eckardt et al., 2004; Korets-Smith et al., 2004) and spontaneous loss of Cre activity (Schulz et al., 2007; Requardt et al., 2009). These critical limitations required developing a reliable method of quality control in the transgenic mice.

4.1 Quality control of the widely used hGFAP-Cre and nestin-Cre transgenes

For gene deletion in the CNS, a Cre transgene driven by promoter elements of the human glial fibrillary acidic protein (hGFAP-Cre) has been used extensively (Zhuo et al., 2001). We and others have used this hGFAP-Cre transgene to study the role of astrocytic gap junction proteins (Theis et al., 2003; Theis et al., 2004; Wallraff et al., 2006; Rouach et al., 2008; Kunze et al., 2009; Maglione et al., 2010; Magnotti et al., 2011; Pannasch et al., 2011). We and others have also used a nestin-Cre transgene (Tronche et al., 1999) to delete the major astrocytic gap junction protein, Cx43 (Cina et al., 2009) or to replace the WT version with mutant versions of Cx43 (Dobrowolski et al., 2008). A previous study showed spontaneous loss of hGFAP-Cre activity in our mouse colony and developed control procedures to maintain stably active hGFAP-Cre in our animal facility (Requardt et al., 2009). Now we found that there is in addition germ-line activity of hGFAP-Cre and also of nestin-Cre, two widely used transgenes for astrocyte-directed gene deletion. Ectopic, global deletion of floxed genes occurs with high frequency, which requires an even more rigorous control. I here outline procedures to detect and minimize Cre-mediated germ-line deletion, which is essential to avoid unwanted global deletion of floxed alleles and to maintain the CNS-restricted deletion status of floxed alleles in transgenic mouse colonies.

4.1.1 PCR analysis reveals germ-line hGFAP-Cre activity in Cx43 conditional knock-out mice

In an attempt to create mice in which Cx43 still mediates gap junctional coupling but no longer adhesive interactions via its C-terminal tail (Giaume and Theis, 2010), we raised Cx43fl/K258stop: hGFAP-Cre mice carrying one Cx43K258stop allele (Maass et al., 2004) and a Cx43fl allele (Theis et al., 2001) which is deleted in the CNS by virtue of the hGFAP-Cre transgene (Theis et al., 2003). In order to express solely mutant connexins which still mediate coupling but lack adhesive function in astrocytes, we crossed these mice with Cx30 deficient mice to obtain Cx30-/-; Cx43fl/K258stop: hGFAP-Cre mice. Mice homozygous for the Cx43K258stop allele are not viable (Maass et al., 2004), similar to the perinatal lethality of the homozygous Cx43 deletion (Reaume et al., 1995; Theis et al., 2001). However, mice carrying a Cx43K258stop allele and a deleted floxed Cx43 allele (also called Cx43del allele) are viable (Maass et al., 2004). We observed that Cx43K258stop/del mice also survive when Cx30 is lacking in addition. When breeding Cx43fl/fl: hGFAP-Cre mice with Cx43fl/K258stop mice (irrespective of Cx30 deletion status), we obtained 'impossible' genotyping results from tail tip PCR, indicating the presence of a Cx43fl allele in combination with a deleted floxed Cx43 allele even when these mice did not carry the hGFAP-Cre transgene (Fig. 4.1 a). PCR strategies for identifying the Cx43 WT and Cx43K258stop allele as well as the floxed Cx43 allele and the deleted Cx43 allele are schematically depicted in Figure 4.1 b. In order to exclude genotyping errors, we next performed a PCR specific for the hGFAP-Cre transgene and a general Cre PCR (internal Cre PCR) and got consistent results with both PCRs. From 15 Cx43fl/fl: hGFAP-Cre x Cx43fl/K258stop breedings, we obtained a total of 224 mice in the offspring. In 7 of these breedings, Cre-transgenic females were used as parents, while in 8 breedings, Cre-bearing male mice were employed. A total of 114 hGFAP-Cre negative mice were among the offspring of which 38 (33 %) exhibited ectopic recombination measured by the Cx43del PCR. Of those, 34 (89 %) were offspring from Cre-bearing mothers and only 4 (11 %) were from Cre-transgenic fathers.

We went back to analyse possible ectopic hGFAP-Cre activity in Cx30-/-; Cx43fl/fl x Cx30-/-; Cx43fl/fl: hGFAP-Cre breedings. A total of 58 hGFAP-Cre negative mice were among the offspring of which 15 (26 %) exhibited ectopic recombination measured by the Cx43 del PCR. In 4 breedings, Cre-transgenic mothers were employed and in 7 breedings, Cre-transgenic fathers were used. Eight out of 16 Cre-negative animals from Cre-bearing mothers showed recombination (50 %), while only 7 out of 42 Cre-negative offspring from Cre-transgenic fathers exhibited ectopic Cre activity (17 %). We never observed mice with homozygous deletion due to the perinatal lethality of global Cx43 deletion (Reaume et al., 1995; Theis et al., 2001). We tested if the activity was due to Cre-mediated recombination or

due to spontaneous recombination of loxP sites. None out of 38 mice from Cx30-/-; Cx43fl/fl x Cx30-/-; Cx43fl/fl breedings (without hGFAP-Cre) was positive in the Cx43del PCR, disfavoring spontaneous recombination of loxP sites without recombinase. We conclude that the hGFAP-Cre transgene exhibited germ-line activity. Germ-line recombination occurred more often in the offspring of Cre-transgenic females.

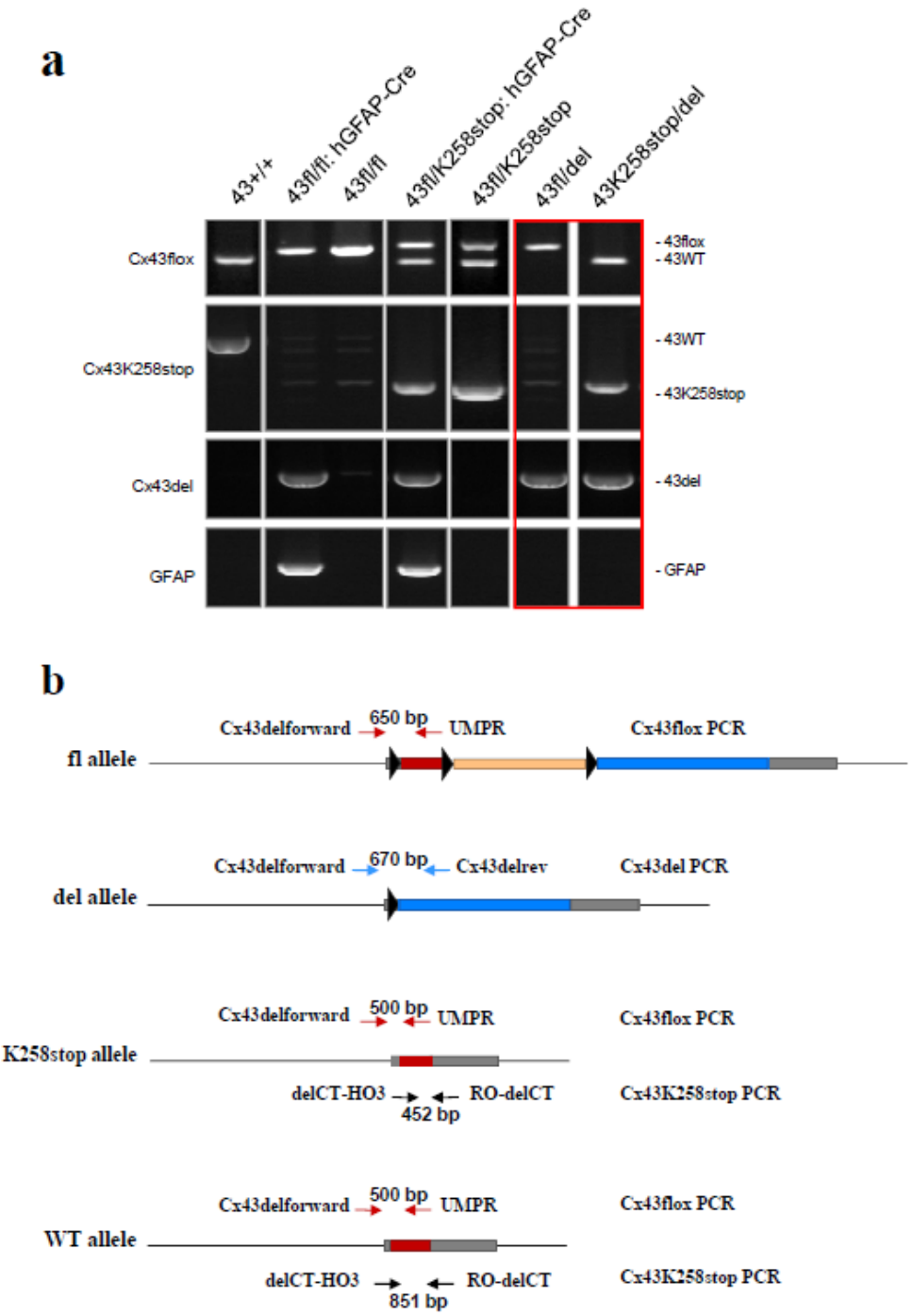

Fig. 4.1: PCR strategies for different Cx43 alleles reveal unexpected results indicative of ectopic hGFAP-Cre activity. a: Analysis of Cx43 alleles and for the presence of the hGFAP-Cre transgene by four different PCRs of offspring from Cx43fl/fl: hGFAP-Cre X Cx43fl/K258stop breedings and of WT mice. The Cx43flox PCR generated a 0.5 kb WT amplicon and, in case of Cx43fl alleles, a 0.65 kb amplicon. The Cx43K258stop PCR led to a 0.45 kb amplicon (Cx43K258stop allele) and a 0.85 kb amplicon (Cx43 WT allele). The Cx43del PCR led to a

0.67 kb amplicon (Cx43del allele). Unexpectedly, we observed mice which carried a Cx43del allele in the absence of the hGFAP-Cre transgene (red box). **b:** Scheme of Cx43 alleles. Solid boxes: transcribed regions. Dark grey boxes: 5' and 3' untranslated region. Red boxes: Cx43 coding region. Yellow box: selection marker cassette. Blue box: *lacZ* reporter gene. Arrowheads: loxP sites. Arrows: primers used for Cx43flox/WT PCR (red), Cx43del PCR (blue), and Cx43K258stop/WT PCR (black).

4.1.2 ß-Gal immunoreactivity in the CNS confirms germ-line activity of the hGFAP-Cre transgene

To confirm our PCR results, we next evaluated *lacZ* reporter gene expression by immunofluorescence staining for β-Gal in the brains of Cre-negative mice, in which the Cx43del PCR indicated germ-line deletion (Fig. 4.1 a, b). Mice lacking Cx30 in all cells of the body showed β-Gal expression representing Cx30 transcription in the granule cell layer and the leptomeninges of the cerebellum (Fig. 4.2 a), but only very weak labeling in the hippocampus (Fig. 4.2 b). Cre negative mice which show germ-line deletion of one Cx43fl allele (Cx43fl/del mice) mediated by parental Cre expression show strongly increased labeling for β-Gal in the granule cell layer and in the Purkinje cell layer of the cerebellum (Fig. 4.2 c), consistent with expression of Cx43 driven β-Gal in Bergmann glia (Theis et al., 2003; Theis et al., 2005) and highly abundant expression in the hippocampus (Fig. 4.2 d). This expression was very similar to the staining of DKO mice (Fig. 4.2 e, f).

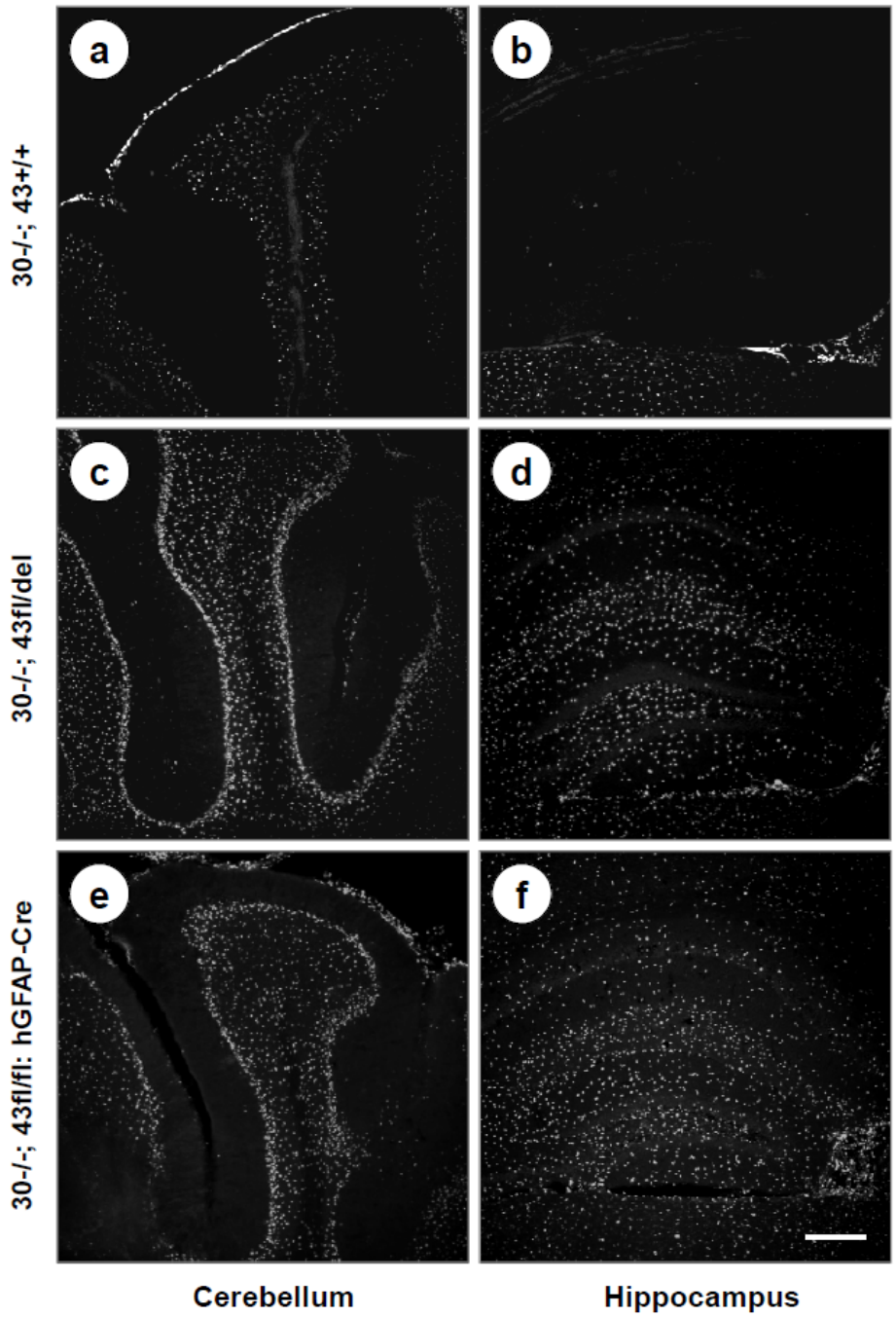

Fig. 4.2: β-Gal immunoreactivity in cerebellum and hippocampus indicates ectopic activity of the hGFAP-Cre transgene. a, b: antibody staining of Cx30-/- mice shows the distribution of β-Gal expression derived from the Cx30 locus. The β-Gal expression pattern matches that of Cx30 deficient mice (Theis et al., 2005; Gosejacob et al., 2011). Expression is moderate in the granule cell layer and leptomeninges of the cerebellum (a), and virtually absent in hippocampus (b). **c, d:** β-Gal staining of Cx30-/-; Cx43fl/del mice with ectopic deletion shows much stronger β-Gal expression in cerebellum (c) and hippocampus (d) which largely matches that of DKO mice shown below. **e, f:** β-Gal staining of Cx30-/-; Cx43fl/fl: hGFAP-Cre mice show the distribution of β-Gal expression derived from the Cx43 locus and the Cx30 locus. The β-Gal expression is strong both in cerebellum (e) and hippocampus (f). Bar: 200 µm.

4.1.3 ß-Gal expression is colocalized with the astrocytic marker GFAP in the dentate gyrus of animal with germ-line deletion

Since β-Gal immunoreactivity from the Cx30 knock-out disturbed the analysis of Cx43 driven β-Gal expression, we next tested mice which carried Cx30 WT alleles: Cx43/Cx30 WT mice were negative for β-Gal (Fig. 4.3 a). The β-Gal immunoreactivity of deleted floxed Cx43 mice (Cx43fl/del), i. e. with germ-line deletion of one Cx43fl allele, showed localization in cells which were positive for the astrocytic marker GFAP (Fig. 4.3 b).

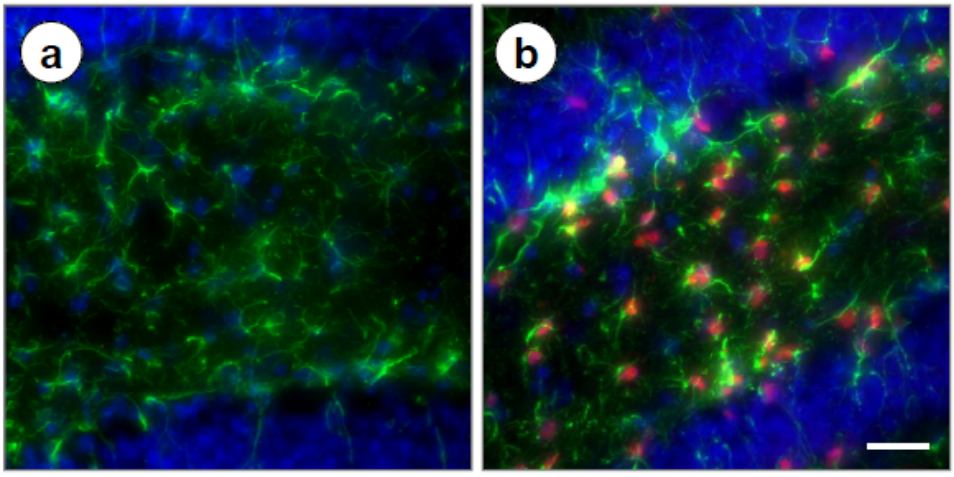

Fig. 4.3: Double immunofluorescence staining for GFAP and β-Gal in the dentate gyrus. a: WT animals show absence of β-Gal expression in the dentate gyrus. **b:** Cx43fl/del animal with germ-line deletion showing abundant β-Gal expression colocalized with the astrocytic marker GFAP similar to DKO mice. Scale bar: 50 µm.

4.1.4 ß-Gal immunoreactivity occurs even in the absence of hGFAP-Cre immunoreactivity in mice with germ-line deletion

In the next step, we correlated Cre expression with Cx43 ablation *in situ* by immunofluorescence detection of Cre recombinase and of β-Gal in cerebellar and hippocampal cryosections. WT mice were negative both for β-Gal and Cre (Fig. 4.4 a, b). Mice lacking Cx30 showed Cx30 driven β-Gal expression in the cerebellum, very weak labeling in the hippocampus and were likewise Cre negative (Fig. 4.4 c, d). Mice which experienced germ-line deletion of one Cx43fl allele showed strong immunoreactivity for β-Gal, but lacked Cre immunoreactivity (Fig. 4.4 e, f). Immunoreactivity for β-Gal was very similar in DKO mice lacking both Cx43 and Cx30, which showed robust Cre immunoreactivity (Fig. 4.4 g, h), in contrast to the mice with germ-line deletion which show no Cre immunoreactivity (Fig. 4.4 e, f).

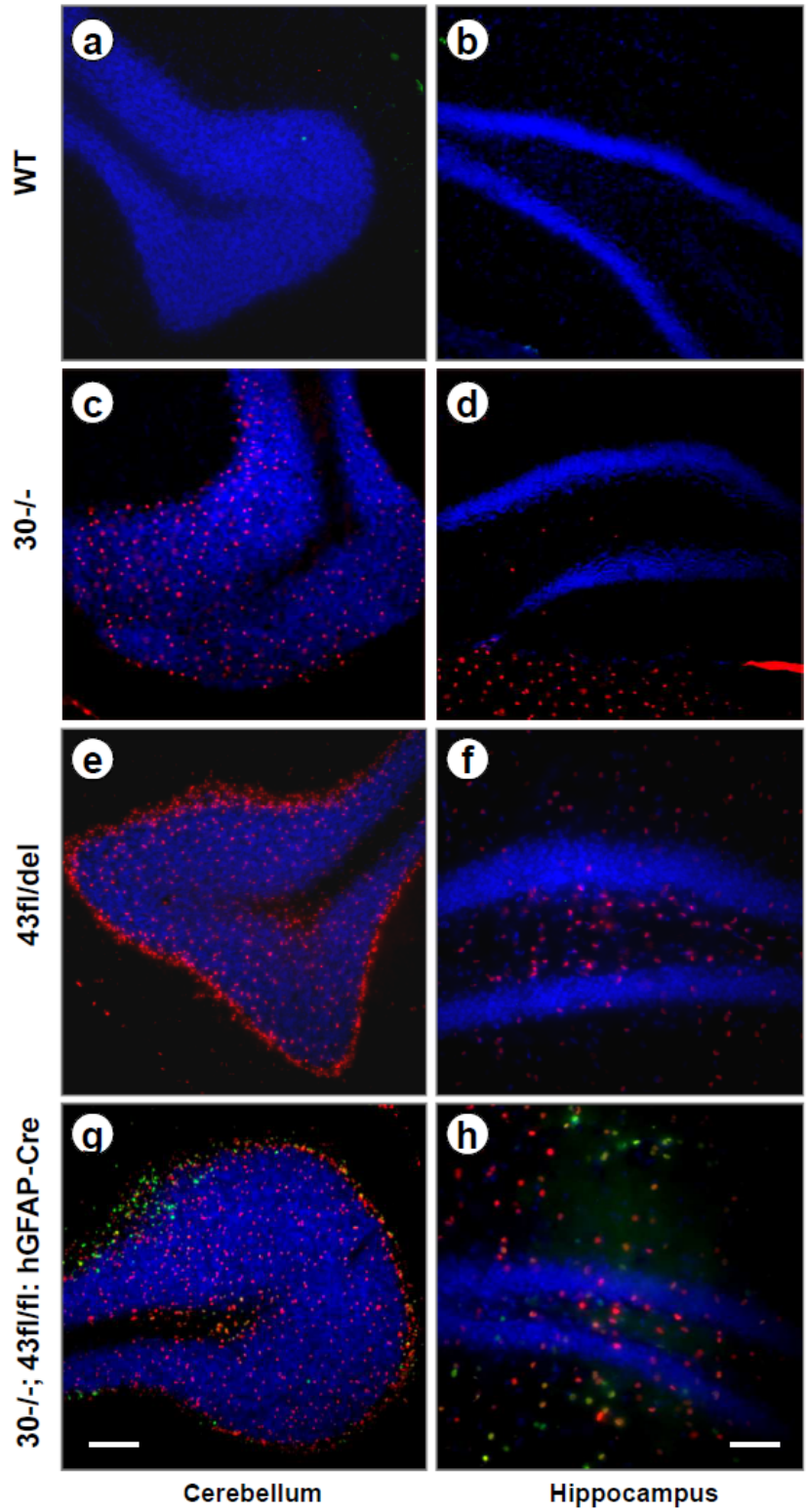

Fig. 4.4: Cx43-driven β-Gal immunoreactivity occurs even in the absence of Cre immunoreactivity in mice with ectopic deletion. a-h: Immunofluorescence analysis for Cre expression (green) and β-Gal (red). Hoechst staining in blue. a, c, e, g: Cerebellum. b, d, f, h: Hippocampus. **a, b:** WT mice express neither β-Gal nor Cre protein. **c, d:** Cx30-/- mice show moderate β-Gal expression in cerebellum and very weak expression in hippocampus. **e, f:** Cx43fl/del mice exhibit strong immunoreactivity for β-Gal in both brain areas, but no Cre expression. **g, h:** DKO mice show β-Gal immunoreactivity essentially identical to mice with ectopic deletion and prominent expression of Cre in both brain areas. Bar: 100 µm (50 µm for f and h).

4.1.5 Immunoblot analysis confirms loss of Cx43 expression in the absence of Cre protein

Immunoblot analysis of hippocampal lysates confirmed that Cx43K258stop/del mice with germ-line deletion of Cx43 indeed have lost immunoreactivity for the full length Cx43. The Cx43 antibody used detected the C-terminus of Cx43, which is lacking in the truncated Cx43K258stop form. WT mice and mice carrying Cx43fl alleles show Cx43 expression with an antibody directed to the C-terminus at a Mw of 43 kDa (upper row), but lack immunoreactivity for an N-terminal Cx43 antibody at a Mw of 28 kDa (corresponding to the Cx43K258stop protein; second row). Cx43fl/fl: hGFAP-Cre mice show strongly decreased expression of Cx43 at 43 kDa, corresponding with their immunoreactivity for Cre in hippocampal lysates (third row). Cx43fl/fl mice show less abundant Cx43 protein expression compared to WT mice due to the targeted modification of the Cx43 locus, as already reported (Theis et al., 2001). Consistently, in deleted floxed Cx43 mice (Cx43fl/del; green box in Fig. 4.5), immunoreactivity for Cx43 is further reduced by about 50% due to loss of one Cx43fl allele in spite of the absence of Cre protein. Mice carrying the Cx43K258stop allele show immunoreactivity for the 28 kDa truncated protein with the N-terminal antibody and, depending on the presence of a Cx43fl allele, immunoreactivity for the full length Cx43 protein at 43 kDa. Cx43fl/K258stop: hGFAP-Cre mice show strongly decreased immunoreactivity for the full length Cx43 protein, corresponding with immunoreactivity for Cre, while the levels of the truncated protein are not changed compared to Cx43fl/K258stop mice lacking Cre. No Cre protein is expressed, but immunoreactivity for the full length Cx43 is completely lost in deleted floxed Cx43 (Cx43K258stop/del mice; red box in Fig. 4.5). We here demonstrate with *in situ* immunolocalization and immunoblotting that ectopic activity occurs frequently in Cx43fl/fl x Cx43fl/fl: hGFAP-Cre breedings and in Cx43fl/K258stop x Cx43 fl/fl: hGFAP-Cre breedings. This happens even in the absence of Cre protein, indicating germ-line recombination mediated by hGFAP-Cre.

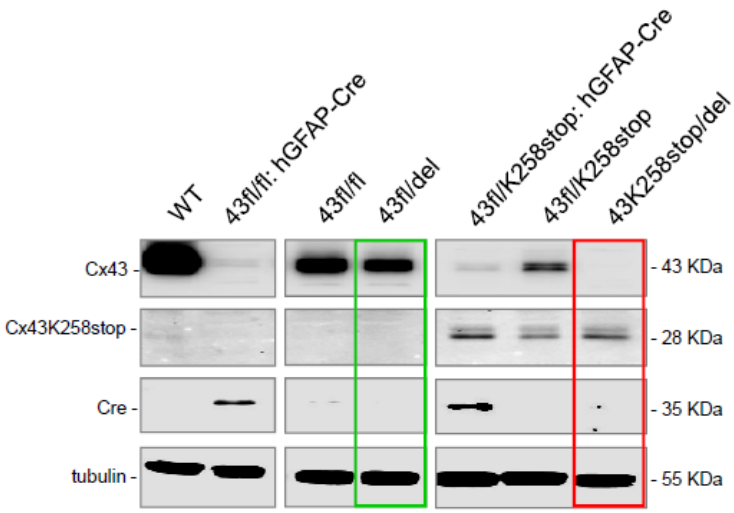

Fig. 4.5: Immunoblot analysis of hippocampal lysates for Cre and Cx43 protein indicates loss of Cx43 expression in the absence of Cre protein. In Cx43fl/del mice (green box), immunoreactivity for Cx43 is reduced by about 50% compared to Cx43fl/fl mice. Immunoreactivity for the full length Cx43 is completely lost in Cx43K258stop/del mice (red box). Please note absence of Cre immunoreactivity in the Cx43fl/del and Cx43K258stop/del lanes, consistent with negative PCR results for hGFAP-Cre and internal cre PCRs. Upper row: Cx43 immunoreactivity at 43 kDa (full length protein, Cx43) with an antibody directed to the C-terminus. Second row: Cx43 immunoreactivity at 28 kDa (truncated protein, Cx43K258stop) with an antibody directed to the N-terminus. Third row: Immunoreactivity for the Cre recombinase (Cre). Fourth row: Tubulin loading control. WT: Cx43+/+. 43 fl/fl; hGFAP-Cre: Cx43fl/fl: hGFAP-Cre. 43fl/fl: Cx43fl/fl. 43fl/del: Cx43fl/del. 43fl/K258stop; hGFAP-Cre: Cx43fl/K258stop; hGFAP-Cre. 43fl/K258stop: Cx43fl/K258stop. 43K258stop/del: Cx43K258stop/del. KDa: Kilodalton.

4.1.6 Germ-line activity of the hGFAP-Cre transgene in the heart

Besides astrocytes and leptomeningeal cells in the CNS, Cx43 is also prominently expressed in the heart (Reaume et al., 1995), and likewise Cx43-driven β-Gal reporter expression has been demonstrated in the heart (Theis et al., 2001). Any germ-line activity mediated by hGFAP-Cre in the zygote or early embryo should therefore as well lead to recombination in the adult heart, an organ which is not targeted by hGFAP-Cre (Zhuo et al., 2001). We therefore investigated heart sections of mice with germ-line deletion of Cx43 for β-Gal activity by X-gal staining (Fig. 4.6). WT mice lack β-Gal (Fig. 4.6 a). By contrast, hGFAP-Cre negative offspring from Cx43fl/fl: hGFAP-Cre x Cx43fl/K258stop breedings carrying the deleted floxed Cx43 (Cx43fl/del) genotype, i.e. showing germ-line deletion, exhibited prominent β-Gal activity in the heart visualized by X-gal staining which was localized to the nucleus (the engineered β-Gal contained a nuclear localization signal). Together with Mrs. Alexandra Klein, we also assessed Cx43 immunoreactivity in heart sections of Cx43K258stop/del mice from the same breedings, using an antibody directed to the 20 C-terminal amino acids of Cx43 which are lacking in the truncated variant of Cx43. While we

obtained typical labeling of gap junction plaques in the intercalated discs between ventricular cardiomyocytes of WT mice (Fig. 4.6 c, e; Maass et al., 2004), we did not observe any labeling in heart sections of Cx43K258stop/del mice using this antibody (Fig. 4.6 d, f), confirming germ-line deletion of full length Cx43 by parental hGFAP-Cre protein. Similarly, we observed loss of immunoreactivity for the C-terminal epitope of Cx43 concomitant with gain of β-Gal immunoreactivity in the hippocampus of Cx43K258stop/del mice when compared to WT mice (Fig. 4.6 g, h).

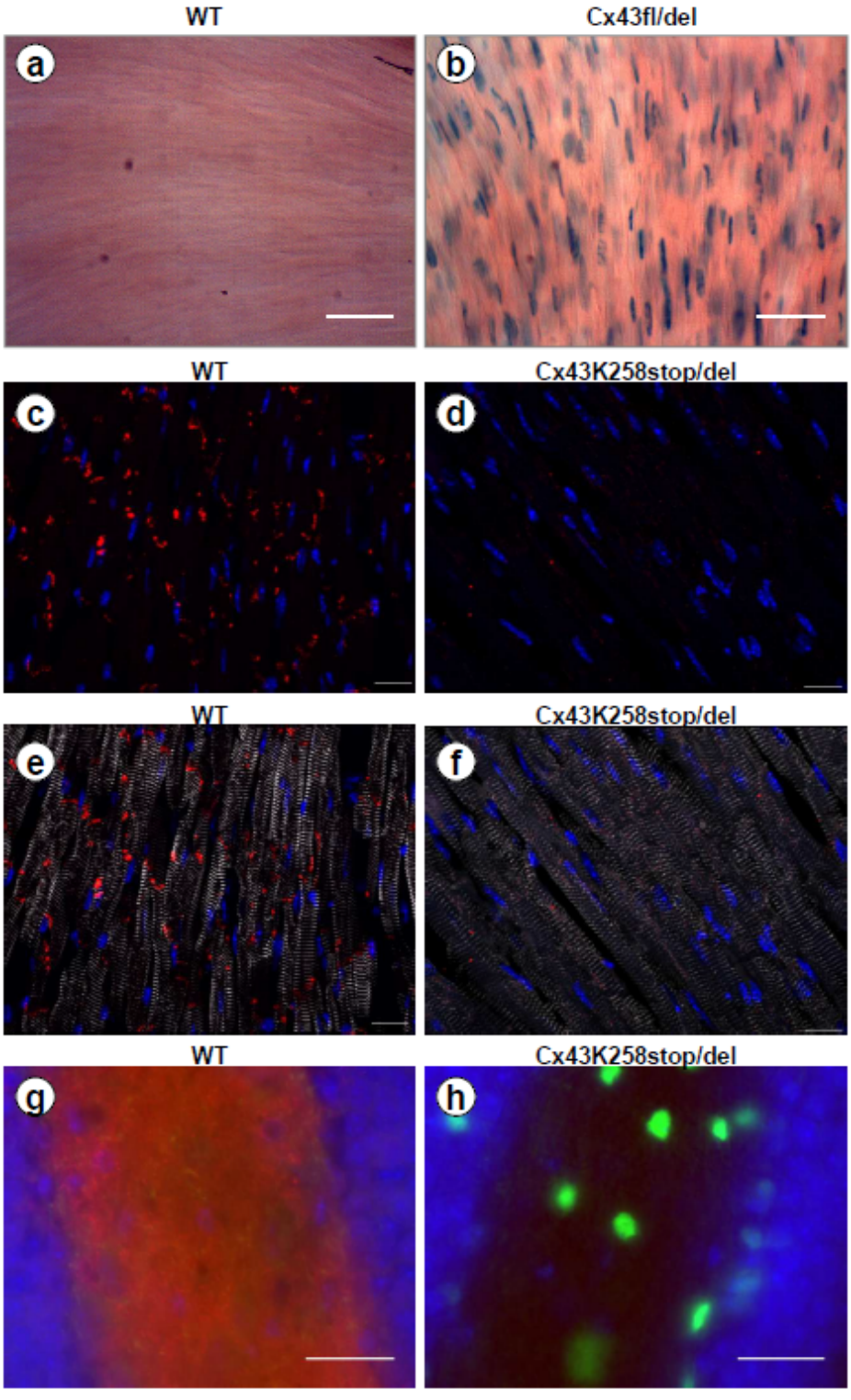

Fig. 4.6: Ectopic activity of the hGFAP-Cre transgene in the heart and brain. a, b: X-gal staining of sections from the left ventricle. WT mice do not show X-gal staining (a), while Cx43fl/del mice derived from Cx43fl/fl: hGFAP-Cre x Cx43fl/K258stop breedings exhibit β-Gal activity which is confined to the nucleus of cardiomyocytes (b). **c, d** and **e, f:** Antibody staining of sections from the left ventricle with an antibody directed to the 20 C-terminal amino acids of Cx43 (red) together with Hoechst nuclear stain (blue). e and f show additionally an antibody directed to sarcomeric α-actinin (white). WT mice show prominent labelling of gap junctional plaques at intercalated disks between cardiomyocytes (c and e), while Cx43K258stop/del mice lack immunoreactivity, consistent with absence of the Cx43 C-terminus (d and f). **g, h:** Triple staining for the Hoechst nuclear stain (blue), β-Gal (green) and the C-terminal epitope of Cx43 (red). WT mice show prominent Cx43 expression in the hilus of the dentate gyrus and no β-Gal expression (g). By contrast, Cx43K258stop/del mice do not show immunoreactivity for the C-terminal epitope of Cx43 but show strong β-Gal expression, consistent with deletion of the Cx43fl allele (h). Bar: 50 µm for A and B, 20 µm for c-f and 25 µm for g and h.

4.1.7 EGFP immunoreactivity in hippocampal dentate gyrus and CA1 region indicates germ-line activity of the nestin-Cre transgene

We have recently investigated conditional knock-in mice with a replacement of WT Cx43 by the Cx43G138R point mutation (Dobrowolski et al., 2008) directed to astrocytes via a nestin-Cre transgene (Tronche et al., 1999). In these mice, Cre-mediated recombination leads to expression of the Cx43G138R point mutation together with EGFP. Germ-line nestin-Cre activity in Cx43G138R point mutated mice was assessed by negativity for both the nestin-Cre PCR and the internal cre PCR and GFP immunostaining (Fig. 4.7 a-f). In 4 out of 14 Cre-negative mice investigated, we observed eGFP-reporter expression in the hippocampus, indicating ectopic deletion mediated by nestin-Cre (Fig. 4.7 e, f). Thus, germ-line Cre activity occurs in the CNS-restricted nestin-Cre transgene as well.

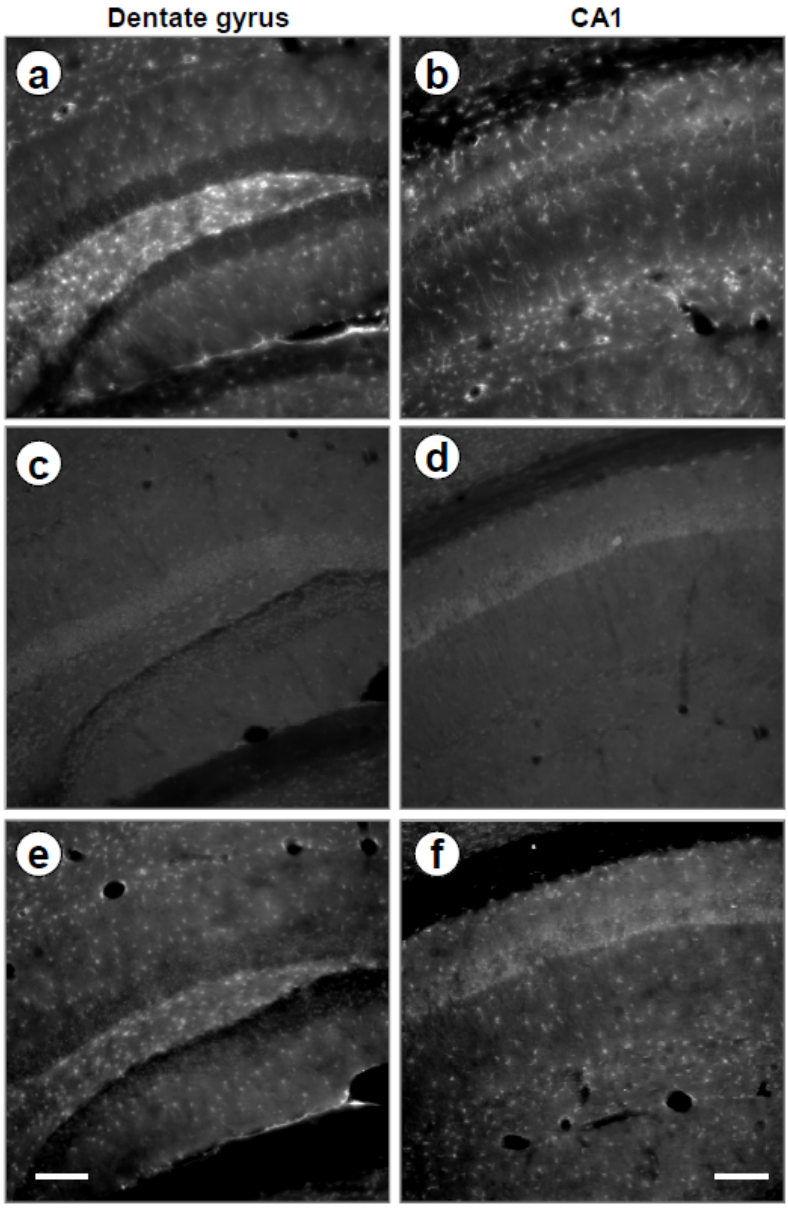

Fig. 4.7: GFP immunoreactivity in hippocampal dentate gyrus and CA1 region indicates ectopic activity of the nestin-Cre transgene. a, b: Chicken anti-GFP antibody staining of Cx30-/-; Cx43flG138R/flG138R: nestin-Cre mice show the distribution of EGFP expression under control of Cx43 regulatory elements. Expression is stronger in the dentate gyrus (a), especially in the hilus, compared to the CA1 region (b). **c, d:** Cx30-/-; Cx43flG138R/flG138R mice exhibit no immunoreactivity for GFP in both hippocampal regions. **e, f:** Cx30-/-; Cx43flG138R/flG138R mice with ectopic activity of nestin-Cre in the parents show GFP staining in the dentate gyrus (e) and the CA1 region (f) with similar density as in Cx30-/-;Cx43flG138R/flG138R: nestin-Cre mice. Bar: 100 µm.

4.1.8 Assessment of germ-line hGFAP-Cre activity in testis and ovary

To investigate the possibility of a germ-line recombination (deletion) underlying the phenomenon of germ-line expression of hGFAP expression, the following experiment was performed: analysis of a Cre induced germ cell recombination using β-Gal

immunofluorescence in combination with either a (testicular) Sertoli cell-specific marker (TIF-2) and/or a germ cell-specific marker (VASA).

Human TIF2 (hTIF2) is a member of the p160 family of nuclear receptor coactivators and TIF2-/- mice are viable, but fertility of both sexes is impaired (Gehin et al., 2002). Testicular TIF2 expression is Sertoli cell-specific and appears to be essential for adhesion of somatic Sertoli cells to germ cells (Gehin et al., 2002; Mark et al., 2004; Ye et al., 2005).

Characterization of germ cells was conducted using Vasa, a member of the DEAD box helicase family (alternative names: DDX4 or MVH). Vasa as a known specific marker for germ cells in general is localized in the cytoplasm or perinuclear region of male and female germ cells (Castrillon et al., 2000; Toyooka et al., 2000; Tanaka et al., 2000).

Testes from genotyped transgenic prepubertal male mice (day 9 post partum (p9)) showed no morphological differences (data not shown). Neither in male transgenic mice of prepubertal (data not shown) and adult (Fig. 4.8 a-f) nor in adult female transgenic mice (Fig. 4.8 g-i), any germ cells could be found “deleted / recombined” using immunofluorescence stainings. By means, spermatogonia, spermatocytes, spermatids as well as all stages of oocyte development remained immunonegative for β-Gal (Fig. 4.8 a-i). However, it cannot be excluded that recombination of one floxed Cx43 allele occurred during fetal gonadal development, which is in line with the fertility of the parents.

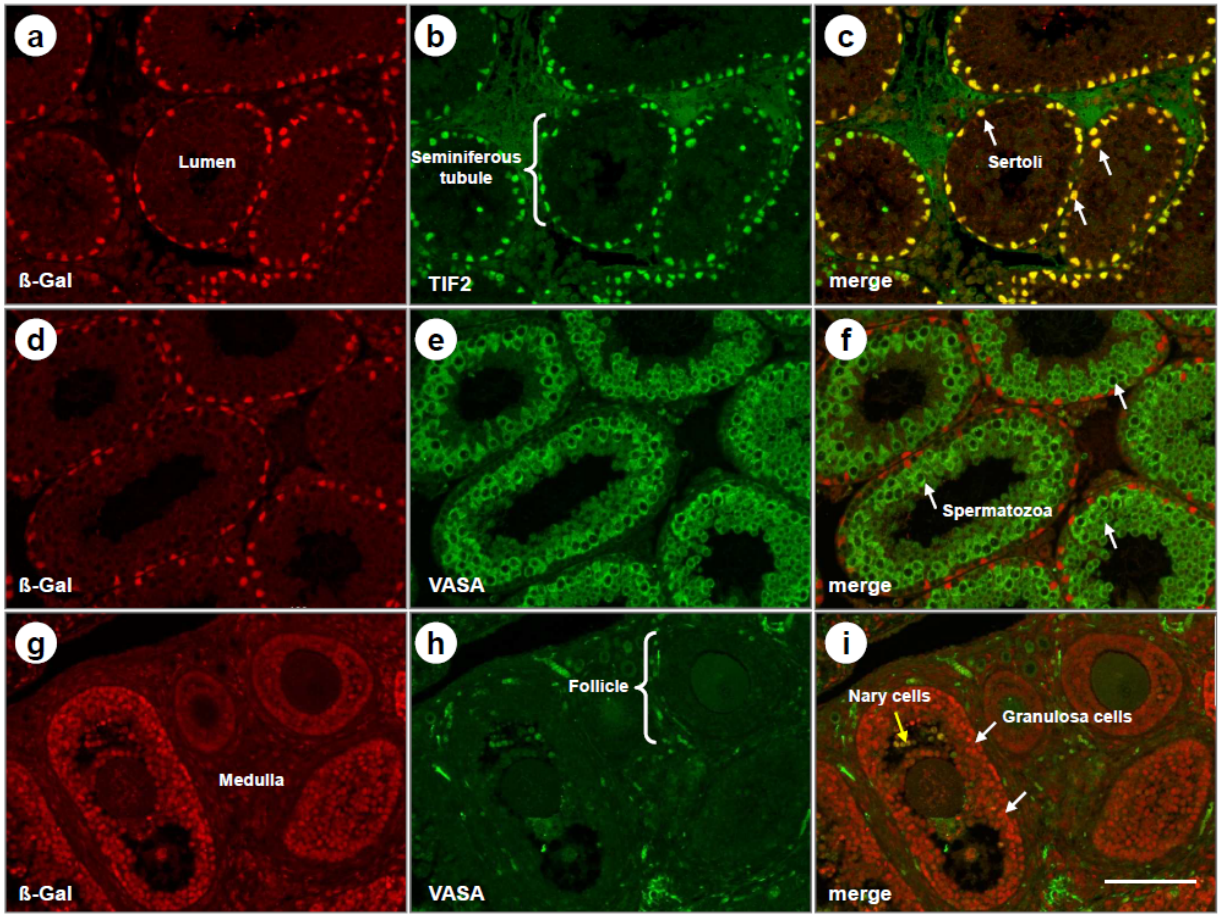

Fig. 4.8: Double immunofluorescence staining in adult Cx43/del mice testis and ovary (p35). a-c: ß-Gal and TIF2 double-labelling showed that only somatic Sertoli cells (TIF2-positive, white arrow) were immunoreactivity for ß-Gal but not in germ cells. **d-f:** Somatic Sertoli cells showed a nuclear labelling for β-Gal but no cytoplasmic immunoreaction for VASA. Germ cell nuclei (white arrow) were always immunonegative for β-Gal but immunopositive in the cytoplasm for VASA, indicating germ cells were not "deleted/recombined". **g-i:** In ovaries predominantly somatic follicle cells (white arrow) showed a nuclear immunoreaction for β-Gal, whereas different generations of oocytes showed a characteristic staining for VASA but remained immunonegative for β-Gal. Nary cells (yellow arrow) showed a double-labelling for both markers. In adult Cx43/del female mice no oocytes had been found "deleted/recombined". Identification of oocytes was performed with VASA. Bar: 100 µm.

4.2 Functional insights of astroglial Cx30 and Cx43 in adult hippocampal neurogenesis

In the SGZ of the adult DG, astrocytes with RG-like morphology are considered putative neural stem cells (Kempermann et al., 2004). The mechanisms that regulate RG-like precursor proliferation to new neuron maturation, synaptic integration and survival are not clearly understood. However, the local environment in the neurogenic niche may be required for the control of proliferation and differentiation of adult neural precursor in the DG (Li and Xie, 2005; Ninkovic and Gotz, 2007; Morrison and Spradling, 2008; Suh et al., 2009). One possible molecular pathway by which they receive signals is coupling through gap junctions. Gap junctional channels are comprised of connexins. Astrocytic connexins are involved in metabolite supply of neurons and extracellular K^+ homeostasis, thus modulating neuronal activity (Wallraff et al., 2006; Rouach et al., 2008). In the DG, Cx30 and Cx43 are expressed in RG-like cells of the SGZ. Mice lacking Cx30 and Cx43 displayed almost complete inhibition of proliferation and a significant decline in numbers of RG-like cells and granule neurons. This data clearly showed astroglial Cx43 and/or Cx30 are required for adult neurogenesis (Kunze et al., 2009).

4.2.1 Cx43, but not Cx30, is crucial for hippocampal adult neurogenesis

Previous single cell RT-PCR data showed that RG-like cells express three distinct connexin isoforms in the SGZ with Cx43 being most abundant, followed by Cx30 and Cx26. In the SGZ a significant proportion of RG-like cells are gap junction coupled, predominantly via Cx43 and Cx30. Ablation of these two majority astroglial connexins within RG-like cells leads

to strongly impaired neurogenesis in the DG (Kunze et al., 2009). However, it has not been clearly demonstrated which connexin is crucial for adult hippocampal neurogenesis. One recent study showed that gap junctional coupling of glomerular astrocytes is reduced after Cx30 ablation but not in Cx43 knock-out mice, indicating that Cx30 formed channels are the molecular targets of neuronal activity dependent modulation for olfactory information processing (Roux et al., 2011).

4.2.1.1 Constitutive ablation of Cx30 has no impact on proliferation and neurogenesis assessed by Ki67, Prox1 and BLBP immunostaining

To compare the role of Cx30 and Cx43 in adult hippocampal neurogenesis we performed NeuN and Ki67 immunostainings in Cx30-/- and Cx43fl/fl: hGFAP-Cre mice. NeuN is a neuronal specific nuclear antigen, which is present in most CNS and PNS neuronal cell types of all vertebrates (Mullen et al., 1992). NeuN immunoreactivity becomes obvious as neurons mature, a marker seen in the late stages of neuronal development. The name Ki67 is derived from the city of origin (Kiel, Germany) and the number of the original clone in a 96-well plate (Gerdes et al., 1983). Ki67 as endogenous proliferation marker is expressed in all phases of the cell cycle except the resting phase and at the beginning of the G1 phase (Zacchetti et al., 2003).

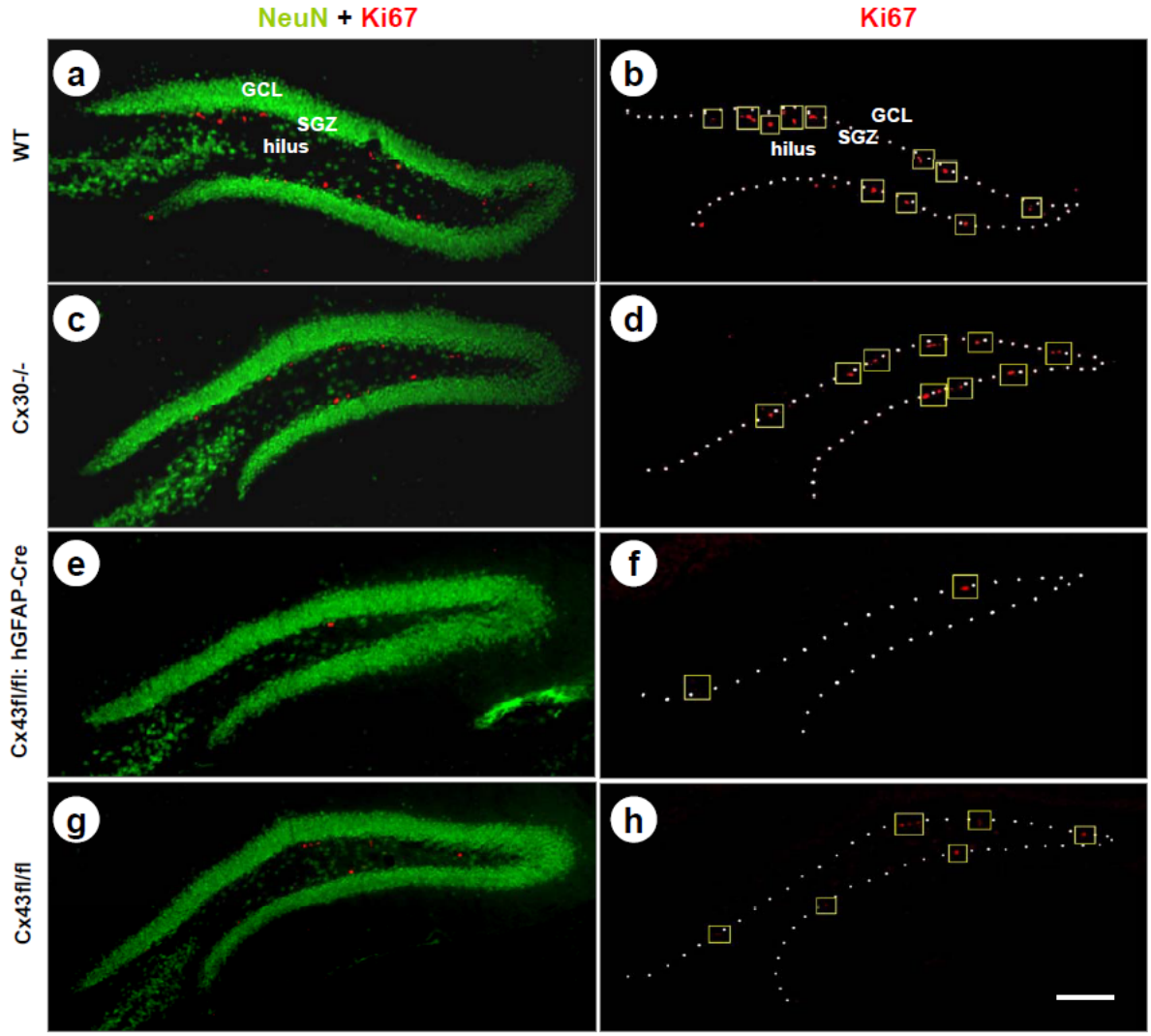

Fig. 4.9: Reduced proliferation in the SGZ of Cx43fl/fl: hGFAP-Cre and Cx43fl/fl mice, but not Cx30-/- mice (p60). a-h: Double immunostaining for NeuN (green) and Ki67 (red) in the DG of WT (a, b), Cx30-/- (c, d), Cx43fl/fl: hGFAP-Cre (e, f) and Cx43fl/fl mouse (g, h). The coronal slices represent approximately the same z-position in rostrocaudal extension of the hippocampus, respectively. Ki67-positive cells were framed in yellow scale in the same section (b, d, f and h) as in (a, c, e and g), indicated lower proliferative activity in the Cx43fl/fl: hGFAP-Cre (e, f) and Cx43fl/fl mouse (g, h), but not Cx30-/- (c, d) mouse. Dotted lines indicate the border between SGZ and GCL. Bar: 100 µm.

In addition, to investigate whether lack of Cx30 or Cx43 directly affects neurogenesis, Prox1 immunostaining was performed in DG of adult mice. Prox1, a prospero-related homeobox gene (Oliver et al., 1993), is expressed in DG granule cells throughout embryonic development and into adulthood. Prox1 is sequentially required for maturation and survival of new neurons in the adult hippocampus (Lavado et al., 2010). Therefore, Prox1 is commonly used as a specific marker for newborn neurons in the DG (Jessberger et al., 2008).

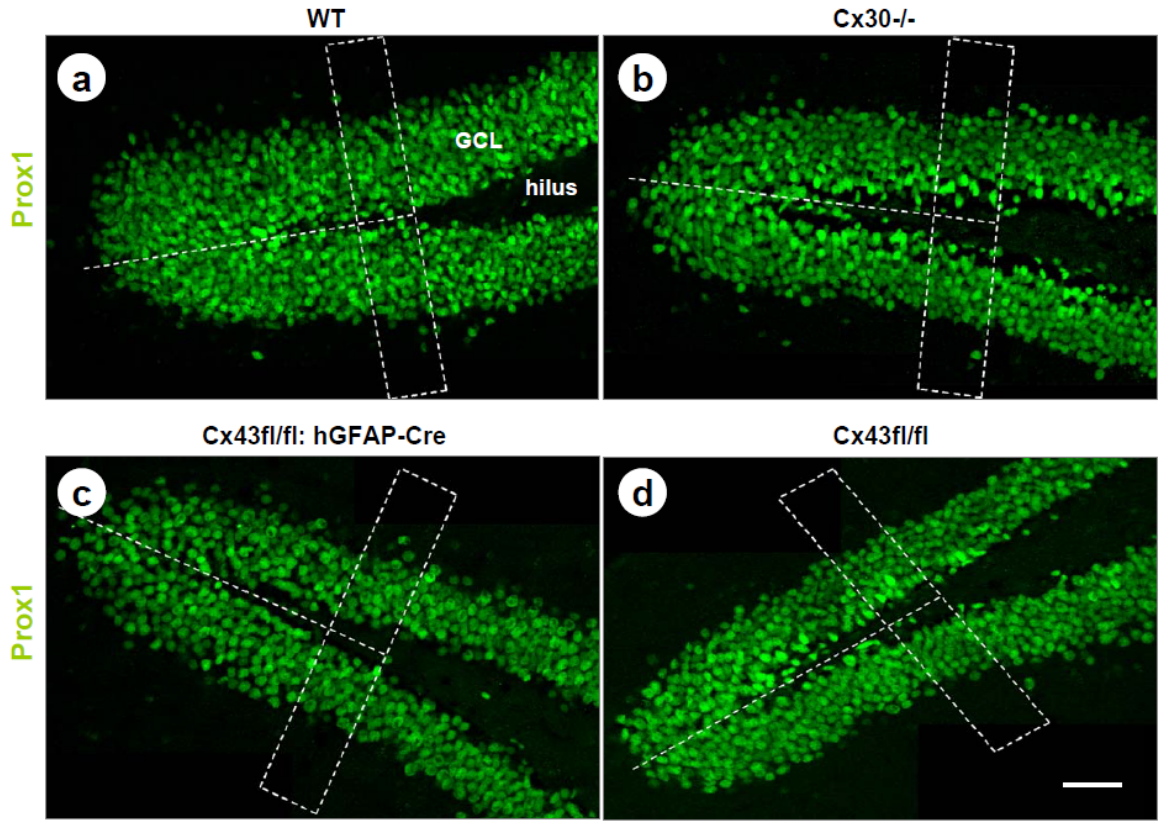

Fig. 4.10: Decreased granular cell numbers in the DG of Cx43fl/fl: hGFAP-Cre and Cx43fl/fl mice, but not Cx30-/- mice (p60). Confocal images of Prox1 immunostaining on the DG of WT (a), Cx30-/- (b), Cx43fl/fl: hGFAP-Cre (c) and Cx43fl/fl mouse (d). Reduced numbers of Prox1-positive cells were observed in Cx43fl/fl: hGFAP-Cre and Cx43fl/fl mouse vs. Cx43WT animal. Frames in (a-d) indicate counting boxes (150 x 50 x 4 μm^3). Bar: 50 µm.

To get a first hint as to whether Cx30 deletion affected the number or arrangement of RG-like cells in the adult DG, expression of the RG marker, brain lipid-binding protein (BLBP), was assessed in mutated mice versus control animals at p60. BLBP is transiently expressed during fetal brain development (Feng et al., 1994) and actively blocks differentiation, presumably as a direct target gene of Notch signalling in RG cells (Anthony et al., 2005). Except RG-like cell (type-1) BLBP are also expressed in type-2 cell but label only a small percentage of the proliferating cells (Steiner et al., 2006). The number of BLBP-positive RG-like cells in the SGZ of Cx30-/- mice was not significantly decreased compared to controls (Fig. 4.11).

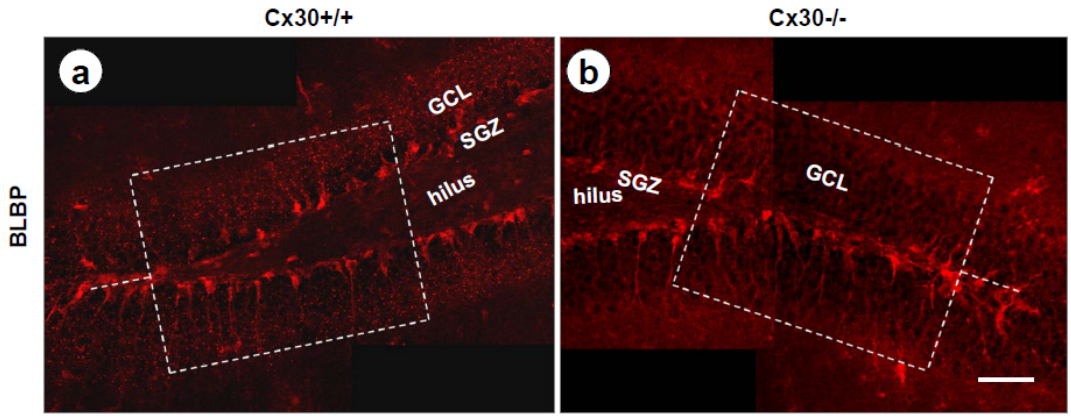

Fig. 4.11: BLBP-positive cell numbers were similar between Cx30+/+ and Cx30-/- mice (p60). Representative images revealed similar numbers of BLBP labeled cells in the SGZ of Cx30+/+ control (a) and Cx30-/- mice (b). Frames indicate counting boxes (220 x 170 x 30 µm^3). Scale bar: 50 µm.

These findings indicated that only Cx43, but not Cx30, is crucial for proliferation, neurogenesis and RG-like cell numbers in the DG. Quantitative data is summarized in Figure 4.12.

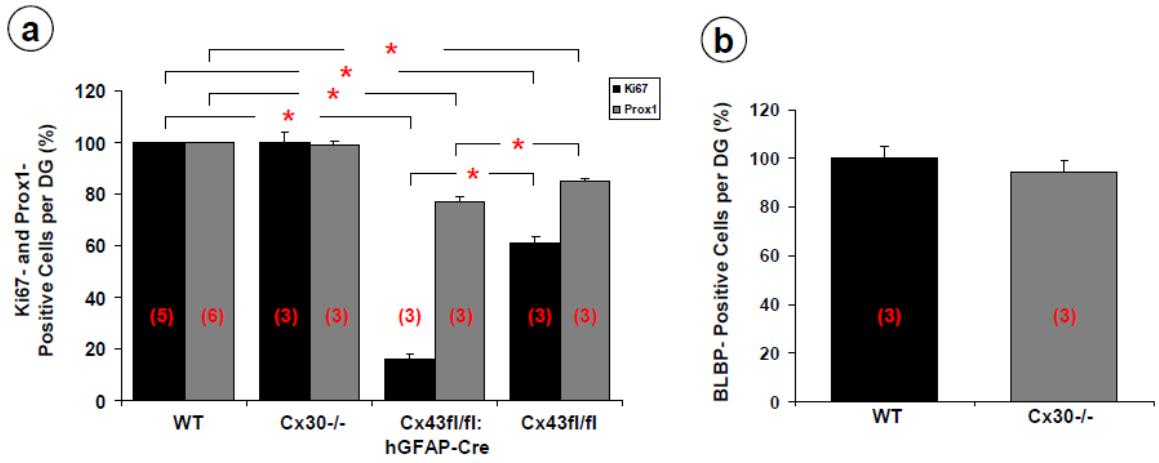

Fig. 4.12: Deletion of Cx30 in astroglial cells has no impact on adult neurogenesis (p60). a: Complete deletion of Cx43 in astrocytes led to a strong reduction of Ki67-positive nuclei to 83 % in the SGZ and a significant decrease in the number of granule neurons to 21 % as compared with WT mice. In addition, comparative counting of Ki67- (35 %) and Prox1- (13 %) labelled cells demonstrated significant lower number in Cx43fl/fl mice vs. WT mice. However, in the Cx30-/- mice i observed a similar number of Ki67- and Prox1-positive cells in comparison to WT, indicating the proliferation and neurogenesis in Cx30-/- mice remained unchanged. **b**: The number of BLBP-positive cells were very similar between Cx30-/- and WT mice. Significant differences are indicated by asterisk. Significance level was set at $P < 0.05$ (Mann-Whitney U-test and Kruskal-Wallis H-test). Number of animals in each group is shown in brackets.

4.2.1.2 Cx43 is not upregulated after Cx30 ablation in the hippocampus

Former studies demonstrated that specific deletion of Cx43 in astrocytes of Cx43fl/fl: hGFAP-Cre mice can lead to the compensatory up-regulation of Cx30 (Theis et al., 2003; Nakase et al., 2004; Unger et al., 2012). More recently, gene deletion of Cx30 led to almost total elimination of immunofluorescence labelling for Cx26 in astrocytes of brain parenchyma and down-regulation of Cx26 mRNA in the brain. Moreover, ablation of astrocytic Cx30 resulted in the loss of its coupling partner Cx32 on the oligodendrocyte side of astrocyte-oligodendrocyte (A/O) gap junctions (Lynn et al., 2011). To assess whether compensatory up-regulation of Cx43 after Cx30 deletion would likewise lead to unaltered adult neurogenesis between WT and Cx30-/- mice, we determined Cx43 protein levels in the hippocampus of WT and Cx30-/- mice by Western blot analysis. Importantly, by immunoblot we did not observe any increased Cx43 protein expression upon ablation of Cx30 when compared to WT controls (n = 4; Fig. 4.13). In contrast to Cx43, Cx30 protein levels were very low in the hippocampus of WT mice and completely absent in Cx30-/- mice, as we expected. Combining results of immunolabelling with immunoblotting, we demonstrate that significantly reduced proliferation and neurogenesis in Cx43fl/fl: hGFAP-Cre and Cx43fl/fl mice, but not in Cx30-/- mice might be a direct effect of ablation or mutation of Cx43, indicating that astrocytic Cx43, but not Cx30, is crucial for hippocampal adult neurogenesis.

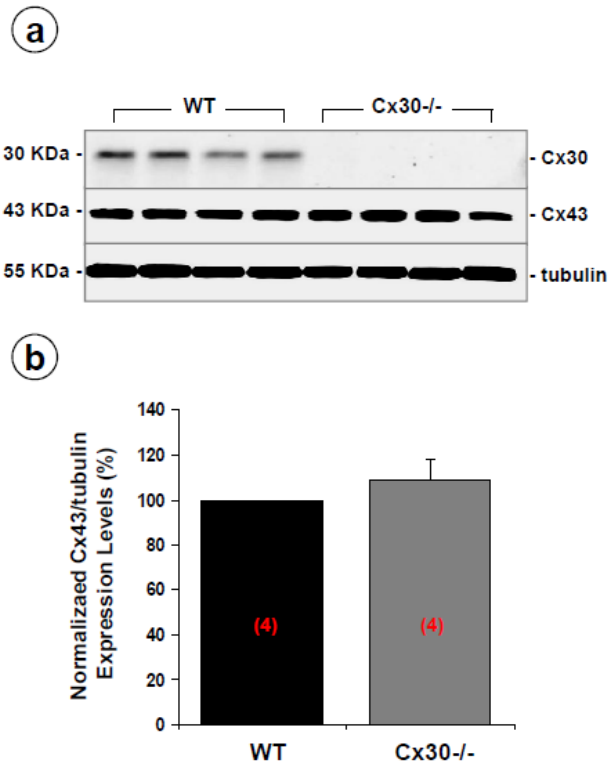

Fig. 4.13: Hippocampal immunoblot with antibodies directed to Cx30 and Cx43. a: In WT mice, a band occurred at 30 KDa but not in Cx30-/- mice. Cx43 antibody detected a band at 43 KDa in both genotypes. Tubulin was used as a loading control. **b:** Quantitative analysis of Cx43 expression. Relative expression levels of Cx43

are shown normalized to tubulin levels; Cx43 expression in WT is set to 100 %. Changes were not statistically significant. Significance level was set at $P < 0.05$ (student's t-test).

4.2.1.3 BrdU incorporation and fate mapping in the DG of Cx30-/- mice

To confirm Ki67 immunostaining results and compare the proliferative activity we analyzed the incorporation of BrdU into the SGZ of Cx30-/- mice, 2 h and 4 weeks after last BrdU administration. BrdU labeling can be visualized with immunocytochemical techniques and does not require autoradiography. This technique allows stereological estimation of the total number of cells as well as demonstration that the new cells express markers of specific cell types. To study the fate of proliferating cells we performed BrdU, Prox1 and Doublecortin (DCX) triple immunostaining in Cx30-/- mice, 4 weeks after last BrdU injection. DCX is a cytoskeleton-associated protein that is expressed transiently in the course of adult neurogenesis (Brown et al., 2003). DCX has recently been used as a marker associated with normal differentiation of new born neurons in the DG (Couillard-Despres et al., 2005).

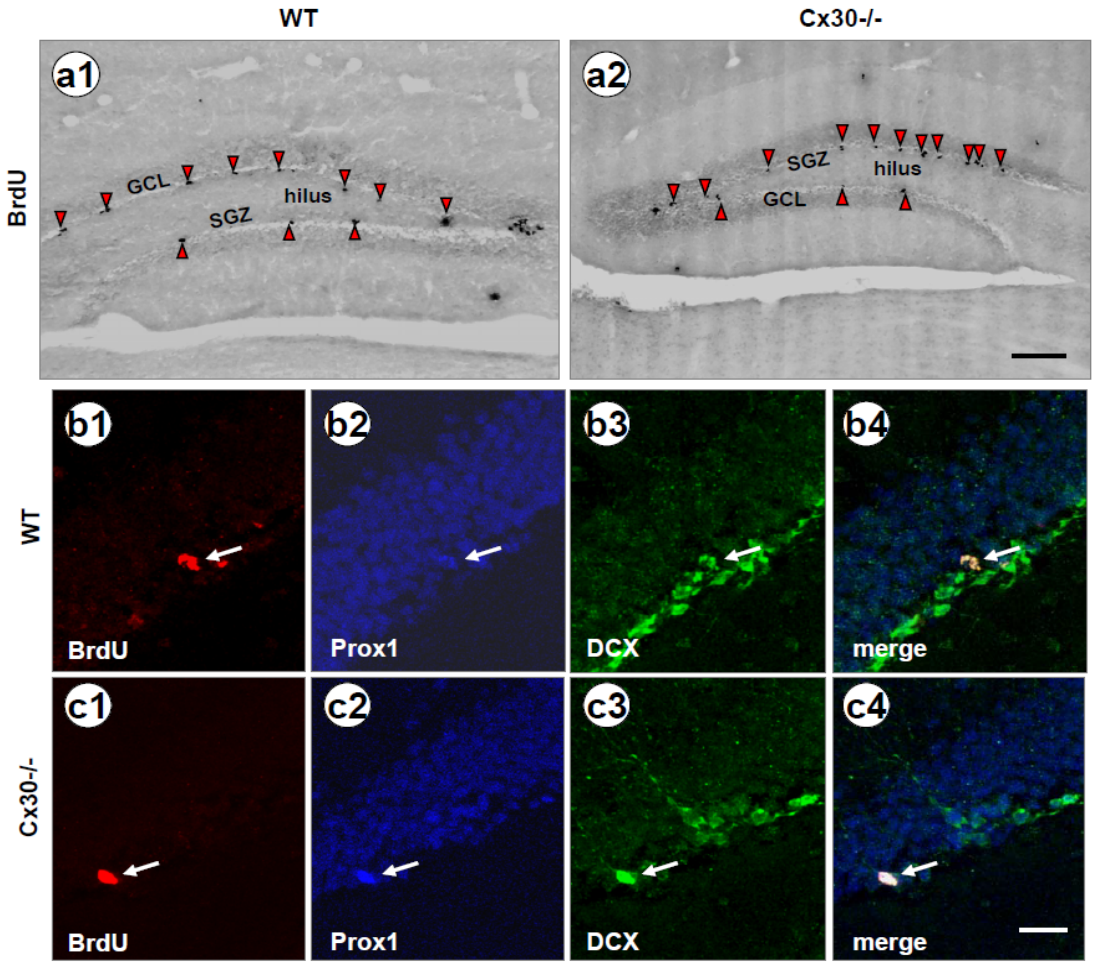

Fig. 4.14: BrdU incorporation was similar between WT and Cx30-/- mice (p60). a1, a2: Peroxidase based immunohistochemical BrdU-detection revealed similar numbers of labeled cells (red arrowheads) in the SGZ between WT (a1) and Cx30-/- mice (a2). Images were obtained from 40 µm thick coronal sections through the

hippocampus 2 h after the last BrdU injection. Scale bar: 100 µm. **b-c:** Fate mapping analysis of BrdU-positive cells in the DG. Confocal images of triple-labeled immunofluorescent sections showing the colocalization of BrdU (red), Prox1 (blue) and DCX (green) positive cells (white arrow) in SGZ of WT (b1-b4) and Cx30-/- (c1-c4) mice. Images were taken 4 weeks after the last BrdU injection. Scale bar: 25 µm

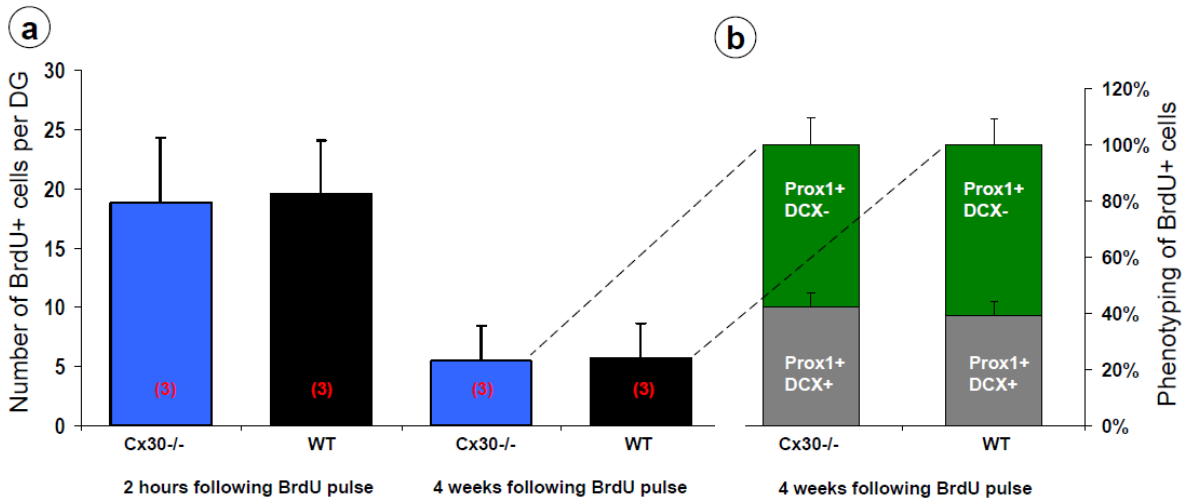

Fig. 4.15: Fate mapping of BrdU-positive cells in the SGZ of Cx30-/- mice. a: The histogram illustrates the number of BrdU-positive cells per DG of WT (black) and Cx30-/- (blue) mice, 2 h and 4 weeks after the last BrdU injections. At both time points no significant alteration of BrdU labeling was detected. **b:** Percentage of BrdU-positive cells expressing Prox1 only, or Prox1 and DCX 4 weeks after the last BrdU injection. Note that all BrdU-labeled cells adopted a neuronal phenotype, and that the proportion of Prox1-positive/DCX-positive cells (gray) did not differ between Cx30-/- and WT mice. Number of animals in each group is shown in brackets.

4.2.2 Analysis of Cx43G138R mutant mice in adult neurogenesis

Since Cx30 ablation has no impact on the proliferation and neurogenesis in the adult brain and a massive decrease in the number of dividing cells and granule neurons in response to Cx43 deletion during postnatal development, a key question is: which mechanisms in mice with Cx43-deficient in astroglia might underlie the observed reduction in proliferation and neurogenesis? However, previous work used Cx30-/-; Cx43fl/fl: hGFAP-Cre mice, in which both major astrocytic connexins completely lack (Kunze et al., 2009). Connexins mediate not only intercellular exchange of small molecules but also adhesive interaction between cells via the cytoplasmic C-terminal tail, as well as gene expression and hemichannel activity which might be required for neurogenesis (Giaume and Theis, 2010). To circumvent this limitation, we employed a panel of Cx43 mutant mice, which allowed us to gain the mechanistic insight into connexin function related to adult neurogenesis.

4.2.2.1 Quality control of Cx43G138R mice

In Cx43flG138R/flG138R: nestin-Cre mutants, Cre recombination leads to expression of the Cx43G138R point mutation together with EGFP reporter gene driven by the Cx43 promotor. It was important to know whether the EGFP reporter protein indicated specific expression of the point mutated Cx43 in astrocytes. Immunfluorescence analysis using anti-EGFP and anti-GFAP antibodies revealed a very high colocalization of the reporter protein with GFAP in astrocytes in the DG (Fig. 4.16 a, b). As mentioned in section 4.1.7, we revealed limitations of the widely used nestin-Cre transgenes, that is, spontaneous germ-line recombination activity of the Cre that required a rigorous quality control. To test for this pleiotropic effect, we compared the expression of cytoplasmic EGFP in the hippocampus of Cx43flG138R/flG138R and Cx43flG138R/flG138R: nestin-Cre mice with the Ki67 and NeuN immunostaining (Fig. 4.16 c, d), or Prox1 labelling (Fig. 4.16 e, f). We found in nestin-Cre positive hippocampus a strong expression of EGFP immunoreactivity but not in the Cre negative control mice. In addition, we observed a lower number of Ki67-positive cells in the SGZ of nestin-Cre positive mice versus controls. These data confirm the proper expression of Cx43G138R in the astrocytes and ensure the faithful nestin-Cre mediated expression of astrocytic Cx43.

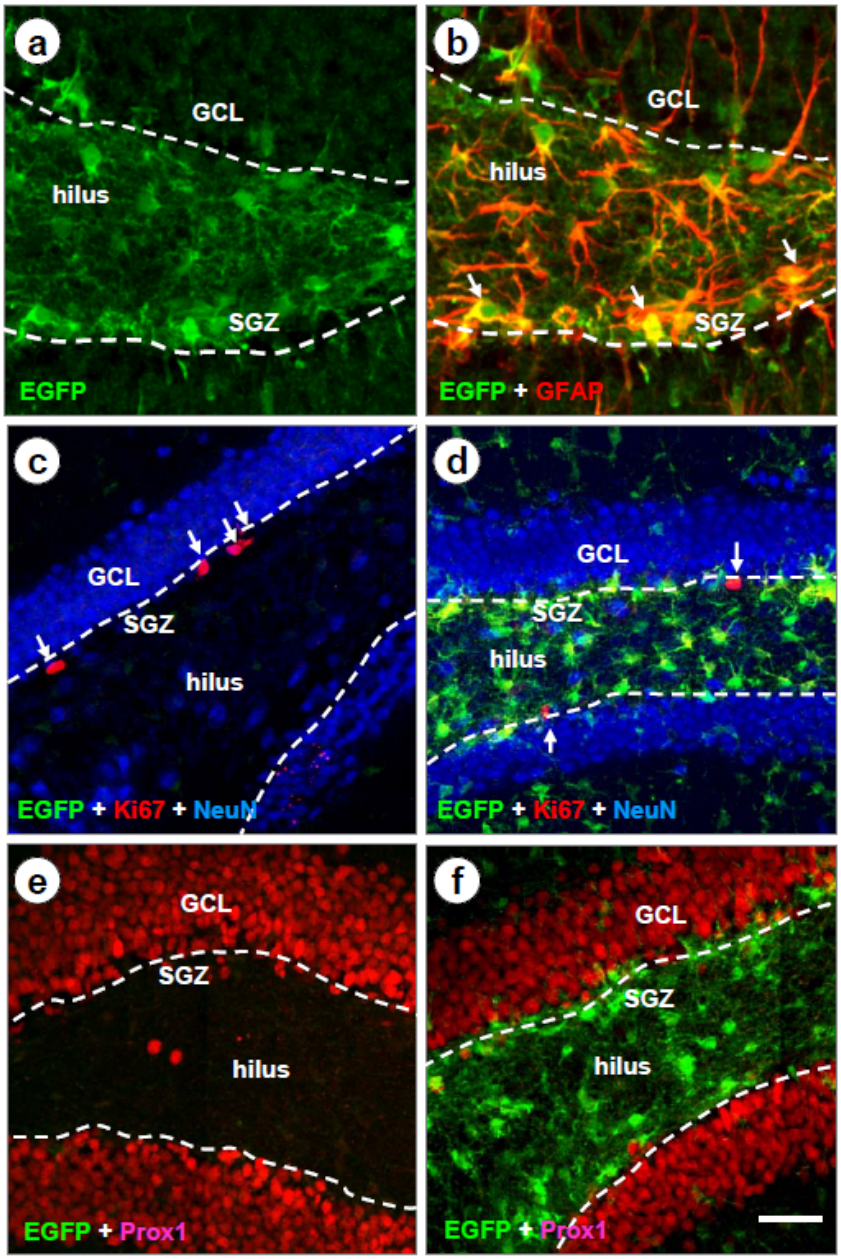

Fig. 4.16: Nestin-Cre mediated recombination leads to expression of the Cx43G138R point mutation in hippocampal DG. a: nestin-Cre activity in Cx43G138R point mutated mice were assessed by GFP immunostaining (green). The distribution of EGFP-reporter expression is under control of Cx43 regulatory elements, indicating the Cx43G138R protein expression in the DG. **b:** Double immunofluorescence staining for GFAP (red) and eGFP (green) in the DG of Cx43G138R point mutated mice. Animal with nestin-Cre mediated recombination showing the high level of colocalization of GFP expression with the astrocytic marker GFAP in the hilus, which points out astrocytic-specific expression of Cx43G138R protein in the CNS-restricted nestin-Cre transgenic animal. **c, d:** Confocal images of a Cx43flG138R/flG138R (c) and a Cx43flG138R/flG138R: nestin-Cre (d) mouse. eGFP (green) monitors Cre-mediated activation of the EGFP reporter. Ki67 (red, thin white arrow) and NeuN (blue) immunostaining indicates lower proliferative activity in the Cx43flG138R/flG138R: nestin-Cre mouse. **e, f:** Double labelling for Prox1(red) and eGFP (green) in Cx43flG138R/flG138R (e) and a Cx43flG138R/flG138R: nestin-Cre (f) mouse, dotted lines indicate the border between GCL and SGZ. Scale bar, 50 µm.

4.2.2.2 The Cx43G138R mutation decreases proliferation and the numbers of granule cells and RG-like cells in the DG

The available evidence strongly indicates that gap junction mediated coupling of glial cells plays a crucial role in regulating neurogenesis, and deletion of Cx43 disturbs cell proliferation not only during early developmental period of neocortex, but also in the postnatal hippocampal neurogenic region (Sutor and Hagerty, 2005; Wiencken-Barger et al., 2007; Kunze et al., 2009). With respect to gap junction coupling, previous experimental data suggested that mice expressing the point mutation Cx43G138R selectively lost intercellular coupling in primary cardiomyocytes, as well as in mutant Cx43 transfected HeLa and embryonic stem (ES) cells (Dobrowolski et al., 2008). However, those mutant mice still contain the intact C-terminal region, indicating cell adhesive interaction via the cytoplasmic C-terminal domain of Cx43, so neuronal migration should be preserved (Cina et al., 2009).

To elucidate the impact of the point mutation Cx43G138R on RG-like precursor cell proliferation in the adult brain, we compared the proliferative activity in the SGZ assessed by Ki67 immunostaining. We observed a strong decrease in the number of Ki67-positive cells in mice expressing Cx43G138R (Cx30+/+; Cx43flG138R/flG138R: nestin-Cre) compared to “floxed” control animals, which are still expressing wild-type Cx43 (Cx30+/+; Cx43flG138R/flG138R; Fig. 4.17 a-d; Fig. 4.20 a). In order to abolish residual astrocytic coupling, Cx43 point mutated mice were crossed with Cx30-/- mice (Teubner et al., 2003). Additional deletion of Cx30 revealed also a significant reduction of Ki67-positive cells in Cx30-/-; Cx43flG138R/flG138R: nestin-Cre mice relative to Cx30-/-; Cx43flG138R/flG138R mice (Fig. 4.17 e-h; Fig. 4.20 b). However, within control (Cx30+/+; Cx43flG138R/flG138R vs. Cx30-/-; Cx43flG138R/flG138R) and point mutation groups (Cx30+/+; Cx43flG138R/flG138R: nestin-Cre vs. Cx30-/-; Cx43flG138R/flG138R: nestin-Cre) the number of Ki67-positive cells was similar irrespective of the Cx30 knockout. This indicates that reduced proliferative activity is caused alone by the Cx43G138R point mutation in precursor cells but not by Cx30.

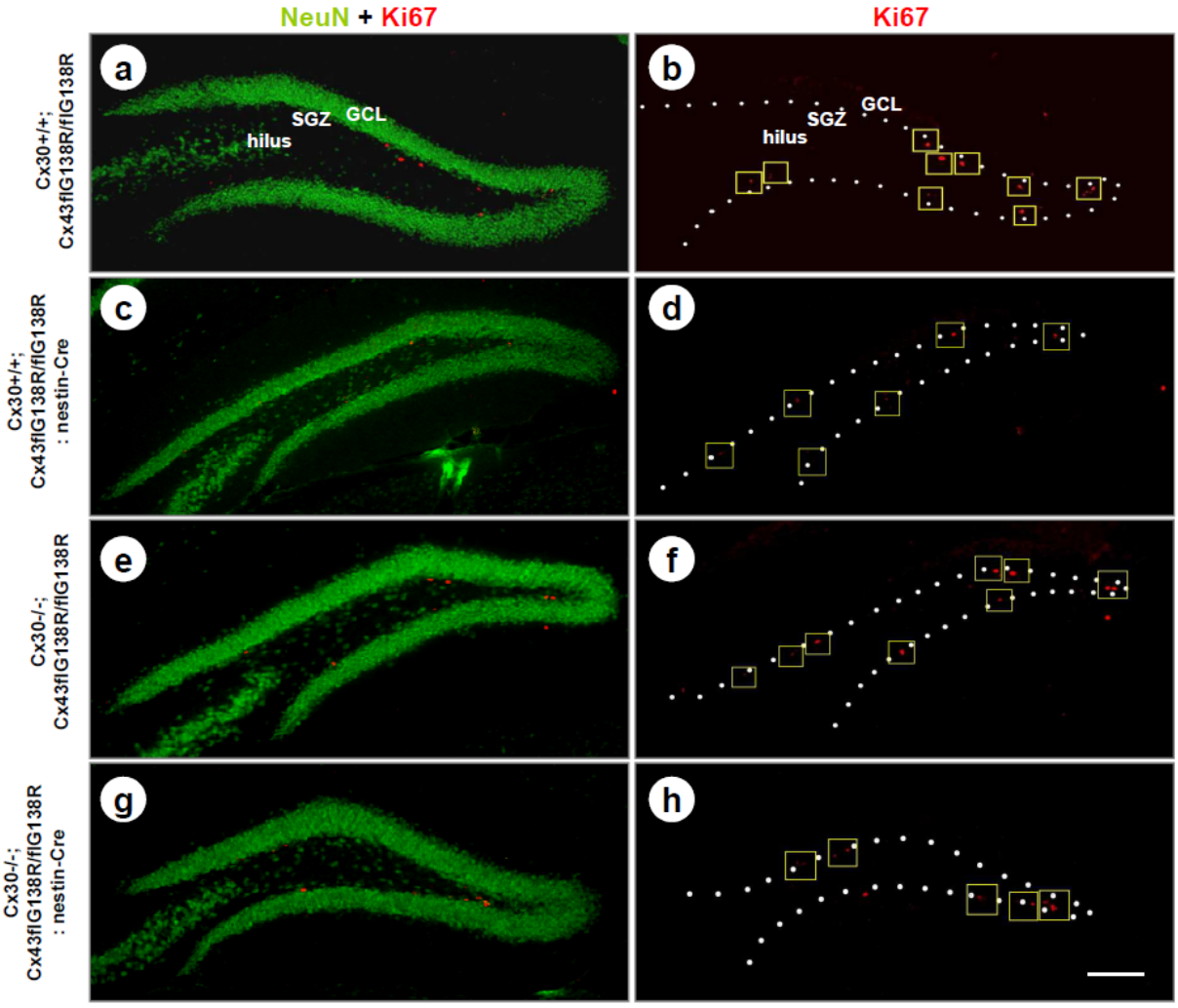

Fig. 4.17: Reduced proliferative activity in the SGZ of Cx43G138R mutant mice is independent of Cx30 (p60). a-h: Double labelling for Ki67 (red) and NeuN (green) in the DG of Cx30+/+; Cx43flG138R/flG138R (a, b), Cx30+/+; Cx43flG138R/flG138R: nestin-Cre (c, d), Cx30-/-; Cx43flG138R/flG138R (e, f) and Cx30-/-; Cx43flG138R/flG138R: nestin-Cre mice (g, h). Ki67-positive cells were framed in yellow boxes in the same section (b, d, f and h) as in (a, c, e and g), indicating strongly reduced proliferative activity in Cx43flG138R/flG138R: nestin-Cre mice (c, d, g and h) in comparison to Cx43flG138R/flG138R mice (a, b, e and f) independent of the Cx30 status. Dotted lines indicate the border between SGZ and GCL Scale bar: 100 µm.

The majority of dividing precursors in the SGZ are directed to the neuronal fate and develop into mature dentate granule neurons during the following several weeks as they migrate radially from SGZ into the inner third of the granular layer (Zhao et al., 2006; Zhao et al., 2008). To find out if there was any effect on the neurogenesis in response to strongly decreased proliferation in the Cx43G138R mutant, we subsequently investigated the number of granule neurons by the neuron marker Prox1, which is persistently and strongly expressed in the DG granule cells of the postnatal and adult hippocampus. Confocal Z-stack images were taken and counting boxes were used to estimate the number of Prox1-positive cells. For better comparison with the above described Ki67 immunostaining results, experiments

were performed in same transgenic mouse lines. A significant reduction in the number of granule neurons was observed in both Cx43 point mutated mice (Cx30+/+; Cx43flG138R/flG138R: nestin-Cre and Cx30-/-; Cx43flG138R/flG138R: nestin-Cre) compared to their corresponding control (Cx30+/+; Cx43flG138R/flG138R and Cx30-/-; Cx43flG138R/flG138R) independent of Cx30 status (Fig. 4.18; Fig. 4.20 a-b).

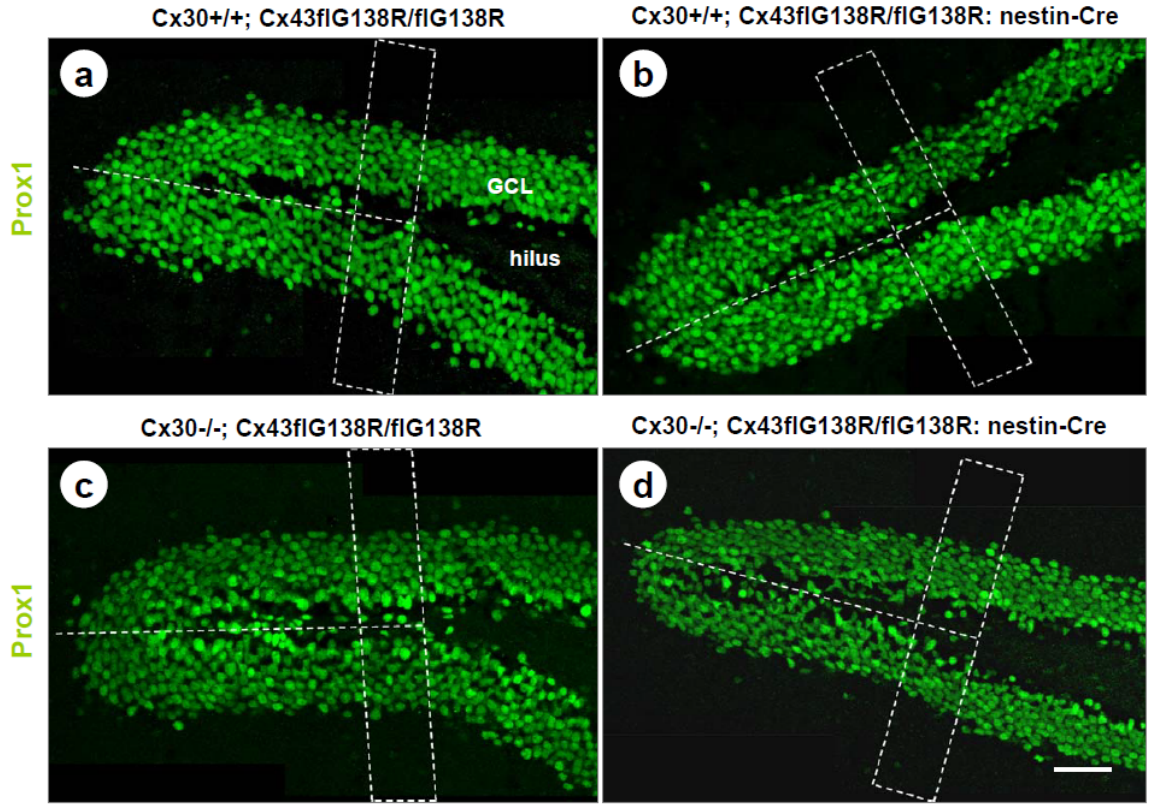

Fig. 4.18: Decreased granular neuron numbers in the DG of Cx43G138R mutant mice independent of the Cx30 expression (p60). a-d: Confocal images of Prox1 immunostaining (green) in the DG of Cx30+/+; Cx43flG138R/flG138R (a), Cx30+/+; Cx43flG138R/flG138R: nestin-Cre (b), Cx30-/-; Cx43flG138R/flG138R (c) and Cx30-/-; Cx43flG138R/flG138R: nestin-Cre mice (d). Representive images showing reduced numbers of Prox1-positive cells in the GCL of Cx43G138R point mutated mice (b, d) versus Cx43flG138R/flG138R mice (a, c) independent of the Cx30 conditions. Frames in (a-d) indicate counting boxes. Scale bar: 50 µm.

To identify if there was any change in the number and the arrangement of the RG-like cells in the SGZ, expression of BLBP was assessed in mice expressing Cx43G138R. Upon quantifying the number of BLBP-positive cells in the SGZ we observed a strong reduction in the number of RG-like cells by 40 % in Cx43G138R mice relative to controls (Fig. 4.19; Fig. 4.20 d).

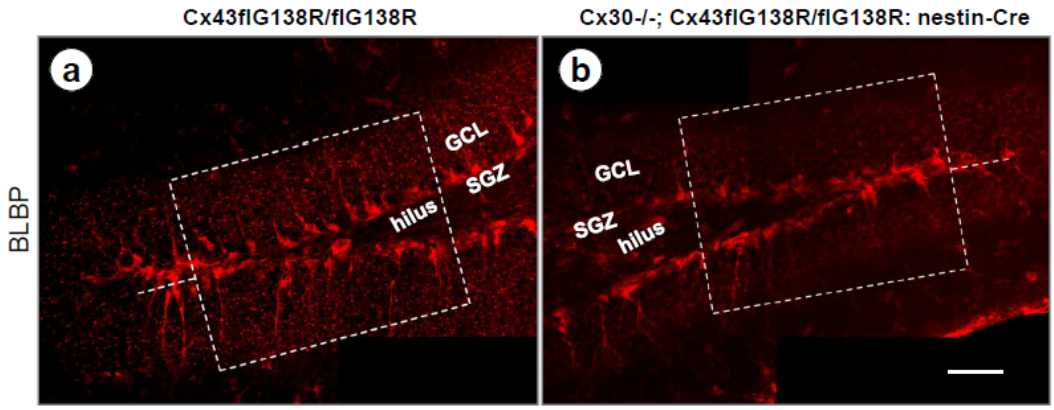

Fig. 4.19: Reduced number of BLBP-positive cells in the Cx43G138R mice (p60). Confocal images revealed significantly decreased numbers of BLBP labeled cells in the SGZ of Cx30-/-; Cx43flG138R/flG138R; nestin-Cre (b) vs. Cx43flG138R/flG138R control mice (a). Frames indicate counting boxes. Scale bar: 50 µm.

Together, these findings indicated that the Cx43G138R point mutation expression is a critical determinant of decreased number of RG-like cells, neural precursor proliferation and subsequently reduced neurogenesis in the adult mouse hippocampus. Quantitative data are summarized in Figure 4.20.

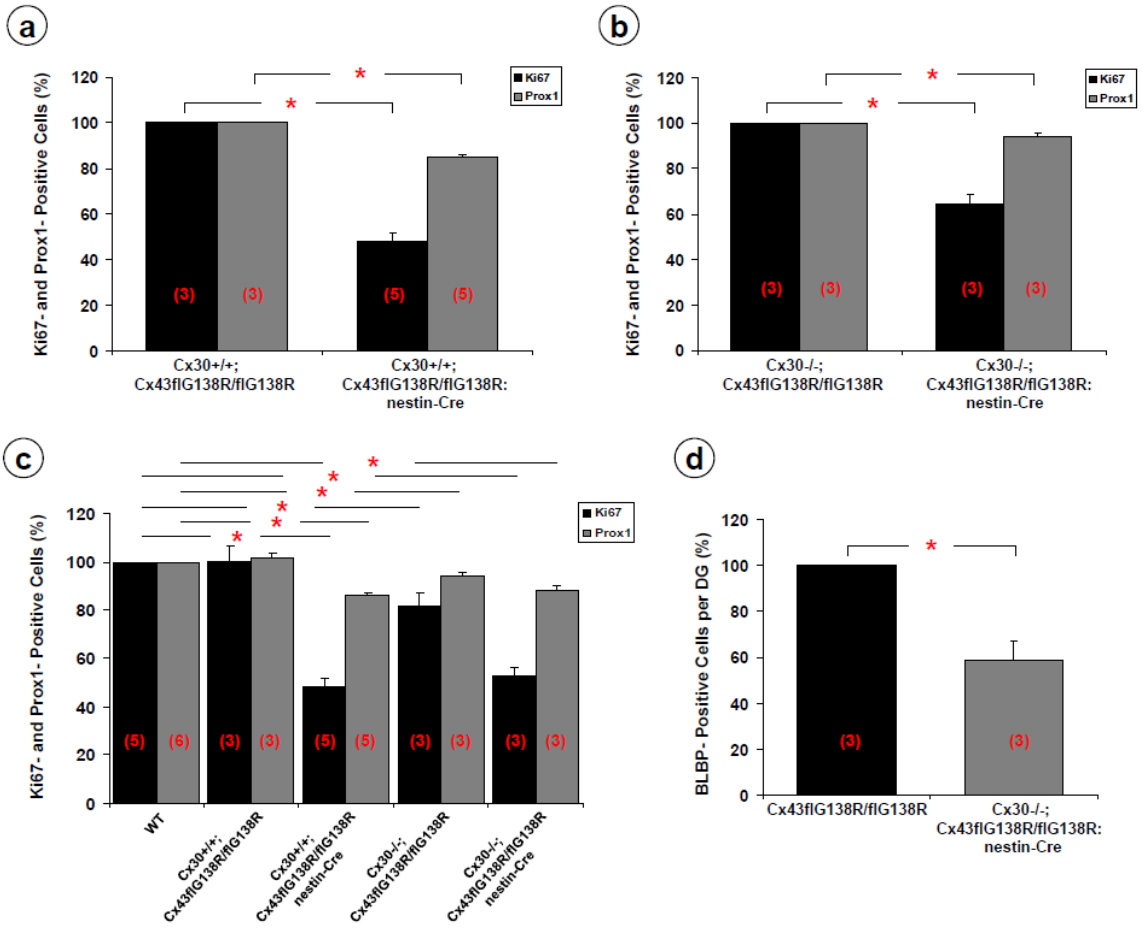

Fig. 4.20: Expression of Cx43G138R point mutations in astroglia decreases proliferation and neurogenesis in the adult mice DG (p60). a-b: Quantitative analysis of Ki67- and Prox1-positive cell numbers of

Cx43G138R point mutated mice with (a) or without Cx30 (b). Both positive cell numbers were significantly lower in nestin-Cre positive animals comparing to control mice, which still express wild-type Cx43. **c:** Histogram comparing the proliferation and neurogenesis between Cx43G138R point mutant mice and WT animals. Mice expressing Cx43G138R show significantly decreased numbers of Ki67- and Prox1-positive cells compared to WT, irrespective of Cx30 conditions. In the Cx30-/-; Cx43flG138R/flG138R mice we observed also lower numbers of Ki67- and Prox1-positive cells, whereas the proliferation and neurogenesis were not significantly changed in Cx30+/+; Cx43flG138R/flG138R mice compared with WT. **d:** Quantitative evaluation showing a significant reduction of BLBP-positive cells in Cx43G138R mutant mice. Asterisks mark significant differences. Significance level was set at $P < 0.05$ (Mann-Whitney U-test and Kruskal-Wallis H-test). Number of animals in each group is shown in brackets.

4.2.2.3 Cx43 protein expression levels are similar in Cx43flG138R/flG138R and Cx43flG138R/flG138R; nestin-Cre mouse hippocampus

A previous study demonstrated a strong down-regulation of Cx43 expression in whole brain lysate of Cx43flG138R/flG138R: nestin-Cre mice to approx. 40% of WT animals (Dobrowoski, 2008, Dissertation). To investigate the expression level of Cx43G138R in the hippocampus and its influence on the adult neurogenesis, we determined Cx43 protein levels in the hippocampus of WT, Cx43fl/fl: hGFAP-Cre, Cx43flG138R/flG138R and Cx43flG138R/flG138R: nestin-Cre mice by Western blot (Fig. 4.21 a). Here, a significant down-regulation of Cx43 was detected in nestin-Cre positive mice relative to WT mice. This finding is consistent with former whole brain immunoblotting results. We further noted lower Cx43 protein levels also in the Cx43flG138R/flG138R mice, this originates from the fact that “floxed” Cx43 alleles result in decreased endogenous protein expression (Theis et al., 2003). Residual Cx43 protein levels in the Cx43 KO samples, used as negative control, are due to remaining expression of Cx43 in cell types not targeted by hGFAP-Cre, such as endothelial cells and leptomeningeal cells (Theis et al., 2003). Most importantly, however, expression levels of Cx30 and Cx43 in Cx43flG138R/flG138R mice were similar to those of Cx43flG138R/flG138R: nestin-Cre mice (Fig. 4.21 b, c). Moreover, additional knock-out of Cx30 to the same comparing groups revealed the similarity in Cx43 expression strength (Fig. 4.21 d, e). Combining Ki67 and Prox1 immunostaining results (Fig. 4.20), these findings imply that the decline of wild-type Cx43 in Cx43flG138R/flG138R mice has no impact on the adult neurogenesis, reduced proliferation and neurogenesis are associated with the expression of the Cx43 point mutation in the DG.

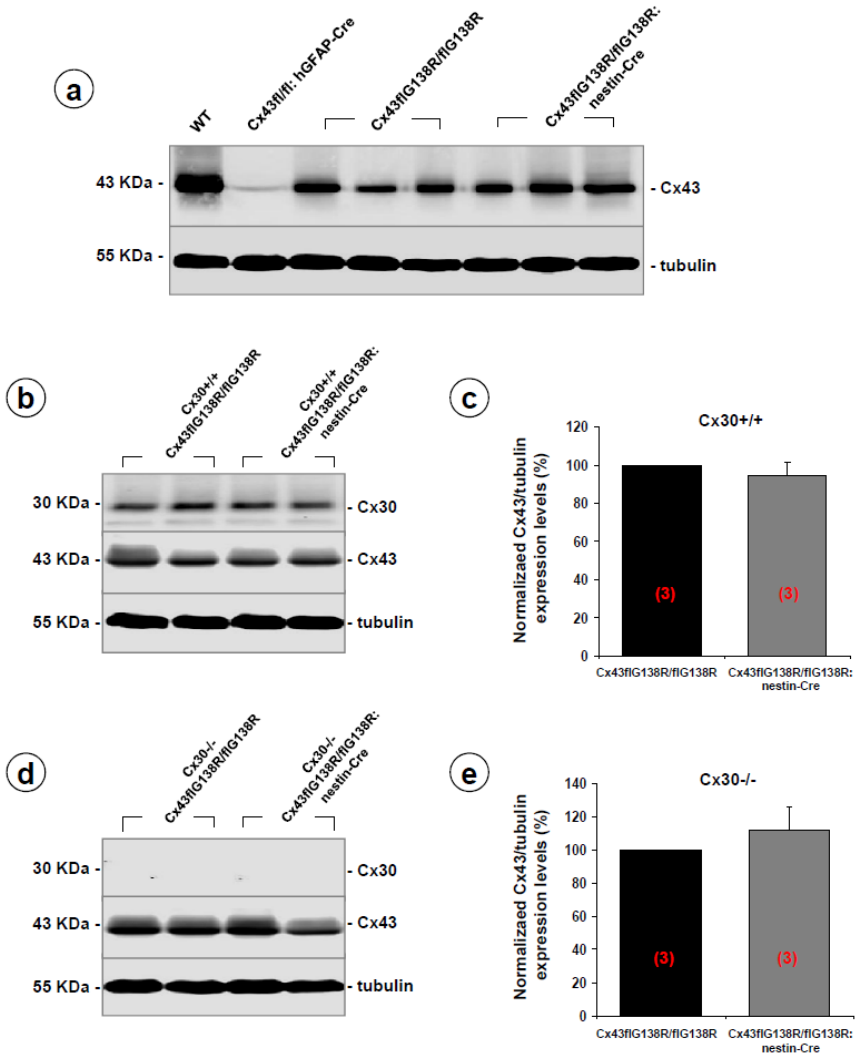

Fig. 4.21: Cx43 protein expression level in Cx43G138R mutant mouse hippocampus. a: Immunoblot showing a down-regulation of Cx43 expression in Cx43flG138R/flG138R and Cx43flG138R/flG138R: nestin-Cre mice in contrast to WT. **b, d:** Comparison of Cx43 and Cx30 expression levels in Cx43flG138R/flG138R: nestin-Cre and Cx43flG138R/flG138R control animals. Cx30 expression level was not up-regulated in Cx43flG138R/flG138R: nestin-Cre mice compared to control. No Cx30-band was observed in lysates after Cx30 deletion. **c, e:** Quantitative analysis showing a similar Cx43 expression level between groups independent of Cx30 status. Relative expression levels of Cx43 were normalized to tubulin levels. Cx43 expression in control mouse hippocampus is set to 100%. Significance level was set at $P < 0.05$ (student's t-test). Number of animals is shown in red.

4.2.2.4 BrdU incorporation and fate mapping in the DG of Cx43G138R mice

To map the fate of proliferating cells we used BrdU immunohistochemistry in Cx43G138R point mutant mice 2 h and 4 weeks after last BrdU injection. To characterize whether Cx43 point mutation has any impact on differentiation, maturation and integration of newborn granule neurons, we employed BrdU, Prox1 and DCX triple immmunostaining. This revealed a 48 % (2 h) and 33 % (4 weeks) lower number of BrdU labeled cells in Cx30-/-;

Cx43flG138R/flG138R; nestin-Cre mice compared to WT, respectively (Fig. 4.23 a). Importantly, almost all of the BrdU-positive cells expressed Prox1 (with or without DCX) in both comparing groups (Fig. 4.32 b). The proportion of Prox1-positive/DCX-positive cells among the BrdU-positive cells in Cx43G138R mice and control animals remained unchanged (Fig. 4. 31 b).

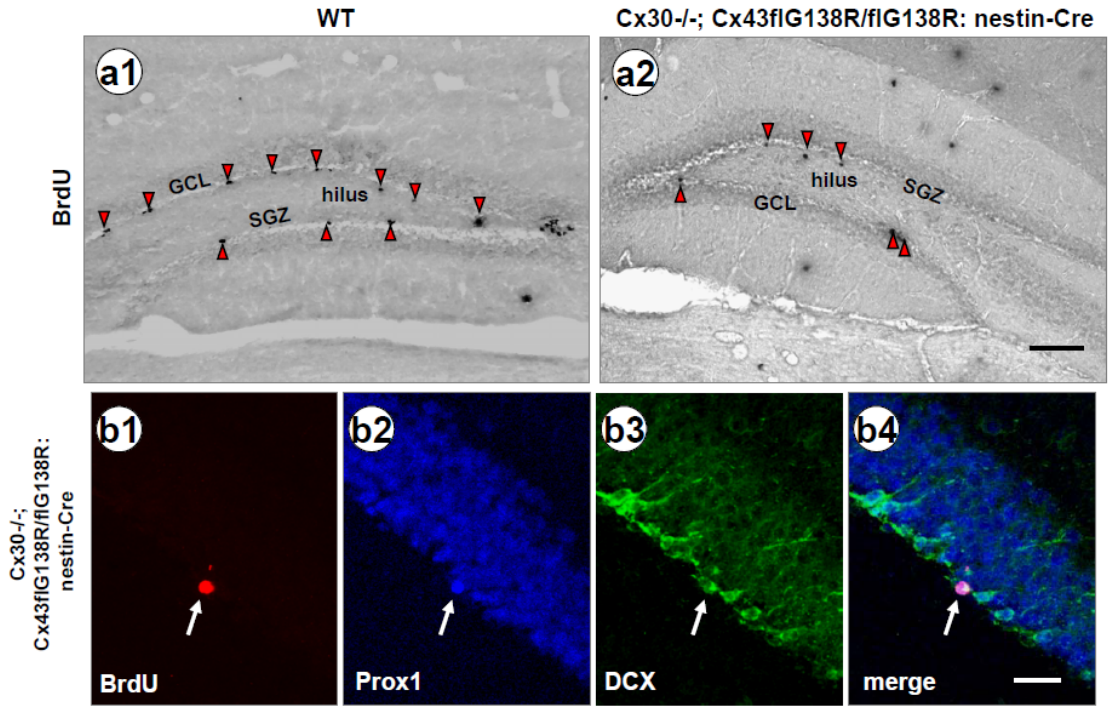

Fig. 4.22: Reduced number of BrdU-positive cells in Cx43 point mutant mice (p60). a: Peroxidase based immunohistochemical BrdU-detection revealed a significantly decreased number of BrdU-labeled cells (red arrowheads) in the SGZ of Cx30-/-; Cx43flG138R/flG138R: nestin-Cre mice (a2) vs. WT (a1). Representative images were obtained 2 h after the last BrdU injection. Scale bar: 100 µm. **b:** Confocal images of a cell (white arrow) expressing BrdU (red), Prox1 (blue) and DCX (green) in the SGZ. Images were taken 4 weeks after the last BrdU injection. Scale bar: 25 µm

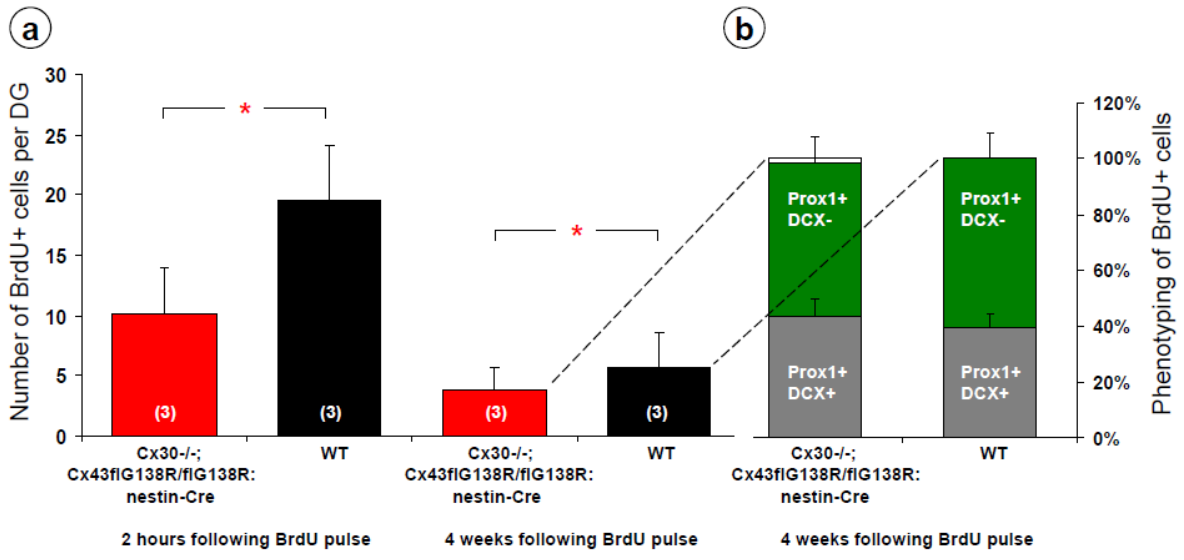

Fig. 4.23: Fate mapping of BrdU-positive cells in the SGZ of Cx43 point mutant mice. a: The histogram illustrates the number of BrdU-positive cells per DG of WT (black) and Cx30-/-; Cx43flG138R/flG138R; nestin-Cre (red) mice, 2 h and 4 weeks after the last BrdU injections. At both time points a significantly decreased number of BrdU-labeled cells were detected in Cx43 point mutant mice. **b:** Percentage of BrdU-positive cells expressing Prox1 only, or Prox1 and DCX 4 weeks after the last BrdU pulse. Almost all BrdU-positive cells adopted a neuronal phenotype, but the proportion of Prox1-positive/DCX-positive cells (gray) did not differ between groups. In Cx43 point mutated mice 0 to 1,7% of the BrdU-positive cells expressed neither Prox1 nor DCX (left bar, open). Asterisks mark significant differences. Significance level was set at $P < 0.05$ (Mann-Whitney U-test).

4.2.2.5 Biocytin coupling in the astrocytes of Cx43G138R mice

Extensive gap junction mediated coupling is considered a prominent feature of astrocytes. The two main astrocytic connexins, Cx30 and Cx43, are involved in interastrocytic distribution of energetic substrates and extracellular ion homeostasis, as well as metabolite supply of neurons (Giaume et al., 1997, Theis et al., 2003a; Wallraff et al., 2006; Rouach et al., 2008; Gosejacob et al., 2011). To investigate the impact of Cx30 and mutated Cx43 on adult hippocampal neurogenesis, together with Dr. Peter Bedner, we performed a functional assay, i.e., analysis of intercellular tracer diffusion from one injected astrocytes to their gap junction-coupled neighbours, as described previously (Wallraff et al., 2004). Briefly, coupling experiments were performed in acute hippocampal slices (P90-P120) by dialyzing an astrocyte in the CA1 stratum radiatum recorded in the whole-cell configuration with biocytin, a gap junction channel-permeant dye. In order to abolish residual astrocytic coupling, Cx43 mutants were crossed with Cx30-/- mice (Teubner et al., 2003). Upon staining for biocytin and quantifying the number of cells coupled from the Z-stack images, an almost complete absence of interastrocytic coupling was observed in Cx43flG138R/flG138R: nestin-Cre mice compared to Cx43flG138R/flG138R animals, used as a reference (Fig. 4.24 a1, b1; 1 ± 4 coupled cells vs. 78 ± 36 coupled cells). Additional EGFP immunolabelling on the same section served as quality control (Fig. 4.24 a2, b2). Quantitative data are summarized in Figure 4.25.

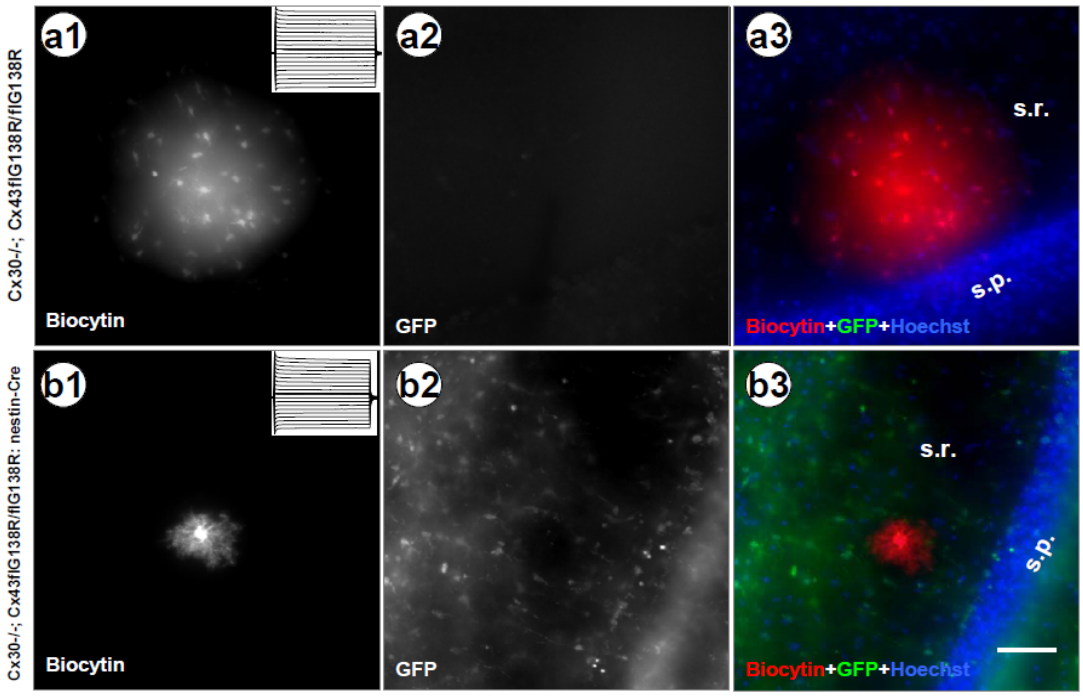

Fig. 4.24: Expression of Cx43 point mutation in hippocampal astrocytes strongly reduces tracer coupling (p90-p120). a1: Tracer-coupled astrocytes in Cx30-/-; Cx43flG138R/flG138R control hippocampal slices, as obtained after biocytin diffusion from a single cell, held in whole-cell voltage clamp for 20 min. **b1:** Strongly reduced numbers of tracer-coupled astrocytes in hippocampal slices of a Cx43 point mutant mouse. **a2, b2:** Immunostaining images of anti-GFP on control (a2) and Cx43 point mutated mice (b2) in the slices shown in a1 and b1, respectively. Note, that no GFP signals were detected in control animals. **a3, b3:** Merged pictures of triple staining. Red, biocytin; green, GFP; blue, Hoechst. Insets give the current profiles of recorded cells. Slices, 200 µm thick; Scale bar, 50 µm; s.p., Stratum pyramidale; s.r., stratum radiatum.

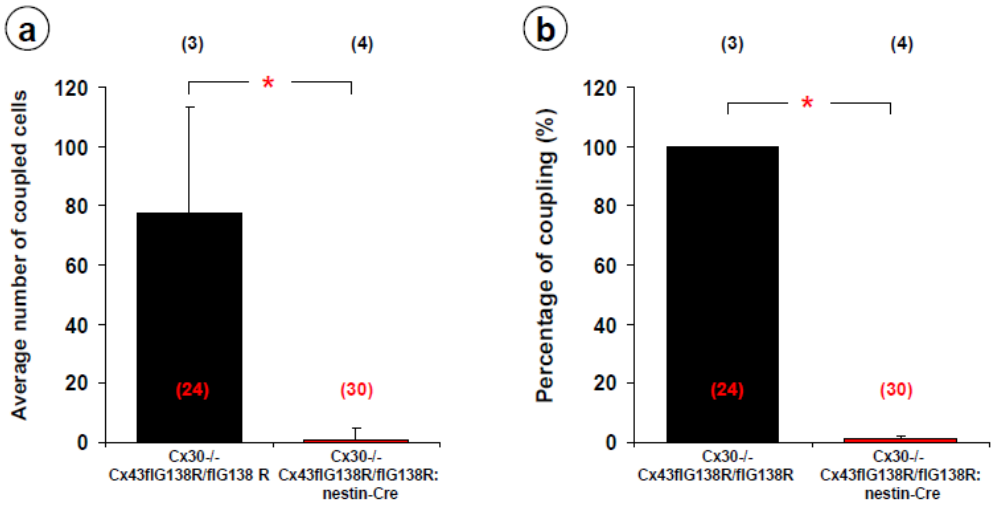

Fig. 4.25: Reduced astroglial tracer coupling in CA1 region of Cx43 point mutant mice. a: Quantitative evaluation revealed that coupling was almost completely lacking in Cx30-/-; Cx43flG138R/flG138R: nestin-Cre mice, as expected. **b:** Percentage of coupling normalized to control mice reveals a 98,8 % significant decrease in Cx43G138R mice. Asterisks mark significant differences. Significance level was set at $P < 0.05$ (Mann-Whitney U-test). Number of analyzed brains is shown in black and corresponding slices in red per genotype.

4.2.2.6 Biocytin coupling in the RG-like cells of Cx43G138R mice

To determine whether decreased proliferation and differentiation of granule neurons is due to reduction of RG-like cell coupling, together with Mrs. Stephanie Griemsmann, the same protocols described in Kunze et al. (2009) were applied to adult Cx30-/-; Cx43flG138R/flG138R: nestin-Cre mice. Only passive RG-like cells having cell soma located in the SGZ and having a radial process spanning the GCL, as revealed through postrecording immunostaining, were considered (Fig 4.26 a, b). Biocytin immunostaining revealed a significant decrease in the number of coupled RG-like cells in Cx30-/-; Cx43flG138R/flG138R: nestin-Cre mice as compared to WT (Fig. 4.27 a; 12 ± 1 coupled cells vs. 8 ± 2 coupled cells). Moreover, a higher proportion of passive RG-like cells completely lack coupling in the mutated mice (Fig. 4.27 b). In conclusion, Cx43G138R mutants exhibited a significantly decreased RG-like cell coupling.

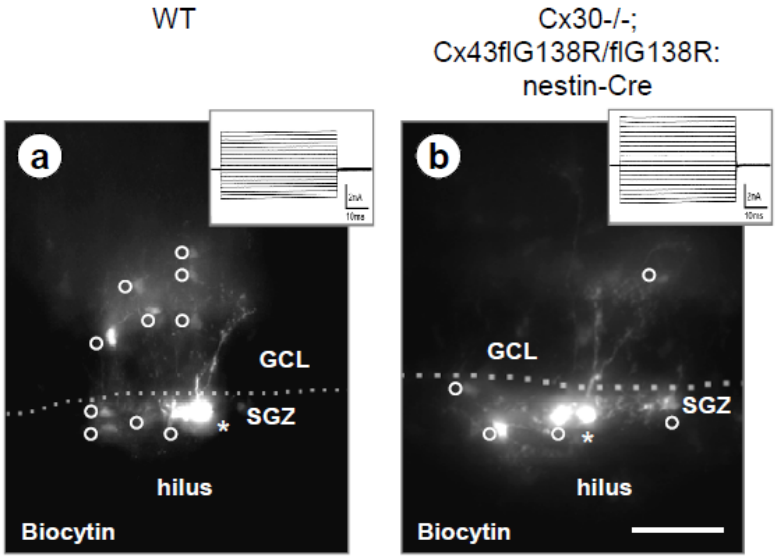

Fig. 4.26: Decreased biocytin coupling in the SGZ of Cx30-/-, Cx43flG138R/flG138R: nestin-Cre mice (p90-p120). Representative images of a coupled RG-like cells in WT control (a) and Cx30-/-; Cx43flG138R/flG138R; nestin-Cre (b) mice. Tracer spread from the recorded cell (*) to neighbouring cells (ʕ). Note that the tracer spread to a few neighbouring cells in Cx43G138R point muation mice comparing to WT animals. Cells were filled with biocytin during recording (20 min). Insets give the current pattern of recorded cells. Broken lines indicate the border between SGZ and GCL. Slices, 200 µm thick; Scale bar, 50 µm.

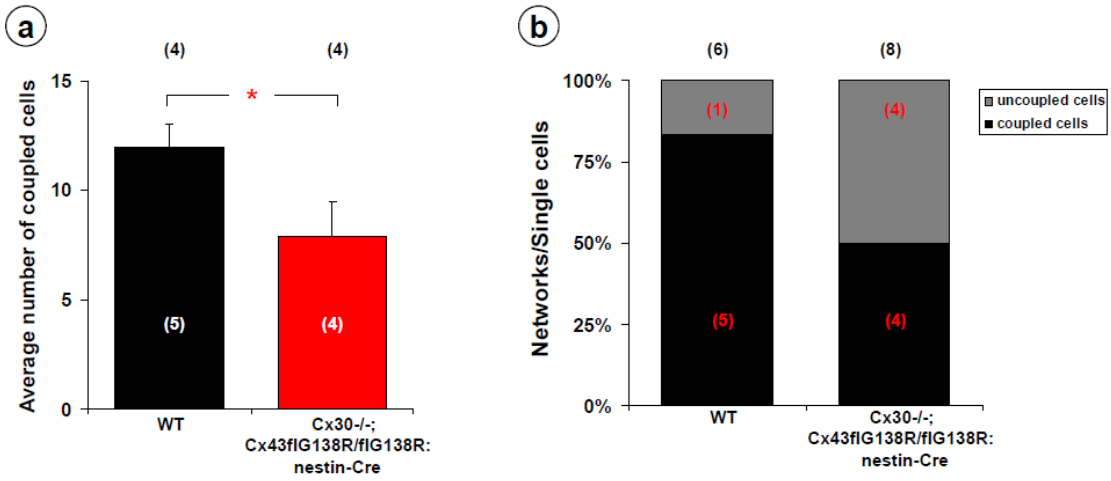

Fig. 4.27: Quantitative evaluation of RG-like cell tracer coupling in Cx43G138R point mutation mice. a: Mice expressing Cx43G138R mutations show a significantly decreased number of biocytin coupled RG-like cells in the SGZ versus WT animals. Number of analyzed brains is shown in black and corresponding cells in white. **b:** Percentage of tracer coupled and uncoupled cells in control and Cx30-/-; Cx43flG138R/flG138R: nestin-Cre mice. Asterisk marks significant differences. Significance level was set at $P < 0.05$ (Mann-Whitney U-test).

4.2.3 Analysis of Cx43K258stop mutant mice in adult neurogenesis

Although Cx43-mediated intercellular coupling between RG-like cells in the DG has a strong impact on adult neurogenesis (Kunze et al., 2009), several studies have indicated that Cx43 plays important, non-channel roles during embryonic cortical development by affecting neuronal migration. The molecular mechanisms controlling directly and/or indirectly the cellular motility is not yet fully understood. A former study using shRNA techniques has shown that gap junction adhesion, rather than channels or the C-terminus of Cx43 is responsible for the radial migration during early cortical development (Elias et al., 2007). In contrast, other studies using RNA interference or Cx43K258stop mice have indicated that the C-terminus is required for cortical neuronal migration that were mainly attributed to adhesive interactions (Bates et al., 2007; Cina et al., 2009). Cx43K258stop mice carry a C-terminal truncation of Cx43, which still showed robust intercellular coupling in transfected HeLa cells (Maass et al., 2004), but adhesive functions should be decreased because of loss of protein-protein binding motifs on the C-terminal domain (Giepmans, 2004; Laird, 2006; Kozoriz et al., 2010). In this regard, we are asked whether a truncation of the C-terminus of Cx43 alters cell adhesion and may subsequently influence adult neurogenesis.

4.2.3.1 Quality control of Cx43K258stop mice

For this reason, we analyzed Cx43fl/K258stop: hGFAP-Cre mice expressing only the truncated C-terminus of Cx43 (Cx43K258stop) following conditional ablation of wild-type Cx43 upon hGFAP-Cre mediated recombination in the CNS. hGFAP-Cre activity leading to

loss of Cx43 expression in astrocytes was monitored by gain of ß-Gal reporter expression in immunfluorescence analysis using anti-ß-Gal antibodies (Fig. 4.28 a). We observed a high degree of colocalization of the astrocytic marker GFAP with the Cx43 promotor driven reporter ß-Gal (Fig. 4.28 b). However, the widely used hGFAP-Cre transgene required a rigorous quality control due to spontaneous ectopic Cre activity (Zhang et al., in revision) and spontaneous loss of Cre activity (Requardt et al., 2009). We compared the ß-Gal immunoreactivity in the hippocampus of Cx43fl/K258stop and Cx43fl/K258stop: hGFAP-Cre mice with Ki67 and NeuN labelling (Fig. 4.28 c, d), or Prox1 immunostaining (Fig. 4.28 e, f). We found in hGFAP-Cre positive hippocampus a strong expression of the ß-Gal signal, but not in the Cre negative control mice. These data confirm the proper expression of Cx43K258stop in the astrocytes and corroborate the faithfulness of hGFAP-Cre mediated deletion of astrocytic connexins. Importantly, we observed a low number of Ki67-positive cells in the SGZ of Cx43fl/K258stop: hGFAP-Cre mice versus Cx43fl/K258stop control.

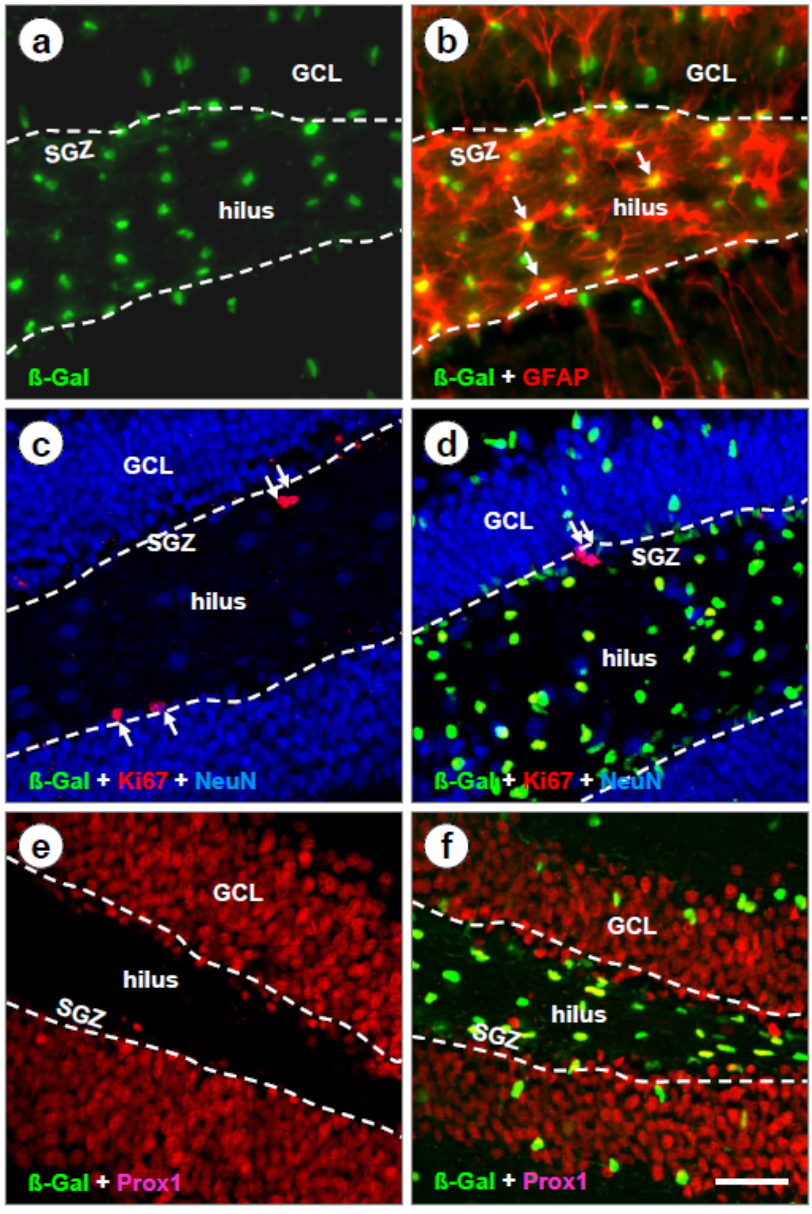

Fig. 4.28: hGFAP-Cre mediated recombination leads to deletion of wild-type Cx43 in Cx43K258stop truncated mouse DG. a: hGFAP-Cre activity in a Cx43K258stop truncated mouse was evaluated by ß-Gal immunoreactivity (green). β-Gal staining of Cx43fl/K258stop: hGFAP-Cre mice shows the distribution of β-Gal expression derived from the Cx43 locus. After deletion of wild-type Cx43 mice carry only truncated Cx43K258stop protein in astrocytes. **b:** Double immunofluorescence staining for GFAP (red) and ß-Gal (green) in the DG of a Cx43K258stop truncated mouse. Animals with hGFAP-Cre mediated recombination show abundant ß-Gal expression, colocalized with the astrocytic marker GFAP in the DG. **c-d:** Confocal images of triple immunostaining of ß-Gal (green), Ki67 (red, white arrow) and NeuN (blue) in a Cx43fl/K258stop (c) and a Cx43fl/K258stop: hGFAP-Cre (d) mouse. **e-f:** Double labelling for Prox1(red) and ß-Gal (green) in a Cx43fl/K258stop (e) and a Cx43fl/K258stop: hGFAP-Cre (f) mouse, dotted lines indicate the border between GCL and SGZ. Scale bar: 50 µm.

4.2.3.2 The Cx43K258stop mutation leads to a reduction of proliferation and neurogenesis in the DG and is independent of Cx30

We subsequently investigated the impact of Cx43K258stop on RG-like cell proliferation in the adult SGZ by using the proliferation marker Ki67, as was shown in Cx43G138R mice (Fig. 4.17). In adult Cx43fl/K258stop: hGFAP-Cre mice, expression of Cx43K258stop in astrocytes led to a strong reduction of Ki67-positive cells in the SGZ, as compared with Cx43fl/K258stop control mice, which still express wild-type Cx43 in addition to the C-terminal truncated Cx43 (Fig. 4.29 a-d). For better comparison with the above described Ki67 immunolabelling results in Cx43G138R mice, we assessed the proliferative activity also in Cx30-/-; Cx43fl/K258stop: hGFAP-Cre mice which arose from the mating of Cx30-/- (Teubner et al., 2003) with Cx43fl/K258stop: hGFAP-Cre mice. Additional ablation of Cx30 revealed also a significant reduction of Ki67-positive cells in hGFAP-Cre mice relative to Cx30-/-; Cx43fl/K258stop mice (Fig. 4.29 e-h). Again, we found the number of Ki67-positive cells was not significantly different within Cx43K258stop groups (Cx30+/+; Cx43fl/K258stop: hGFAP-Cre vs. Cx30-/-; Cx43fl/K258stop: hGFAP-Cre) or between their controls (Cx30+/+; Cx43fl/K258stop vs. Cx30-/-; Cx43fl/K258stop), similar to Cx43G138R point mutation mice. Thus, Cx43 decreased proliferation in the SGZ is only due to the C-terminus truncation, but not influenced by Cx30.

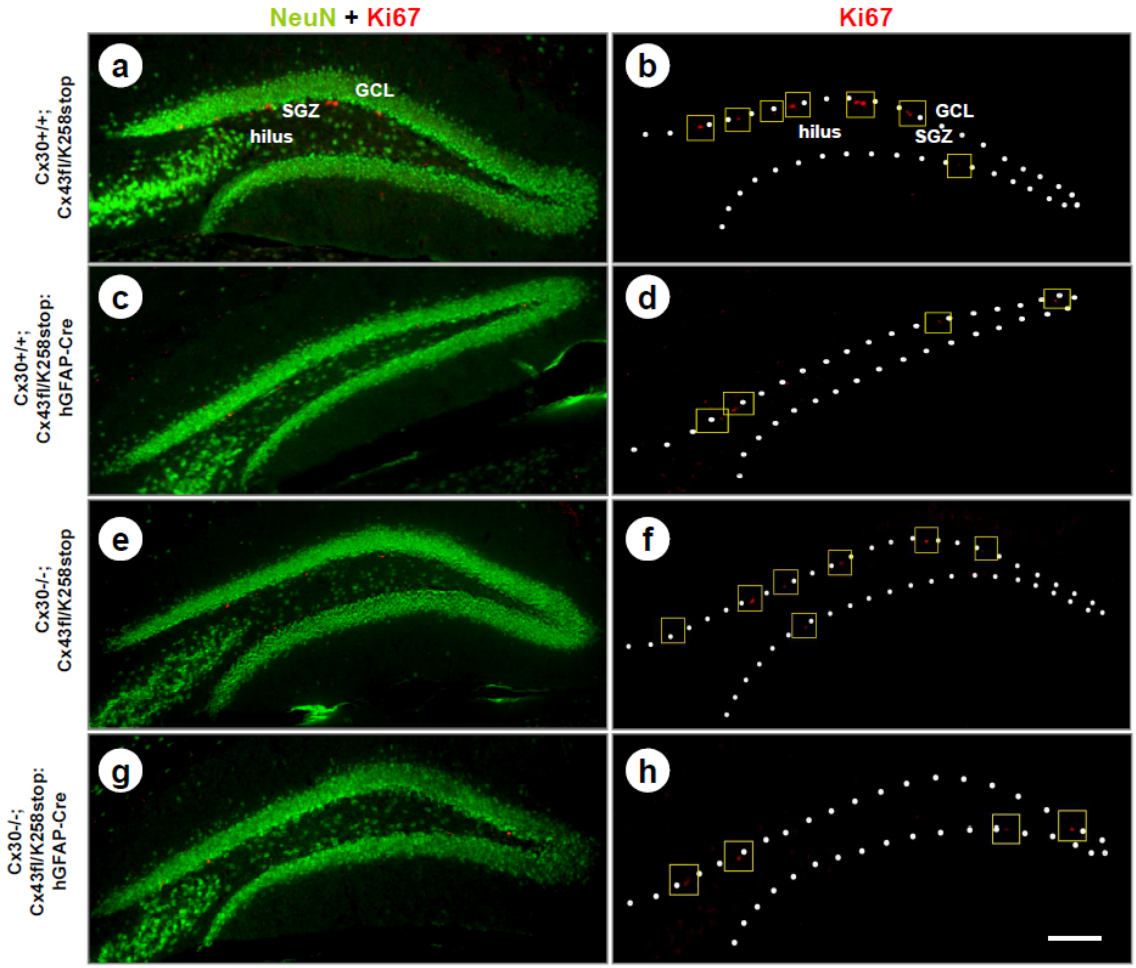

Fig. 4.29: Reduced proliferation in the SGZ of Cx43K258stop truncated mice (p60). a-h: Double labelling for Ki67 (red) and NeuN (green) in the DG of Cx30+/+; Cx43fl/K258stop (a, b), Cx30+/+; Cx43fl/K258stop: hGFAP-Cre (c, d), Cx30-/-; Cx43fl/K258stop (e, f) and Cx30-/-; Cx43fl/K258stop: hGFAP-Cre mice (g, h). Ki67-positive cells were framed in yellow scales in the same section (b, d, f and h) as in (a, c, e and g) indicated lower proliferative activity in Cx43fl/K258stop: hGFAP-Cre mice (c, d, g and h), independent of the Cx30 status. Dotted lines indicate the border between SGZ and GCL. Scale bar: 100 µm.

As mentioned previously, a positive correlation had been demonstrated between decreased proliferation in the SGZ and a reduction of granule neurons in the DG of Cx43G138R mice. We were curious about whether the Cx43K258stop expression is involved in granule neuron development. Therefore, we compared the number of granule cells employing Prox1 labelling. Interestingly, this revealed that the total number of Prox1-positive cells was comparable in the Cx43fl/K258stop: hGFAP-Cre and Cx43fl/K258stop control mice (Fig. 4.30 a, b and Fig. 4.32 a). Moreover, following Cx30 ablation the proportion of Prox1-positive cells in the Cx43K258stop and control mice remained unchanged (Fig. 4.30 c, d and Fig 4.32 b). However, we observed that the number of granule neurons in the GCL was significantly reduced in all Cx43 mutants comparing to WT (Fig. 4.32 c). In this context it is important to note that only a subpopulation of the newly generated neurons integrates into the adult GCL,

while the majority undergoes programmed cell death. Cx30-/-; Cx43fl/fl: hGFAP-Cre mice with an almost complete inhibition of proliferation showed only a 21% decline of neurogenesis compared to WT (Kunze et al., 2009). Furthermore, both animals (Cx43fl/K258stop and Cx43fl/K258stop: hGFAP-Cre) showed strongly decreased proliferation compared to WT. These situations might explain why a significant reduction of diving cells as observed in Cx43fl/K258stop and Cx43fl/K258stop: hGFAP-Cre mice caused no decrease of Prox1-positive cells.

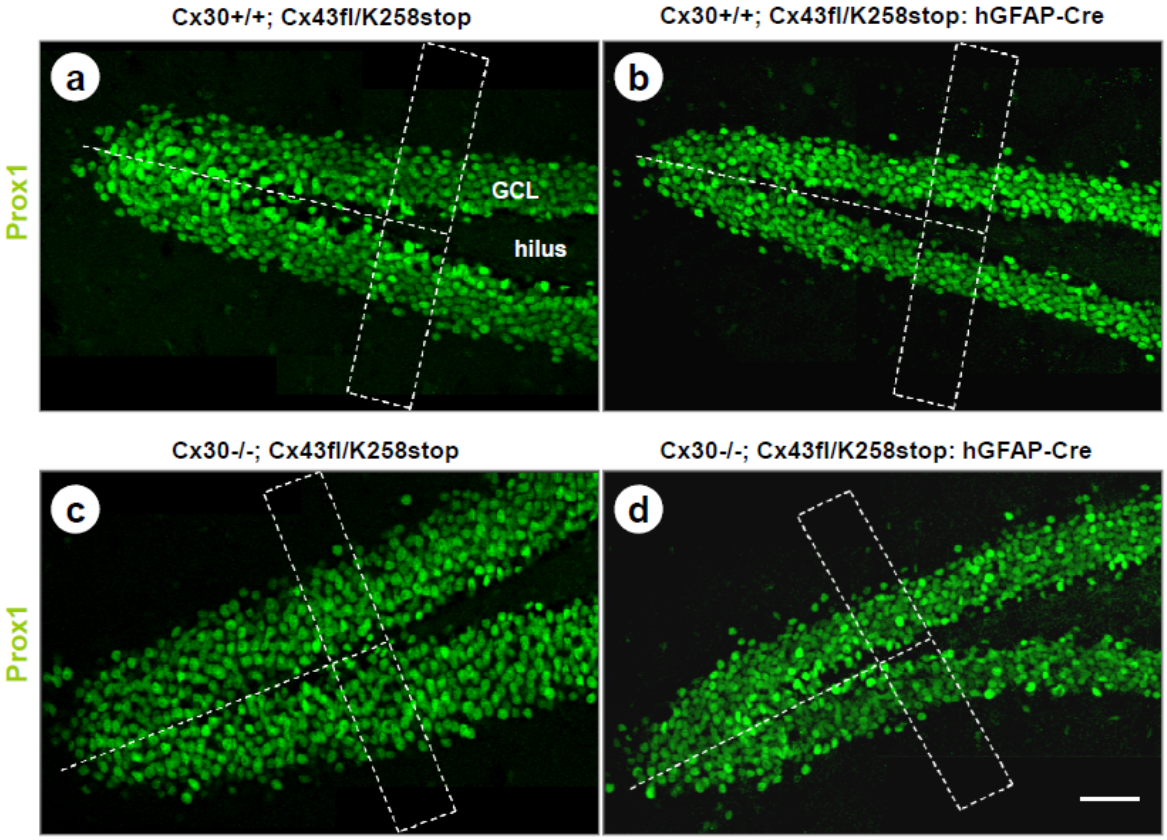

Fig. 4.30: Decreased granular neuron numbers in the DG of Cx43K258stop truncated mice (p60). a-d: Confocal images of Prox1 immunostaining (green) in the DG of Cx30+/+; Cx43fl/K258stop (a), Cx30+/+; Cx43fl/K258stop: hGFAP-Cre (b), Cx30-/-; Cx43fl/K258stop (c) and Cx30-/-; Cx43fl/K258stop: hGFAP-Cre mice (d). Representive images show similar numbers of Prox1-positive cells in the GCL of Cx43K258stop truncated mice (b, d) and Cx43fl/K258stop mice (a, c) independent of the Cx30 status. Frames in (a-d) indicate counting boxes. Scale bar: 50 µm.

In the Cx43K258stop mice, many of the BLBP-positive cells displayed a nonradial morphology and might represent transient amplifying type-2 cells which initially may still show BLBP immunoreactivity as well (Steiner et al., 2006). Moreover, we found the number of BLBP-positive cells was significantly decreased in Cx43K258stop mice versus control animals (Fig. 4.31).

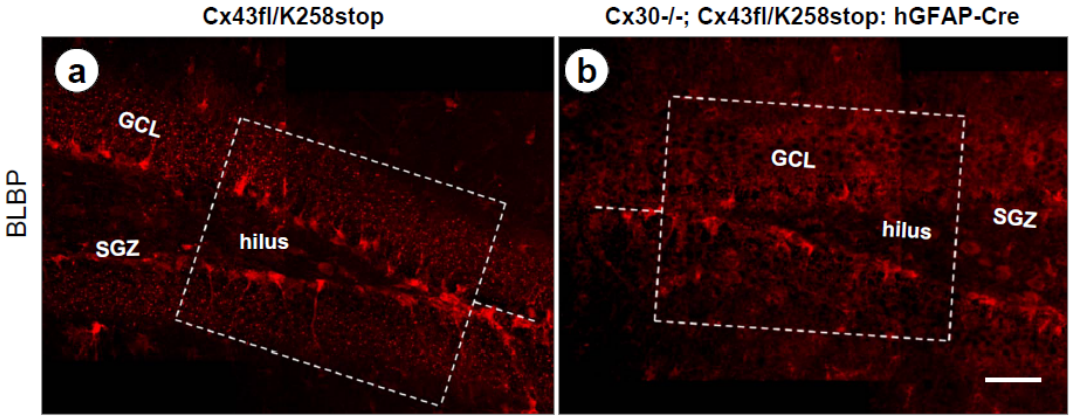

Fig. 4.31: Reduced number of BLBP-positive cells in the Cx43K258stop mice (p60). Confocal images revealed significantly decreased numbers of BLBP labeled cells in the SGZ of Cx30-/-; Cx43fl/K258stop: hGFAP-Cre (b) vs. Cx43fl/K258stop control mice (a). Frames indicated counting boxes. Scale bar: 50 µm.

In general, these observations suggest that Cx43K258stop truncation resulted in strong proliferative reduction of RG-like cells and a decrease of granule neurons in the adult DG compared to WT mice. Moreover, the numbers and the arrangement of BLBP-positive cells were significantly different between both groups. Quantitative data are summarized in Figure 4.32.

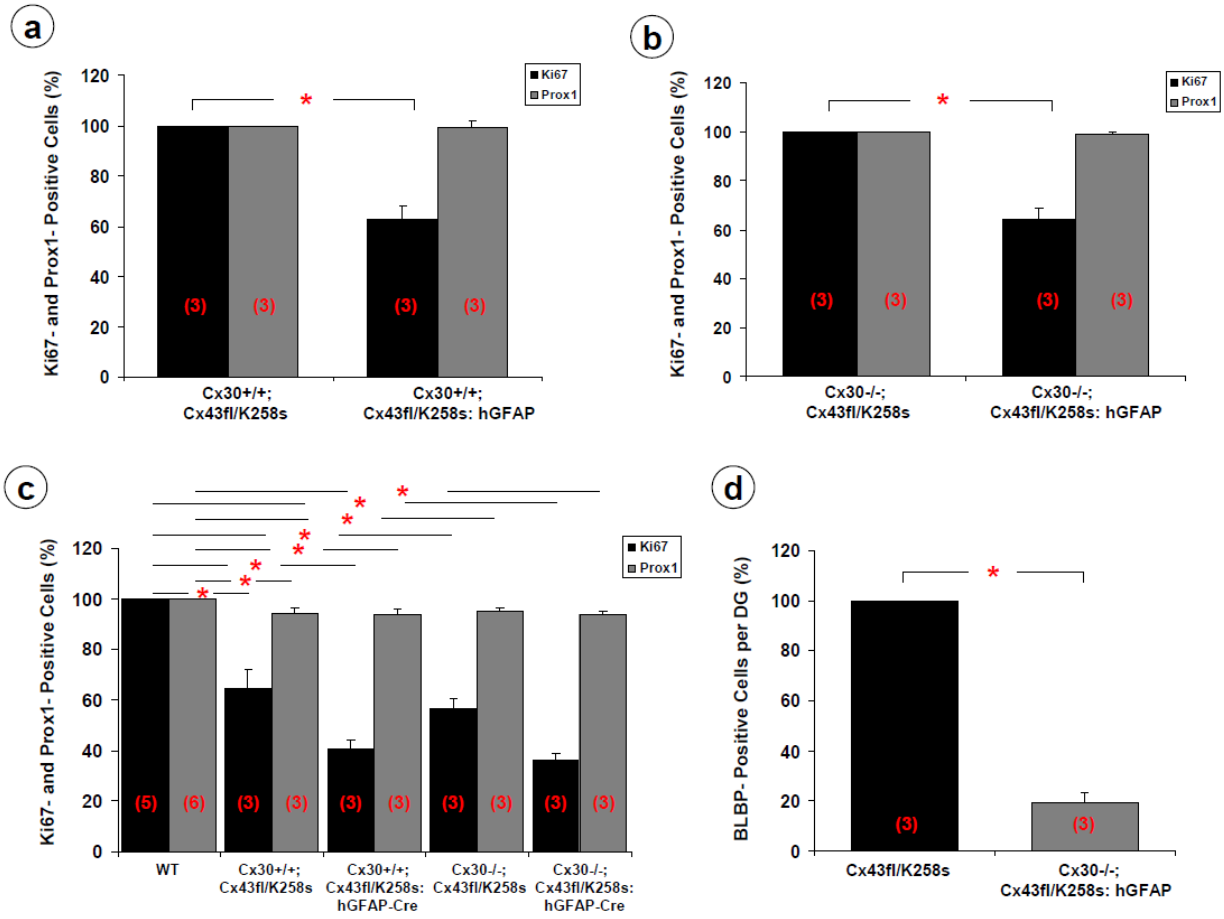

Fig. 4.32: Expression of Cx43K258stop truncation in astroglia decreases proliferation and neurogenesis in the adult mouse DG (p60). a-b: Quantitative analysis of Ki67- and Prox1-positive cell numbers of Cx43K258stop truncated mice with (a) or without Cx30 (b). Ki67-positive cell numbers were lower in hGFAP-Cre positive animals comparing to control mice, whereas the number of Prox1-positive cells was similar between both groups. **c**: Histogram comparing the proliferation and neurogenesis between Cx43K258stop mutated mice and WT animals. Mice expressing only Cx43K258stop show significantly decreased numbers of Ki67- and Prox1-positive cells compared to WT mice, irrespective of Cx30 status. In Cx43fl/K258stop mice we observed also lower numbers of Ki67- and Prox1-positive cells independent of Cx30, indicating the proliferation and neurogenesis were affected if mice express Cx43K258stop, as well as strongly reduced WT Cx43. **d:** Quantitative evaluation showing a significant reduction of BLBP-positive cells in Cx43K258stop mutated mice. Asterisks mark significant differences. Significance level was set at $P < 0.05$ (Mann-Whitney U-test and Kruskal-Wallis H-test). Number of animals in each group is shown in brackets.

4.2.3.3 No alteration of Cx43K258stop protein expression levels between Cx43fl/K258stop and Cx43fl/K258stop; hGFAP-Cre mouse hippocampus

As a previous study reported, Cx43 protein content is over 75 % decreased in heart lysates of Cx43K258stop/- comparing to Cx43+/- mice (Maass et al., 2007), whereas other groups indicated a similarly decreased Cx43 expression levels in astrocyte cultures and cortical brain tissue relative to WT (Kozoriz et al., 2010). To characterize Cx43K258stop expression and demonstrate the removal of WT Cx43 in hGFAP-Cre expressing astrocytes, Western blots were performed on hippocampal lysates using an antibody against the N-terminal domain of Cx43 (Fig. 4.33 a). Bands representing Cx43 at approximately 43 kDa were observed in Cx43+/+ and Cx43CFP/+ mice, but not in Cx43CFP/K258stop and Cx43fl/K258stop: hGFAP-Cre mice, which are lacking WT Cx43. However, the use of the N-terminal antibody resulted in additional bands at about 28 kDa in Cx43K258stop expressing mice, representing the truncated form of Cx43. Here, a significant down-regulation of Cx43 was detected in Cx43fl/K258stop: hGFAP-Cre mice relative to WT. This finding is consistent with former immunoblotting results of whole brain and heart. Most importantly, however, expression levels of Cx43 in Cx43fl/K258stop mice were similar to those of Cx43fl/K258stop: hGFAP-Cre mice (Fig. 4.33 b, c). We found that Cx30 levels were not changed in both groups. Moreover, additional knock-out of Cx30 revealed similar Cx43K258stop expression (Fig. 4.33 d, e). Immunoblotting confirmed that Cx43fl/K258stop: hGFAP-Cre mice indeed have lost immunoreactivity for the full length Cx43 and contain only strongly decreased Cx43K258stop protein. Combining proliferation and neurogenesis findings, immunoblotting results imply that significantly reduced Cx43K258stop protein levels decrease adult neurogenesis. In spite of unchanged amount of Cx43, Cx43fl/K258stop: hGFAP-Cre mice

shown significantly decreased numbers of Ki67-positive cells compared to Cx43fl/K258stop mice, indicating the C-terminus of Cx43 is required for neural stem cell proliferation.

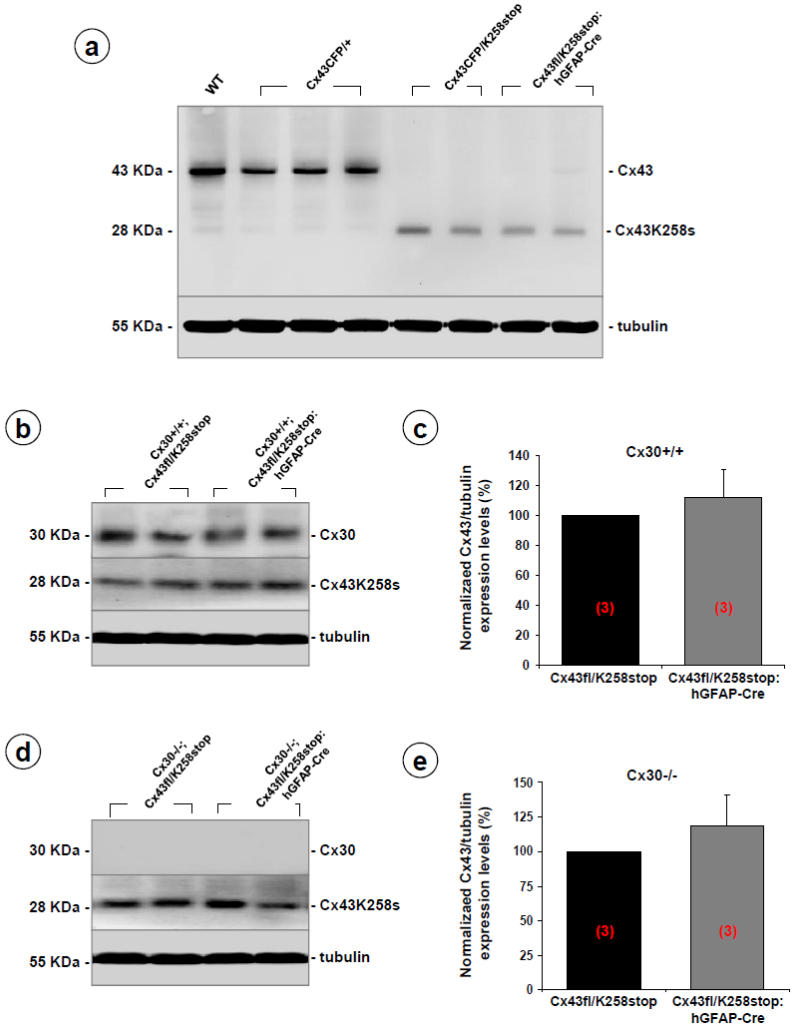

Fig. 4.33: Cx43 protein expression levels in Cx43K258stop truncated hippocampi. a: Western blot showing that the Cx43NT1 antibody recognizes the Cx43K258stop isoform (28 KDa) and WT Cx43 (43 KDa). We observed a strong down-regulation of Cx43 expression in Cx43CFP/K258stop and Cx43fl/K258stop: hGFAP-Cre mice versus WT animals. Note, that no WT Cx43 bands were detected in Cx43fl/K258stop: hGFAP mice, and in the Cx43CFP/K258stop animals. **b, d:** Comparion of Cx43 protein levels in Cx43fl/K258stop: hGFAP-Cre and Cx43fl/K258stop control animals. Cx30 expression levels were not significantly alterated between groups. **c, e:** Quantitative analysis showing a similar Cx43 protein level between groups, irrespective of Cx30. Relative expression levels of Cx43 was normalized to tubulin levels. Cx43 expression in control mice hippocampus is set to 100%. Significance level was set at $P < 0.05$ (student's t-test).

4.2.3.4 BrdU incorporation and fate mapping in the DG of Cx43K258stop mice

With an approach similar to the Cx43G138R mice used to characterize the fate of newborn neurons, the BrdU incorporation analysis was performed in Cx43K258stop mice and WT animals. This revealed a 46% (2 h) and 32% (4 weeks) lower number of BrdU labeled cells in Cx30-/-; Cx43fl/K258stop; hGFAP-Cre mice compared to WT, respectively (Fig. 4.35 a).

Importantly, almost all of the BrdU-positive cells expressed Prox1 (with or without DCX) in the 4 weeks group (Fig. 4.35 b). The proportion of Prox1-positive/Dcx-positive cells among the BrdU-positive cells in Cx43K258stop mice and control animals remained unchanged (Fig. 4. 35 b).

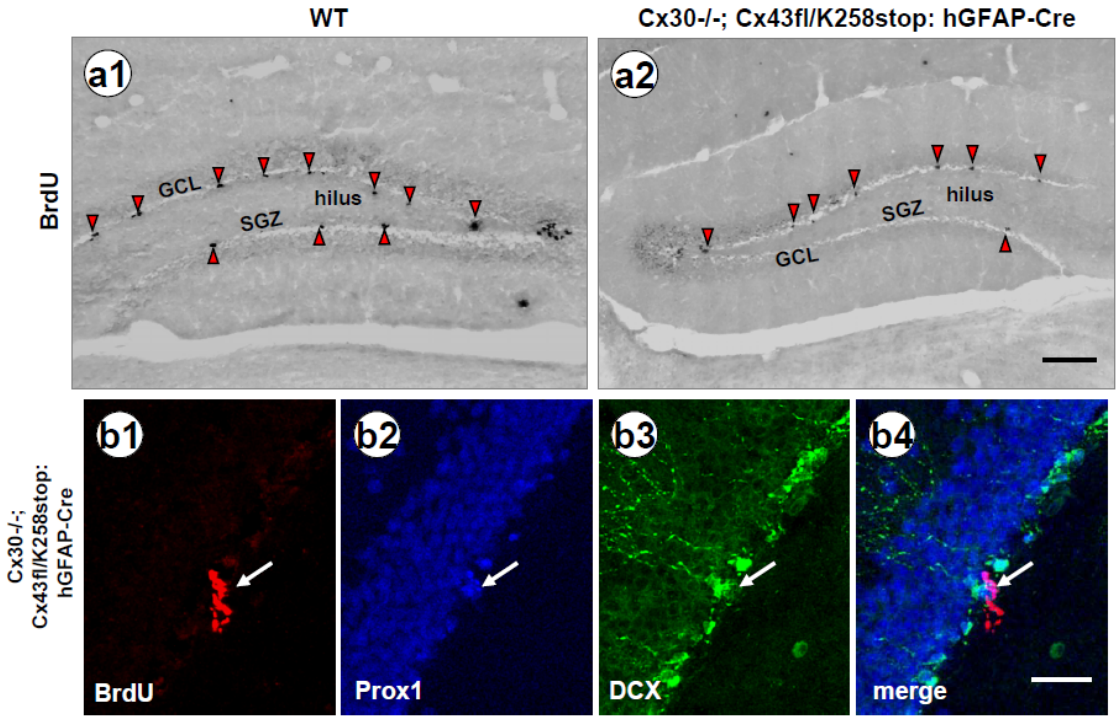

Fig. 4.34: Reduced BrdU-positive cells in Cx43K258stop mice (p60). a1-a2: Peroxidase based immunohistochemical BrdU-detection revealed a significantly decreased number of BrdU-labeled cells (red arrowheads) in the SGZ of Cx30-/-; Cx43fl/K258stop: hGFAP-Cre mice (a2) vs. WT (a1). Representative images were obtained 2 h after the last BrdU injection. Scale bar: 100 µm. **b:** Confocal images of a cell (white arrow) expressing BrdU (red), Prox1 (blue) and DCX (green) in the SGZ. Images were taken 4 weeks after the last BrdU injection. Scale bar: 25 µm

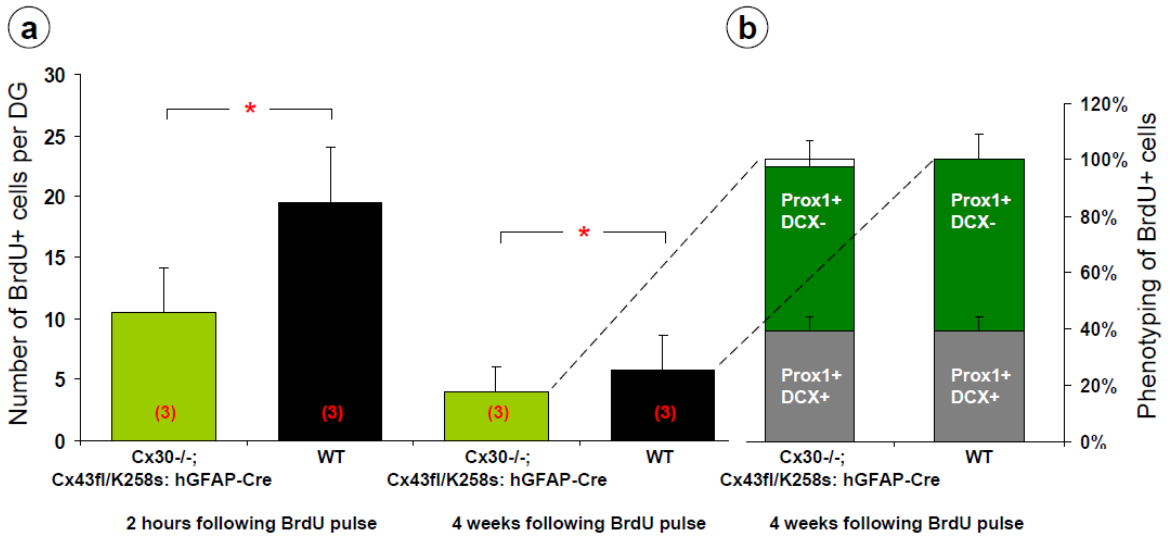

Fig. 4.35: Fate mapping of BrdU-positive cells in the SGZ of Cx43K258stop mice. a: Histogram illustrates the number of BrdU-positive cells per DG of WT (black) and Cx30-/-; Cx43fl/K258stop: hGFAP-Cre (green) mice, 2 h and 4 weeks after the last BrdU injections. At both time points a significantly decreased number of BrdU-positive cells were detected in Cx43K258stop mice. **b:** Percentage of BrdU-positive cells expressing Prox1 only, or Prox1 and DCX 4 weeks after the last BrdU pulse. Almost all BrdU-positive cells adopted a neuronal phenotype, but the proportion of Prox1-positive/DCX-positive cells (gray) did not differ between groups. In Cx43K258stop mice 0 to 2,6% of the BrdU-positive cells expressed neither Prox1 nor DCX (left bar, open). Asterisks mark significant differences. Significance level was set at $P < 0.05$ (Mann-Whitney U-test).

4.2.3.5 Biocytin coupling in the astrocytes of Cx43K258stop mice

To our surprise, tracer-coupling studies in the adult CA1 region revealed a near complete disruption in coupling of astrocytes in Cx43fl/K258stop: hGFAP-Cre mice as compared to Cx43fl/fl mice, used as control (Fig. 4.36 a1, b1; 2 ± 4 coupled cells vs. 53 ± 30 coupled cells). To confirm the Cre activity, ß-Gal immunostaining was performed in the same slice (Fig. 4.36 a2, b2). Altogether, our data indicate that not only the Cx43 point mutation but also the Cx43 truncation in astrocytes may result in complete uncoupling of astrocytes in hippocampus.

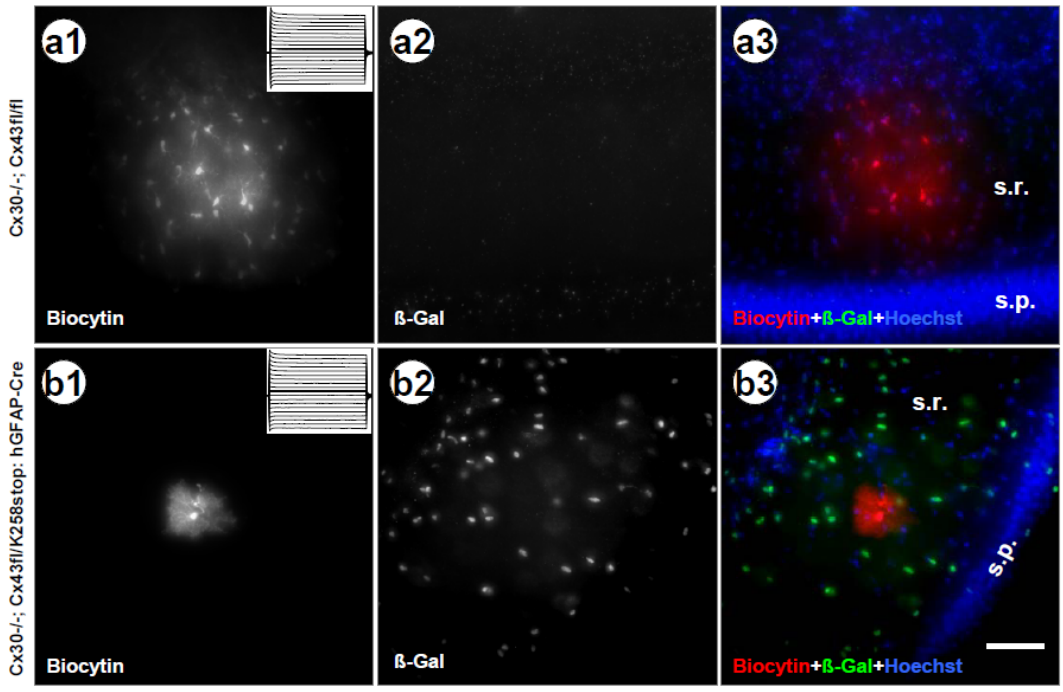

Fig. 4.36: Expression of Cx43K258stop truncation in hippocampal astrocytes strongly reduces tracer coupling (p90-p120). a1: Tracer-coupled astrocytes in Cx30-/-; Cx43fl/fl control hippocampal slices, as obtained after biocytin diffusion from a single cell, held in whole-cell voltage clamp for 20 min. **b1:** Reduced numbers of tracer-coupled astrocytes in hippocampal slices of a Cx43K258stop mutated mouse. **a2, b2:** Immunostaining of anti-ß-Gal on control (a2) and Cx43K258stop mutated mice (b2) in the same slices, respectively. Note, that no ß-Gal signals were detected in control animals. **a3, b3:** Merged pictures of triple staining. Red, biocytin; green, ß-

Gal; blue, Hoechst. Insets give the current profiles of recorded cells. Slices, 200 µm thick; Scale bar, 50 µm; s.p., Stratum pyramidale; s.r., stratum radiatum.

Quantitative data is summarized in Figure 4.37.

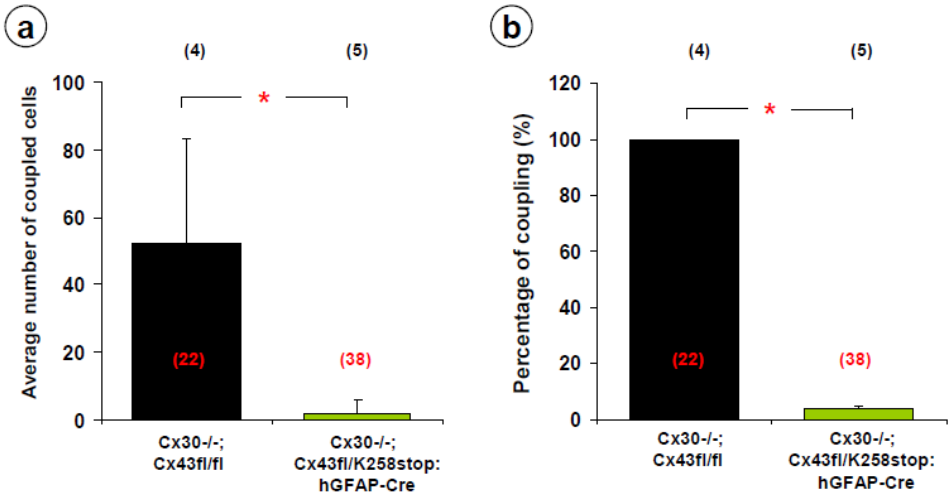

Fig. 4.37: Reduced astroglial tracer coupling in CA1 region of Cx43K258stop mice. a: Coupling was almost completely abolished in Cx43K258stop mice. **b:** Percentage of coupling normalized to control mice reveals a 96% reduction in coupling in Cx43K258stop mice. Asterisks mark significant differences. Significance level was set at $P < 0.05$ (Mann-Whitney U-test). Number of analyzed brains is shown in black and corresponding slices in red per group.

4.2.3.6 Biocytin coupling in the RG-like cells of Cx43K258stop mice

Compared to Cx43G138R mice, Cx30-/-, Cx43fl/K258stop: hGFAP mice displayed a stronger reduction in RG-like cell coupling to about 58% of control (Fig. 4.39 a; 5 ± 1 coupled cells vs. 12 ± 1 coupled cells). Quantification of biocytin spread identified a coupling ratio of 62,5% in Cx43K258stop mice (5 out of 8 cells; Fig. 4.39 b), whereas WT mice shown a coupling ratio of 83,3% among RG-like cells (5 out of 6 cells; Fig. 4.39 b). In conclusion, the Cx43 truncation exhibited a significantly reduced RG-like cell coupling. Moreover, a high proportion of passive RG-like cells are completely uncoupled by this gap junction mutation.

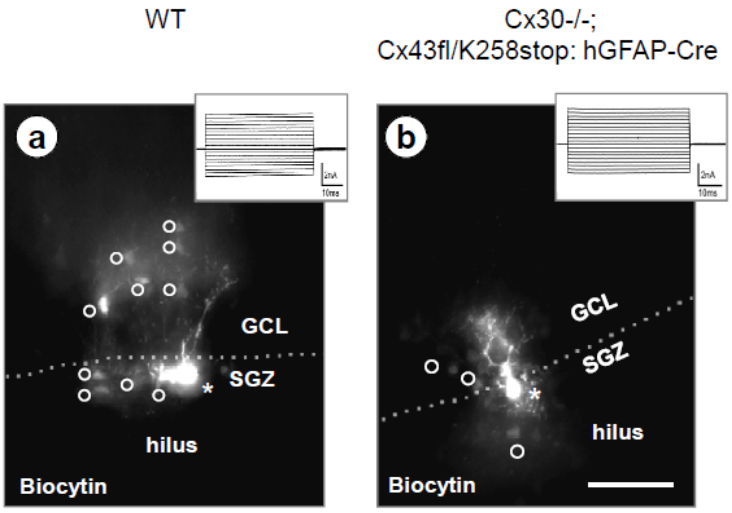

Fig. 4.38: Decreased biocytin coupling in the SGZ of Cx43K258stop mice (p90-p120). Representative images of a coupled RG-like cells in WT control (a) and Cx30-/-; Cx43fl/K258stop: hGFAP-Cre (b) mice. Tracer spread from the recorded cell (*) to neighbouring cells (ٮ). Note that the tracer spread to a few neig hbouring cells in Cx43K258stop mice comparing to WT animals. Insets give the current pattern of recorded cells. Broken lines indicate the border between SGZ and GCL. Slices, 200 µm thick; Scale bar, 50 µm.

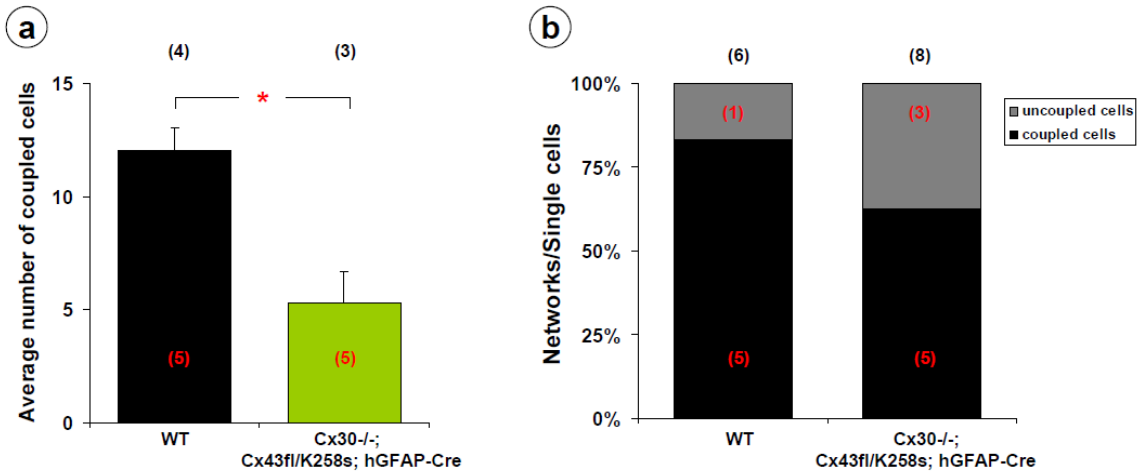

Fig. 4.39: Quantitative evaluation of RG-like cell tracer coupling in Cx43K258stop mice. a: Mice expressing Cx43K258stop truncation show significantly decreased numbers of biocytin coupled RG-like cells in the SGZ versus WT animals. Number of analyzed brains is shown in black and corresponding cells in red. **b:** Percentage of tracer coupled and uncoupled cells in control and Cx43K258stop mice. Asterisks mark significant differences. Significance level was set at $P < 0.05$ (Mann-Whitney U-test).

4.2.4 Analysis of Cx43D378stop mutant mice in adult neurogenesis

4.2.4.1 Proliferation and neurogenesis of Cx43D378stop mice

Cx43D378stop mice lacking the last five amino acid residues of the C-terminal binding motif for ZO-1 still reveal functional gap junction channels and normal coupling properties in cardiomyocytes (Lubkemeier et al., 2013). However, the intracellular adhesion mediated by

C-terminus should be impaired in this mouse. With immunostaining, we found that the proliferative activity in the SGZ but not the number of newborn neurons in the DG was significantly changed in astroglia-specific Cx43D378stop mice.

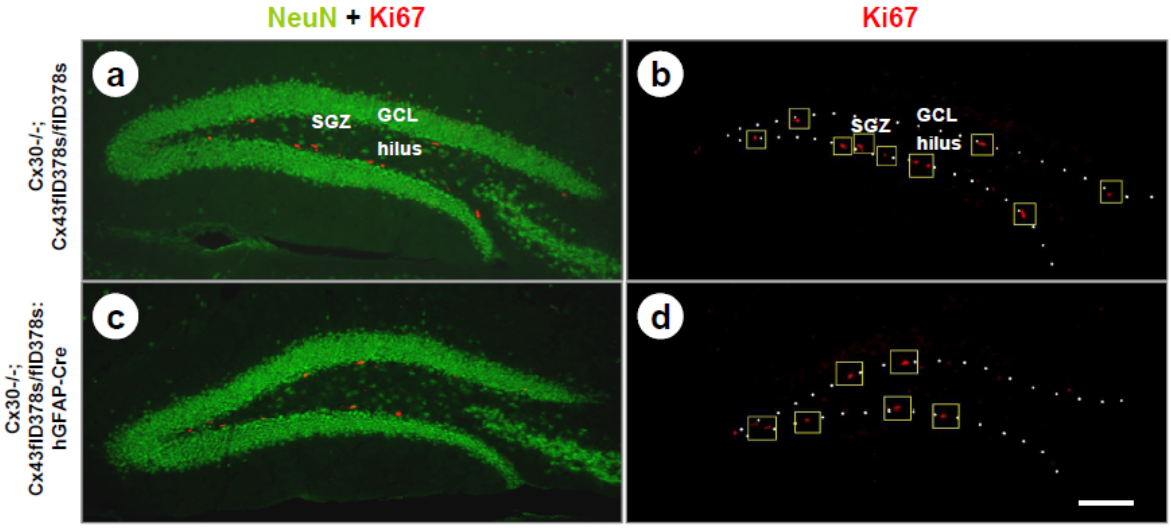

Fig. 4.40: Reduced proliferative activity in the SGZ of Cx43D378stop mutated mice (p60). a-d: Double labelling for Ki67 (red) and NeuN (green) in the DG of Cx30-/-; Cx43flD378stop/flD378stop (a, b) and Cx30-/-; Cx43flD378stop/flD378stop: hGFAP-Cre mouse (c, d). The coronal images represent approximately the same z-position in rostrocaudal extension of the hippocampus, respectively. Ki67 positive cells were framed in yellow boxes in the same section (b, d) as in (a, c), indicating significantly decreased proliferation in the Cx43flD378stop/flD378stop: hGFAP-Cre mouse. Dotted lines indicate the border between SGZ and GCL. Scale bar: 100 µm.

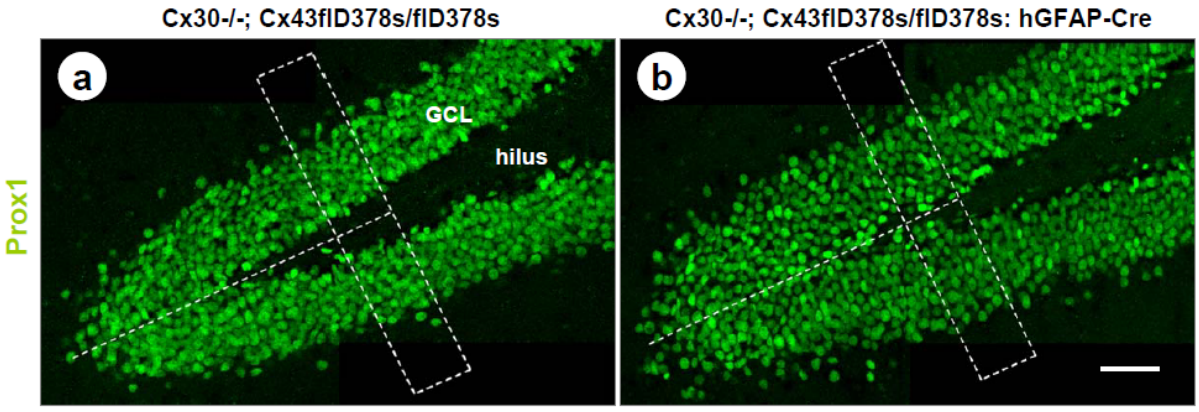

Fig. 4.41: Unchanged granular neuron numbers in the DG of Cx43D378stop mutated mice (p60). Confocal images of Prox1 immunostaining (green) on the DG of Cx30-/-; Cx43flD378stop/flD378stop (a) and Cx30-/-; Cx43flD378stop/flD378stop: hGFAP-Cre mouse (b). Representive images show similar numbers of Prox1-positive cells in the GCL of Cx43D378stop mutated (b) versus Cx43flD378stop/flD378stop mice (a). Frames in (a, c) indicated counting boxes. Scale bar: 50 µm.

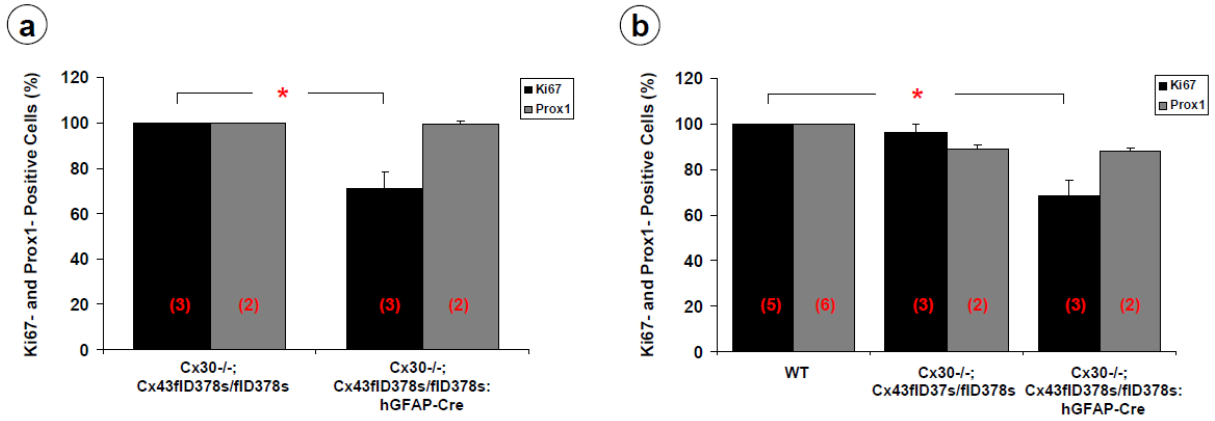

Fig. 4.42: Expression of Cx43D378stop mutations in astroglia decreases proliferation in the adult DG (p60). a: Quantitative analysis of Ki67- and Prox1-positive cell numbers of Cx43D378stop mutated mice. Ki67-positive cell numbers were lower in hGFAP-Cre positive animals compared to control mice, which express still wild type Cx43. **b:** Histogram comparing the proliferation and neurogenesis between Cx43D378stop mutated mice and wild type animals. Mice expressing Cx43D378stop show significantly decreased numbers of Ki67- and Prox1-positive cells compared to WT mice. Asterisks mark significant differences. Significance level was set at $P < 0.05$ (Mann-Whitney U-test and Kruskal-Wallis H-test). Number of animals in each group is shown in brackets.

4.2.4.2 Biocytin coupling in the astrocytes of Cx43D378stop mice

Our results so far suggest that there is a significantly reduced astrocytic coupling in Cx43D378stop mice compared to control animals, which was not consistent with former findings in primary cadiomyocytes and transfected HeLa-cells (Lubkemeier et al., 2013).

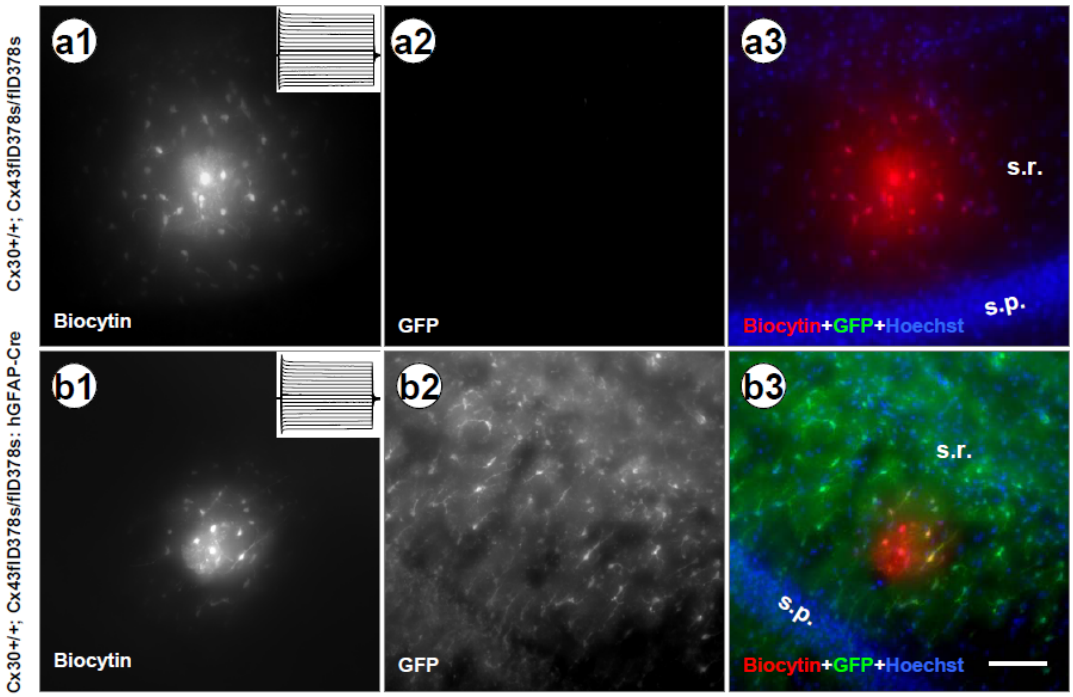

Fig. 4.43: Expression of Cx43D378stop mutation in hippocampal astrocytes strongly reduces tracer coupling (p90-p120). a1: Tracer-coupled astrocytes in Cx30+/+; Cx43flD378stop/flD378stop control hippocampal slices, as obtained after biocytin diffusion from a single cell, held in whole-cell voltage clamp for 20 min. **b1:** Reduced numbers of tracer-coupled astrocytes in hippocampal slices of a Cx43D378stop mutated mouse. **a2, b2:** Immunostaining of anti-GFP on control (a2) and Cx43D378stop mutated mice (b2) in the same slices, respectively. Note, that no GFP signals were detected in control animals. **a3, b3:** Merged pictures of triple staining. Red, biocytin; green, GFP; blue, Hoechst. Insets give the current profiles of recorded cells. Slices, 200 µm thick; Scale bar, 50 µm; s.p., Stratum pyramidale; s.r., stratum radiatum.

Quantitative data is summarized in Figure 4.44.

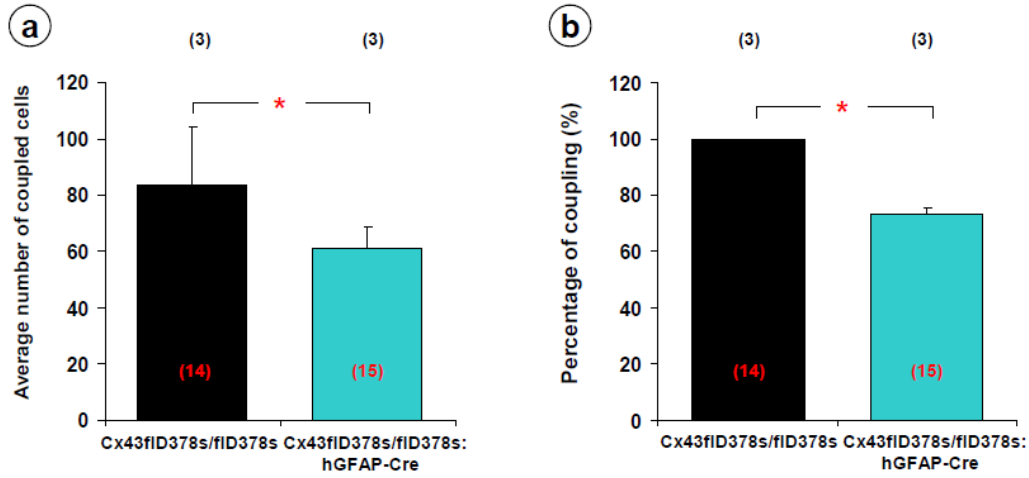

Fig. 4.44: Reduced astroglial tracer coupling in CA1 region of Cx43D378stop mutated mice. a: Quantitative evaluation revealed that average numbers of coupled cells were significantly decreased in Cx43D378stop mice. **b:** Percentage of coupling normalized to control mice reveals a 30 % significant decrease in Cx43D378stop mice. Asterisks mark significant differences. Significance level was set at $P < 0.05$ (Mann-Whitney U-test). Number of analyzed brains is shown in black and corresponding slices in red per group.

4.3 Cx43 phosphorylation as a regulatory event linked to gap junction coupling

To study the role of glial connexins in epilepsy, mice were subjected to a Temporal Lobe Epilepsy (TLE) model which closely mimics human TLE with a sclerotic hippocampus (HS) in the mouse. A significant decrease of astrocytic coupling was observed ipsilaterally compared to the contralateral side on the same slice 5 days after kainate injection (5 dpi; Bedner et al., unpublished). A former study has shown that the coupling of astrocytes in the hippocampus predominately depends on Cx43 (Gosejacob et al., 2011). However, Cx43 mRNA or protein expression in astrocytes of kainate-treated rats was nearly normal or slightly increased at various survival times. Immunofluorescence analysis indicated that cellular localization of Cx43 was indistinguishable from control animals 4 weeks after the last kainate administration (Hossain et al., 1994; Sohl et al., 2000). Previous work has demonstrated that Cx43 phosphorylation state is to some extent correlated with alterations in junctional coupling (Warn-Cramer et al., 1998; Nagy and Li, 2000; Lampe and Lau, 2004). To investigate how Cx43 posttranslational phosphorylation regulates astrocytic junctional coupling and identify of potential protein kinases that contribute to this regulation we performed immunoblotting, immunoprecipitation and mass spectrometry studies.

4.3.1 Comparison of Cx43 phosphorylation in dorsal ipsi- and contralateral hippocampus following intracortical kainate injection

To determine whether reduced astrocytic coupling in kainate-treated tissue is due to an altered expression pattern of Cx43, Western blot was performed using 100 µg homogenized hippocampal lysates of the injected hemisphere and the respective contralateral side from the same animal 5 days after injection. We examined the total protein level employing an antibody against the C-terminus of Cx43, which recognizes both phosphorylated and unphosphorylated isoforms. The result from this study indicated that nonphosphorylated isoform (P0) of Cx43 can be found mainly on the contralateral side, whereas phosphorylated isoforms (P) are remarkably upregulated on the ipsilateral side. The observed total Cx43 amount shows a significant 2,5-fold increase on the ipsilateral versus contralateral side (Fig. 4.45).

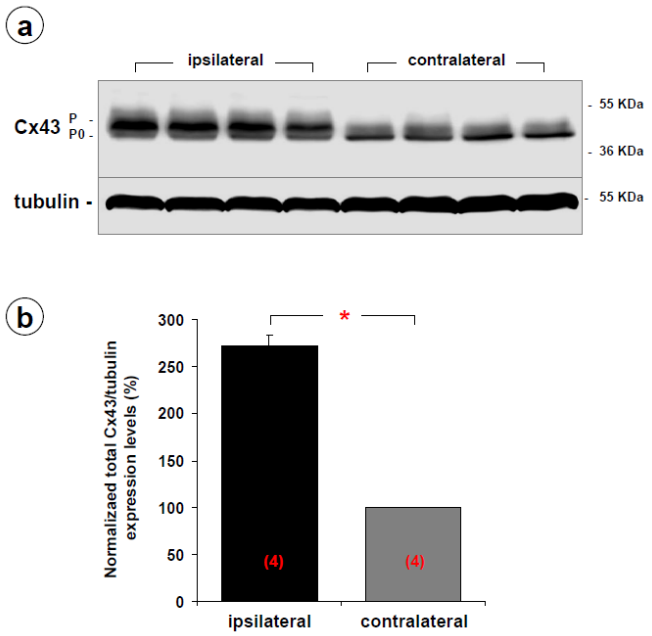

Fig. 4.45: Cx43 phosphorylation profiles in ipsi- and contralateral hippocampus following intracortical kainate injection (5 dpi). a: Immunoblot showing a up-regulation of phosphorylated Cx43 isoform in ipsilateral side comparing with contralateral hippocampus using an antibody recognizes C-terminal of both phosphorylated and nonphsphorylated Cx43 isoforms. α-Tubulin is shown as a loading control. P, position of the phospho-isoform; P0, position of the unphospho-isoform. **b:** Quantitative analysis of total Cx43 amount in ipsi- and contralateral hippocampus. A significant increase of total Cx43 protein levels was observed on the ipsilateral vs. contralateral side. Significance level was set at $P < 0.05$ (student's t-test).

Former studies demonstrated that Cx43 from cultured cells or heart lysates have multiple electrophoretic isoforms when analyzed by SDS-PAGE. It includes a fast migrating form (P0) for non-phosphorylated and two slowly migrating forms (P1 and P2) of phosphorylated Cx43 (Musil and Goodenough, 1991; Lampe et al., 2006). Treatment of such sample with alkaline phosphatases collapses most of the Cx43-associated bands to its fastest migrating isoform (P0) (Musil et al., 1990). To characterize whether in hippocampal lysates similar multiple electrophoretic isoforms of Cx43 in SDS-PAGE occur we tested different protein amounts and gel running conditions. According to our immunoblot results, we found that 30 µg protein lysates is sufficient to detect all three isoforms of Cx43 (Fig. 4.46 a), indicating a hippocampal Cx43 expressing pattern similar to heart or cultured kidney cells. In agreement with our previous studies, the Cx43 P2 isoform in the ipsilateral side was significantly increased compared with those in contralateral tissue (Fig. 4.46 b, c). Following alkaline phosphatase treatment, the phosphorylated isoforms collapsed to the fastest migrating form as shown in Fig. 4.46 d, indicating a reduction in the level of phosphorylation of these residues and confirming that the bands detected with same antibody are indeed phospho-Cx43. Quantification of P0 signals normalized to tubulin revealed no increased protein of the ipsilateral side (Fig. 4.46 e).

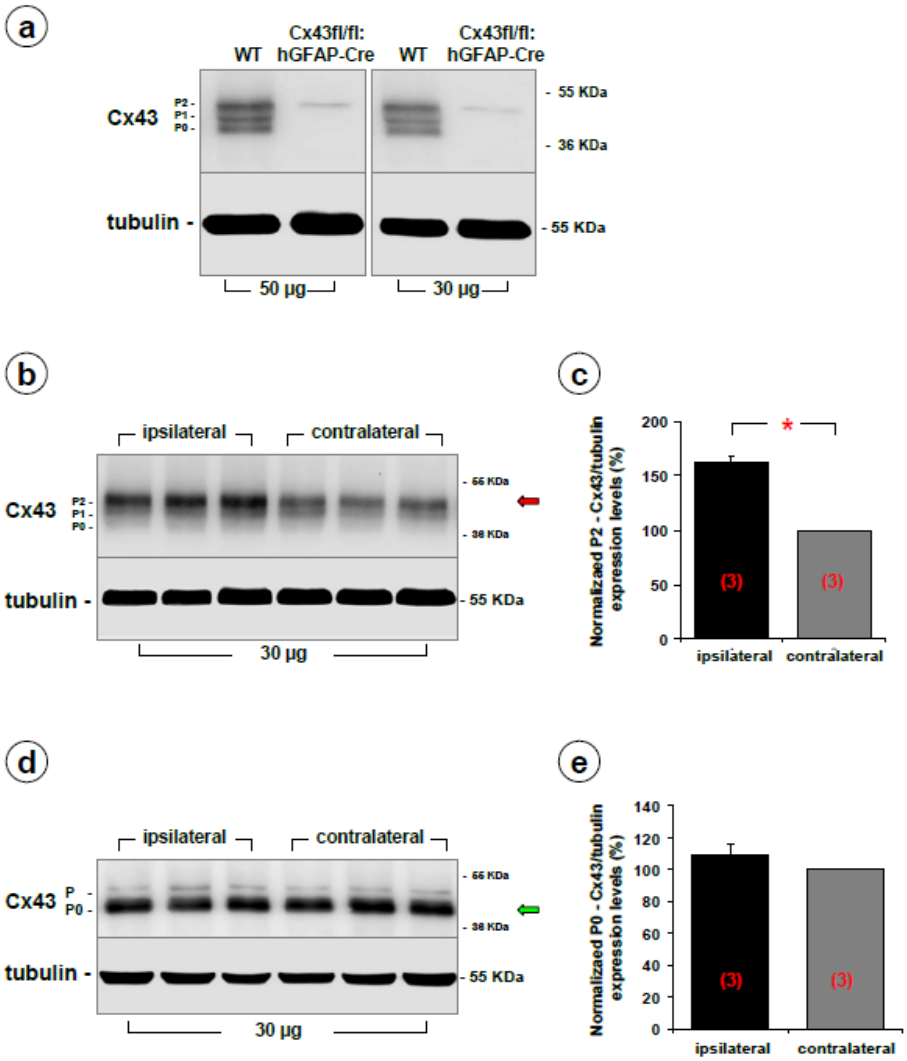

Fig. 4.46: Specificity of the C-terminal antibody by immunoblotting. a: Western blot analysis of hippocampal lysates from WT and Cx43fl/fl: hGFAP-Cre mice. Increased Cx43 level was observed in the 50 µg WT group relative to those in the 30 µg group. Here, we found phosphorylated and nonphosphorylated Cx43 using the antibody against the CT domain. **b, d:** Equal amounts of protein lysate from dorsal hippocampus were either untreated (b) after intracortical kainate injection and probed with the C-terminal Cx43 antibody or treated with alkaline phosphatase (d). We observed an increase in the P2 isoform of Cx43 on the ipsilateral side (red arrow). However, the same lysates after alkaline phosphatase treatment show a disappearance of the P2 isoforms and reduced P1 isoforms, but increased P0 isoforms (green, arrow). **c, e:** Quantitative analysis of P2- (c) or P0-isoforms (e) of Cx43 amount in ipsi- and contralateral side. The P2 isoform of Cx43 shows a significant increase in ipsilateral vs. contralateral, but P0 Cx43 was similar on both sides. Significance level was set at $P < 0.05$ (student's t-test). Animal numbers are marked in red.

4.3.2 Using specific antibodies that recognize Cx43 phosphorylated residues in the carboxy-terminal region

In the C-terminal region of Cx43 there are at least 14 serines and 2 tyrosines that are phosphorylated by a variety of kinases (Marquez-Rosado et al., 2012). It has been shown that phosphorylation of these residues can result in decreased or increased conductivity of the gap junction channel (Lampe et al., 2000; Lampe and Lau, 2004; Pahujaa et al., 2007). Understanding the phosphorylation sites, patterns and corresponding kinases is absolutely critical to our study. One of the most classical examinations regarding this issue is assessment by Western blot with a set of Cx43 phospho-specific antibodies. Together with Prof. Dr. Lampe (FHCRC, Seattle, USA), the dorsal parts of hippocampal lysates were analyzed for any impact of phosphorylation on gap junctional communication. Using an antibody against the N-terminus of Cx43 (Cx43NT1), which recognizes both phosphorylated and unphosphorylated isoforms of Cx43, we found a significant increase of Cx43 phosphorylation in the ipsilateral versus contralateral samples (Fig. 4.47 a). This observation confirmed our previous immunoblotting results using a C-terminal antibody (Cx43CT) (Fig. 4.45 and Fig. 4.46 b). Surprisingly, we observed a significant increase in the pS373-Cx43 signal of ipsilateral samples which has previously been shown to associate with improved gap junction functionality via a protein kinase A (PKA)-dependent mechanism (Fig. 4.47 b). As pY247 has been identified as a Src phosphorylation site (Pahujaa et al., 2007), we expected to find an increase in the active, phosphorylated form of Src concomitant with increased phospho-Cx43 in the injected side. However, unfortunately, pY247-Cx43 was undetectable at both lateral sides (Fig. 4.47 c). In addition, when pS279/282- and pS365-Cx43 antibodies were probed on the same membrane, we can see a slightly increased pS279/282-Cx43 signal and an almost unchanged pS365-Cx43 amount in the ipsilateral samples (Fig. 4.47 c), indicating a reduction of gap junctional functionality by the mitogen-activated protein kinase (MAPK) pathway. In contrast, we observed a slightly reduced phosphorylation of residue pS368 in the ipsilateral tissue. These results suggested that after kainate injection the activation of PKA and MAPK can lead to increased phosphorylation at pS373 and pS279/282 residues in the C-terminus of Cx43, respectively, which would be expected to lead opposite effect on gap junction mediated conductance.

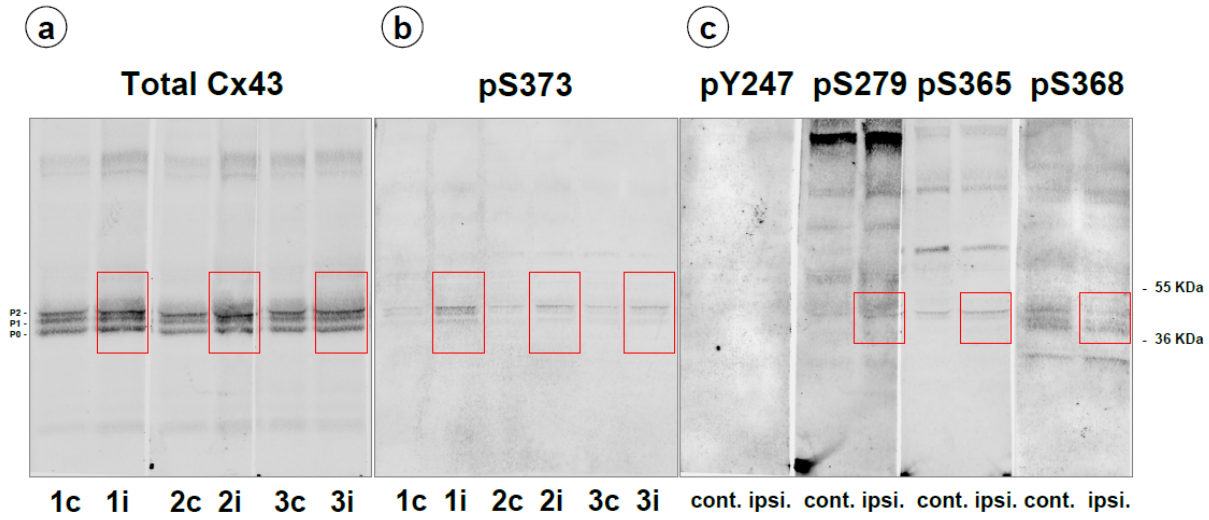

Fig. 4.47: Comparison of Cx43 expression profile using phospho-specific antibodies. a: Western blot of hippcampal protein lysates isolated from three WT animals (lanes 1, 3, 5, contralateral and lanes 2, 4, 6, ipsilateral, respectively) simultaneously probed for total Cx43 antibody against N-terminal (Cx43NT1). Notice the increased Cx43 phosphorylated content in the ipsilateral samples. **b:** The pS373-Cx43 antibody reprobed on the same blot show increased P2 isoform of Cx43 in the ipsilateral groups relative to contralateral. **c:** Same blot reprobed for Cx43 phosphorylated at S247, S279/282, S365 and S368. Western blots demonstrating an increased pS279/282-Cx43 and an unchanged pS365-Cx43, but decreased pS368-Cx43 in the ipsilateral comparing to contralateral. The pS247-Cx43 antibody did not detect any band from both sides.

4.3.3 Isolation and concentration of Cx43 for phosphorylation analysis by mass spectrometry

Because of conflicting results and limited by the availability, affinity and specificity of commercial antibodies directed toward phosphorylated residues in Cx43, we applied mass spectrometry (MS) to characterize site-specific changes in Cx43 phosphorylation. With the growing prominence of MS, this technique is being applied to fill the gaps in understanding of connexin post-translational regulation. The protein purification and preparation procedures can have the most significant impact on the outcome of an MS-based investigation. Because the proteome is so complex, there is no standard method for preparing protein samples for MS analysis. In our study, an immunoprecipitation (IP)-based procedure was performed to isolate purified and reasonable amounts of Cx43 protein preserved in its native phosphorylation state. Two different anti-Cx43 C-terminus (Cx43CT) rabbit polyclonal antibodies and 1000 µg homogenized hippocampal protein lysate were tested for their antibody-antigen interaction. As shown in Fig. 4.48, the concentrated Cx43 was successfully recovered and fractionated by SDS-PAGE and evaluated by immunoblotting with one antibody against the C-terminus of Cx43 after elution of target antigen (lanes A1 and B1). Before elution, the supernatant (“Pre-elution” in lanes A2 and B2) corresponding to the IP

samples were loaded on the same gel and used as control. A “pseudo-IP” sample without binding of Cx43 antibody was separated on the same blot as negative reference (lane C1 and C2). Moreover, normal WT hippocampal lysate (lane D), transfected Cx43 HeLa cell extracts (lane E) and Cx43fl/fl: hGFAP-Cre hippocampal lysate (lane F) served as positive or negative loading control, respectively. Cx43 IP-samples separated on SDS-PAGE were visualized using Coomassie staining. Cx43 protein bands are then excised from the gel and digested *in situ*. The peptides are extracted from the gel matrix and prepared for MS analysis.

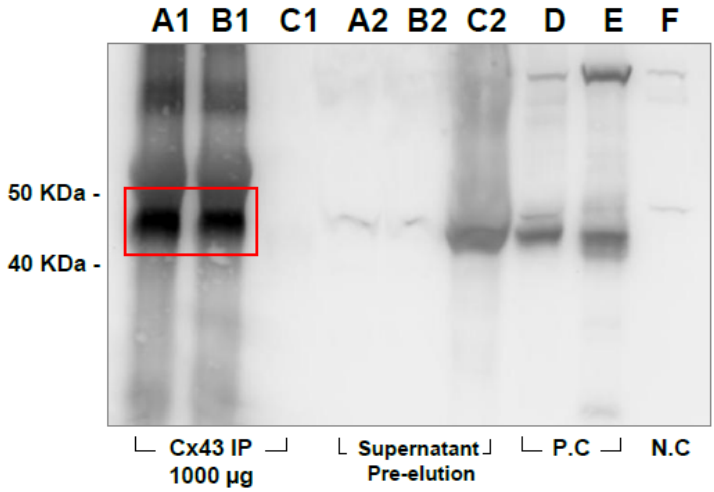

Fig. 4.48: Immunoprecipitation to Isolate and concentrate total Cx43 for MS analysis. Immunoprecipitated Cx43 protein was probed by Cx43 C-terminal antibody. Immunoblotting shows precipitate using two different Cx43 C-terminus antibodies (lane A1, B1) and a control immunoprecipitate with non anti-Cx43 antibody was analyzed in parallel (lane C1). Prior to elution, transfer supernatants from corresponding bead-Ab-Ag complexes to clean tubes for the following control as shown in lane A2, B2 and C2. WT hippocampal lysate (lane D), transfected Cx43 HeLa cell extracts (lane E) and Cx43KO hippocampal lysate (lane F) served as positive or negative loading control, respectively. Bands of interest are indicated by red boxes.

4.3.4 Identification of phosphorylation sites in Cx43 using mass spectrometry

Protein lysates from five WT mice hippocampi were subjected to IP with anti Cx43-antibodies (section 4.3.3). Proteins were separated by SDS-PAGE and a slice corresponding to the molecular weight of Cx43 was excised. After in-gel digestion nanoLC-MS was performed at the MS service unit at the Institute of Biochemistry and Molecular Biology (Dr. Marc Sylvester, University Hospital Bonn) in order to identify Cx43 peptides carrying phosphorylation sites on serine, theonine, or tyrosine. Overall intensities of Cx43 peptide signals were low but three phosphopeptides could be identified in two experiments. The peptide D190 to S217 is unambiguously phosphorylated at its C-terminal serine (Fig. 4.49). The majority of peaks could be identified. Consecutive ions from one ion series were found for several charge states. Several phosphorylation losses and neutral losses of water and ammonia were found.

A peptide covering G242 to K258 was found to be singly phosphorylated; however the exact position can not be assigned due to the low number of fragmentation of phosphopeptides. The most probable assignments are pS244 and pY247. A mixture of both singly phosphorylated peptides is conceivable as well (Fig. 4.50). A third phosphopeptide was identified: A370 to I382 (C-terminus of Cx43) contains a phosphorylation on position S372 or S373 or a mixture of both isoforms (Fig. 4.51). Consecutive ions from one ion series were found for both charge states. Many peaks could be identified and characteristic y_6- and y_8-ions were found at proline sites while the corresponding b-ions are suppressed. Co-isolation of other precursors was 15% which can account for unassigned fragments. The proximal position of phosphate hampers unambiguous assignment of the phosphorylated position.

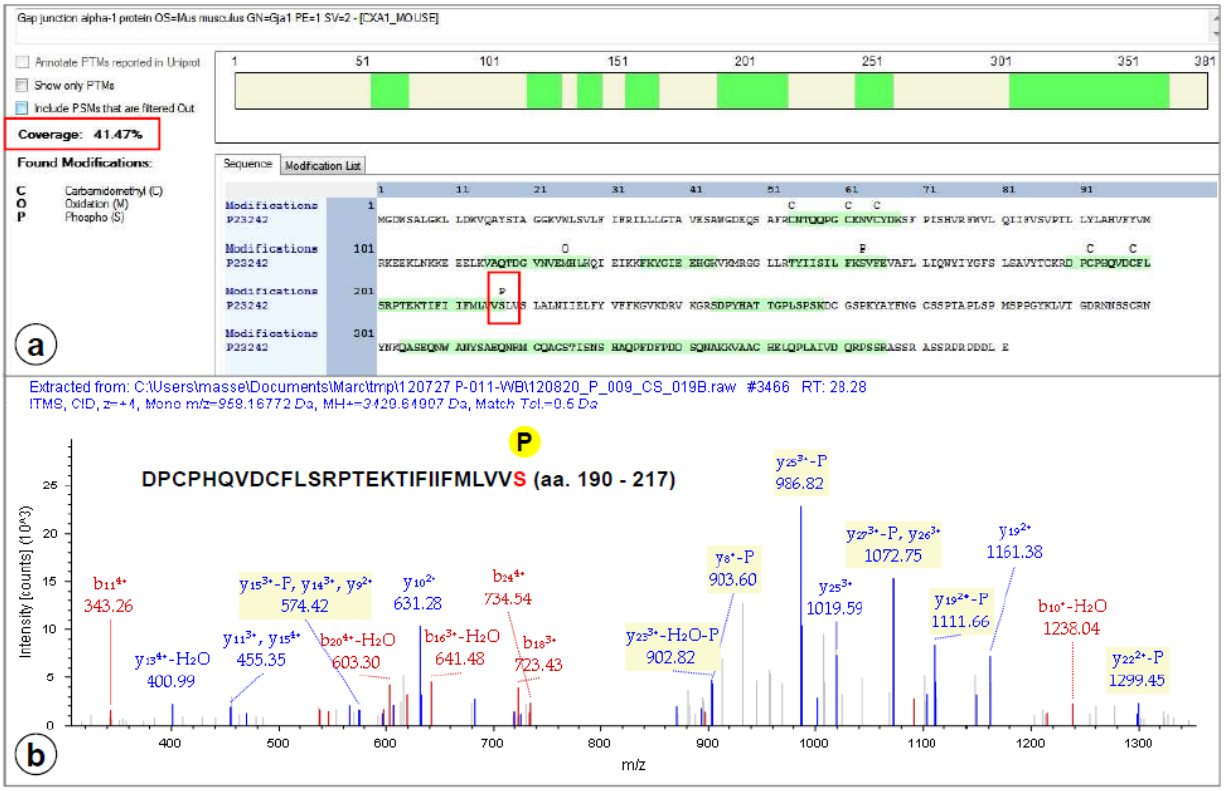

Fig. 4.49: SEQUEST search of reduced Cx43 database. **a:** Sequence coverage of Cx43 (SwissProt P23242) with phosphorylation site S217. **b:** Fragment ion spectrum of highest scoring assignment of m/z 868.168 (z=4, 1.29 ppm error, Xcorr=2.60) as identified by Proteome Discoverer Software: ^{190}DPc(CaM)PHQVDc(CaM)FLSRPTEKTIFIIFMLVVs^{217}(phospho). b-ions are shown in red, y-ions in blue. Several phosphorylation losses (yellow shaded annotations) and neutral losses of water and ammonia were found.

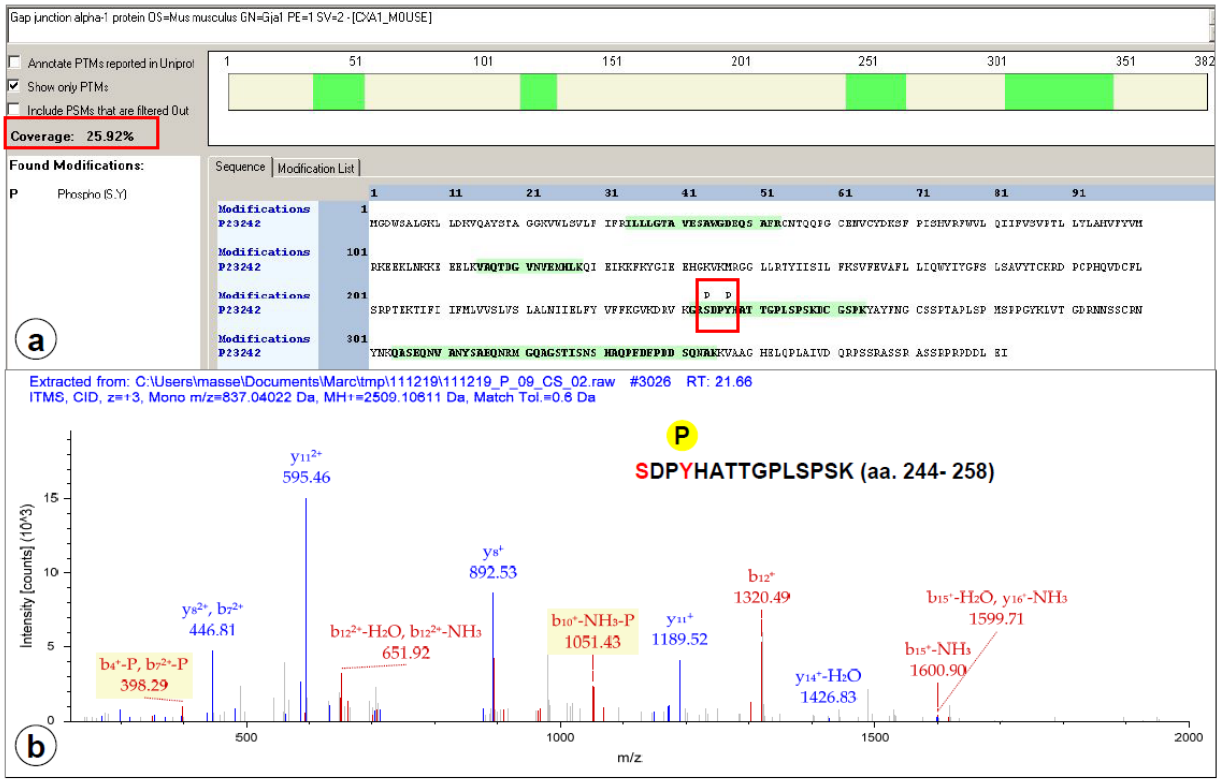

Fig. 4.50: SEQUEST search of SwissProt (mouse sequences). a: Sequence coverage of Cx43 (SwissProt P23242) with phosphorylation site S244 or Y247. **b:** Fragment ion spectrum of highest scoring assignment of m/z 837.040 (z=3, -4.67 ppm error, Xcorr=2.13) as identified by Proteome Discoverer Software: ^{242}GRs(phospho)DPYHATTGPLSPSKDc(CaM)GSPK^{258}. b-ions are shown in red, y-ions in blue. Most major peaks were assigned, but some lower remained unassigned.

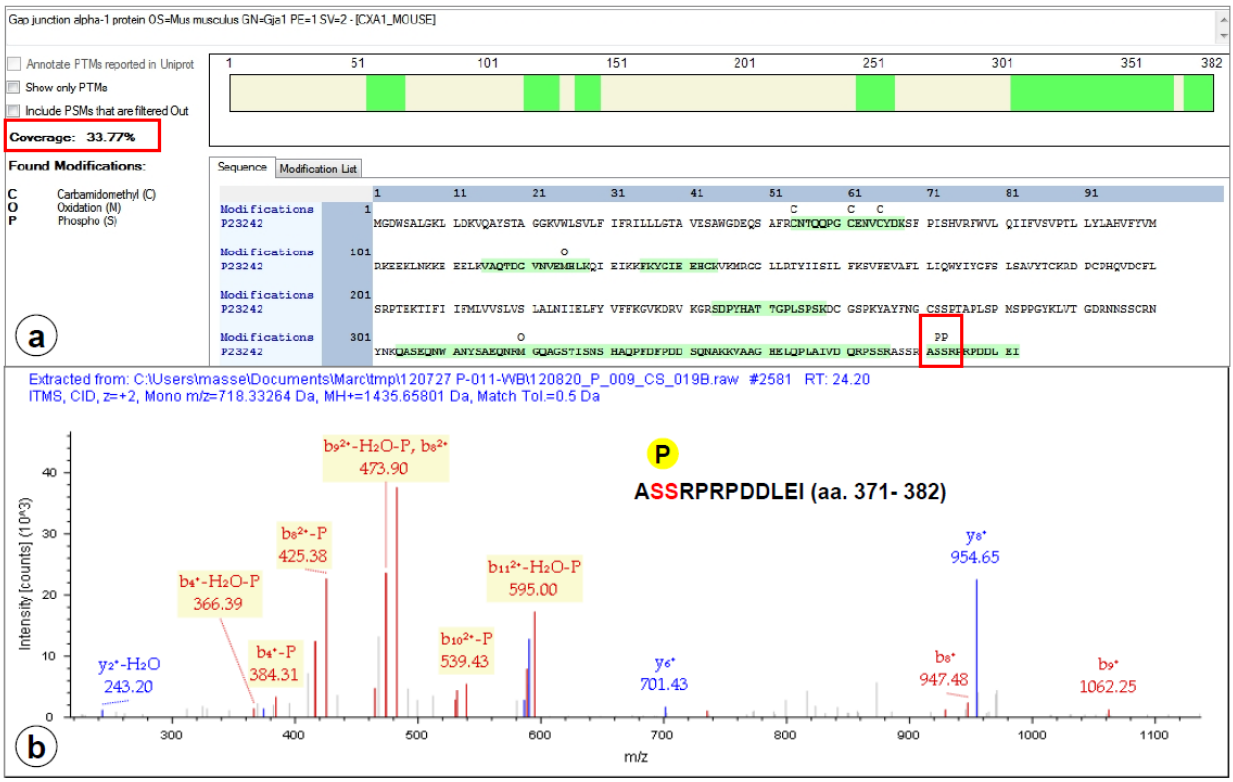

Fig. 4.51: Mascot search of reduced Cx43 database. a: Sequence coverage of Cx43 (SwissProt P23242) with phosphorylation site S372/373. **b:** Fragment ion spectrum of highest scoring assignment of m/z 718.333 (z=2, 0.16 ppm error, Mascot ion score 15) as identified by Proteome Discoverer Software: ^{371}ASs(phospho)RPRPDDLEI^{382}. b-ions are shown in red, y-ions in blue. Several phosphorylation losses (yellow shaded annotations) and neutral losses of water and ammonia were found.

5. Discussion

5.1 Quality control of hGFAP-Cre and nestin-Cre mediated recombination

5.1.1 Spontaneous germ-line recombination activity of different Cre transgenes

Here we describe a spontaneous germ-line recombination activity of an hGFAP-Cre transgene (Zhuo et al., 2001) and of a nestin-Cre transgene (Tronche et al., 1999) when bred to Cx43 conditional alleles. Following the initial characterization and confirmation of faithful recombination mediated by hGFAP-Cre, we kept mice with astrocyte-specific deletion in a homozygous floxed state for several years. Global homozygous deletion of Cx43 in all cells of the body is perinatally lethal due to morphological disturbances of the right ventricular outflow tract (Reaume et al., 1995; Theis et al., 2001). However, deletion of one allele in all cells of the body has remained undetected. We now observed germ-line activity of hGFAP-Cre in an allelic setting compatible with survival of global Cx43 deletion (i.e. in combination with the Cx43K258Stop allele; Maass et al., 2004). The germ-line activity occurred mostly in the offspring of Cre-transgenic females and was not linked to hGFAP-Cre transgene transmission to the offspring. The offspring of Cre-transgenic males was less affected. Although the exact mechanism responsible for hGFAP-Cre germ-line activity remains elusive, the occurrence of germ-line deletion can be minimized by using male with Cre-recombinase. We observed the same phenomenon in nestin-Cre mice. Such an inheritance pattern of ectopic recombination even in Cre-negative offspring is already known from the PGK-Cre transgene (Lallemand et al., 1998), a Keratin5-Cre transgene (Ramirez et al., 2004), and an αMHC-Cre line (Eckardt et al., 2004). Once we have observed germ-line recombination activity of hGFAP-Cre in combination with the Cx43K258Stop allele, we tested our Cx43fl/fl: hGFAP-Cre colony and frequently found germ-line deletion of single floxed alleles. Cx43 protein expression from a Cx43 floxed allele is already rather low (~ 50% of a WT allele). The expression of a ‘control’ mouse with hidden germ-line deletion of one Cx43 floxed allele is thus minimally different from a full Cx43 knockout. Compared to lack of hGFAP-Cre activity giving rise to pseudo KO mice (Requardt et al., 2009), the germ-line activity of hGFAP-Cre and nestin-Cre activity we show here is much more frequent.

A rigid quality control of mice with astrocyte-directed gene inactivation is required to exclude germ-line deletion by hGFAP-Cre and nestin-Cre within transgenic colonies. We here present strategies for pre- and post-experimental assessment of astrocyte-directed Cx43 KO

mice by DNA analysis, immunohistochemistry and immunodetection. Deletion status measured by the Cx43del PCR for deletion of the Cx43 floxed allele in tail tip DNA was consistent with the deletion status in brain and heart measured by reporter gene expression, immunoblotting and immunofluorescence. We found that PCR analysis of tail-tip DNA is suited to detect hGFAP-Cre negative mice which experienced germ-line deletion. Thus, the tail-tip genotyping allows pre-experimental assessment of animals in order to estimate the deletion status of Cx43 floxed alleles in mice lacking the hGFAP-Cre or nestin-Cre transgenes. In case of lacking reporter genes, PCR for detection of a deleted floxed allele should be employed. Since germ-line deletion also occurs in the presence of hGFAP-Cre and nestin-Cre, it is not possible to differentiate faithful deletion from germ-line deletion in the tail of hGFAP-Cre positive mice. Post-experimental screening for β-Gal expression in the heart is required to exclude germ-line recombination of the Cx43 floxed allele, as we showed here exemplarity for hGFAP-Cre positive mice.

Several other GFAP-Cre transgenic mice have been generated using identical or similar hGFAP promoter elements (Kwon et al., 2001; Bajenaru et al., 2002; Fraser et al., 2004; Casper and McCarthy, 2006). Since a recent report indicated that a tamoxifen-inducible RIP-CreER transgene for timed recombination in beta cells of the pancreas is active even without inducer (Liu et al., 2010b), ectopic activity of hGFAP-Cre may even constitute a problem for inducible gene switches employing hGFAP promoter elements (Ganat et al., 2006; Hirrlinger et al., 2006). Our findings on germ-line recombination of the hGFAP-Cre and nestin-Cre transgenes are therefore highly relevant to other groups working in the field of astroglial gene function.

Especially if global deletion of a floxed gene is not lethal, the mouse colony may, with time, become contaminated by global knockouts. We recommend to closely monitor the activity status of GFAP-Cre and of nestin-Cre transgenic lines.

5.1.2 Potential mechanism for the spontaneous Cre recombinase activity

Our results imply that there is no direct germ-line recombination in the hGFAP-Cre mice. However, it may be speculated for this transgenic system that there might exist an indirect germ-line recombination in both male and female gonads via adjacent Sertoli cells in the testis and granulosa (follicle) cells in the ovary as only these somatic cell populations seem to be primarily affected by the hGFAP-Cre induced deletion. Usually it is assumed that the Cre recombinase needs FGF or TAT peptides to cross membranes (Peitz et al., 2002). However, it has also been shown that unmodified Cre recombinase can cross membranes (Will et al., 2002).

In the testis, intercellular communication is regulated through different mechanisms including direct junctions like tight, adherens and gap junctions. Within the seminiferous epithelium, communication is mainly mediated by somatic Sertoli cells and Cx43 is the predominantly expressed gap junctional protein (Risley et al., 1992; Risley, 2000; Brehm et al., 2007).

Cx43 is expressed between Sertoli cells and between Sertoli cells and different generations of germ cells (Risley et al., 1992; Bravo-Moreno et al., 2001) and plays a role in Sertoli cell and germ cell maturation (Pelletier, 1995). In addition, a severe loss of germ cells has been found in general Cx43 knockout (KO) mice (Reaume et al., 1995) indicating an indispensable role of Cx43 mediated cell coupling for germ cell development (Juneja et al., 1999). Also a conditional Sertoli cell specific KO of the Cx43 gene (SCCx43 KO) revealed Cx43 expression in Sertoli cells as an absolute requirement for normal testicular development and initiation of spermatogenesis. Compared to the generalized KO, the SCCx43 KO mice are viable, but infertile and adult SCCx43KO mice showed a significantly reduced number of germ cells per tubule (Brehm et al., 2007; Sridharan et al., 2007). In addition, dye-coupling studies demonstrated that Cx43 participates in the coupling between SC and between SC and GC, with the dye transfer from SC to GC being mostly unidirectional (Decrouy et al., 2004).

A similar constellation can be found in the ovary (Kidder and Mhawi, 2002; Winterhager et al., 2007). In developing follicles, gap junctions couple the growing oocyte and its surrounding follicle cells into a functional syncytium. Gap junctions between cumulus cells contain predominantly Cx43 and follicles lacking this Cx show an arrest in early folliculogenesis (Juneja et al., 1999). In addition to Cx43, also other Cx like Cx37 appear to play a role in different stages of folliculogenesis (Simon et al., 1997).

In the present study, neither in male nor in female transgenic mice of different genotypes any germ cells could be found “deleted/recombined” using double immunofluorescence stainings. It means, spermatogonia, spermatocytes, spermatids as well as all stages of oocyte development remained immunonegative for β-Gal. These results are supported by the fact that GFAP-immunoreactivity has so far been only predominantly detected in the cytoplasm of interstitial Leydig cells of adult human and rat testes, and in the cytoplasm of Sertoli cells in human testes during prenatal development (Davidoff et al., 2002; Davidoff et al., 2004; Ortega et al., 2006). To the best of our knowledge there are no data available on the spatiotemporal expression pattern of GFAP in the normal ovary. Only single tumour cells in ovarian carcinomas were found to express a glial filament protein (Moll et al., 1991). It can not be excluded that a recombination occurred during fetal gonadal development in hGFAP-Cre mice (Francis and Lo, 2006): At E9.5 coupling was significantly decreased in Cx43 KOs compared to Cx43 WT mice. Primordial germ cell (PGC) speed was decreased both at E8.5 and E11.5, and directionality of PGCs was significantly decreased at E8.5. It was found that PGCs underwent apoptosis by activated p53.

As for nestin expression: vascular smooth muscle cells (VSMCs) and pericytes (PCs) have been identified as progenitors of all testicular Leydig cell phenotypes in rats, with VSMCs and PCs, but not endothelial cells, being the sites of nestin immunoreactivity (Davidoff et al., 2004). Same results were also shown for adult mice. Most interestingly for the interpretation of the results from the present study, analyses of nestin-GFP transgenic mice confirmed the expression of nestin only in interstitial Leydig cells and their vascular progenitors but not in intratubular Sertoli or germ cells (Davidoff et al., 2004). Fröjdman et al. showed that nestin was transiently found in Sertoli cells, interstitial cells, most prominent in differentiating myoid cells but not in germ cells (Frojdman et al., 1997). After birth, nestin gradually disappeared and was found only in the endothelial cells of some blood vessels. Hutchinson et al. demonstrated that nestin is located in the basal compartment of Sertoli cells and in blood vessels. In somatic Sertoli cells it is switched off between days 15 and 25 as the Sertoli cell matures (Hutchison et al., 2008). In the ovary of adult rats, nestin was mainly localized to capillary endothelial cells of the *theca interna* in follicles with more than two layers of granulosa cells. In addition, its expression increased with follicle growth indicating that this intermediate filament might be involved in angiogenesis in the follicle which is followed by ovulation. No immunopositive oocytes or granulosa cells were detected (Takahashi et al., 2008). In another study, nestin expression was only demonstrated in endothelial cells of blood vessels intruding among granulosa-luteal cells of the ovary (Mokry et al., 2004).

5.2 Astroglial connexins in adult hippocampal neurogenesis

5.2.1 Cx30 is not important for adult neurogenesis in the SGZ

Expression of Cx30 in hippocampal astrocytes and RG-like cells in SGZ has been demonstrated at the level of mRNA and protein previously (Nagy et al., 1999; Rouach et al., 2008; Kunze et al., 2009; Gosejacob et al., 2011). Deletion of astrocytic Cx30 and Cx43 leads to a strongly decreased proliferation and neurogenesis in DG of adult mice (Kunze et al., 2009). This previous data showed that Cx43 and/or Cx30 are required for proliferation of RG-like cells and adult neurogenesis. However, it is impossible to differentiate which one might exert more important functions in postnatal neurogenesis due to the ablation of both major connexins in RG-like cells. To determine the extent of Cx30 involvement in adult neurogenesis, we therefore performed a series of studies using single Cx30 KO mice. Our results indicated that both proliferative activity and neurogenesis are not impaired in the DG of Cx30 KO mice. The numbers of RG-like cells (BLBP-positive), diving neuronal precursor

cells (Ki67- and BrdU-positive) and mature neurons (Prox1-positive) was similar between Cx30 KO and wild-type mice (Fig. 4.12). Moreover, fate mapping studies have shown that the relative expression of DCX, a marker associated with differentiation of newborn neurons in the DG, appeared to be unaffected in Cx30 KO mice versus the WT animals (Fig. 4.15). These findings suggest that differentiation, maturation and integration pathways were not changed. In comparison, Cx43fl/fl: hGFAP-Cre mice showed an 83 % decrease in the number of Ki67-positive cells, and a 21 % reduction in the number of Prox1- positive cells. Interestingly, we also observed a significantly reduced neurogenesis in adult Cx43fl/fl mice, even though the entire Cx43 coding region was not deleted, but only floxed. The reasons for the observed effects might be the overall distinct difference in Cx30 and Cx43 mRNA extent, protein expression levels and astrocytic coupling. By single cell RT-PCR analysis, it was revealed that almost 50 % of the RG-like cells express Cx43 and about 30 % express Cx30 (Kunze et al., 2009), indicating RG-like cells in the postnatal DG predominantly express Cx43 mRNA and a lower extent of Cx30 mRNA. In contrast to Cx43, Cx30 protein levels were extremely low in the hippocampus using immunoblotting and immunoflourescence analysis (Sohl et al., 2000; Gosejacob et al., 2011; Unger et al., 2012). Moreover, previous evidence suggested that floxed Cx43 alleles result in significantly decreased endogenous protein expression (Theis et al., 2003). The most important function of connexins in the hippocampus is forming functional intercellular gap junctional coupling for the exchange of small molecules, metabolites and ions (Giaume and Theis, 2010). Dye-coupling experiments revealed a 50 % reduction in astrocytic coupling in the Cx43 deficient mice (Theis et al., 2003), whereas in Cx30 KO mice only a 20 % reduction of the interastrocytic coupling in the hippocampus was observed (Gosejacob et al., 2011). Cx30-/-; Cx43fl/fl: hGFAP-Cre mice are completely uncoupled in the hippocampus (Wallraff et al., 2006; Rouach et al., 2008; Pannasch et al., 2011). In this study, we observed that intercellular coupling in the hippocampus of Cx43fl/fl mice was also strongly inhibited compared to WT mice (Fig. 4.37). To check for a functional compensation by expression changes of Cx43, we performed immunoblot analysis in the hippocampus of adult Cx30 KO mice. Our data revealed no apparent upregulation or downregulation of Cx43 following lack of Cx30 (Fig 4.13). Taken together, these results strongly suggest that the deletion of Cx30 protein alone did not affect proliferation and neurogenesis. However, Cx43 is critically linked to the regulation of adult hippocampal neurogenesis.

5.2.2 Impact of the Cx43G138R mutation on adult neurogenesis

Similar to the Cx30/Cx43 DKO mice, a strongly decreased proliferation and neurogenesis was observed in mice lacking astrocytic Cx43 (Fig. 4.12). However, the underlying molecular mechanism is not revealed due to the complete deletion of Cx43 in astrocytes. Some lines of evidences indicate that Cx43 mediates not only intercellular coupling of small molecules but also adhesive interaction between cells via the cytoplasmic C-terminal tail which might be required for neurogenesis (Elias et al., 2007; Kunze et al., 2009; Cina et al., 2009). Moreover, hemichannel activity and gene expression control can be also exerted by Cx43 (Neijssen et al., 2005; Valiunas et al., 2005; Rouach et al., 2008; Kang et al., 2008).

In order to receive further mechanistic insight into connexin function in adult neurogenesis, a mouse carrying a conditional point mutation of Cx43 was employed. Cx43G138R mice exhibited lack of intercellular coupling but preserved hemichannel (HC) activity (Dobrowolski et al., 2008; Dobrowolski et al., 2009). This mutant still contains the C-terminal cytoplasmic tail and thus one can assume that adhesion and control of gene expression exerted by Cx43 are still preserved. For instance, scaffolding protein Zonula occludens-1 (ZO-1) binds the carboxy terminus of Cx43 and a previous study has shown that changes in the Cx43/ZO-1 interaction have complementary effects on gap junctional intercellular communication and hemichannel function (Rhett et al., 2011). Since Cx43G138R protein contains the intact C-terminal tail, the interaction between ZO-1 and Cx43 should be maintained. Our data show that the Cx43 point mutation causes a significant reduction of proliferative precursor cells and newborn neurons in the DG of adult mice irrespective of Cx30 expression (Fig. 4.20). Our immunoblotting results demonstrated that total Cx43 protein expression level is not significantly altered between the groups compared (Fig. 4.21). Moreover, we found well distinguishable and multiple junctional plaques in the cell membrane of astrocytes in immunostaining studies (data not shown). This result is consistent with an earlier finding which indicated an unhindered trafficking and a slightly altered localization of the mutated protein in intercalated discs of cardiomyocytes (Dobrowolski et al., 2008). As expected, the astroglia-specific Cx43 point mutation in mice lacking Cx30 showed complete absence of interastrocytic coupling in CA1 region (Fig. 4.25) similar to the Cx30-/-; Cx43fl/fl: hGFAP-Cre mice (Wallraff et al., 2006). Importantly, coupling between RG-like cells in Cx43G138R mice was strongly affected (Fig. 4.26), but not completely inhibited like in Cx30-/-; Cx43fl/fl: hGFAP-Cre mice (Kunze et al., 2009). This situation might explain why the Cx43 point mutation caused a restricted although significant, decline in Ki67-, Prox1- and BLBP-postive cells, but not such a dramatic reduction like in DKO mice. Fate mapping analysis of the proportion of Prox1-positive/DCX-positive cells among the BrdU-positive cells in Cx43 point mutant mice and control animals showed no difference (Fig. 4.23). Together, our findings

suggest that the proliferation and neurogenesis are strongly impacted by the point mutation of Cx43 due to remarkable loss of RG-like cell coupling in the SGZ. However, the differentiation and cell fate determination were not significantly affected, as has also been shown in Cx30/Cx43 DKO mice (Kunze et al., 2009).

Functional intercellular coupling has been suggested to be crucial for the proliferation of RG-like cells in the adult neurogenesis (Kunze et al., 2009; this work). However, which signaling molecules can be regulated by Cx43 mediated coupling in RG-like cells is not clear. Recently, it has been shown that Cx43-mediated gap junctional coupling is essential to maintain morphogen expression, such as sonic hedgehog (Shh) and bone morphogenetic proteins (BMPs), in the mesenchyme of limb buds (Dobrowolski et al., 2009). Morphogens are a group of proteins that not only are vital for the embryonic development and patterning of the brain but also function to regulate the self-renewal and differentiation of RG cells in the adult brain. In the adult brain, the morphogenic proteins continue to subtly modulate the number and differentiation of neural precursor cells. In both the SGZ and the SVZ, Shh is essential for the maintenance of RG-like cells (Ahn and Joyner, 2005; Balordi and Fishell, 2007; Han et al., 2008), whereas BMP determines the fate of NSCs (Lim et al., 2000; Bonaguidi et al., 2005; Mira et al., 2010). Therefore, reduced expression of Shh and BMPs in the Cx43 point mutation mice might be the cause for the decreased proliferation of RG-like cells via impaired intercellular coupling. However, the precise molecular mechanism how Cx43 mediated coupling influences the expression of these morphogens is not known. Small molecular messengers are also involved in the regulation process of adult neurogenesis. Several approaches have shown that serotonin (5-HT) increases neural progenitor proliferation and enhances survival of newborn neurons in the adult hippocampus (Warner-Schmidt and Duman, 2006; Sahay and Hen, 2007). The transfer of serotonin through gap junctional channels was described (Esser et al., 2006).

Unlike gap junctional coupling, hemichannels mediate direct communication between the extracellular environment and the cells (Bennett et al., 2003). Within the neurogenic niche, Cx43 is further described as being involved in hemichannel mediated ATP release, contributing to the initiation and propagation of calcium waves between clusters of cells during cortical neurogenesis (Weissman et al., 2004). Thus, Cx43 in adult neurogenic regions may coordinate the communication between neighboring and distant cells within the niche also through hemichannels. As recently reported the Cx43G138R mutation leads to an increased number of open hemichannels and increased ATP release (Dobrowolski et al., 2008), which can be correlated with the calcium wave propagation needed to regulate of NSCs cell cycle entry and thus proliferation (Owens and Kriegstein, 1998). Recently, it has been shown that Cx43 hemichannels are also permeable to calcium and regulated by calcium (De et al., 2009; De et al., 2012).

5.2.3 Impact of the Cx43K258stop mutation on adult neurogenesis

The C-terminal region of Cx43 has a variety of protein interacting sites and is known to be important in control of gap junctional channel gating (Moreno et al., 2002; Maass et al., 2004; Lampe and Lau, 2004; Herve et al., 2007). For this reason, we wanted to assess the role of the Cx43CT in adult neurogenesis using a truncated Cx43 mutated mouse. The Cx43K258stop mouse lacks the last 125 amino acids in the CT tail, which implicated a loss of cell-cell adhesion and control of gene expression (Giaume and Theis, 2010). However, Cx43K258stop transfected HeLa cells show still robust intercellular coupling (Maass et al., 2004). Interestingly, it is important to point out that Cx43K258stop and ZO-1 protein were still found in the same immunoprecipitate after the deletion of ZO-1 binding motifs in the Cx43CT. It seems likely that the interaction between ZO-1 and Cx43K258stop was preserved (Maass et al., 2007).

Similar to Cx43G138R mice, our data indicated that proliferation and neurogenesis are strongly reduced in Cx43K258stop mice (Fig. 4.32). Again, in the Western blot of adult hippocampal tissue, we observed no significant alteration of the truncated Cx43 protein levels between Cx43K258stop mice and their control independent of Cx30 status (Fig. 4.33). Immunostaining of brain sections using antibodies against the N-terminal residues revealed membrane localization of Cx43K258stop plaques in astrocytes, but expression seemed to be reduced overall (data not shown). These findings are in line with a previous observation, which has shown a reduction in plaque formation combined with increased plaque size in the heart. Moreover, these gap junctions showed a tendency to accumulate towards the periphery of the intercalated disc, indicating changes in the localization and formation of intermolecular complexes (Maass et al., 2007). Thus, it is important to detect the potential localization changes of Cx43K258stop gap junction plaques in astrocytes using higher level of resolution i.e., transmission electron microscopy. The contribution of potentially changed localization in adult neurogenesis remains to be determined. To our surprise, astroglia-specific Cx43 truncated mice lacking Cx30 exhibited uncoupling in the CA1 region (Fig. 4.37), contrary to the studies in HeLa cells, but such decreased coupling was earlier detected in cultured astrocytes from Cx43 truncated mice (Kozoriz et al., 2010). Tracer coupling of RG-like cells was also significantly reduced in Cx43K258stop mice, but not completely abolished (Fig. 4.38). These data suggest that the reduction of proliferative activity and decreased number of newborn neurons was not due to Cx43 protein levels and disfavours adhesion as relevant aspect of connexin function, but suggests loss of RG-like coupling in mice expressing the truncated Cx43 protein as a cause for impaired neurogenesis.

The data on the role of the CT tail in postnatal and embryonic neurogenesis is somewhat conflicting. Several experiments suggested that the CT domain is a negative modulator of

neuronal proliferation and differentiation (Moorby and Patel, 2001; Santiago et al., 2010), whereas other studies point to a positive regulator of Cx43 to maintain cells in a proliferative state in adult hippocampus and embryonic cortex (Cheng et al., 2004; Kunze et al., 2009). The results presented in this study have led us to propose that the CT domain of Cx43 acts as a positive effector for adult hippocampal neurogenesis, in a manner consistent with gap junctional channel regulation. A number of structure-function studies have shown that the C-terminal region of Cx43 controls the gating of gap junction channels via a chemical mechanism ("ball-and-chain" model; Duffy et al., 2002), including phosphorylation (Moreno et al., 1994; Kanemitsu et al., 1997; Solan and Lampe, 2009). Moreover, some lines of evidence point to the C-terminal domain as a gating particle also for voltage regulation of the Cx43 channel. Cx43 channels are gated between three states under normal conditions: closed, open and residual. In transfected murine neuroblastoma (N2a) cells the truncation of CT domain of Cx43 eliminates the residual state, indicating that channels transit directly between open and closed states in response to a transjunctional voltage gradient (Moreno et al., 2002). The same paper also reported the CT region as independent voltage-gating partner for interacting with the pore-forming domain of Cx43 to regulate channel conductance. Moreover, the truncation of Cx43 causes a significant prolongation of the open time, as well as an extension of the closed configuration. These observations were confirmed by two other studies in primary cardiomyocyte and astrocyte cultures using Cx43K258stop mice (Maass et al., 2007; Kozoriz et al., 2010). Astrocytes expressing the truncated Cx43 form functional gap junction channels with single channel conductance of about 110 pS similar to those of WT control, but the open time of these channels is much longer, indicating a reduced sensitivity to transjunctional voltage (Kozoriz et al., 2010). Furthermore, the hemichannel activity was disturbed in cultured astrocytes from Cx43K258stop mice in comparison with WT astrocytes. As described above, calcium signaling is important in astrocyte and blood vessel regulation (Mulligan and MacVicar, 2004), indicating that the calcium wave propagation was reduced in Cx43K258stop mice.

It has been reported that the association of the CT domain with protein partners regulate Cx43 assembly and degradation and, therefore, stabilizes the Cx43 anchoring in plasma membranes (Giepmans and Moolenaar, 1998; Gumpert et al., 2008). Recently, the functional relevance of three amino acid (aa) regions in the CT domain of Cx43 was disclosed: first, the region 235-242aa is important for gap junction plaque formation at the plasma membrane; second, the region 271-302aa is crucial for gap junction plaque size; third, the specific region 325-342aa plays an important role in the direction of internalization as annular gap junction (Wayakanon et al., 2012). These findings suggested a function of the Cx43 CT domain in gap junction expression and its turnover.

5.2.4 The role of the Cx43D378stop mutation in adult neurogenesis

To confirm our conclusion that Cx43-mediated intercellular coupling is important for adult neurogenesis in the hippocampus, we investigated the Cx43D378stop mouse, which expresses a mini-truncated form of the Cx43 gene lacking the last five CT amino acid residues (378-382aa) of the protein (Lubkemeier et al., 2013). In comparison with the two other Cx43 mutated animals, our results suggest that there is slightly, however significant, reduced astrocytic coupling in the CA1 region of Cx43D378stop mice and proliferation was also significantly altered (Fig 4.42). Interestingly, our coupling study data are not consistent with previous findings, which reported dye transfer between cadiomyocytes isolated from Cx43D378stop mice and coupling between Cx43D378stop transfected HeLa cells which showed no apparent changes (Lubkemeier et al., 2013). The discrepancy of our findings with those of Lübkemeier et al., (2013) might be because of different cell types, tissue preparation and higher molecular weight of Lucifer Yellow used in the latter study. Moreover, these mice expressing the mini-truncation of Cx43 still express Cx30, so we can expect a further decrease in coupling upon loss of Cx30. Loss of Cx43 leads to an up-regulation of Cx30 (Theis et al., 2003). It has been previously shown that the region 378-382aa of Cx43 is important for interaction between Cx43 and its scaffolding protein ZO-1 (Giepmans and Moolenaar, 1998; Sorgen et al., 2004; Hunter et al., 2005). A physiological role of ZO-1, an actin-binding protein, is the interaction with Cx43 for the modulation of transition of undocked hemichannels into gap junction plaques in the cell membrane. It has been shown that new hemichannels are added to gap junctions at the periphery of the aggregates (Gaietta et al., 2002). Moreover, previous studies revealed that disruption of the Cx43 and ZO-1 interaction leads to increased gap junction size and a decrease or loss of colocalization between Cx43 and ZO-1 at plaque edges of cadiomyocytes, respectively (Maass et al., 2007; Palatinus et al., 2011; Rhett et al., 2012). To explain the remarkable changed coupling in Cx43D378stop expressing astrocytes one model was speculated. The binding of ZO-1 to Cx43 at the periphery of GJ plaques restricts the hemichannel addition to the plaques, whereas inhibition of the interaction results in larger size, but lower number of gap junction plaques and fewer hemichannels. The predicted functional consequences of the path are reduced hemichannel activity and decreased gap junctional communication (Rhett et al., 2012).

Our coupling analysis in astrocytes did not find changed in intercellular coupling, in contrast it was shown that the cell-cell communication was decreased. The reason might be that ZO-1 still interacts with the Cx43D378stop protein as suggested in the IP study (Lubkemeier et al., 2013). New observations in adult Cx43D378stop mice showed that Cx43 and ZO-1 still colocalized to the intercalated disc of heart and the Cx43D378stop protein amount was not significantly different compared to controls. These results indicated that ablation of the ZO-1

binding motif of Cx43 may still allow the interactions between both proteins via other potential binding domains of Cx43 or indirectly through linked partners (Sorgen et al., 2004; Severs, 2007). In mouse cadiomyocytes Cx45 tends to colocalize with Cx43 in the same junctions (Kanter et al., 1993). A previous study reported that the interaction of Cx45 with ZO-1 (Laing et al., 2001), and possibly of Cx45 with Cx43D378stop protein, could explain, at least in part, the presence of ZO-1 in the Cx43D378stop precipitates. However, so far no evidence revealed that Cx45 is expressed in astrocytes or RG-like cells in the SGZ neurogenic zones. Thus, the question arises as to whether Cx43 and ZO-1 still colocalize in the membrane of astrocytes or RG-like cells after ablation of the binding residues? If the Cx43D378stop mutation changes the formation of a gap junctional plaque, does this lead to a reduced interastrocytic coupling? Interestingly, pull-down assays and co-IPs indicated binding of Cx30 to the second PDZ domains in ZO-1. Moreover, ZO-1 associated nucleic acid-binding protein (ZONAB) is a transcription factor (Balda and Matter, 2000), and it was suggested that ZO-1/ZONAB interaction regulates gene expression and glial homeostasis in combination with Cx30 and Cx43 (Penes et al., 2005). In conclusion, our data again strongly favor a role of Cx43-mediated intercellular coupling rather than Cx43-mediated adhesive interaction for adult hippocampal neurogenesis. This holds true for the point mutation (Cx43G138R), the large truncation (Cx43K258stop) and for the small truncation (Cx43D378stop).

5.3 Cx43 phosphorylation modulates gap junctional coupling

5.3.1 Decreased astrocytic coupling due to increased Cx43 phosphorylation

An understanding of the molecular mechanism behind the reduced gap junction coupling induced by kainate injection is still outstanding. More and more evidence suggests that changes in Cx43 post-translational phosphorylation affect gap junctional communication and have an impact on intercellular signalling (reviewed by Solan and Lampe, 2009). Using an antibody against the CT domains of Cx43, our data show that the phosphorylated isoforms were significantly increased in ipsilateral versus contralateral side after kainate injection (Fig. 4.45 and Fig. 4.46). Treatment of the same samples with alkaline phosphatase collapsed most of Cx43 phosphorylation associated bands to its non-phosphorylated isoforms, indicating that in SDS-PAGE detected bands are indeed phospho-Cx43. These results were confirmed in the following immunoblotting studies using the same samples probed by an antibody against the N-terminus of Cx43 (Fig. 4.45). Therefore, a firm conclusion can be made that the decreased intrastrocytic coupling in CA1 is correlated with an increased Cx43 phosphorylation after kainate injection.

The Cx43 CT domain is extensively phosphorylated by different protein kinases at different motifs leading to decreased conductivity of the gap junction. The phosphorylation of connexins by tyrosine protein kinases, especially Src, is now considered as one main regulatory mechanism (Lau, 2005; Pahujaa et al., 2007). It has been indicated that the initial activation of v-Src occurs through the interaction of the 274-284aa proline-rich region of Cx43 with the SH3 domain of the v-Src (Lin et al., 2001; Warn-Cramer and Lau, 2004). This interaction leads to the phosphorylation of Cx43 at the Tyr265 residue, which stabilizes the binding of Cx43 and v-Src and promotes the second tyrosine phosphorylation on Tyr247 of Cx43. Phosphorylation on Tyr247 may be the key molecular event that triggers the gap junction channel closure, as measured by decreases in dye transfer or inhibited channel open probability (Filson et al., 1990; Loo et al., 1995; Lin et al., 2001; Cottrell et al., 2003). Similar to v-Src, the interaction of Cx43 with c-Src on Tyr265 decreases the binding of Cx43 with the ZO-1 cytoskeletal protein and diminishes gap junctional channel conductance (Toyofuku et al., 1999; Toyofuku et al., 2001; Giepmans et al., 2001). A recent paper provides evidence that the disruption of gap junctional communication in ischemic or hypoxic astrocytes is associated with c-Src induced phosphorylation of Cx43 (Li et al., 2005). In primary mouse cortical astrocytes, intracellular acidification induced by ischemia triggers the uncoupling of Cx43 gap junctions (known as “pH-gating”) due to the binding of c-Src to Cx43, which is believed to play a crucial role in attenuating damage to tissues surrounding the lesion focus (Peters et al., 1997; Lin et al., 1998). Furthermore, Src can not only block gap junctional communication by directly phosphorylating Cx43 at tyrosine sites, it may recruit MAPK, PKC and CDC2 to phosphorylate Cx43 on serine residues to disrupt intercellular coupling as well (Pahujaa et al., 2007; Solan and Lampe, 2008). Additionally, Src may affect intercellular communication via regulation of transcriptome and proteome expression pattern. For instance, Src can increase PDGF receptor expression, which leads to increases in MAPK and PKC activity to reduce channels formed by Cx43 (Warn-Cramer and Lau, 2004; Shen et al., 2007). Unfortunately, our Cx43-pY247 phospho-specific antibody did not detect any signals (Fig. 4.47 c). This study should be performed again and it will be also important to know whether the Src induced phosphorylation of the second tyrosine site (Tyr265) is associated with reduced coupling between astrocytes.

Down-regulation of gap junctional communication was also reported by phosphorylation of the Ser279/282 target by MAPK due to decreased channel open time and probability (Cottrell et al., 2003). Indeed, we observed an increased phosphorylation of Cx43 at Ser279/282 using Cx43-pS279 specific antibody (Fig. 4.47 c). Recently, phosphorylation at Ser365 has been described as a “gatekeeper” event for Cx43 forming channels, which may represent a mechanism to prevent cells from ischemia via increased assembly of Cx43 to gap junction plaques (Solan et al., 2007). In addition, the same paper suggested that PKC dependent

phosphorylation of Ser368 was dramatically reduced when Ser365 was phosphorylated arguing that Ser365 dephosphorylation likely precedes Ser368 phosphorylation during hypoxia. The interrelationship of Cx43 phosphorylation at Ser365 and Ser368 indicates that PKA enhances while PKC suppresses phosphorylation of Cx43 (Yogo et al., 2006; Solan and Lampe, 2007). Our data demonstrate that pSer365-Cx43 amount was almost similar between ipsi-and contralateral samples and the phosphorylation on Ser368 was slightly reduced in the ipsilateral tissue, indicating that the PKA and PKC kinases might not be efficiently active to regulate the phosphorylation of Cx43. Therefore, there is no significant impact on the gap junction coupling after an excitotoxic insult. Interestingly, a slightly increased pSer373-Cx43 amount was observed at the ipsilateral side, indicating an increased gap junction communication induced by PKA activity. This result is in opposition to the fact that reduced coupling was found at the ipsilateral side. However, previous data showed that Src prevents positive Cx43-mediated coupling by modulating PKA, either directly, or by inducing counteractive phosphatase activity. Thus, sufficient PKA activity that is required for gap junctional communication may be suppressed by Src. Moreover, a previous study has indicated that initial phosphorylation of Ser364 is necessary for subsequent sufficient phosphorylation of Ser373 by PKC (Shah et al., 2002). Since the lacking of Ser364 phosphorylation data it is difficult to determine whether this slightly increased phosphorylation of Ser373 is indeed due to PKC. All of these data indicate that gap junction coupling via Cx43 is a highly co-ordinated regulatory process, including phosphorylation on multiple sites through multiple signaling pathways. It will be important to know whether one residue is phosphorylated only by one kinase or several kinases. One point however seems clear: we need more phospho-specific antibodies to identify the potential sites involved in the regulation of Cx43 gap junctional communication.

5.3.2 Evaluation of Cx43 phosphorylation sites by mass spectrometry

Liquid chromatography-MS (LC-MS) on immunoprecipitated Cx43 provided information on the phosphorylation status on several positions, namely Ser217, Ser244/Tyr247, and Ser372/373. Evidence could be found for single phosphorylation on the peptides but unequivocal localization of the phosphorylation positions was only possible for pS217. This identified serine residue localizes in the fourth transmembrane domain of Cx43, which has not previously been described. It is unlikely that this residue is phosphorylated, since it is within a transmembrane domain. The functional consequence for gap junctional communication remains to be investigated. Ser244 and Tyr247 have previously been

described as phosphorylation sites in the Cx43 CT domain using phosphoproteomic strategies (Lin et al., 2001; Huang et al., 2011). Moreover, the phosphorylation of Ser372/373 was also reported in the primary references (Yogo et al., 2002; Axelsen et al., 2006). However, the interpretation of the accurate phosphorylation site regarding Ser372/373 and Ser244/Tyr247 are complicated by the close proximity of the two residues introducing an uncertainty to the conclusion. It should also be noted that the total amount of precipitated Cx43 was low as indicated by absence of enrichment of Coomassie staining at the expected molecular weight after IP. The sequence coverage reached about 40%, but varied between experiments. Due to the still low abundance and unfavourable ionization and fragmentation of phosphopeptides no quantitative conclusions can be drawn from the obtained LC-MS data. Attempts to enrich phosphopeptides by titanium dioxide (TiO_2) and immobilized chelated metal ions (Fe-IMAC) from whole brain lysates did not lead to identification of Cx43 phosphopeptides. The reason is not known but the low abundance of these phosphorylated peptides might result in suppression by other phosphopeptides during MS analysis or might be lost during sample preparation.

6. Future perspectives

In the first part of my work I describe the repeated, spontaneous germ-line recombination activity of the widely used hGFAP-Cre and nestin-Cre transgenes when bred to Cx43 conditional alleles. Interestingly, we found that this phenomenon more frequently appears in the offspring of Cre-transgenic females than male mice in both Cre transgenic lines. Moreover, compared to spontaneous loss of hGFAP-Cre activity, the germ-line hGFAP-Cre and nestin-Cre recombination is much more frequent. In view of these findings, using males with Cre-recombinase, the occurrence of germ-line deletion/activation in the future breeding can be minimized, which can seriously influence the experimental outcome. Using double immunofluorescence stainings in testis and ovary of prepubertal and juvenile mice we investigated the potential mechanism responsible for hGFAP-Cre germ-line activity. Our results imply that there might exist an indirect germ-line recombination in both male and female gonads via adjacent Sertoli cells in the testis and follicle cells in the ovary, because we found only these somatic cell types, seem to be immunopositive for ß-Gal staining. It has been shown that unmodified Cre recombinase possesses an intrinsic ability to cross cellular membranes, enter the nucleus and catalyze recombination at loxP sites (Will et al., 2002). In addition, dye-coupling studies demonstrated that the dye transfer from Sertoli cell to spermatogonia is mostly unidirectional via Cx43 (Decrouy et al., 2004). One way in which the Cre protein can cross membranes is by annular gap junctions (Jordan et al., 2001; Laird, 2010) or tunneling nanotubes (Gerdes and Carvalho, 2008; Abounit and Zurzolo, 2012). Transient Cre expression during preimplantation stages for mosaic and partial recombination has been described for different Cre lines (Eckardt et al., 2004). Therefore, ectopic Cre expression in early embryonic developmental stages of conditional Cx43 floxed mouse might be very useful to find out whether other promoters lead to unexpected Cre expression.

In the adult neurogenesis studies we show that gap junctional coupling plays a crucial role in regulating neurogenesis, and decreased intercellular communication is closely correlated with decreased proliferation in all of the three Cx43 mutant mice. To understand the molecular mechanisms underlying the modulation of adult neurogenesis by gap junctional coupling further *in vivo* and *in vitro* experiments should be performed. In order to test the expression of morphogens, e.g. Shh, BMP and 5-HT, single cell RT-PCR analyses in the RG-like cells should be performed. The possible regulation of these morphogens by Ca^{2+} and IP_3 signaling pathways can be monitored using two photon imaging. Within the neurogenic niche are RG-like cells, astrocytes and endothelial cells, all of which exhibit gap junction mediated coupling (Mirzadeh et al., 2008). Moreover, astrocytic processes form endfeet on the basal lamina of blood vessels, which facilitate intercellular transfer of small molecules from the blood to the RG-like cells. A variety of growth factors and hormones, including these

molecules above are known to regulate adult proliferation. Therefore, further analyses of gap junctional plaques in astrocytic endfeet are required to examine whether the decreased coupling is due to mislocalization or low expression of Cx43 in the cell membrane of endfeet region. This can be tested with scanning electron microscopy. In addition, the C-terminal domains of Cx43 can exert intrinsic functionality independent of channel activity, which appears to regulate signaling/adaptor proteins (Giepmans, 2004). Since the neurogenic factors Wnt and ephrin-B were suggested to be important for adult hippocampal neurogenesis (Lie et al., 2005; Ashton et al., 2012) *in vivo* gain and loss of function studies using RNAi might be improve our knowledge about the role of the Cx43 CT. To validate our conclusion that gap junctional coupling is more important than cell adhesion for adult neurogenesis, additional work in an adhesion assay can be done. For instance, confocal microscopy can be applied to study the live cell adhesion/migration imaging in the rostral migratory stream (RMS) *in vivo*. An investigation in a 3D cell adhesion assay in primary hippocampal astrocytes culture can also be done *in vitro*. Finally, Cx43 is further thought to be involved in hemichannel mediated ATP release within the NSC microenvironment via Ca^{2+} wave propagation (Weissman et al., 2004; Dale, 2008). This mechanism regulates NSC/NPC cell cycle entry and thus proliferation (Owens and Kriegstein, 1998). It would be interesting, for example, to study the hemichannel activity of these three Cx43 mutants using photolysis of diazo-2 triggered ATP release and astrocytic Ca^{2+} waves (Torres et al., 2012). This real-time imaging of cellular processes allows us to investigate astrocytes releasing ATP *in vivo* and precisely examine their cellular behaviour as well as their influence on neighbouring cells in the neurogenic niche.

Results from the third part of my study suggest that strongly reduced gap junctional coupling is directly linked to the phosphorylation of Cx43 in TLE pathology. However, the phosphorylation sites, patterns and correlated functions should be investigated in more detail. Using a set of more phospho-specific antibodies we can maybe identify the putative crucial phophorylated residues involved in down-regulation of Cx43 mediated cell-cell communication. Since the Src kinase is now considered as one main regulator for the inhibited gap junctional coupling (Lau, 2005; Pahujaa et al., 2007), it might be possible to test Tyr247/265 specific antibodies first in Western blotting. Subsequently, it would also be promising to use phospho-specific antibodies to target multiple serines, which in turn cause reduced coupling. It should be noted that the phospho-analysis in present work is not quantitative, it only reveals if the identified sites are highly phosphorylated or not. Thus, it is reasonable to quantify the serine/tyrosine specific phosphorylated Cx43 isoform between ipsi- and contra-lateral sides in the future. Within the context of our MS findings, a particular challenge of studying phosphorylation arises from the difficulties of isolating and purification

reasonable amount of Cx43 protein. The IP method appears to be successfull in covering phosphorylated Cx43 for MS analysis. However, the total amount of precipitated Cx43 was still low after IP. Thus, residues observed to be phosphorylated in the present study are required to validate using improved IP or phosphopeptide enrichment. To further characterise the phosphorylation pattern MS analysis should be performed using ipsilateral versus contralateral tissues following different time points after kainate injection. Moreover, an important element of understanding Cx43 phosphorylation is to determine their structural composition and how all the kinases work together as an integrated system. A variety of phosphoproteomic datasets demonstrated that Cx43 likely serves as a highly integrated hub capable of consolidating a set of phosphate based signaling cascades (Chen et al., 2013). Therefore, it will be important to systematically examine the subcellular fractionation using discovery proteomics, targeted technologies (i.e. multiple reaction monitoring MS) and quantitative proteomics (i.e. heat map analysis) together as a valuable framework towards fully understanding Cx43 phosphorylation.

7. Summary

For astrocyte restricted connexin mutations/deletions the Cre/loxP system of site-specific recombination method was applied in this study. However, the Cre recombinase mediated gene deletion/activation is not free of limitations (Eckardt et al., 2004; Requardt et al., 2009). Since it affects every process in our adult neurogenesis study, it is critical to overcome such pitfalls using a series of quality assessment. With PCR, immunodetection and reporter gene approaches, we show that the widely used hGFAP-Cre transgene exhibits spontaneous germ-line recombination leading to deletion of Cx43 gene in brain, heart, ovary, testis and tail tissue with high frequency. The ectopic activity of hGFAP-Cre requires a rigorous control. We also observed the nestin-Cre transgene shows germ-line deletion. Here we describe procedures to identify mice with germ-line recombination mediated by the hGFAP-Cre and nestin-Cre transgenes. Such control is essential to avoid pleiotropic effects due to germ-line deletion of loxP-flanked target genes and to maintain the astrocytes-restricted deletion status of Cx43 in transgenic mouse colonies.

Adult hippocampal neurogenesis generates functional new granule neurons that become integrated into the DG throughout whole mammalian lifespan (Gage, 2000). Despite of the growing number of studies in the past decade, the exact regulatory mechanisms as well as the functional significance of adult neurogenesis are still not fully elucidated. Moreover, only few parameters have been assessed to characterize the regulation of adult neurogenesis, i.e. cell proliferation in the SGZ, cell survival and neuronal differentiation (Kempermann et al., 2004). Astrocytes with RG-like morphology are considered neural stem cells (type-1) in the SGZ of the DG (Kempermann et al., 2004). Recently, Cx30 and Cx43, two major astrocytic gap junction proteins have been shown critical for proliferation and neurogenesis in the adult hippocampus (Kunze et al., 2009). However, the underlying mechnisms of the obseved decrease on adult neurogenesis are not clarified. To gain the mechanistic insight into connexin function related to adult neurogenesis, we employed several Cx30 and Cx43 mutations in the present work.

In the second part of my work I first analyzed the influence of Cx30 and Cx43 on adult neurogenesis. In contrast to WT mice, single knockout of Cx30 did not impair the number of dividing neuronal precursor cells and mature neurons in the DG of adult mice. However, the complete deletion of Cx43 in astrocytes significantly decreases the proliferation and granule cell numbers. These effects are similar to those obtained in Cx30/Cx43 DKO mice (Kunze et al., 2009). Moreover, utilizing a fate mapping approach it has been shown that differentiation, maturation and integration of newly born neurons were not altered in Cx30KO mice compared to WT. In the immunoblot analysis our data revealed no apparent alteration of

Cx43 protein amount in the hippocampus following deletion of Cx30, indicating that unchanged adult neurogenesis in Cx30KO mice is not due to up-regulation of Cx43. Our findings suggest that Cx43, but not Cx30, is required for normal adult neurogenesis. The Cx43G138R expressing mice present a conditional mouse model to study the mechanism linking connexin mutation and coupling to proliferation in the adult hippocampus. The main finding of this mouse suggests that the strong decrease of Cx43G138R mediated astrocyte and RG-like cell coupling is responsible for the observed reduction of adult neurogenesis. Moreover, this impaired proliferation appears to be not associated with the alteration of the mutant Cx43 protein level in the hippocampus. However, the expression of the point mutation Cx43 in the RG-like cells determines the different rate of intercellular coupling and its corresponding effects on adult neurogenesis. To our surprise, astroglia-specific Cx43K258stop mice lacking Cx30 also exhibited significantly decreased coupling between astrocytes and RG-like cells, contrary to the studies in cultured HeLa cells. The functional consequence of the Cx43K258stop truncation is the strongly decreased proliferative activity in the SGZ and the number of newborn neurons in the GCL. Again, our immunoblot data evaluated that the expression of Cx43 amount is similar between comparing groups. Furthermore, fate analysis of BrdU-positive cells associated with the relative expression of DCX appeared to be unaffected in both astroglia-specific Cx43G138R and Cx43K258stop mice. Interestingly, compared to the WT animal the Cx43D378stop mouse also shows significantly decreased astrocytic coupling as well as decreased proliferation. However, the average rate of coupling and proliferation is much higher than the above two Cx43 mutants. Together, our findings strongly favour a role of Cx43-mediated intercellular coupling between RG-like cells rather than Cx43-mediated adhesive interactions for adult neurogenesis in the hippocampus.

In order to investigate the impact of Cx43 post-translational phosphorylation on pathogenesis of TLE, homogenized hippocampal lysates were established and further characterized in immunoblot, IP and MS analysis. An overall changed Cx43 phosphorylation pattern was found in ipsilateral (i.e., the kainate-injected site) versus contralateral (the non-injected site) using an antibody against the Cx43 CT domain. To confirm our results the same samples were assessed again using an antibody which recognized the N-terminus of Cx43, and our data are consistent with the former results. This suggests that *in vivo* phosphorylation of Cx43 is not only a response to epileptic neuronal activity but is also coupled to the decrease of interastrocytic coupling. A more detailed analysis using phospho-specific antibodies revealed several site-specific phosphorylation patterns of Cx43. Our data indicate that a co-ordinated regulation of gap junction occurs via mutiple kinase signaling pathways, leading to phosphorylation on mutiple sites of Cx43 CT domain. This complex interplay between

mutiple kinases made it difficult to determine specific aspects of Cx43 regulation and interpret its functional relevance for gap junctional communication. To overcome the limitation, we developed and established a reliable IP-based method for Cx43 phosphorylation study by MS analysis. Using control hippocampi, three of the phosphorylated sites (i.e. Ser217, Ser244/Tyr247, and Ser372/373) were successfully identified in our MS study. These are the first *in vivo* data, to our knowledge, to show that phosphorylation of Cx43 in the mouse hippocampus using MS-based discovery proteomics, and our data offer a new possibility for the study of connexin post-translational regulation in TLE mouse model.

8. References

Ables,J.L., DeCarolis,N.A., Johnson,M.A., Rivera,P.D., Gao,Z., Cooper,D.C., Radtke,F., Hsieh,J., and Eisch,A.J. (2010). Notch1 is required for maintenance of the reservoir of adult hippocampal stem cells. J. Neurosci. *30*, 10484-10492.

Abounit,S. and Zurzolo,C. (2012). Wiring through tunneling nanotubes--from electrical signals to organelle transfer. J. Cell Sci. *125*, 1089-1098.

Ahn,S. and Joyner,A.L. (2005). In vivo analysis of quiescent adult neural stem cells responding to Sonic hedgehog. Nature *437*, 894-897.

Aimone,J.B. and Gage,F.H. (2011). Modeling new neuron function: a history of using computational neuroscience to study adult neurogenesis. Eur. J. Neurosci. *33*, 1160-1169.

Allen,E. (1912). The cessation of mitosis in the central nervous system of the albino rat. J. Comp. Neurol. 19, 547-568.

Allen,N.J. and Barres,B.A. (2009). Neuroscience: Glia - more than just brain glue. Nature *457*, 675-677.

Altman,J. (1969). Autoradiographic and histological studies of postnatal neurogenesis. IV. Cell proliferation and migration in the anterior forebrain, with special reference to persisting neurogenesis in the olfactory bulb. J. Comp Neurol. *137*, 433-457.

Altman,J. (2011). Memoir: The discovery of adult mammalian neurogenesis, Springer.

Altman,J. and Bayer,S.A. (1975). Postnatal development of the hippocampal dentate gyrus under normal and experimental conditions. In: R. L. Isaacson and K. J. Pribram (eds) The Hippocampus: A Comprehensive Treatise, Vol. 1, pp. 95-122. New York: Plenum Press.

Altman,J. and Das,G.D. (1965). Autoradiographic and histological evidence of postnatal hippocampal neurogenesis in rats. J. Comp Neurol. *124*, 319-335.

Altman,J. and Das,G.D. (1966). Autoradiographic and histological studies of postnatal neurogenesis. I. A longitudinal investigation of the kinetics, migration and transformation of cells incorporating tritiated thymidine in neonate rats, with special reference to postnatal neurogenesis in some brain regions. J. Comp Neurol. *126*, 337-389.

Amaral,D.G. and Witter,M.P. (1995). Hippocampal formation. In: The rat nervous system, second edition (Paxinos G, ed), pp 443-493. San Diego, CA: Academic Press.

Amaral,D.G., Dolorfo,C., and varez-Royo,P. (1991). Organization of CA1 projections to the subiculum: a PHA-L analysis in the rat. Hippocampus *1*, 415-435.

Anthony,T.E., Mason,H.A., Gridley,T., Fishell,G., and Heintz,N. (2005). Brain lipid-binding protein is a direct target of Notch signaling in radial glial cells. Genes Dev. *19*, 1028-1033.

Ashton,R.S., Conway,A., Pangarkar,C., Bergen,J., Lim,K.I., Shah,P., Bissell,M., and Schaffer,D.V. (2012). Astrocytes regulate adult hippocampal neurogenesis through ephrin-B signaling. Nat. Neurosci. *15*, 1399-1406.

Atkinson,M.M., Lampe,P.D., Lin,H.H., Kollander,R., Li,X.R., and Kiang,D.T. (1995). Cyclic AMP modifies the cellular distribution of connexin43 and induces a persistent increase in the junctional permeability of mouse mammary tumor cells. J. Cell Sci. *108 (Pt 9)*, 3079-3090.

Axelsen,L.N., Stahlhut,M., Mohammed,S., Larsen,B.D., Nielsen,M.S., Holstein-Rathlou,N.H., Andersen,S., Jensen,O.N., Hennan,J.K., and Kjolbye,A.L. (2006). Identification of ischemia-regulated

phosphorylation sites in connexin43: A possible target for the antiarrhythmic peptide analogue rotigaptide (ZP123). J. Mol. Cell Cardiol. *40*, 790-798.

Bajenaru,M.L., Zhu,Y., Hedrick,N.M., Donahoe,J., Parada,L.F., and Gutmann,D.H. (2002). Astrocyte-specific inactivation of the neurofibromatosis 1 gene (NF1) is insufficient for astrocytoma formation. Mol. Cell Biol. *22*, 5100-5113.

Balda,M.S. and Matter,K. (2000). The tight junction protein ZO-1 and an interacting transcription factor regulate ErbB-2 expression. EMBO J. *19*, 2024-2033.

Balordi,F. and Fishell,G. (2007). Hedgehog signaling in the subventricular zone is required for both the maintenance of stem cells and the migration of newborn neurons. J. Neurosci. *27*, 5936-5947.

Barkho,B.Z., Song,H., Aimone,J.B., Smrt,R.D., Kuwabara,T., Nakashima,K., Gage,F.H., and Zhao,X. (2006). Identification of astrocyte-expressed factors that modulate neural stem/progenitor cell differentiation. Stem Cells Dev. *15*, 407-421.

Bates,D.C., Sin,W.C., Aftab,Q., and Naus,C.C. (2007). Connexin43 enhances glioma invasion by a mechanism involving the carboxy terminus. Glia *55*, 1554-1564.

Bedner,P., Steinhauser,C., and Theis,M. (2012). Functional redundancy and compensation among members of gap junction protein families? Biochim. Biophys. Acta *1818*, 1971-1984.

Bennett,M.V., Contreras,J.E., Bukauskas,F.F., and Saez,J.C. (2003). New roles for astrocytes: gap junction hemichannels have something to communicate. Trends Neurosci. *26*, 610-617.

Bennett,M.V. and Verselis,V.K. (1992). Biophysics of gap junctions. Semin. Cell Biol. *3*, 29-47.

Bennett,M.V. and Zukin,R.S. (2004). Electrical coupling and neuronal synchronization in the Mammalian brain. Neuron *41*, 495-511.

Bergami,M., Rimondini,R., Santi,S., Blum,R., Gotz,M., and Canossa,M. (2008). Deletion of TrkB in adult progenitors alters newborn neuron integration into hippocampal circuits and increases anxiety-like behavior. Proc. Natl. Acad. Sci. U. S. A *105*, 15570-15575.

Beyer,E.C., Kistler,J., Paul,D.L., and Goodenough,D.A. (1989). Antisera directed against connexin43 peptides react with a 43-kD protein localized to gap junctions in myocardium and other tissues. J. Cell Biol. *108*, 595-605.

Bignami,A., Eng,L.F., Dahl,D., and Uyeda,C.T. (1972). Localization of the glial fibrillary acidic protein in astrocytes by immunofluorescence. Brain Res. *43*, 429-435.

Bjorklund,A. and Lindvall,O. (2000). Parkinson disease gene therapy moves toward the clinic. Nat. Med. *6*, 1207-1208.

Blomstrand,F., Venance,L., Siren,A.L., Ezan,P., Hanse,E., Glowinski,J., Ehrenreich,H., and Giaume,C. (2004). Endothelins regulate astrocyte gap junctions in rat hippocampal slices. Eur. J. Neurosci. *19*, 1005-1015.

Bonaguidi,M.A., McGuire,T., Hu,M., Kan,L., Samanta,J., and Kessler,J.A. (2005). LIF and BMP signaling generate separate and discrete types of GFAP-expressing cells. Development *132*, 5503-5514.

Boyes,B.E., Kim,S.U., Lee,V., and Sung,S.C. (1986). Immunohistochemical co-localization of S-100b and the glial fibrillary acidic protein in rat brain. Neuroscience *17*, 857-865.

Bravo-Moreno,J.F., az-Sanchez,V., Montoya-Flores,J.G., Lamoyi,E., Saez,J.C., and Perez-Armendariz,E.M. (2001). Expression of connexin43 in mouse Leydig, Sertoli, and germinal cells at different stages of postnatal development. Anat. Rec. *264*, 13-24.

Brehm,R., Zeiler,M., Ruttinger,C., Herde,K., Kibschull,M., Winterhager,E., Willecke,K., Guillou,F., Lecureuil,C., Steger,K., Konrad,L., Biermann,K., Failing,K., and Bergmann,M. (2007). A sertoli cell-specific knockout of connexin43 prevents initiation of spermatogenesis. Am. J. Pathol. *171*, 19-31.

Breunig,J.J., Silbereis,J., Vaccarino,F.M., Sestan,N., and Rakic,P. (2007). Notch regulates cell fate and dendrite morphology of newborn neurons in the postnatal dentate gyrus. Proc. Natl. Acad. Sci. U. S. A *104*, 20558-20563.

Brown,J.P., Couillard-Despres,S., Cooper-Kuhn,C.M., Winkler,J., Aigner,L., and Kuhn,H.G. (2003). Transient expression of doublecortin during adult neurogenesis. J. Comp Neurol. *467*, 1-10.

Brozzi,F., Arcuri,C., Giambanco,I., and Donato,R. (2009). S100B Protein Regulates Astrocyte Shape and Migration via Interaction with Src Kinase: IMPLICATIONS FOR ASTROCYTE DEVELOPMENT, ACTIVATION, AND TUMOR GROWTH. J. Biol. Chem. *284*, 8797-8811.

Bruzzone,S., Guida,L., Zocchi,E., Franco,L., and De,F.A. (2001). Connexin 43 hemi channels mediate Ca2+-regulated transmembrane NAD+ fluxes in intact cells. FASEB J. *15*, 10-12.

Butt,A.M. and Ransom,B.R. (1989). Visualization of oligodendrocytes and astrocytes in the intact rat optic nerve by intracellular injection of lucifer yellow and horseradish peroxidase. Glia *2*, 470-475.

Cameron,H.A., McEwen,B.S., and Gould,E. (1995). Regulation of adult neurogenesis by excitatory input and NMDA receptor activation in the dentate gyrus. J. Neurosci. *15*, 4687-4692.

Cameron,S.J., Malik,S., Akaike,M., Lerner-Marmarosh,N., Yan,C., Lee,J.D., Abe,J., and Yang,J. (2003). Regulation of epidermal growth factor-induced connexin 43 gap junction communication by big mitogen-activated protein kinase1/ERK5 but not ERK1/2 kinase activation. J. Biol. Chem. *278*, 18682-18688.

Casper,K.B. and McCarthy,K.D. (2006). GFAP-positive progenitor cells produce neurons and oligodendrocytes throughout the CNS. Mol. Cell Neurosci. *31*, 676-684.

Castrillon,D.H., Quade,B.J., Wang,T.Y., Quigley,C., and Crum,C.P. (2000). The human VASA gene is specifically expressed in the germ cell lineage. Proc. Natl. Acad. Sci. U. S. A *97*, 9585-9590.

Chen,V.C., Gouw,J.W., Naus,C.C., and Foster,L.J. (2013). Connexin multi-site phosphorylation: mass spectrometry-based proteomics fills the gap. Biochim. Biophys. Acta *1828*, 23-34.

Cheng,A., Tang,H., Cai,J., Zhu,M., Zhang,X., Rao,M., and Mattson,M.P. (2004). Gap junctional communication is required to maintain mouse cortical neural progenitor cells in a proliferative state. Dev. Biol. *272*, 203-216.

Cina,C., Maass,K., Theis,M., Willecke,K., Bechberger,J.F., and Naus,C.C. (2009). Involvement of the cytoplasmic C-terminal domain of connexin43 in neuronal migration. J. Neurosci. *29*, 2009-2021.

Cooper,C.D. and Lampe,P.D. (2002). Casein kinase 1 regulates connexin-43 gap junction assembly. J. Biol. Chem. *277*, 44962-44968.

Cottrell,G.T., Lin,R., Warn-Cramer,B.J., Lau,A.F., and Burt,J.M. (2003). Mechanism of v-Src- and mitogen-activated protein kinase-induced reduction of gap junction communication. Am. J. Physiol Cell Physiol *284*, C511-C520.

Couillard-Despres,S., Winner,B., Schaubeck,S., Aigner,R., Vroemen,M., Weidner,N., Bogdahn,U., Winkler,J., Kuhn,H.G., and Aigner,L. (2005). Doublecortin expression levels in adult brain reflect neurogenesis. Eur. J. Neurosci. *21*, 1-14.

Dale,N. (2008). Dynamic ATP signalling and neural development. J. Physiol *586*, 2429-2436.

Davidoff,M.S., Middendorff,R., Enikolopov,G., Riethmacher,D., Holstein,A.F., and Muller,D. (2004). Progenitor cells of the testosterone-producing Leydig cells revealed. J. Cell Biol. *167*, 935-944.

Davidoff,M.S., Middendorff,R., Kofuncu,E., Muller,D., Jezek,D., and Holstein,A.F. (2002). Leydig cells of the human testis possess astrocyte and oligodendrocyte marker molecules. Acta Histochem. *104*, 39-49.

De,B.M., Wang,N., Bol,M., Decrock,E., Ponsaerts,R., Bultynck,G., Dupont,G., and Leybaert,L. (2012). Connexin 43 hemichannels contribute to cytoplasmic Ca2+ oscillations by providing a bimodal Ca2+-dependent Ca2+ entry pathway. J. Biol. Chem. *287*, 12250-12266.

De,V.E., Wang,N., Decrock,E., De,B.M., Vinken,M., Van,M.M., Lai,C., Culot,M., Rogiers,V., Cecchelli,R., Naus,C.C., Evans,W.H., and Leybaert,L. (2009). Ca(2+) regulation of connexin 43 hemichannels in C6 glioma and glial cells. Cell Calcium *46*, 176-187.

Decrouy,X., Gasc,J.M., Pointis,G., and Segretain,D. (2004). Functional characterization of Cx43 based gap junctions during spermatogenesis. J. Cell Physiol *200*, 146-154.

Degen,J., Dublin,P., Zhang,J., Dobrowolski,R., Jokwitz,M., Karram,K., Trotter,J., Jabs,R., Willecke,K., Steinhauser,C., and Theis,M. (2012). Dual reporter approaches for identification of Cre efficacy and astrocyte heterogeneity. FASEB J. *26*, 4576-4583.

Dermietzel,R., Gao,Y., Scemes,E., Vieira,D., Urban,M., Kremer,M., Bennett,M.V., and Spray,D.C. (2000). Connexin43 null mice reveal that astrocytes express multiple connexins. Brain Res. Brain Res. Rev. *32*, 45-56.

Dermietzel,R., Traub,O., Hwang,T.K., Beyer,E., Bennett,M.V., Spray,D.C., and Willecke,K. (1989). Differential expression of three gap junction proteins in developing and mature brain tissues. Proc. Natl. Acad. Sci. U. S. A *86*, 10148-10152.

Dobrowolski,R., Hertig,G., Lechner,H., Worsdorfer,P., Wulf,V., Dicke,N., Eckert,D., Bauer,R., Schorle,H., and Willecke,K. (2009). Loss of connexin43-mediated gap junctional coupling in the mesenchyme of limb buds leads to altered expression of morphogens in mice. Hum. Mol. Genet. *18*, 2899-2911.

Dobrowolski,R., Sasse,P., Schrickel,J.W., Watkins,M., Kim,J.S., Rackauskas,M., Troatz,C., Ghanem,A., Tiemann,K., Degen,J., Bukauskas,F.F., Civitelli,R., Lewalter,T., Fleischmann,B.K., and Willecke,K. (2008). The conditional connexin43G138R mouse mutant represents a new model of hereditary oculodentodigital dysplasia in humans. Hum. Mol. Genet. *17*, 539-554.

Doetsch,F. (2003). The glial identity of neural stem cells. Nat. Neurosci. *6*, 1127-1134.

Doetsch,F., Garcia-Verdugo,J.M., and varez-Buylla,A. (1997). Cellular composition and three-dimensional organization of the subventricular germinal zone in the adult mammalian brain. J. Neurosci. *17*, 5046-5061.

Domingues,A.M., Taylor,M., and Fern,R. (2010). Glia as transmitter sources and sensors in health and disease. Neurochem. Int. *57*, 359-366.

Dranovsky,A., Picchini,A.M., Moadel,T., Sisti,A.C., Yamada,A., Kimura,S., Leonardo,E.D., and Hen,R. (2011). Experience dictates stem cell fate in the adult hippocampus. Neuron *70*, 908-923.

Duan,X., Chang,J.H., Ge,S., Faulkner,R.L., Kim,J.Y., Kitabatake,Y., Liu,X.B., Yang,C.H., Jordan,J.D., Ma,D.K., Liu,C.Y., Ganesan,S., Cheng,H.J., Ming,G.L., Lu,B., and Song,H. (2007). Disrupted-In-Schizophrenia 1 regulates integration of newly generated neurons in the adult brain. Cell *130*, 1146-1158.

Eckardt,D., Theis,M., Doring,B., Speidel,D., Willecke,K., and Ott,T. (2004). Spontaneous ectopic recombination in cell-type-specific Cre mice removes loxP-flanked marker cassettes in vivo. Genesis. *38*, 159-165.

Elias,L.A., Wang,D.D., and Kriegstein,A.R. (2007). Gap junction adhesion is necessary for radial migration in the neocortex. Nature *448*, 901-907.

Eng,L.F., Ghirnikar,R.S., and Lee,Y.L. (2000). Glial fibrillary acidic protein: GFAP-thirty-one years (1969-2000). Neurochem. Res. *25*, 1439-1451.

Eriksson,P.S., Perfilieva,E., Bjork-Eriksson,T., Alborn,A.M., Nordborg,C., Peterson,D.A., and Gage,F.H. (1998). Neurogenesis in the adult human hippocampus. Nat. Med. *4*, 1313-1317.

Esser,A.T., Smith,K.C., Weaver,J.C., and Levin,M. (2006). Mathematical model of morphogen electrophoresis through gap junctions. Dev. Dyn. *235*, 2144-2159.

Evans,M.J. and Kaufman,M.H. (1981). Establishment in culture of pluripotential cells from mouse embryos. Nature *292*, 154-156.

Feng,L., Hatten,M.E., and Heintz,N. (1994). Brain lipid-binding protein (BLBP): a novel signaling system in the developing mammalian CNS. Neuron *12*, 895-908.

Ferri,A.L., Cavallaro,M., Braida,D., Di,C.A., Canta,A., Vezzani,A., Ottolenghi,S., Pandolfi,P.P., Sala,M., DeBiasi,S., and Nicolis,S.K. (2004). Sox2 deficiency causes neurodegeneration and impaired neurogenesis in the adult mouse brain. Development *131*, 3805-3819.

Filippov,V., Kronenberg,G., Pivneva,T., Reuter,K., Steiner,B., Wang,L.P., Yamaguchi,M., Kettenmann,H., and Kempermann,G. (2003). Subpopulation of nestin-expressing progenitor cells in the adult murine hippocampus shows electrophysiological and morphological characteristics of astrocytes. Mol. Cell Neurosci. *23*, 373-382.

Filson,A.J., Azarnia,R., Beyer,E.C., Loewenstein,W.R., and Brugge,J.S. (1990). Tyrosine phosphorylation of a gap junction protein correlates with inhibition of cell-to-cell communication. Cell Growth Differ. *1*, 661-668.

Forni,P.E., Scuoppo,C., Imayoshi,I., Taulli,R., Dastru,W., Sala,V., Betz,U.A., Muzzi,P., Martinuzzi,D., Vercelli,A.E., Kageyama,R., and Ponzetto,C. (2006). High levels of Cre expression in neuronal progenitors cause defects in brain development leading to microencephaly and hydrocephaly. J. Neurosci. *26*, 9593-9602.

Francis,R.J. and Lo,C.W. (2006). Primordial germ cell deficiency in the connexin 43 knockout mouse arises from apoptosis associated with abnormal p53 activation. Development *133*, 3451-3460.

Fraser,M.M., Zhu,X., Kwon,C.H., Uhlmann,E.J., Gutmann,D.H., and Baker,S.J. (2004). Pten loss causes hypertrophy and increased proliferation of astrocytes in vivo. Cancer Res. *64*, 7773-7779.

Frojdman,K., Pelliniemi,L.J., Lendahl,U., Virtanen,I., and Eriksson,J.E. (1997). The intermediate filament protein nestin occurs transiently in differentiating testis of rat and mouse. Differentiation *61*, 243-249.

Fukuda,S., Kato,F., Tozuka,Y., Yamaguchi,M., Miyamoto,Y., and Hisatsune,T. (2003). Two distinct subpopulations of nestin-positive cells in adult mouse dentate gyrus. J. Neurosci. *23*, 9357-9366.

Gage,F.H. (2000). Mammalian neural stem cells. Science *287*, 1433-1438.

Gage,F.H., Ray,J., and Fisher,L.J. (1995). Isolation, characterization, and use of stem cells from the CNS. Annu. Rev. Neurosci. *18*, 159-192.

Gaietta,G., Deerinck,T.J., Adams,S.R., Bouwer,J., Tour,O., Laird,D.W., Sosinsky,G.E., Tsien,R.Y., and Ellisman,M.H. (2002). Multicolor and electron microscopic imaging of connexin trafficking. Science *296*, 503-507.

Ganat,Y.M., Silbereis,J., Cave,C., Ngu,H., Anderson,G.M., Ohkubo,Y., Ment,L.R., and Vaccarino,F.M. (2006). Early postnatal astroglial cells produce multilineage precursors and neural stem cells in vivo. J. Neurosci. *26*, 8609-8621.

Gangoso,E., Ezan,P., Valle-Casuso,J.C., Herrero-Gonzalez,S., Koulakoff,A., Medina,J.M., Giaume,C., and Tabernero,A. (2012). Reduced connexin43 expression correlates with c-Src activation, proliferation, and glucose uptake in reactive astrocytes after an excitotoxic insult. Glia *60*, 2040-2049.

Gao,Z., Ure,K., Ables,J.L., Lagace,D.C., Nave,K.A., Goebbels,S., Eisch,A.J., and Hsieh,J. (2009). Neurod1 is essential for the survival and maturation of adult-born neurons. Nat. Neurosci. *12*, 1090-1092.

Garcia,A.D., Doan,N.B., Imura,T., Bush,T.G., and Sofroniew,M.V. (2004). GFAP-expressing progenitors are the principal source of constitutive neurogenesis in adult mouse forebrain. Nat. Neurosci. *7*, 1233-1241.

Gaveriaux-Ruff,C. and Kieffer,B.L. (2007). Conditional gene targeting in the mouse nervous system: Insights into brain function and diseases. Pharmacol. Ther. *113*, 619-634.

Ge,S., Goh,E.L., Sailor,K.A., Kitabatake,Y., Ming,G.L., and Song,H. (2006). GABA regulates synaptic integration of newly generated neurons in the adult brain. Nature *439*, 589-593.

Ge,S., Sailor,K.A., Ming,G.L., and Song,H. (2008). Synaptic integration and plasticity of new neurons in the adult hippocampus. J. Physiol *586*, 3759-3765.

Gehin,M., Mark,M., Dennefeld,C., Dierich,A., Gronemeyer,H., and Chambon,P. (2002). The function of TIF2/GRIP1 in mouse reproduction is distinct from those of SRC-1 and p/CIP. Mol. Cell Biol. *22*, 5923-5937.

Gerdes,H.H. and Carvalho,R.N. (2008). Intercellular transfer mediated by tunneling nanotubes. Curr. Opin. Cell Biol. *20*, 470-475.

Gerdes,J., Schwab,U., Lemke,H., and Stein,H. (1983). Production of a mouse monoclonal antibody reactive with a human nuclear antigen associated with cell proliferation. Int. J. Cancer *31*, 13-20.

Giaume,C., Koulakoff,A., Roux,L., Holcman,D., and Rouach,N. (2010). Astroglial networks: a step further in neuroglial and gliovascular interactions. Nat. Rev. Neurosci. *11*, 87-99.

Giaume,C. and Theis,M. (2010). Pharmacological and genetic approaches to study connexin-mediated channels in glial cells of the central nervous system. Brain Res. Rev. *63*, 160-176.

Giepmans,B.N. (2004). Gap junctions and connexin-interacting proteins. Cardiovasc. Res. *62*, 233-245.

Giepmans,B.N. and Moolenaar,W.H. (1998). The gap junction protein connexin43 interacts with the second PDZ domain of the zona occludens-1 protein. Curr. Biol. *8*, 931-934.

Giepmans,B.N., Verlaan,I., and Moolenaar,W.H. (2001). Connexin-43 interactions with ZO-1 and alpha- and beta-tubulin. Cell Commun. Adhes. *8*, 219-223.

Gilula,N.B., Epstein,M.L., and Beers,W.H. (1978). Cell-to-cell communication and ovulation. A study of the cumulus-oocyte complex. J. Cell Biol. *78*, 58-75.

Godwin,A.J., Green,L.M., Walsh,M.P., McDonald,J.R., Walsh,D.A., and Fletcher,W.H. (1993). In situ regulation of cell-cell communication by the cAMP-dependent protein kinase and protein kinase C. Mol. Cell Biochem. *127-128*, 293-307.

Gong,C., Wang,T.W., Huang,H.S., and Parent,J.M. (2007). Reelin regulates neuronal progenitor migration in intact and epileptic hippocampus. J. Neurosci. *27*, 1803-1811.

Gosejacob,D., Dublin,P., Bedner,P., Huttmann,K., Zhang,J., Tress,O., Willecke,K., Pfrieger,F., Steinhauser,C., and Theis,M. (2011). Role of astroglial connexin30 in hippocampal gap junction coupling. Glia *59*, 511-519.

Gould,E. (2007). How widespread is adult neurogenesis in mammals? Nat. Rev. Neurosci. *8*, 481-488.

Gratzner,H.G. (1982). Monoclonal antibody to 5-bromo- and 5-iododeoxyuridine: A new reagent for detection of DNA replication. Science *218*, 474-475.

Gross,C.G. (2000). Neurogenesis in the adult brain: death of a dogma. Nat. Rev. Neurosci. *1*, 67-73.

Gumpert,A.M., Varco,J.S., Baker,S.M., Piehl,M., and Falk,M.M. (2008). Double-membrane gap junction internalization requires the clathrin-mediated endocytic machinery. FEBS Lett. *582*, 2887-2892.

Hafting,T., Fyhn,M., Molden,S., Moser,M.B., and Moser,E.I. (2005). Microstructure of a spatial map in the entorhinal cortex. Nature *436*, 801-806.

Hamilton,A. (1901). The division of differentiated cells in the central nervous system of the white rat. J. Comp. Neurol. 11, 297-320.

Han,Y.G., Spassky,N., Romaguera-Ros,M., Garcia-Verdugo,J.M., Aguilar,A., Schneider-Maunoury,S., and varez-Buylla,A. (2008). Hedgehog signaling and primary cilia are required for the formation of adult neural stem cells. Nat. Neurosci. *11*, 277-284.

Harris,A.L. (2007). Connexin channel permeability to cytoplasmic molecules. Prog. Biophys. Mol. Biol. *94*, 120-143.

Heinemann,U. and Lux,H.D. (1977). Ceiling of stimulus induced rises in extracellular potassium concentration in the cerebral cortex of cat. Brain Res. *120*, 231-249.

Herve,J.C., Bourmeyster,N., Sarrouilhe,D., and Duffy,H.S. (2007). Gap junctional complexes: from partners to functions. Prog. Biophys. Mol. Biol. *94*, 29-65.

Hirrlinger,P.G., Scheller,A., Braun,C., Hirrlinger,J., and Kirchhoff,F. (2006). Temporal control of gene recombination in astrocytes by transgenic expression of the tamoxifen-inducible DNA recombinase variant CreERT2. Glia *54*, 11-20.

Hodge,R.D., Nelson,B.R., Kahoud,R.J., Yang,R., Mussar,K.E., Reiner,S.L., and Hevner,R.F. (2012). Tbr2 is essential for hippocampal lineage progression from neural stem cells to intermediate progenitors and neurons. J. Neurosci. *32*, 6275-6287.

Hossain,M.Z., Sawchuk,M.A., Murphy,L.J., Hertzberg,E.L., and Nagy,J.I. (1994). Kainic acid induced alterations in antibody recognition of connexin43 and loss of astrocytic gap junctions in rat brain. Glia *10*, 250-265.

Hsieh,J. (2012). Orchestrating transcriptional control of adult neurogenesis. Genes Dev. *26*, 1010-1021.

Huang,R.Y., Laing,J.G., Kanter,E.M., Berthoud,V.M., Bao,M., Rohrs,H.W., Townsend,R.R., and Yamada,K.A. (2011). Identification of CaMKII phosphorylation sites in Connexin43 by high-resolution mass spectrometry. J. Proteome. Res. *10*, 1098-1109.

Hunter,A.W., Barker,R.J., Zhu,C., and Gourdie,R.G. (2005). Zonula occludens-1 alters connexin43 gap junction size and organization by influencing channel accretion. Mol. Biol. Cell *16*, 5686-5698.

Hutchison,G.R., Scott,H.M., Walker,M., McKinnell,C., Ferrara,D., Mahood,I.K., and Sharpe,R.M. (2008). Sertoli cell development and function in an animal model of testicular dysgenesis syndrome. Biol. Reprod. *78*, 352-360.

Imbeault,S., Gauvin,L.G., Toeg,H.D., Pettit,A., Sorbara,C.D., Migahed,L., DesRoches,R., Menzies,A.S., Nishii,K., Paul,D.L., Simon,A.M., and Bennett,S.A. (2009). The extracellular matrix controls gap junction protein expression and function in postnatal hippocampal neural progenitor cells. BMC. Neurosci. *10*, 13.

Jagasia,R., Steib,K., Englberger,E., Herold,S., Faus-Kessler,T., Saxe,M., Gage,F.H., Song,H., and Lie,D.C. (2009). GABA-cAMP response element-binding protein signaling regulates maturation and survival of newly generated neurons in the adult hippocampus. J. Neurosci. *29*, 7966-7977.

Jeno,P., Mini,T., Moes,S., Hintermann,E., and Horst,M. (1995). Internal sequences from proteins digested in polyacrylamide gels. Anal. Biochem. *224*, 75-82.

Jessberger,S., Toni,N., Clemenson,G.D., Jr., Ray,J., and Gage,F.H. (2008). Directed differentiation of hippocampal stem/progenitor cells in the adult brain. Nat. Neurosci. *11*, 888-893.

Jin,K., Zhu,Y., Sun,Y., Mao,X.O., Xie,L., and Greenberg,D.A. (2002). Vascular endothelial growth factor (VEGF) stimulates neurogenesis in vitro and in vivo. Proc. Natl. Acad. Sci. U. S. A *99*, 11946-11950.

Jordan,K., Chodock,R., Hand,A.R., and Laird,D.W. (2001). The origin of annular junctions: a mechanism of gap junction internalization. J. Cell Sci. *114*, 763-773.

Judisch,G.F., Martin-Casals,A., Hanson,J.W., and Olin,W.H. (1979). Oculodentodigital dysplasia. Four new reports and a literature review. Arch. Ophthalmol. *97*, 878-884.

Juneja,S.C., Barr,K.J., Enders,G.C., and Kidder,G.M. (1999). Defects in the germ line and gonads of mice lacking connexin43. Biol. Reprod. *60*, 1263-1270.

Kafitz,K.W., Meier,S.D., Stephan,J., and Rose,C.R. (2008). Developmental profile and properties of sulforhodamine 101--Labeled glial cells in acute brain slices of rat hippocampus. J. Neurosci. Methods *169*, 84-92.

Kall,L., Storey,J.D., MacCoss,M.J., and Noble,W.S. (2008). Assigning significance to peptides identified by tandem mass spectrometry using decoy databases. J. Proteome. Res. *7*, 29-34.

Kanemitsu,M.Y., Jiang,W., and Eckhart,W. (1998). Cdc2-mediated phosphorylation of the gap junction protein, connexin43, during mitosis. Cell Growth Differ. *9*, 13-21.

Kanemitsu,M.Y., Loo,L.W., Simon,S., Lau,A.F., and Eckhart,W. (1997). Tyrosine phosphorylation of connexin 43 by v-Src is mediated by SH2 and SH3 domain interactions. J. Biol. Chem. *272*, 22824-22831.

Kang,J., Kang,N., Lovatt,D., Torres,A., Zhao,Z., Lin,J., and Nedergaard,M. (2008). Connexin 43 hemichannels are permeable to ATP. J. Neurosci. *28*, 4702-4711.

Kanter,H.L., Laing,J.G., Beyer,E.C., Green,K.G., and Saffitz,J.E. (1993). Multiple connexins colocalize in canine ventricular myocyte gap junctions. Circ. Res. *73*, 344-350.

Kaplan,M.S. and Bell,D.H. (1983). Neuronal proliferation in the 9-month-old rodent-radioautographic study of granule cells in the hippocampus. Exp. Brain Res. *52*, 1-5.

Kaplan,M.S. and Hinds,J.W. (1977). Neurogenesis in the adult rat: electron microscopic analysis of light radioautographs. Science *197*, 1092-1094.

Kee,N., Teixeira,C.M., Wang,A.H., and Frankland,P.W. (2007). Preferential incorporation of adult-generated granule cells into spatial memory networks in the dentate gyrus. Nat. Neurosci. *10*, 355-362.

Kempermann,G. and Gage,F.H. (2002). Genetic determinants of adult hippocampal neurogenesis correlate with acquisition, but not probe trial performance, in the water maze task. Eur. J. Neurosci. *16*, 129-136.

Kempermann,G., Jessberger,S., Steiner,B., and Kronenberg,G. (2004). Milestones of neuronal development in the adult hippocampus. Trends Neurosci. *27*, 447-452.

Kettenmann,H. and Ransom,B.R. (1988). Electrical coupling between astrocytes and between oligodendrocytes studied in mammalian cell cultures. Glia *1*, 64-73.

Khodosevich,K., Zuccotti,A., Kreuzberg,M.M., Le,M.C., Frank,M., Willecke,K., and Monyer,H. (2012). Connexin45 modulates the proliferation of transit-amplifying precursor cells in the mouse subventricular zone. Proc. Natl. Acad. Sci. U. S. A *109*, 20107-20112.

Kidder,G.M. and Mhawi,A.A. (2002). Gap junctions and ovarian folliculogenesis. Reproduction. *123*, 613-620.

Kimelberg,H.K. and Nedergaard,M. (2010). Functions of astrocytes and their potential as therapeutic targets. Neurotherapeutics. *7*, 338-353.

Kofuji,P. and Newman,E.A. (2004). Potassium buffering in the central nervous system. Neuroscience *129*, 1045-1056.

Korets-Smith,E., Lindemann,L., Tucker,K.L., Jiang,C., Kabacs,N., Belteki,G., Haigh,J., Gertsenstein,M., and Nagy,A. (2004). Cre recombinase specificity defined by the tau locus. Genesis. *40*, 131-138.

Kozoriz,M.G., Bechberger,J.F., Bechberger,G.R., Suen,M.W., Moreno,A.P., Maass,K., Willecke,K., and Naus,C.C. (2010). The connexin43 C-terminal region mediates neuroprotection during stroke. J. Neuropathol. Exp. Neurol. *69*, 196-206.

Kuhn,H.G., ckinson-Anson,H., and Gage,F.H. (1996). Neurogenesis in the dentate gyrus of the adult rat: age-related decrease of neuronal progenitor proliferation. J. Neurosci. *16*, 2027-2033.

Kukekov,V.G., Laywell,E.D., Suslov,O., Davies,K., Scheffler,B., Thomas,L.B., O'Brien,T.F., Kusakabe,M., and Steindler,D.A. (1999). Multipotent stem/progenitor cells with similar properties arise from two neurogenic regions of adult human brain. Exp. Neurol. *156*, 333-344.

Kumar,N.M. and Gilula,N.B. (1996). The gap junction communication channel. Cell *84*, 381-388.

Kunze,A., Congreso,M.R., Hartmann,C., Wallraff-Beck,A., Huttmann,K., Bedner,P., Requardt,R., Seifert,G., Redecker,C., Willecke,K., Hofmann,A., Pfeifer,A., Theis,M., and Steinhauser,C. (2009). Connexin expression by radial glia-like cells is required for neurogenesis in the adult dentate gyrus. Proc. Natl. Acad. Sci. U. S. A *106*, 11336-11341.

Kuwabara,T., Hsieh,J., Muotri,A., Yeo,G., Warashina,M., Lie,D.C., Moore,L., Nakashima,K., Asashima,M., and Gage,F.H. (2009). Wnt-mediated activation of NeuroD1 and retro-elements during adult neurogenesis. Nat. Neurosci. *12*, 1097-1105.

Kwon,C.H., Zhu,X., Zhang,J., Knoop,L.L., Tharp,R., Smeyne,R.J., Eberhart,C.G., Burger,P.C., and Baker,S.J. (2001). Pten regulates neuronal soma size: a mouse model of Lhermitte-Duclos disease. Nat. Genet. *29*, 404-411.

Lagace,D.C., Whitman,M.C., Noonan,M.A., Ables,J.L., DeCarolis,N.A., Arguello,A.A., Donovan,M.H., Fischer,S.J., Farnbauch,L.A., Beech,R.D., DiLeone,R.J., Greer,C.A., Mandyam,C.D., and Eisch,A.J. (2007). Dynamic contribution of nestin-expressing stem cells to adult neurogenesis. J. Neurosci. *27*, 12623-12629.

Lai,K., Kaspar,B.K., Gage,F.H., and Schaffer,D.V. (2003). Sonic hedgehog regulates adult neural progenitor proliferation in vitro and in vivo. Nat. Neurosci. *6*, 21-27.

Laing,J.G., Manley-Markowski,R.N., Koval,M., Civitelli,R., and Steinberg,T.H. (2001). Connexin45 interacts with zonula occludens-1 and connexin43 in osteoblastic cells. J. Biol. Chem. *276*, 23051-23055.

Laird,D.W. (2005). Connexin phosphorylation as a regulatory event linked to gap junction internalization and degradation. Biochim. Biophys. Acta *1711*, 172-182.

Laird,D.W. (2006). Life cycle of connexins in health and disease. Biochem. J. *394*, 527-543.

Laird,D.W. (2010). The gap junction proteome and its relationship to disease. Trends Cell Biol. *20*, 92-101.

Laird,P.W., Zijderveld,A., Linders,K., Rudnicki,M.A., Jaenisch,R., and Berns,A. (1991). Simplified mammalian DNA isolation procedure. Nucleic Acids Res. *19*, 4293.

Lallemand,Y., Luria,V., Haffner-Krausz,R., and Lonai,P. (1998). Maternally expressed PGK-Cre transgene as a tool for early and uniform activation of the Cre site-specific recombinase. Transgenic Res. *7*, 105-112.

Lampe,P.D. (1994). Analyzing phorbol ester effects on gap junctional communication: a dramatic inhibition of assembly. J. Cell Biol. *127*, 1895-1905.

Lampe,P.D., Cooper,C.D., King,T.J., and Burt,J.M. (2006). Analysis of Connexin43 phosphorylated at S325, S328 and S330 in normoxic and ischemic heart. J. Cell Sci. *119*, 3435-3442.

Lampe,P.D., Kurata,W.E., Warn-Cramer,B.J., and Lau,A.F. (1998). Formation of a distinct connexin43 phosphoisoform in mitotic cells is dependent upon p34cdc2 kinase. J. Cell Sci. *111 (Pt 6)*, 833-841.

Lampe,P.D. and Lau,A.F. (2004). The effects of connexin phosphorylation on gap junctional communication. Int. J. Biochem. Cell Biol. *36*, 1171-1186.

Lampe,P.D., TenBroek,E.M., Burt,J.M., Kurata,W.E., Johnson,R.G., and Lau,A.F. (2000). Phosphorylation of connexin43 on serine368 by protein kinase C regulates gap junctional communication. J. Cell Biol. *149*, 1503-1512.

Langer,J., Stephan,J., Theis,M., and Rose,C.R. (2012). Gap junctions mediate intercellular spread of sodium between hippocampal astrocytes in situ. Glia *60*, 239-252.

Lau,A.F. (2005). c-Src: bridging the gap between phosphorylation- and acidification-induced gap junction channel closure. Sci. STKE. *2005*, e33.

Lau,A.F., Kanemitsu,M.Y., Kurata,W.E., Danesh,S., and Boynton,A.L. (1992). Epidermal growth factor disrupts gap-junctional communication and induces phosphorylation of connexin43 on serine. Mol. Biol. Cell *3*, 865-874.

Lavado,A., Lagutin,O.V., Chow,L.M., Baker,S.J., and Oliver,G. (2010). Prox1 is required for granule cell maturation and intermediate progenitor maintenance during brain neurogenesis. PLoS. Biol. *8*.

Lee,J.Y., Ristow,M., Lin,X., White,M.F., Magnuson,M.A., and Hennighausen,L. (2006). RIP-Cre revisited, evidence for impairments of pancreatic beta-cell function. J. Biol. Chem. *281*, 2649-2653.

Lewandoski,M. (2001). Conditional control of gene expression in the mouse. Nat. Rev. Genet. *2*, 743-755.

Li,L. and Xie,T. (2005). Stem cell niche: structure and function. Annu. Rev. Cell Dev. Biol. *21*, 605-631.

Li,W., Hertzberg,E.L., and Spray,D.C. (2005). Regulation of connexin43-protein binding in astrocytes in response to chemical ischemia/hypoxia. J. Biol. Chem. *280*, 7941-7948.

Lie,D.C., Colamarino,S.A., Song,H.J., Desire,L., Mira,H., Consiglio,A., Lein,E.S., Jessberger,S., Lansford,H., Dearie,A.R., and Gage,F.H. (2005). Wnt signalling regulates adult hippocampal neurogenesis. Nature *437*, 1370-1375.

Liedtke,W., Edelmann,W., Chiu,F.C., Kucherlapati,R., and Raine,C.S. (1998). Experimental autoimmune encephalomyelitis in mice lacking glial fibrillary acidic protein is characterized by a more severe clinical course and an infiltrative central nervous system lesion. Am. J. Pathol. *152*, 251-259.

Lim,D.A., Tramontin,A.D., Trevejo,J.M., Herrera,D.G., Garcia-Verdugo,J.M., and varez-Buylla,A. (2000). Noggin antagonizes BMP signaling to create a niche for adult neurogenesis. Neuron *28*, 713-726.

Lin,J.H., Takano,T., Cotrina,M.L., Arcuino,G., Kang,J., Liu,S., Gao,Q., Jiang,L., Li,F., Lichtenberg-Frate,H., Haubrich,S., Willecke,K., Goldman,S.A., and Nedergaard,M. (2002). Connexin 43 enhances the adhesivity and mediates the invasion of malignant glioma cells. J. Neurosci. *22*, 4302-4311.

Lin,J.H., Weigel,H., Cotrina,M.L., Liu,S., Bueno,E., Hansen,A.J., Hansen,T.W., Goldman,S., and Nedergaard,M. (1998). Gap-junction-mediated propagation and amplification of cell injury. Nat. Neurosci. *1*, 494-500.

Lin,R., Warn-Cramer,B.J., Kurata,W.E., and Lau,A.F. (2001). v-Src phosphorylation of connexin 43 on Tyr247 and Tyr265 disrupts gap junctional communication. J. Cell Biol. *154*, 815-827.

Liu,X., Hashimoto-Torii,K., Torii,M., Ding,C., and Rakic,P. (2010a). Gap junctions/hemichannels modulate interkinetic nuclear migration in the forebrain precursors. J. Neurosci. *30*, 4197-4209.

Liu,Y., Suckale,J., Masjkur,J., Magro,M.G., Steffen,A., Anastassiadis,K., and Solimena,M. (2010b). Tamoxifen-independent recombination in the RIP-CreER mouse. PLoS. One. *5*, e13533.

Lois,C. and varez-Buylla,A. (1993). Proliferating subventricular zone cells in the adult mammalian forebrain can differentiate into neurons and glia. Proc. Natl. Acad. Sci. U. S. A *90*, 2074-2077.

Loo,L.W., Berestecky,J.M., Kanemitsu,M.Y., and Lau,A.F. (1995). pp60src-mediated phosphorylation of connexin 43, a gap junction protein. J. Biol. Chem. *270*, 12751-12761.

Lorente de No R. (1934). Studies on the structure of the cerebral cortex - II. Continuation of the study of the ammonic system.

Lubkemeier,I., Requardt,R.P., Lin,X., Sasse,P., Andrie,R., Schrickel,J.W., Chkourko,H., Bukauskas,F.F., Kim,J.S., Frank,M., Malan,D., Zhang,J., Wirth,A., Dobrowolski,R., Mohler,P.J., Offermanns,S., Fleischmann,B.K., Delmar,M., and Willecke,K. (2013). Deletion of the last five C-terminal amino acid residues of connexin43 leads to lethal ventricular arrhythmias in mice without affecting coupling via gap junction channels. Basic Res. Cardiol. *108*, 348.

Ludwin,S.K., Kosek,J.C., and Eng,L.F. (1976). The topographical distribution of S-100 and GFA proteins in the adult rat brain: an immunohistochemical study using horseradish peroxidase-labelled antibodies. J. Comp Neurol. *165*, 197-207.

Lynn,B.D., Tress,O., May,D., Willecke,K., and Nagy,J.I. (2011). Ablation of connexin30 in transgenic mice alters expression patterns of connexin26 and connexin32 in glial cells and leptomeninges. Eur. J. Neurosci. *34*, 1783-1793.

Maass,K., Ghanem,A., Kim,J.S., Saathoff,M., Urschel,S., Kirfel,G., Grummer,R., Kretz,M., Lewalter,T., Tiemann,K., Winterhager,E., Herzog,V., and Willecke,K. (2004). Defective epidermal barrier in neonatal mice lacking the C-terminal region of connexin43. Mol. Biol. Cell *15*, 4597-4608.

Maass,K., Shibayama,J., Chase,S.E., Willecke,K., and Delmar,M. (2007). C-terminal truncation of connexin43 changes number, size, and localization of cardiac gap junction plaques. Circ. Res. *101*, 1283-1291.

Maglione,M., Tress,O., Haas,B., Karram,K., Trotter,J., Willecke,K., and Kettenmann,H. (2010). Oligodendrocytes in mouse corpus callosum are coupled via gap junction channels formed by connexin47 and connexin32. Glia *58*, 1104-1117.

Magnotti,L.M., Goodenough,D.A., and Paul,D.L. (2011). Deletion of oligodendrocyte Cx32 and astrocyte Cx43 causes white matter vacuolation, astrocyte loss and early mortality. Glia *59*, 1064-1074.

Malatesta,P., Hack,M.A., Hartfuss,E., Kettenmann,H., Klinkert,W., Kirchhoff,F., and Gotz,M. (2003). Neuronal or glial progeny: regional differences in radial glia fate. Neuron *37*, 751-764.

Mark,M., Yoshida-Komiya,H., Gehin,M., Liao,L., Tsai,M.J., O'Malley,B.W., Chambon,P., and Xu,J. (2004). Partially redundant functions of SRC-1 and TIF2 in postnatal survival and male reproduction. Proc. Natl. Acad. Sci. U. S. A *101*, 4453-4458.

Marquez-Rosado,L., Solan,J.L., Dunn,C.A., Norris,R.P., and Lampe,P.D. (2012). Connexin43 phosphorylation in brain, cardiac, endothelial and epithelial tissues. Biochim. Biophys. Acta *1818*, 1985-1992.

Martens,K., Bottelbergs,A., and Baes,M. (2010). Ectopic recombination in the central and peripheral nervous system by aP2/FABP4-Cre mice: implications for metabolism research. FEBS Lett. *584*, 1054-1058.

Martin,S.J. and Morris,R.G. (2002). New life in an old idea: the synaptic plasticity and memory hypothesis revisited. Hippocampus *12*, 609-636.

Menezes,J.R., Froes,M.M., Moura,N., V, and Lent,R. (2000). Gap junction-mediated coupling in the postnatal anterior subventricular zone. Dev. Neurosci. *22*, 34-43.

Mercier,F. and Hatton,G.I. (2001). Connexin 26 and basic fibroblast growth factor are expressed primarily in the subpial and subependymal layers in adult brain parenchyma: roles in stem cell proliferation and morphological plasticity? J. Comp Neurol. *431*, 88-104.

Metzger,D., Clifford,J., Chiba,H., and Chambon,P. (1995). Conditional site-specific recombination in mammalian cells using a ligand-dependent chimeric Cre recombinase. Proc. Natl. Acad. Sci. U. S. A *92*, 6991-6995.

Middeldorp,J. and Hol,E.M. (2011). GFAP in health and disease. Prog. Neurobiol. *93*, 421-443.

Miller,M.W. and Nowakowski,R.S. (1988). Use of bromodeoxyuridine-immunohistochemistry to examine the proliferation, migration and time of origin of cells in the central nervous system. Brain Res. *457*, 44-52.

Ming,G.L. and Song,H. (2005). Adult neurogenesis in the mammalian central nervous system. Annu. Rev. Neurosci. *28*, 223-250.

Ming,G.L. and Song,H. (2011). Adult neurogenesis in the mammalian brain: significant answers and significant questions. Neuron *70*, 687-702.

Mira,H., Andreu,Z., Suh,H., Lie,D.C., Jessberger,S., Consiglio,A., San,E.J., Hortiguela,R., Marques-Torrejon,M.A., Nakashima,K., Colak,D., Gotz,M., Farinas,I., and Gage,F.H. (2010). Signaling through BMPR-IA regulates quiescence and long-term activity of neural stem cells in the adult hippocampus. Cell Stem Cell *7*, 78-89.

Miragall,F., Albiez,P., Bartels,H., de,V.U., and Dermietzel,R. (1997). Expression of the gap junction protein connexin43 in the subependymal layer and the rostral migratory stream of the mouse: evidence for an inverse correlation between intensity of connexin43 expression and cell proliferation activity. Cell Tissue Res. *287*, 243-253.

Mirzadeh,Z., Merkle,F.T., Soriano-Navarro,M., Garcia-Verdugo,J.M., and varez-Buylla,A. (2008). Neural stem cells confer unique pinwheel architecture to the ventricular surface in neurogenic regions of the adult brain. Cell Stem Cell *3*, 265-278.

Miyake,T. and Kitamura,T. (1992). Glutamine synthetase immunoreactivity in two types of mouse brain glial cells. Brain Res. *586*, 53-60.

Mokry,J., Cizkova,D., Filip,S., Ehrmann,J., Osterreicher,J., Kolar,Z., and English,D. (2004). Nestin expression by newly formed human blood vessels. Stem Cells Dev. *13*, 658-664.

Moll,R., Pitz,S., Levy,R., Weikel,W., Franke,W.W., and Czernobilsky,B. (1991). Complexity of expression of intermediate filament proteins, including glial filament protein, in endometrial and ovarian adenocarcinomas. Hum. Pathol. *22*, 989-1001.

Moorby,C. and Patel,M. (2001). Dual functions for connexins: Cx43 regulates growth independently of gap junction formation. Exp. Cell Res. *271*, 238-248.

Moreno,A.P., Chanson,M., Elenes,S., Anumonwo,J., Scerri,I., Gu,H., Taffet,S.M., and Delmar,M. (2002). Role of the carboxyl terminal of connexin43 in transjunctional fast voltage gating. Circ. Res. *90*, 450-457.

Moreno,A.P., Saez,J.C., Fishman,G.I., and Spray,D.C. (1994). Human connexin43 gap junction channels. Regulation of unitary conductances by phosphorylation. Circ. Res. *74*, 1050-1057.

Morrison,S.J. and Spradling,A.C. (2008). Stem cells and niches: mechanisms that promote stem cell maintenance throughout life. Cell *132*, 598-611.

Mullen,R.J., Buck,C.R., and Smith,A.M. (1992). NeuN, a neuronal specific nuclear protein in vertebrates. Development *116*, 201-211.

Mulligan,S.J. and MacVicar,B.A. (2004). Calcium transients in astrocyte endfeet cause cerebrovascular constrictions. Nature *431*, 195-199.

Mullis,K.B. and Faloona,F.A. (1987). Specific synthesis of DNA in vitro via a polymerase-catalyzed chain reaction. Methods Enzymol. *155*, 335-350.

Musil,L.S., Cunningham,B.A., Edelman,G.M., and Goodenough,D.A. (1990). Differential phosphorylation of the gap junction protein connexin43 in junctional communication-competent and -deficient cell lines. J. Cell Biol. *111*, 2077-2088.

Musil,L.S. and Goodenough,D.A. (1991). Biochemical analysis of connexin43 intracellular transport, phosphorylation, and assembly into gap junctional plaques. J. Cell Biol. *115*, 1357-1374.

Nagy,A. (2000). Cre recombinase: the universal reagent for genome tailoring. Genesis. *26*, 99-109.

Nagy,J.I., Ionescu,A.V., Lynn,B.D., and Rash,J.E. (2003). Connexin29 and connexin32 at oligodendrocyte and astrocyte gap junctions and in myelin of the mouse central nervous system. J. Comp Neurol. *464*, 356-370.

Nagy,J.I. and Li,W.E. (2000). A brain slice model for in vitro analyses of astrocytic gap junction and connexin43 regulation: actions of ischemia, glutamate and elevated potassium. Eur. J. Neurosci. *12*, 4567-4572.

Nagy,J.I., Patel,D., Ochalski,P.A., and Stelmack,G.L. (1999). Connexin30 in rodent, cat and human brain: selective expression in gray matter astrocytes, co-localization with connexin43 at gap junctions and late developmental appearance. Neuroscience *88*, 447-468.

Nagy,J.I. and Rash,J.E. (2000). Connexins and gap junctions of astrocytes and oligodendrocytes in the CNS. Brain Res. Brain Res. Rev. *32*, 29-44.

Nakase,T., Sohl,G., Theis,M., Willecke,K., and Naus,C.C. (2004). Increased apoptosis and inflammation after focal brain ischemia in mice lacking connexin43 in astrocytes. Am. J. Pathol. *164*, 2067-2075.

Neijssen,J., Herberts,C., Drijfhout,J.W., Reits,E., Janssen,L., and Neefjes,J. (2005). Cross-presentation by intercellular peptide transfer through gap junctions. Nature *434*, 83-88.

Newman,E. and Reichenbach,A. (1996). The Muller cell: a functional element of the retina. Trends Neurosci. *19*, 307-312.

Nimmerjahn,A., Kirchhoff,F., Kerr,J.N., and Helmchen,F. (2004). Sulforhodamine 101 as a specific marker of astroglia in the neocortex in vivo. Nat. Methods *1*, 31-37.

Ninkovic,J. and Gotz,M. (2007). Signaling in adult neurogenesis: from stem cell niche to neuronal networks. Curr. Opin. Neurobiol. *17*, 338-344.

Nishiyama,A., Komitova,M., Suzuki,R., and Zhu,X. (2009). Polydendrocytes (NG2 cells): multifunctional cells with lineage plasticity. Nat. Rev. Neurosci. *10*, 9-22.

Norenberg,M.D. and Martinez-Hernandez,A. (1979). Fine structural localization of glutamine synthetase in astrocytes of rat brain. Brain Res. *161*, 303-310.

Nottebohm,F. (2004). The road we travelled: discovery, choreography, and significance of brain replaceable neurons. Ann. N. Y. Acad. Sci. *1016*, 628-658.

O' Keefe and Nadel (1978). The hippocampus as a cognitive map, Oxford Univ. Press, New York, USA.

O'Mara,S.M., Commins,S., Anderson,M., and Gigg,J. (2001). The subiculum: a review of form, physiology and function. Prog. Neurobiol. *64*, 129-155.

Oelze,I., Kartenbeck,J., Crusius,K., and Alonso,A. (1995). Human papillomavirus type 16 E5 protein affects cell-cell communication in an epithelial cell line. J. Virol. *69*, 4489-4494.

Ogata,K. and Kosaka,T. (2002). Structural and quantitative analysis of astrocytes in the mouse hippocampus. Neuroscience *113*, 221-233.

Oliver,G., Sosa-Pineda,B., Geisendorf,S., Spana,E.P., Doe,C.Q., and Gruss,P. (1993). Prox 1, a prospero-related homeobox gene expressed during mouse development. Mech. Dev. *44*, 3-16.

Ortega,H.H., Salvetti,N.R., Baravalle,C., Lorente,J.A., and Mira,G.A. (2006). Oestradiol induced inhibition of neuroendocrine marker expression in Leydig cells of adult rats. Reprod. Domest. Anim *41*, 204-209.

Owens,D.F. and Kriegstein,A.R. (1998). Patterns of intracellular calcium fluctuation in precursor cells of the neocortical ventricular zone. J. Neurosci. *18*, 5374-5388.

Pahujaa,M., Anikin,M., and Goldberg,G.S. (2007). Phosphorylation of connexin43 induced by Src: regulation of gap junctional communication between transformed cells. Exp. Cell Res. *313*, 4083-4090.

Palatinus,J.A., O'Quinn,M.P., Barker,R.J., Harris,B.S., Jourdan,J., and Gourdie,R.G. (2011). ZO-1 determines adherens and gap junction localization at intercalated disks. Am. J. Physiol Heart Circ. Physiol *300*, H583-H594.

Pannasch,U., Vargova,L., Reingruber,J., Ezan,P., Holcman,D., Giaume,C., Sykova,E., and Rouach,N. (2011). Astroglial networks scale synaptic activity and plasticity. Proc. Natl. Acad. Sci. U. S. A *108*, 8467-8472.

Paxinos,G. and Franklin,K. (2011). The Mouse Brain, 2nd Ed., Academic Press, New York.

Paznekas,W.A., Boyadjiev,S.A., Shapiro,R.E., Daniels,O., Wollnik,B., Keegan,C.E., Innis,J.W., Dinulos,M.B., Christian,C., Hannibal,M.C., and Jabs,E.W. (2003). Connexin 43 (GJA1) mutations cause the pleiotropic phenotype of oculodentodigital dysplasia. Am. J. Hum. Genet. *72*, 408-418.

Pearson,R.A., Luneborg,N.L., Becker,D.L., and Mobbs,P. (2005). Gap junctions modulate interkinetic nuclear movement in retinal progenitor cells. J. Neurosci. *25*, 10803-10814.

Peitz,M., Pfannkuche,K., Rajewsky,K., and Edenhofer,F. (2002). Ability of the hydrophobic FGF and basic TAT peptides to promote cellular uptake of recombinant Cre recombinase: a tool for efficient genetic engineering of mammalian genomes. Proc. Natl. Acad. Sci. U. S. A *99*, 4489-4494.

Pelletier,R.M. (1995). The distribution of connexin 43 is associated with the germ cell differentiation and with the modulation of the Sertoli cell junctional barrier in continual (guinea pig) and seasonal breeders' (mink) testes. J. Androl *16*, 400-409.

Penes,M.C., Li,X., and Nagy,J.I. (2005). Expression of zonula occludens-1 (ZO-1) and the transcription factor ZO-1-associated nucleic acid-binding protein (ZONAB)-MsY3 in glial cells and colocalization at oligodendrocyte and astrocyte gap junctions in mouse brain. Eur. J. Neurosci. *22*, 404-418.

Perea,G., Navarrete,M., and Araque,A. (2009). Tripartite synapses: astrocytes process and control synaptic information. Trends Neurosci. *32*, 421-431.

Peretto,P., Giachino,C., Aimar,P., Fasolo,A., and Bonfanti,L. (2005). Chain formation and glial tube assembly in the shift from neonatal to adult subventricular zone of the rodent forebrain. J. Comp Neurol. *487*, 407-427.

Peters,A. (2004). A fourth type of neuroglial cell in the adult central nervous system. J. Neurocytol. *33*, 345-357.

Peters,N.S., Coromilas,J., Severs,N.J., and Wit,A.L. (1997). Disturbed connexin43 gap junction distribution correlates with the location of reentrant circuits in the epicardial border zone of healing canine infarcts that cause ventricular tachycardia. Circulation *95*, 988-996.

Qu,Q., Sun,G., Li,W., Yang,S., Ye,P., Zhao,C., Yu,R.T., Gage,F.H., Evans,R.M., and Shi,Y. (2010). Orphan nuclear receptor TLX activates Wnt/beta-catenin signalling to stimulate neural stem cell proliferation and self-renewal. Nat. Cell Biol. *12*, 31-40.

Ramirez,A., Page,A., Gandarillas,A., Zanet,J., Pibre,S., Vidal,M., Tusell,L., Genesca,A., Whitaker,D.A., Melton,D.W., and Jorcano,J.L. (2004). A keratin K5Cre transgenic line appropriate for tissue-specific or generalized Cre-mediated recombination. Genesis. *39*, 52-57.

Ramon y Cajal (1913). Degeneration and Regeneration of the Nervous System (Trans. Day, R. M., from the 1913 Spanish edn) (Oxford Univ. Press, London, 1928).

Ransom,B.R. and Kettenmann,H. (1990). Electrical coupling, without dye coupling, between mammalian astrocytes and oligodendrocytes in cell culture. Glia *3*, 258-266.

Ransom,B.R. and Sontheimer,H. (1992). The neurophysiology of glial cells. J. Clin. Neurophysiol. *9*, 224-251.

Reaume,A.G., de Sousa,P.A., Kulkarni,S., Langille,B.L., Zhu,D., Davies,T.C., Juneja,S.C., Kidder,G.M., and Rossant,J. (1995). Cardiac malformation in neonatal mice lacking connexin43. Science *267*, 1831-1834.

Reichenbach,A. and Wolburg,H. (2005). Neuroglia, chap. Astrocytes and ependymal glia., pp. 19-35. (Oxford University Press).

Requardt,R.P., Kaczmarczyk,L., Dublin,P., Wallraff-Beck,A., Mikeska,T., Degen,J., Waha,A., Steinhauser,C., Willecke,K., and Theis,M. (2009). Quality control of astrocyte-directed Cre transgenic mice: the benefits of a direct link between loss of gene expression and reporter activation. Glia *57*, 680-692.

Revel,J.P. and Karnovsky,M.J. (1967). Hexagonal array of subunits in intercellular junctions of the mouse heart and liver. J. Cell Biol. *33*, C7-C12.

Reynhout,J.K., Lampe,P.D., and Johnson,R.G. (1992). An activator of protein kinase C inhibits gap junction communication between cultured bovine lens cells. Exp. Cell Res. *198*, 337-342.

Reynolds,B.A. and Weiss,S. (1992). Generation of neurons and astrocytes from isolated cells of the adult mammalian central nervous system. Science *255*, 1707-1710.

Rhett,J.M., Jourdan,J., and Gourdie,R.G. (2011). Connexin 43 connexon to gap junction transition is regulated by zonula occludens-1. Mol. Biol. Cell *22*, 1516-1528.

Rhett,J.M., Ongstad,E.L., Jourdan,J., and Gourdie,R.G. (2012). Cx43 associates with Na(v)1.5 in the cardiomyocyte perinexus. J. Membr. Biol. *245*, 411-422.

Risley,M.S. (2000). Connexin gene expression in seminiferous tubules of the Sprague-Dawley rat. Biol. Reprod. *62*, 748-754.

Risley,M.S., Tan,I.P., Roy,C., and Saez,J.C. (1992). Cell-, age- and stage-dependent distribution of connexin43 gap junctions in testes. J. Cell Sci. *103 (Pt 1)*, 81-96.

Rosenfeld,J., Capdevielle,J., Guillemot,J.C., and Ferrara,P. (1992). In-gel digestion of proteins for internal sequence analysis after one- or two-dimensional gel electrophoresis. Anal. Biochem. *203*, 173-179.

Rouach,N., Koulakoff,A., Abudara,V., Willecke,K., and Giaume,C. (2008). Astroglial metabolic networks sustain hippocampal synaptic transmission. Science *322*, 1551-1555.

Roux,L., Benchenane,K., Rothstein,J.D., Bonvento,G., and Giaume,C. (2011). Plasticity of astroglial networks in olfactory glomeruli. Proc. Natl. Acad. Sci. U. S. A *108*, 18442-18446.

Sahay,A. and Hen,R. (2007). Adult hippocampal neurogenesis in depression. Nat. Neurosci. *10*, 1110-1115.

Santiago,M.F., Alcami,P., Striedinger,K.M., Spray,D.C., and Scemes,E. (2010). The carboxyl-terminal domain of connexin43 is a negative modulator of neuronal differentiation. J. Biol. Chem. *285*, 11836-11845.

Sauer,B. and Henderson,N. (1988). Site-specific DNA recombination in mammalian cells by the Cre recombinase of bacteriophage P1. Proc. Natl. Acad. Sci. U. S. A *85*, 5166-5170.

Scemes,E. (2008). Modulation of astrocyte P2Y1 receptors by the carboxyl terminal domain of the gap junction protein Cx43. Glia *56*, 145-153.

Scharfman,H., Goodman,J., Macleod,A., Phani,S., Antonelli,C., and Croll,S. (2005). Increased neurogenesis and the ectopic granule cells after intrahippocampal BDNF infusion in adult rats. Exp. Neurol. *192*, 348-356.

Schmechel,D.E. and Rakic,P. (1979). A Golgi study of radial glial cells in developing monkey telencephalon: morphogenesis and transformation into astrocytes. Anat. Embryol. (Berl) *156*, 115-152.

Schmidt,E.E., Taylor,D.S., Prigge,J.R., Barnett,S., and Capecchi,M.R. (2000). Illegitimate Cre-dependent chromosome rearrangements in transgenic mouse spermatids. Proc. Natl. Acad. Sci. U. S. A *97*, 13702-13707.

Schmidt-Hieber,C., Jonas,P., and Bischofberger,J. (2004). Enhanced synaptic plasticity in newly generated granule cells of the adult hippocampus. Nature *429*, 184-187.

Schmidt-Supprian,M. and Rajewsky,K. (2007). Vagaries of conditional gene targeting. Nat. Immunol. *8*, 665-668.

Schulz,T.J., Glaubitz,M., Kuhlow,D., Thierbach,R., Birringer,M., Steinberg,P., Pfeiffer,A.F., and Ristow,M. (2007). Variable expression of Cre recombinase transgenes precludes reliable prediction of tissue-specific gene disruption by tail-biopsy genotyping. PLoS. One. *2*, e1013.

Seki,T. and Arai,Y. (1995). Age-related production of new granule cells in the adult dentate gyrus. Neuroreport *6*, 2479-2482.

Seri,B., Garcia-Verdugo,J.M., Collado-Morente,L., McEwen,B.S., and varez-Buylla,A. (2004). Cell types, lineage, and architecture of the germinal zone in the adult dentate gyrus. J. Comp Neurol. *478*, 359-378.

Seri,B., Garcia-Verdugo,J.M., McEwen,B.S., and varez-Buylla,A. (2001). Astrocytes give rise to new neurons in the adult mammalian hippocampus. J. Neurosci. *21*, 7153-7160.

Severs,N.J. (2007). The carboxy terminal domain of connexin43: from molecular regulation of the gap junction channel to supramolecular organization of the intercalated disk. Circ. Res. *101*, 1213-1215.

Shah,M.M., Martinez,A.M., and Fletcher,W.H. (2002). The connexin43 gap junction protein is phosphorylated by protein kinase A and protein kinase C: in vivo and in vitro studies. Mol. Cell Biochem. *238*, 57-68.

Shen,Y., Khusial,P.R., Li,X., Ichikawa,H., Moreno,A.P., and Goldberg,G.S. (2007). SRC utilizes Cas to block gap junctional communication mediated by connexin43. J. Biol. Chem. *282*, 18914-18921.

Shors,T.J., Miesegaes,G., Beylin,A., Zhao,M., Rydel,T., and Gould,E. (2001). Neurogenesis in the adult is involved in the formation of trace memories. Nature *410*, 372-376.

Sierra,A., Encinas,J.M., Deudero,J.J., Chancey,J.H., Enikolopov,G., Overstreet-Wadiche,L.S., Tsirka,S.E., and Maletic-Savatic,M. (2010). Microglia shape adult hippocampal neurogenesis through apoptosis-coupled phagocytosis. Cell Stem Cell *7*, 483-495.

Simon,A.M., Goodenough,D.A., Li,E., and Paul,D.L. (1997). Female infertility in mice lacking connexin 37. Nature *385*, 525-529.

Slezak,M. and Pfrieger,F.W. (2003). New roles for astrocytes: regulation of CNS synaptogenesis. Trends Neurosci. *26*, 531-535.

Snyder,J.S., Kee,N., and Wojtowicz,J.M. (2001). Effects of adult neurogenesis on synaptic plasticity in the rat dentate gyrus. J. Neurophysiol. *85*, 2423-2431.

Sohl,G., Guldenagel,M., Beck,H., Teubner,B., Traub,O., Gutierrez,R., Heinemann,U., and Willecke,K. (2000). Expression of connexin genes in hippocampus of kainate-treated and kindled rats under conditions of experimental epilepsy. Brain Res. Mol. Brain Res. *83*, 44-51.

Sohl,G., Maxeiner,S., and Willecke,K. (2005). Expression and functions of neuronal gap junctions. Nat. Rev. Neurosci. *6*, 191-200.

Sohl,G. and Willecke,K. (2003). An update on connexin genes and their nomenclature in mouse and man. Cell Commun. Adhes. *10*, 173-180.

Solan,J.L. and Lampe,P.D. (2005). Connexin phosphorylation as a regulatory event linked to gap junction channel assembly. Biochim. Biophys. Acta *1711*, 154-163.

Solan,J.L. and Lampe,P.D. (2007). Key connexin 43 phosphorylation events regulate the gap junction life cycle. J. Membr. Biol. *217*, 35-41.

Solan,J.L. and Lampe,P.D. (2008). Connexin 43 in LA-25 cells with active v-src is phosphorylated on Y247, Y265, S262, S279/282, and S368 via multiple signaling pathways. Cell Commun. Adhes. *15*, 75-84.

Solan,J.L. and Lampe,P.D. (2009). Connexin43 phosphorylation: structural changes and biological effects. Biochem. J. *419*, 261-272.

Solan,J.L., Marquez-Rosado,L., Sorgen,P.L., Thornton,P.J., Gafken,P.R., and Lampe,P.D. (2007). Phosphorylation at S365 is a gatekeeper event that changes the structure of Cx43 and prevents down-regulation by PKC. J. Cell Biol. *179*, 1301-1309.

Song,H., Stevens,C.F., and Gage,F.H. (2002). Astroglia induce neurogenesis from adult neural stem cells. Nature *417*, 39-44.

Song,J., Zhong,C., Bonaguidi,M.A., Sun,G.J., Hsu,D., Gu,Y., Meletis,K., Huang,Z.J., Ge,S., Enikolopov,G., Deisseroth,K., Luscher,B., Christian,K.M., Ming,G.L., and Song,H. (2012). Neuronal circuitry mechanism regulating adult quiescent neural stem-cell fate decision. Nature *489*, 150-154.

Sorgen,P.L., Duffy,H.S., Sahoo,P., Coombs,W., Delmar,M., and Spray,D.C. (2004). Structural changes in the carboxyl terminus of the gap junction protein connexin43 indicates signaling between binding domains for c-Src and zonula occludens-1. J. Biol. Chem. *279*, 54695-54701.

Spray,D.C., Ye,Z.C., and Ransom,B.R. (2006). Functional connexin "hemichannels": a critical appraisal. Glia *54*, 758-773.

Sridharan,S., Simon,L., Meling,D.D., Cyr,D.G., Gutstein,D.E., Fishman,G.I., Guillou,F., and Cooke,P.S. (2007). Proliferation of adult sertoli cells following conditional knockout of the Gap junctional protein GJA1 (connexin 43) in mice. Biol. Reprod. *76*, 804-812.

Stanfield,B.B. and Trice,J.E. (1988). Evidence that granule cells generated in the dentate gyrus of adult rats extend axonal projections. Exp. Brain Res. *72*, 399-406.

Steiner,B., Klempin,F., Wang,L., Kott,M., Kettenmann,H., and Kempermann,G. (2006). Type-2 cells as link between glial and neuronal lineage in adult hippocampal neurogenesis. Glia *54*, 805-814.

Sternberg,N., Sauer,B., Hoess,R., and Abremski,K. (1986). Bacteriophage P1 cre gene and its regulatory region. Evidence for multiple promoters and for regulation by DNA methylation. J. Mol. Biol. *187*, 197-212.

Suh,H., Deng,W., and Gage,F.H. (2009). Signaling in adult neurogenesis. Annu. Rev. Cell Dev. Biol. *25*, 253-275.

Sutor,B. and Hagerty,T. (2005). Involvement of gap junctions in the development of the neocortex. Biochim. Biophys. Acta *1719*, 59-68.

Swanson,R.A. (2005). Astrocyte neurotransmitter uptake. In: Neuroglia, second edition (Kettenmann H, Ransom BR, eds), pp 346-354. New York, NY: Oxford University Press, Inc.

Takahashi,C., Fujito,A., Kazuka,M., Sugiyama,R., Ito,H., and Isaka,K. (2008). Anti-Mullerian hormone substance from follicular fluid is positively associated with success in oocyte fertilization during in vitro fertilization. Fertil. Steril. *89*, 586-591.

Takano,T., Tian,G.F., Peng,W., Lou,N., Libionka,W., Han,X., and Nedergaard,M. (2006). Astrocyte-mediated control of cerebral blood flow. Nat. Neurosci. *9*, 260-267.

Tanaka,S.S., Toyooka,Y., Akasu,R., Katoh-Fukui,Y., Nakahara,Y., Suzuki,R., Yokoyama,M., and Noce,T. (2000). The mouse homolog of Drosophila Vasa is required for the development of male germ cells. Genes Dev. *14*, 841-853.

Tashiro,A., Makino,H., and Gage,F.H. (2007). Experience-specific functional modification of the dentate gyrus through adult neurogenesis: a critical period during an immature stage. J. Neurosci. *27*, 3252-3259.

Tashiro,A., Zhao,C., and Gage,F.H. (2006). Retrovirus-mediated single-cell gene knockout technique in adult newborn neurons in vivo. Nat. Protoc. *1*, 3049-3055.

Taube,J.S., Muller,R.U., and Ranck,J.B., Jr. (1990). Head-direction cells recorded from the postsubiculum in freely moving rats. II. Effects of environmental manipulations. J. Neurosci. *10*, 436-447.

Taus,T., Kocher,T., Pichler,P., Paschke,C., Schmidt,A., Henrich,C., and Mechtler,K. (2011). Universal and confident phosphorylation site localization using phosphoRS. J. Proteome. Res. *10*, 5354-5362.

Teubner,B., Michel,V., Pesch,J., Lautermann,J., Cohen-Salmon,M., Sohl,G., Jahnke,K., Winterhager,E., Herberhold,C., Hardelin,J.P., Petit,C., and Willecke,K. (2003). Connexin30 (Gjb6)-deficiency causes severe hearing impairment and lack of endocochlear potential. Hum. Mol. Genet. *12*, 13-21.

Theis,M., de,W.C., Schlaeger,T.M., Eckardt,D., Kruger,O., Doring,B., Risau,W., Deutsch,U., Pohl,U., and Willecke,K. (2001). Endothelium-specific replacement of the connexin43 coding region by a lacZ reporter gene. Genesis. *29*, 1-13.

Theis,M., Jauch,R., Zhuo,L., Speidel,D., Wallraff,A., Doring,B., Frisch,C., Sohl,G., Teubner,B., Euwens,C., Huston,J., Steinhauser,C., Messing,A., Heinemann,U., and Willecke,K. (2003). Accelerated hippocampal spreading depression and enhanced locomotory activity in mice with astrocyte-directed inactivation of connexin43. J. Neurosci. *23*, 766-776.

Theis,M., Sohl,G., Eiberger,J., and Willecke,K. (2005). Emerging complexities in identity and function of glial connexins. Trends Neurosci. *28*, 188-195.

Theis,M., Speidel,D., and Willecke,K. (2004). Astrocyte cultures from conditional connexin43-deficient mice. Glia *46*, 130-141.

Thomas,K.R. and Capecchi,M.R. (1987). Site-directed mutagenesis by gene targeting in mouse embryo-derived stem cells. Cell *51*, 503-512.

Torres,A., Wang,F., Xu,Q., Fujita,T., Dobrowolski,R., Willecke,K., Takano,T., and Nedergaard,M. (2012). Extracellular Ca(2)(+) acts as a mediator of communication from neurons to glia. Sci. Signal. *5*, ra8.

Toyofuku,T., Akamatsu,Y., Zhang,H., Kuzuya,T., Tada,M., and Hori,M. (2001). c-Src regulates the interaction between connexin-43 and ZO-1 in cardiac myocytes. J. Biol. Chem. *276*, 1780-1788.

Toyofuku,T., Yabuki,M., Otsu,K., Kuzuya,T., Tada,M., and Hori,M. (1999). Functional role of c-Src in gap junctions of the cardiomyopathic heart. Circ. Res. *85*, 672-681.

Toyooka,Y., Tsunekawa,N., Takahashi,Y., Matsui,Y., Satoh,M., and Noce,T. (2000). Expression and intracellular localization of mouse Vasa-homologue protein during germ cell development. Mech. Dev. *93*, 139-149.

Tozuka,Y., Fukuda,S., Namba,T., Seki,T., and Hisatsune,T. (2005). GABAergic excitation promotes neuronal differentiation in adult hippocampal progenitor cells. Neuron *47*, 803-815.

Traub,O., Look,J., Dermietzel,R., Brummer,F., Hulser,D., and Willecke,K. (1989). Comparative characterization of the 21-kD and 26-kD gap junction proteins in murine liver and cultured hepatocytes. J. Cell Biol. *108*, 1039-1051.

Tronche,F., Kellendonk,C., Kretz,O., Gass,P., Anlag,K., Orban,P.C., Bock,R., Klein,R., and Schutz,G. (1999). Disruption of the glucocorticoid receptor gene in the nervous system results in reduced anxiety. Nat. Genet. *23*, 99-103.

Tsien,J.Z., Chen,D.F., Gerber,D., Tom,C., Mercer,E.H., Anderson,D.J., Mayford,M., Kandel,E.R., and Tonegawa,S. (1996). Subregion- and cell type-restricted gene knockout in mouse brain. Cell *87*, 1317-1326.

Ullian,E.M., Sapperstein,S.K., Christopherson,K.S., and Barres,B.A. (2001). Control of synapse number by glia. Science *291*, 657-661.

Unger,T., Bette,S., Zhang,J., Theis,M., and Engele,J. (2012). Connexin-deficiency affects expression levels of glial glutamate transporters within the cerebrum. Neurosci. Lett. *506*, 12-16.

Valiunas,V., Polosina,Y.Y., Miller,H., Potapova,I.A., Valiuniene,L., Doronin,S., Mathias,R.T., Robinson,R.B., Rosen,M.R., Cohen,I.S., and Brink,P.R. (2005). Connexin-specific cell-to-cell transfer of short interfering RNA by gap junctions. J. Physiol *568*, 459-468.

Verkhratsky,A. and Butt,A. (2007). Glial Neurobiology: A text book. John Wiley & Sons Ltd, The Atrium, West Sussex, England.

Verkhratsky,A. and Kirchhoff,F. (2007). NMDA Receptors in glia. Neuroscientist. *13*, 28-37.

Verkhratsky,A. and Steinhauser,C. (2000). Ion channels in glial cells. Brain Res. Brain Res. Rev. *32*, 380-412.

Wallraff,A., Kohling,R., Heinemann,U., Theis,M., Willecke,K., and Steinhauser,C. (2006). The impact of astrocytic gap junctional coupling on potassium buffering in the hippocampus. J. Neurosci. *26*, 5438-5447.

Wallraff,A., Odermatt,B., Willecke,K., and Steinhauser,C. (2004). Distinct types of astroglial cells in the hippocampus differ in gap junction coupling. Glia *48*, 36-43.

Wang,S., Scott,B.W., and Wojtowicz,J.M. (2000). Heterogenous properties of dentate granule neurons in the adult rat. J. Neurobiol. *42*, 248-257.

Warn-Cramer,B.J., Cottrell,G.T., Burt,J.M., and Lau,A.F. (1998). Regulation of connexin-43 gap junctional intercellular communication by mitogen-activated protein kinase. J. Biol. Chem. *273*, 9188-9196.

Warn-Cramer,B.J. and Lau,A.F. (2004). Regulation of gap junctions by tyrosine protein kinases. Biochim. Biophys. Acta *1662*, 81-95.

Warner-Schmidt,J.L. and Duman,R.S. (2006). Hippocampal neurogenesis: opposing effects of stress and antidepressant treatment. Hippocampus *16*, 239-249.

Wayakanon,P., Bhattacharjee,R., Nakahama,K., and Morita,I. (2012). The role of the Cx43 C-terminus in GJ plaque formation and internalization. Biochem. Biophys. Res. Commun. *420*, 456-461.

Weissman,T.A., Riquelme,P.A., Ivic,L., Flint,A.C., and Kriegstein,A.R. (2004). Calcium waves propagate through radial glial cells and modulate proliferation in the developing neocortex. Neuron *43*, 647-661.

Wicksteed,B., Brissova,M., Yan,W., Opland,D.M., Plank,J.L., Reinert,R.B., Dickson,L.M., Tamarina,N.A., Philipson,L.H., Shostak,A., Bernal-Mizrachi,E., Elghazi,L., Roe,M.W., Labosky,P.A., Myers,M.G., Jr., Gannon,M., Powers,A.C., and Dempsey,P.J. (2010). Conditional gene targeting in mouse pancreatic ss-Cells: analysis of ectopic Cre transgene expression in the brain. Diabetes *59*, 3090-3098.

Wiencken-Barger,A.E., Djukic,B., Casper,K.B., and McCarthy,K.D. (2007). A role for Connexin43 during neurodevelopment. Glia *55*, 675-686.

Will,E., Klump,H., Heffner,N., Schwieger,M., Schiedlmeier,B., Ostertag,W., Baum,C., and Stocking,C. (2002). Unmodified Cre recombinase crosses the membrane. Nucleic Acids Res. *30*, e59.

Winterhager,E., Pielensticker,N., Freyer,J., Ghanem,A., Schrickel,J.W., Kim,J.S., Behr,R., Grummer,R., Maass,K., Urschel,S., Lewalter,T., Tiemann,K., Simoni,M., and Willecke,K. (2007). Replacement of connexin43 by connexin26 in transgenic mice leads to dysfunctional reproductive organs and slowed ventricular conduction in the heart. BMC. Dev. Biol. *7*, 26.

Witter,M.P. and Groenewegen,H.J. (1990). The subiculum: cytoarchitectonically a simple structure, but hodologically complex. Prog. Brain Res. *83*, 47-58.

Ye,X., Han,S.J., Tsai,S.Y., DeMayo,F.J., Xu,J., Tsai,M.J., and O'Malley,B.W. (2005). Roles of steroid receptor coactivator (SRC)-1 and transcriptional intermediary factor (TIF) 2 in androgen receptor activity in mice. Proc. Natl. Acad. Sci. U. S. A *102*, 9487-9492.

Yogo,K., Ogawa,T., Akiyama,M., Ishida,N., and Takeya,T. (2002). Identification and functional analysis of novel phosphorylation sites in Cx43 in rat primary granulosa cells. FEBS Lett. *531*, 132-136.

Yogo,K., Ogawa,T., Akiyama,M., Ishida-Kitagawa,N., Sasada,H., Sato,E., and Takeya,T. (2006). PKA implicated in the phosphorylation of Cx43 induced by stimulation with FSH in rat granulosa cells. J. Reprod. Dev. *52*, 321-328.

Zacchetti,A., van,G.E., Teske,E., Nederbragt,H., Dierendonck,J.H., and Rutteman,G.R. (2003). Validation of the use of proliferation markers in canine neoplastic and non-neoplastic tissues: comparison of KI-67 and proliferating cell nuclear antigen (PCNA) expression versus in vivo bromodeoxyuridine labelling by immunohistochemistry. APMIS *111*, 430-438.

Zahs,K.R. (1998). Heterotypic coupling between glial cells of the mammalian central nervous system. Glia *24*, 85-96.

Zhao,C., Deng,W., and Gage,F.H. (2008). Mechanisms and functional implications of adult neurogenesis. Cell *132*, 645-660.

Zhao,C., Teng,E.M., Summers,R.G., Jr., Ming,G.L., and Gage,F.H. (2006). Distinct morphological stages of dentate granule neuron maturation in the adult mouse hippocampus. J. Neurosci. *26*, 3-11.

Zhuo,L., Theis,M., varez-Maya,I., Brenner,M., Willecke,K., and Messing,A. (2001). hGFAP-cre transgenic mice for manipulation of glial and neuronal function in vivo. Genesis. *31*, 85-94.

Zonta,M., Sebelin,A., Gobbo,S., Fellin,T., Pozzan,T., and Carmignoto,G. (2003). Glutamate-mediated cytosolic calcium oscillations regulate a pulsatile prostaglandin release from cultured rat astrocytes. J. Physiol *553*, 407-414.

9. Appendix

Mouse line	Total number of ki67 positive cells	Total number of DG sections analyzed	Ki67 positive cells per DG section (mean ± s.d)
Cx30+/+ (n=5)	825	70	11,78 ± 3,91
Cx30-/- (n=3)	354	30	11,80 ± 2,61
Cx43fl/fl: hGFAP-Cre (n=3)	56	30	1,86 ± 1,28 *
Cx43fl/fl (n=3)	259	36	7,19 ± 1,72 *

Tab. 9.1: Quantitative evaluation of Ki67 expression in the SGZ of Cx30-/-, Cx43fl/fl: hGFAP-Cre and Cx43fl/fl mice. *, $P < 0.05$ Cx30+/+ vs. Cx43fl/fl: hGFAP-Cre and Cx43fl/fl

Mouse line	Total number of ki67 positive cells	Total number of DG sections analyzed	Ki67 positive cells per DG section (mean ± s.d)
Cx30+/+; Cx43+/+ (n=5)	825	70	11,78 ± 3,91
Cx30+/+; Cx43flG138R/flG138R (n=3)	367	31	11,84 ± 4,01
Cx30+/+; Cx43flG138R/flG138R: nestin-Cre (n=5)	319	56	5,70 ± 3,07 *
Cx30-/-; Cx43flG138R/flG138R (n=3)	289	30	9,63 ± 3,54 *
Cx30-/-; Cx43flG138R/flG138R: nestin-Cre (n=3)	372	60	6,20 ± 3,01 *

Tab. 9.2: Quantitative evaluation of Ki67 expression in the SGZ of Cx43G138R mice. *, $P < 0.05$ Cx30+/+; Cx43+/+ vs. Cx30+/+; Cx43flG138R/flG138R: nestin-Cre and Cx30-/-; Cx43flG138R/flG138R, as well as Cx30-/-; Cx43flG138R/flG138R: nestin-Cre

Mouse line	Total number of ki67 positive cells	Total number of DG sections analyzed	Ki67 positive cells per DG section (mean ± s.d)
Cx30+/+; Cx43+/+ (n=5)	825	70	11,78 ± 3,91
Cx30+/+; Cx43fl/K258stop (n=3)	229	30	7,63 ± 4,75 *
Cx30+/+; Cx43fl/K258stop: hGFAP-Cre (n=3)	144	30	4,80 ± 2,19 *
Cx30-/-; Cx43fl/K258stop (n=3)	200	30	6,67 ± 2,47 *
Cx30-/-; Cx43fl/K258stop: hGFAP-Cre (n=3)	171	40	4,28 ± 1,98 *

Tab. 9.3: Quantitative evaluation of Ki67 expression in the SGZ of Cx43K258stop mice. *, $P < 0.05$ Cx30+/+; Cx43+/+ vs. Cx30+/+; Cx43fl/K258stop, Cx30+/+; Cx43fl/K258stop: hGFAP-Cre and Cx30-/-; Cx43fl/K258stop, as well as Cx30-/-; Cx43fl/K258stop: hGFAP-Cre

Mouse line	Total number of ki67 positive cells	Total number of DG sections analyzed	Ki67 positive cells per DG section (mean ± s.d)
Cx30-/-; Cx43flD378stop/flD378stop (n=3)	340	30	11,33 ± 2,41
Cx30-/-; Cx43flD378stop/flD378stop: hGFAP-Cre (n=3)	242	30	8,07 ± 4,53 *

Tab. 9.4: Quantitative evaluation of Ki67 expression in the SGZ of Cx43D378stop mice. *, $P < 0.05$ Cx30-/-; Cx43flD378stop/flD378stop vs. Cx30-/-; Cx43flD378stop/flD378stop: hGFAP-Cre

Mouse line	Total number of Prox1 positive cells	Total number of counting boxes (150 x 50 x 4 µm^3)	Prox1 positive cells per DG section (mean ± s.d)
Cx30+/+ (n=6)	5001	116	43,11 ± 5,93
Cx30-/- (n=3)	2566	60	42,77 ± 5,0
Cx43fl/fl: hGFAP-Cre (n=3)	1997	60	33,28 ± 5,07 *
Cx43fl/fl (n=3)	2638	72	36,64 ± 4,18 *

Tab. 9.5: Quantitative evaluation of Prox1 expression in the GCL of Cx30-/-, Cx43fl/fl: hGFAP-Cre and Cx43fl/fl mice. *, $P < 0.05$ Cx30+/+ vs. Cx43fl/fl: hGFAP-Cre and Cx43fl/fl

Mouse line	Total number of Prox1 positive cells	Total number of counting boxes (150 x 50 x 4 µm^3)	Prox1 positive cells per DG section (mean ± s.d)
Cx30+/+; Cx43+/+ (n=6)	5001	116	43,11 ± 5,93
Cx30+/+; Cx43flG138R/flG138R (n=3)	2811	64	43,92 ± 5,33
Cx30+/+; Cx43flG138R/flG138R: nestin-Cre (n=5)	5347	144	37,13 ± 6,28 *
Cx30-/-; Cx43flG138R/flG138R (n=3)	2268	56	40,50 ± 4,83 *
Cx30-/-; Cx43flG138R/flG138R: nestin-Cre (n=3)	2214	58	38,17 ± 4,73 *

Tab. 9.6: Quantitative evaluation of Prox1 expression in the GCL of Cx43G138R mice. *, $P < 0.05$ Cx30+/+; Cx43+/+ vs. Cx30+/+; Cx43flG138R/flG138R: nestin-Cre and Cx30-/-; Cx43flG138R/flG138R, as well as Cx30-/-; Cx43flG138R/flG138R: nestin-Cre

Mouse line	Total number of Prox1 positive cells	Total number of counting boxes (150 x 50 x 4 µm^3)	Prox1 positive cells per DG section (mean ± s.d)
Cx30+/+; Cx43+/+ (n=6)	5001	116	43,11 ± 5,93
Cx30+/+; Cx43fl/K258stop (n=3)	2439	60	40,65 ± 6,31 *
Cx30+/+; Cx43fl/K258stop: hGFAP-Cre (n=3)	2427	60	40,45 ± 6,48 *
Cx30-/-; Cx43fl/K258stop (n=3)	2457	60	40,95 ± 4,71 *
Cx30-/-; Cx43fl/K258stop: hGFAP-Cre (n=3)	2430	60	40,50 ± 4,04 *

Tab. 9.7: Quantitative evaluation of Prox1 expression in the GCL of Cx43K258stop mice. *, $P < 0.05$ Cx30+/+; Cx43+/+ vs. Cx30+/+; Cx43fl/K258stop, Cx30+/+; Cx43fl/K258stop: hGFAP-Cre and Cx30-/-; Cx43fl/K258stop, as well as Cx30-/-; Cx43fl/K258stop: hGFAP-Cre

Mouse line	Total number of Prox1 positive cells	Total number of counting boxes (150 x 50 x 4 µm^3)	Prox1 positive cells per DG section (mean ± s.d)
Cx30-/-; Cx43flD378stop/flD378stop (n=2)	1529	40	38,23 ± 5,52
Cx30-/-; Cx43flD378stop/flD378stop: hGFAP-Cre (n=2)	1438	38	37,84 ± 4,03

Tab. 9.8: Quantitative evaluation of Prox1 expression in the GCL of Cx43D378stop mice.

Mouse line	Total number of BLBP positive cells	Total number of counting boxes (220 x 170 x 30 µm^3)	BLBP positive cells per DG section (mean ± s.d)
Cx30+/+; Cx43+/+ (n=4)	268	35	7,65 ± 2,0
Cx30-/- (n=3)	195	27	7,22 ± 1,92
Cx30+/+; Cx43flG138R/flG138R (n=3)	212	30	7,07 ± 1,64
Cx30-/-; Cx43flG138R/flG138R: nestin-Cre (n=3)	125	30	4,17 ± 3,15 *
Cx30+/+; Cx43fl/K258stop (n=3)	146	30	4,87 ± 2,37
Cx30-/-; Cx43fl/K258stop: hGFAP-Cre (n=3)	28	30	0,93 ± 1,08 *

Tab. 9.9: Quantitative evaluation of BLBP expression in the DG of Cx30 and Cx43 mutant. *, *P* < 0.05 Cx30+/+; Cx43flG138R/flG138R vs. Cx30-/-; Cx43flG138R/flG138R: nestin-Cre and Cx30+/+; Cx43fl/K258stop vs. Cx30-/-; Cx43fl/K258stop: hGFAP-Cre

Mouse line	Total number of BrdU positive cells (2 h)	Total number of DG sections analyzed	BrdU positive cells per DG section (mean ± s.d)
Cx30+/+; Cx43+/+ (n=3)	585	30	19,50 ± 4,61
Cx30-/- (n=3)	564	30	18,80 ± 5,50
Cx30-/-; Cx43flG138R/flG138R: nestin-Cre (n=3)	306	30	10,20 ± 3,67 *
Cx30-/-; Cx43fl/K258stop: hGFAP-Cre (n=3)	316	30	10,53 ± 3,63 *

Tab. 9.10: Quantitative evaluation of BrdU positive cells 2 h after injection in the Cx30 and Cx43 mutant. *, *P* < 0.05 Cx30+/+; Cx43+/+ vs. Cx30-/-; Cx43flG138R/flG138R: nestin-Cre and Cx30-/-; Cx43fl/K258stop: hGFAP-Cre

Mouse line	Total number of BrdU positive cells (4 w)	Total number of DG sections analyzed	BrdU positive cells per DG section (mean ± s.d)
Cx30+/+; Cx43+/+ (n=3)	171	30	5,70 ± 2,89
Cx30-/- (n=3)	166	30	5,53 ± 2,87
Cx30-/-; Cx43flG138R/flG138R: nestin-Cre (n=3)	115	30	3,83 ± 1,90 *
Cx30-/-; Cx43fl/K258stop: hGFAP-Cre (n=3)	117	30	3,90 ± 2,12 *

Tab. 9.11: Quantitative evaluation of BrdU positive cells 4 weeks after injection in the Cx30 and Cx43 mutant. *, *P* < 0.05 Cx30+/+; Cx43+/+ vs. Cx30-/-; Cx43flG138R/flG138R: nestin-Cre and Cx30-/-; Cx43fl/K258stop: hGFAP-Cre

Mouse line	Total number of coupling cells	Total number of cells analyzed	Coupled cells in the SGZ per section (mean ± s.d)
Cx30+/+; Cx43+/+ (n=4)	60	6 (1)	12,0 ± 2,26
Cx30-/-; Cx43flG138R/flG138R: nestin-Cre (n=4)	31,5	8 (4)	7,88 ± 3,14 *
Cx30-/-; Cx43fl/K258stop: hGFAP-Cre (n=3)	26,5	8 (3)	5,30 ± 3,06 *

Tab. 9.12: Quantitative evaluation of RG-like cell coupling in the SGZ of Cx43 mutant. Nummber of uncoupled cells are indicated in the bracket. *, *P* < 0.05 Cx30+/+; Cx43+/+ vs. Cx30-/-; Cx43flG138R/flG138R: nestin-Cre and Cx30-/-; Cx43fl/K258stop: hGFAP-Cre

Mouse line	Total number of coupling cells	Total number of sections analyzed	Coupled cells in CA1 region per section (mean ± s.d)
Cx30-/-; Cx43flG138R/flG138R (n=3)	1860	24	77,5 ± 35,8
Cx30-/-; Cx43flG138R/flG138R: nestin-Cre (n=4)	28	30	0,9 ± 3,6 *

Tab. 9.13: Quantitative evaluation of astrocytic coupling in the CA1 region of Cx43G138R mice. *, $P < 0.05$ Cx30-/-; Cx43flG138R/flG138R vs. Cx30-/-; Cx43flG138R/flG138R: nestin-Cre

Mouse line	Total number of coupling cells	Total number of sections analyzed	Coupled cells in CA1 region per section (mean ± s.d)
Cx30-/-; Cx43fl/fl (n=4)	1152	22	52,4 ± 30,9
Cx30-/-; Cx43K258stop/- (n=5)	79	38	2,1 ± 3,9 *

Tab. 9.14: Quantitative evaluation of astrocytic coupling in the CA1 region of Cx43K258stop mice. *, $P < 0.05$ Cx30-/-; Cx43fl/fl vs. Cx30-/-; Cx43K258stop/-

Mouse line	Total number of coupling cells	Total number of sections analyzed	Coupled cells in CA1 region per section (mean ± s.d)
Cx30+/+; Cx43flD378stop/flD378stop (n=3)	1172	14	83,7 ± 20,7
Cx30+/+; Cx43flD378stop/flD378stop: hGFAP-Cre (n=3)	916	15	61,1 ± 7,7 *

Tab. 9.15: Quantitative evaluation of astrocytic coupling in the CA1 region of Cx43D378stop mice. *, $P < 0.05$ Cx30+/+; Cx43flD378stop/flD378stop vs. Cx30+/+; Cx43flD378stop/flD378stop: hGFAP-Cre

10. List of figures

11. List of tables